The Dissertation Committee for Travis Allen Reine
certifies that this is the approved version of the following dissertation:

Olefin/Paraffin Separation by Reactive Absorption

Committee:

R. Bruce Eldridge, Co-Supervisor

Benny Freeman, Co-Supervisor

J. J. Lagowski

Gary Rochelle

Grant Willson

Olefin/Paraffin Separation by Reactive Absorption

by

Travis Allen Reine, B.S., M.S.

Dissertation

Presented to the Faculty of the Graduate School of
The University of Texas at Austin
in Partial Fulfillment
of the Requirements
for the Degree of
Doctor of Philosophy

The University of Texas at Austin
December 2004

To my wife and my parents.

Acknowledgments

First of all, thank you to Dr. Eldridge for his guidance and support. His door was always open for technical help with bits of humor, and he helped me to keep the goal in mind from the beginning. Also thank you to my committee members, Dr. Freeman, Dr. Lagowski, Dr. Rochelle, and Dr. Willson who were all influential in my research at UT Austin. Thanks also go out to the undergraduate researchers and visiting scholars who helped out with the experimental portion of this work. Alexander Solberg first introduced me to the copper solution while I watched him run the preliminary flow experiments. Ulrich (Uli) Kniefel helped me run a few autoclave experiments as well as build the continuous flow process which held up just fine even though his tube bending art suffered ridicule. Eric Browning helped me run the continuous flow process, and he deserves much credit for staring into a mirror directed at the liquid level of the absorption column and controlling it for hours at a time. Waynisha Edwards helped me run the many different absorption systems for the CV comparison, and she contributed lots of data pages even staying to help when it was time to remove the pyridine solution. Sean Delcambre helped acquire desorption data and proved to be a very responsible assistant.

As far as technical assistance, Ed Sones with Sasol was very helpful in implementation of the HS-GC technique. He graciously explained the HS-GC fundamentals and allowed me to run samples on Sasol's equipment free of charge. (His knowledge and kindness were not altogether unexpected though since he is a Louisiana Tech graduate!) I would also like to thank the Separations Research Program (SRP) staff: Frank Seibert, Chris Lewis, Robert Montgomery, and Steve Briggs for all of their help along the way with practical pointers and experimental expertise.

Most of all, I would like to thank my wife who stood by me from the first days of graduate school when I thought thermodynamics homework would drive me crazy

to the last days when the hours I spent writing the dissertation just about drove her crazy. She is a fearless example of someone who is always willing to sacrifice for the ones she loves. I owe much gratitude to my parents Wayne and Emilie Reine who have always supported me and never once doubted my abilities. In addition, my other set of parents Chuck and Mary Lynn Branton have been very loving and supportive even though I took their daughter out of north Louisiana to another state for these last four years. Thank you also to my grandparents: Mae Hughes, Gertrude Reine, Charles and Janice Branton, and Della Gregory for their encouragement and blessings.

Finally, thank you to all our close friends we have made in Austin, especially at Hyde Park Baptist Church. They have helped Katherine and me to feel like our time in Austin was too brief, and they will all be dearly missed. My greatest thanks go to the Creator of all life who has blessed the world with the indescribable gift of His Son, Jesus Christ. I am thankful for the realization that all of my earthly accomplishments fade into irrelevance in light of the eternal assurance that I possess through faith in Him alone.

Travis Allen Reine
September 2004

Olefin/Paraffin Separation by Reactive Absorption

Publication No. _____

Travis Allen Reine, Ph.D.
The University of Texas at Austin, 2004

Supervisors: R. Bruce Eldridge, Benny Freeman

A novel solvent for gas absorption was investigated for use in ethylene-ethane separations by reactive absorption. Due to the reactive interactions between olefins and transition metals, selection of the absorption solution required identifying a suitable transition metal salt, coordinating ligand, and solvent. In order to select an appropriate metal-salt:ligand pair, the results from a previous study using bench-top electrochemistry were compared to equilibrium data from a stirred-cell autoclave apparatus. Metal-salt:ligand pairs that were tested included combinations of cuprous chloride and cuprous bromide salts with pyridine, benzylamine, and aniline. Results from both techniques showed qualitative agreement for ethylene capacity, and the solution with the best ethylene capacity consisted of cuprous chloride with aniline as ligand.

The presence of the copper salt was found to increase the ethylene absorption capacity up to 0.6 mol/L more than the physical solubility of ethylene in a similar solution prepared without the copper salt. The mixed gas selectivity, ethylene:ethane, for the metal solution was found to be over 12:1 at optimum conditions. The kinetics of the absorption reaction were measured in a stirred cell after calculating the mass transfer coefficient for physical absorption over a range of stirrer speeds. The observed rate was compared to predictions from five different reaction rate models and was found to show good agreement with the instantaneous, reversible model.

Following the equilibrium and kinetic study, a small-scale continuous process was designed consisting of two one-inch packed columns for absorption and regeneration of a 50% ethylene / 50% ethane molar mixture. The process was operated over a wide range of flow conditions over a period of six weeks, and the solution was found to be very robust showing no significant reduction in ethylene capacity or selectivity for the duration of the experiments. The flow study also confirmed the instantaneous, reversible behavior of the complexation reaction.

Table of Contents

List of Tables

List of Figures

Nomenclature

Chapter 2

a(x)	activity of species x in solution
e	electron
E	electronic potential energy
F	Faraday constant
K_{eq}	equilibrium constant
L	ligand molecule or anion
M	metal species for olefin complexation
n	number of electrons transferred in redox reaction
p	coordination number of ligand before olefin complexation
R	gas constant
T	temperature
x	coordination number of complexed olefin
y	number of ligands displaced by complexing olefin

Greek symbols

Δ	denotes shift in potential due to complexation

Superscripts and subscripts

^{o}	denotes standard reduction potential
$_{1/2}$	denotes half wave potential
$_{k}$	denotes metal-olefin complex
$_{pa}$	denotes peak anodic current
$_{pc}$	denotes peak cathodic current

Chapter 3

B	second virial coefficient
h	parameter in generalized correlation for gases
k	binary interaction parameter
n	number of moles
P	pressure
Q	liquid flowrate, cm^3/min
t	time
V	volume, cm^3
y	mole fraction
Z	compressibility factor

Greek symbols

Δ	denotes change in moles
ω	acentric factor

Superscripts and subscripts

$_c$	denotes critical value
$_i$	denotes initial condition
$_{ij}$	denotes a species in a mixture
$_f$	denotes final condition
$_r$	denotes reduced value

Chapter 4

A	absorbance in UV-Vis; peak area in GC
b	cell path length
c	concentration of solute

K	partition or distribution coefficient

Greek symbols

β	phase ratio
ε	molar absorptivity or extinction coefficient

Superscripts and subscripts

$_G$	denotes gas phase
$_o$	denotes original or initial condition
$_S$	denotes sample liquid

Chapter 5

C_p	specific heat
ΔH	heat of complexation
q	thermal energy

Chapter 6

c^*_{total}	total concentration of ethylene in solution due to both physical and chemical absorption
$c_{\text{Cu total}}$	total copper concentration
m	Henry's law constant for physical solubility
s	ethylene to ethane equilibrium selectivity

Superscripts and subscripts

*	denotes equilibrium condition

Chapter 7

a	interfacial mass transfer area
d_{st}	stirrer diameter
D	diffusion coefficient
k	reaction rate coefficient
k_L^*	physical mass transfer coefficient
M_i	molecular weight of component i
N	stirrer rate
N_i	molar flux of component i
R_i	rate of reaction or mass transfer of component i
Re	Reynolds number
Sc	Schmidt number
Sh	Sherwood number
V_i	molar free volume of component i
x	length coordinate from the gas-liquid interface

Greek symbols

μ	liquid viscosity
Φ	enhancement factor
ρ	liquid density
ξ	association factor

Superscripts and subscripts

$_1$	denotes forward reaction rate
$_2$	denotes reverse reaction rate
$'$	denotes pseudo-first order
$_{A,B,C}$	denotes component

b	denotes bulk condition
i	denotes interfacial condition
L	denotes total length of the film

Chapter 8

G	carrier gas molar flowrate
L	liquid molar flowrate
R	ethylene recovery
V	vapor molar flowrate
x	mole fraction in the liquid phase
y	mole fraction in the vapor phase

Superscripts and subscripts

1	denotes ethylene component
2	denotes ethane component
$'$	denotes quantitative result
f	denotes feed to absorber
p	denotes product from absorber

Appendix A

A	area of heat transfer
D_i	inner diameter of inside tube
D_o	outer diameter of inside tube
$D_{o,i}$	inner diameter of outside tube
f	friction factor from Moody diagram
h	heat transfer coefficient
k	thermal conductivity
L	heat exchanger length

m	mass flow rate
Nu	Nusselt number
Pr	Prandtl number
ΔT_{lm}	log-mean temperature difference
U	overall heat transfer coefficient

Superscripts and subscripts

c	denotes cold fluid
h	denotes hot fluid
i	denotes inlet condition or inside tube
o	denotes outlet condition or outside tube
st	denotes steel tube property

Chapter 1.
Introduction to Olefin/Paraffin Separations

1.1 Importance in industry

The separation of olefins from paraffins is of primary importance to the chemical industry. The production of polymers and other specialty chemicals from mono-olefins such as ethylene and propylene requires the olefin to be of extremely high purity (>99.9%) [33]. Light olefins and paraffins have very close boiling points leading to a relative volatility as low as 1.1 for propylene/propane mixtures and 1.5 for ethylene/ethane mixtures. In order to achieve the required high degree of separation from the close boiling point mixture of olefin/paraffin, distillation towers with an enormous number of trays make up a large portion of the capital cost for an ethylene plant. A typical ethylene/ ethane column contains 80 to 150 trays with a diameter of 15 feet [101]. A propylene/propane fractionator is typically divided into two towers each containing 125 stages with a diameter of 20 feet, and reflux ratios are typically from 12 to 20 due to the close boiling points of propylene and propane [33].

Operating conditions for a typical ethylene/ethane splitter consist of pressures between 100 psia and 400 psia (depending on the flowsheet design) with condenser temperatures between -40ºC and -90ºC. At these cryogenic temperatures, closed heat loops are often used with ethylene or propylene as the working fluid. Even with the high level of heat integration present in a modern ethylene unit, the energy expenditure per pound of product produced is enormous: approximately 6.2 BTU/lb from an ethane feedstock and 9.0 BTU/lb from a naphtha feedstock [33]. The high energy costs associated with operating these large columns under these extreme conditions consumes a significant part of the industry's total energy requirements. A 1991 DOE study revealed that olefin/paraffin separations required 0.12 Quads (1

Quad = 10^{15} BTU) of energy per year which was 6.2% of the total yearly energy requirement of all distillation processes [52]. The low temperatures and high pressures required make cryogenic distillation an energy-intensive separation scheme; however, due to its proven effectiveness and reliability, cryogenic distillation has remained the dominant technology for light olefin/paraffin separations for many years. If a more efficient technique for olefin/paraffin separation is developed, it certainly holds an enormous potential for capital and energy cost savings.

1.1.1 Market size and trends

Ethylene has the largest total market value of all petrochemicals with a world production capacity of approximately 95 million tons in 2002 [3]. Figure 1-1 shows the steadily growing trend of ethylene production since the 1960's.

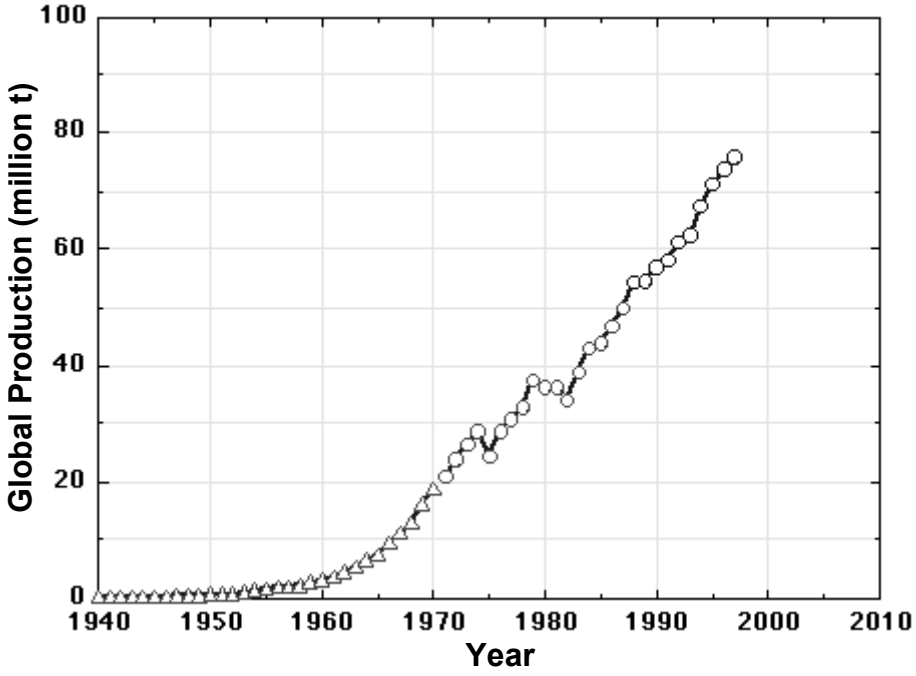

Figure 1-1. Ethylene production (from reference [93])

Based on the current average market price of $0.32 per pound [14], the total market value of ethylene is approximately $60 billion. Most ethylene is bought and sold from common high-pressure (~800 psia) pipelines as a feedstock for further processing; therefore, the purity of ethylene is standardized and highly regulated [101]. Figure 1-2 shows the classification of products from ethylene. Since the polyethylene (high and low density) market makes up the largest segment of ethylene use with nearly 55 million tons per year, this market controls the purity of manufactured ethylene. Typical ethylene purity specifications for polyethylene production are between 99.9% and 99.95% because expensive polymerization catalysts are easily deactivated by significant quantities of impurities [33]. The other ethylene derivatives like ethylene dichloride and ethylbenzene generally do not require such a high purity feed. Occasionally, the ethylene purity is compromised if these end products are manufactured on-site, but any ethylene that is transported via pipeline must be polymer-grade material.

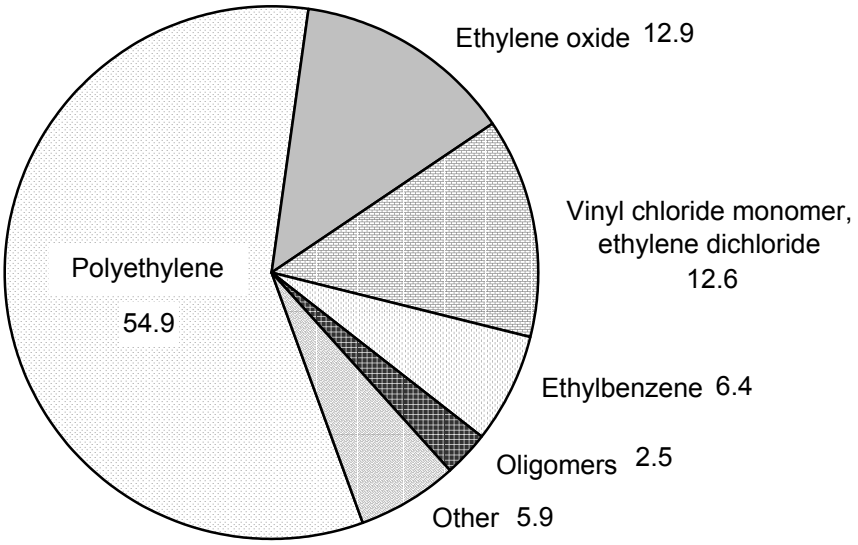

Figure 1-2. 2002 Global ethylene use in million t/yr (from [3])

The United States production capacity of ethylene accounts for nearly 28% of the world capacity, and approximately 70% of U.S. ethylene production is from ethane, propane, and butane [101]. Figure 1-3 shows the production capacity of ethylene from various feedstocks in different regions of the world. From the 1980's to the present day, the use of naphtha as a feedstock has more than doubled, supplanting the use of gas oil as a feedstock to many cracking furnaces. Naphtha feeds are more common in ethylene production overseas, but the abundance of natural gas in the U.S. makes light hydrocarbon feeds more attractive.

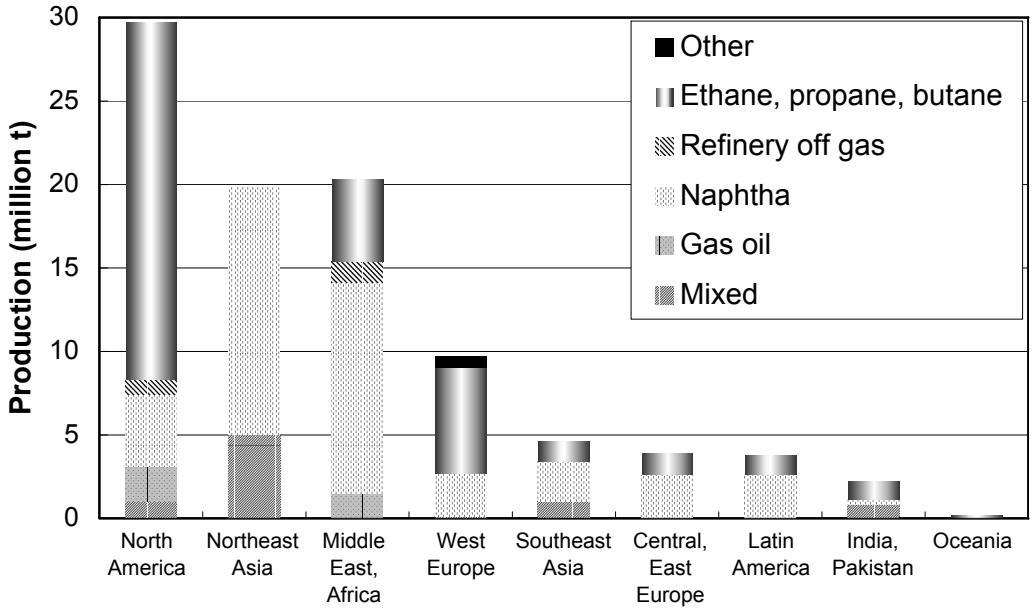

Figure 1-3. Global ethylene sources in 2002 (from [3])

The feedstock used for ethylene production is a major factor in the distribution of products from cracking furnaces. While the product distribution is controlled by many operating variables, Table 1-1 gives typical product distributions for different feedstocks in a cracking furnace with a short residence time coil at 25 psia. These cracking conditions with a light naphtha feed led to a high selectivity of ethylene to ethane of around 10 to 1. Ethane feeds usually result in a substantially greater

ethylene fraction in the product, but the ethane conversion can be quite low leading to a more mixed feed to the ethylene-ethane fractionator.

Table 1-1. Product distribution of different feedstocks* (from [101])

yield, wt%	Feedstock				
	C_2H_6	C_3H_8	*n*-C_4H_{10}	Light naphtha	Light gas oil
H_2	3.93	1.56	1.17	1.00	0.63
CH_4	3.82	25.30	21.70	18.00	11.20
C_2H_2	0.43	0.64	0.78	0.95	0.47
C_2H_4	53.00	39.04	39.20	34.30	26.50
C_2H_6	35.00	3.94	3.02	3.80	3.40
C_3H_4	0.06	0.53	1.15	1.02	0.80
C_3H_6	0.89	11.34	15.34	14.10	13.40
C_3H_8	0.17	5.00	0.16	0.35	0.25
C_4's	1.59	5.39	9.77	8.35	8.80
C_5 +	1.11	6.86	7.13	13.96	19.10
fuel oil	0.00	0.40	0.58	4.17	15.45
Total	*100.00*	*100.00*	*100.00*	*100.00*	*100.00*

* data from a short residence time coil at 25 psia with typical severity

1.1.2 Potential locations for olefin recovery

In the 1970's and 1980's, the capacity of ethylene plants was between 500,000 t/yr and 700,000 t/yr, but technological advances combined with the economic advantages of scale have led to the building of larger and larger plants such that today a world-class ethylene plant can manufacture up to 2,000,000 t/yr. At this massive production rate, the capital and energy costs associated with the separation and purification of product gases are enormous. A block flowsheet of a front-end demethanizer ethylene plant is shown in Figure 1-4.

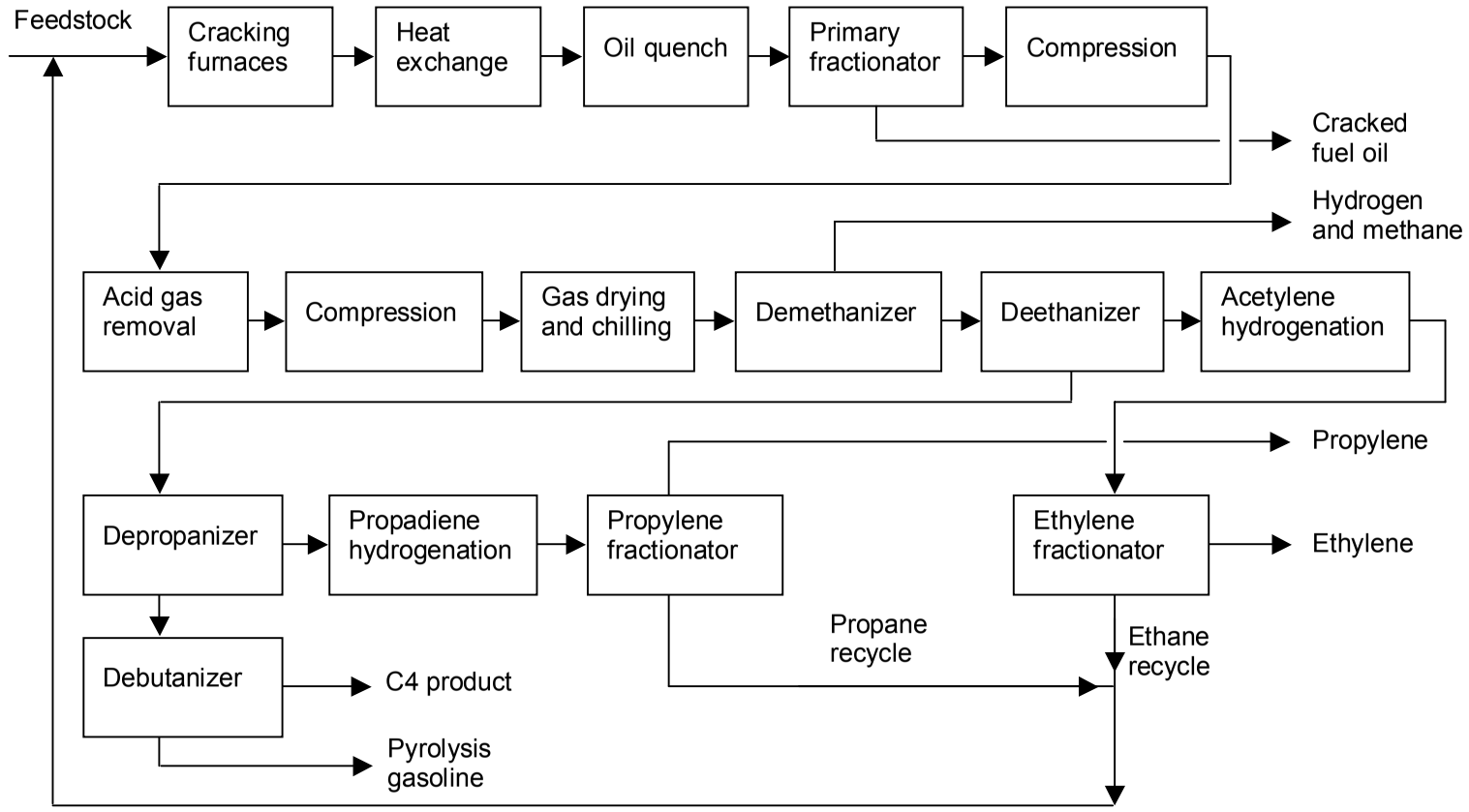

Figure 1-4. Ethylene plant separation scheme (from [33])

The feed stream into the ethylene fractionator in Figure 1-4 has been highly purified by the preceding steps. Since numerous separations must occur before this point, the most cost-saving location for an alternative recovery process is as close to the reaction section as possible; however, trace impurities such as acetylenes, carbon dioxide, hydrogen, and sulfur compounds that are removed in the separation train have adverse effects on nearly all reactive olefin absorption solutions. Because the use of an alternative ethylene-ethane separation process still requires the removal of these components, the target location for ethylene recovery in an ethylene plant is the C_2 splitter. From Table 1-1, the yields of ethylene and ethane produced from an ethane feed are 53wt% and 35wt%, respectively, but none of the other feeds exceed 4wt% ethane in the product. Since the olefin-paraffin stream composition can vary widely depending on the feedstock to the cracking furnaces, a novel separation process must be flexible enough to handle a relatively wide range of ethylene to ethane ratios.

While the ethylene-ethane cryogenic tower handles the bulk of the ethylene-ethane separations, other potential locations are more attractive for the initial application of the alternative process. Locations with a small-scale ethylene-ethane stream that do not deliver enough economic benefit to construct an entire cryogenic unit are more suited for an alternative separation technique. For example, mixtures of light olefins and paraffins produced in the petroleum refining process are often used as fuel because the quantity produced does not justify the cost of recovery by distillation. Other locations include purge streams from polyolefin processes and vent streams from polymer storage facilities. These streams are typically flared, which not only results in a loss of potential value, but also leads to environmental contamination [27]. Federal environmental regulations like the Clean Air Act require the reduction of volatile organic compound emissions by means of responsible accounting for all released pollutants. Moreover, facilities in nonattainment areas can no longer afford the use of flare systems for the destruction of small-volume

hydrocarbon streams because non-compliance can result in heavy penalties from both state and federal agencies [33]. Recovery of ethylene from these small-volume streams would be the best initial application of an alternative process. After successful implementation on a small-scale, the process could be scaled-up for use in an ethylene plant, but the conservative nature of the industry will make it difficult to readily replace the established cryogenic distillation process until the alternative has been firmly demonstrated.

1.2 Alternative separation processes

Due to the high operating and capital costs associated with traditional distillation, many alternatives have been investigated. Some of the main techniques described by Eldridge [27] are extractive distillation, absorption, adsorption, and membranes. Extractive distillation has proven useful for purifying C4's and heavier olefin-paraffin streams; however, the vapor stream still requires condensation – a significant drawback for light olefin/paraffin streams. For ethylene/ethane separations, this would still require high pressures and refrigeration to condense the vapor effluent. If the condensation step is precluded, the process becomes absorption, and the absorbing solvent can either function by physical or reactive means. Reactive absorption solvents are generally preferred over physical absorption solvents due to higher capacities and selectivities. Physical solvents, while possessing lower energy requirements for regeneration, have not yet provided the selectivities necessary for light olefin separations. Reactive solvents possess the most attractive characteristics of the gas-liquid processes; therefore, they are the focus of this dissertation.

Solid based separation processes like physical and chemical adsorption have also been the subject of significant research efforts. By using size selective molecular sieves, some degree of olefin-paraffin separation has been demonstrated for purely physical adsorbents [22]. Like in absorption, chemical adsorbents generally have a much higher capacity and selectivity for olefins. Section 2.3.1 will discuss the state

of the present art of chemical adsorbents in more detail. The use of membranes for olefin-paraffin separations is another quickly advancing field. While most of the literature is concerned with transition metal-based facilitated transport membranes (see section 2.3.2), size selective membranes for olefin-paraffin separations have also been studied and found to exhibit good olefin selectivity [8].

1.3 Olefin π-complexation with transition metals

All of the chemical-based processes mentioned above have the common feature of a transition metal used to selectively bind the olefin. Paraffins do not react with the metal ion, and in many cases the presence of the metal serves to reduce the paraffin's affinity for the separating media (liquid, solid, or membrane). From a practical standpoint, only silver and copper metals are reversible and inexpensive enough to consider using as separating agents. While the knowledge of the reactive behavior of these metals with olefins is not new, commercialization of these chemical processes has encountered many difficulties (primarily metal stability). This has left π-complexation to metals as a seldom-employed technology with a relatively long history of academic and industrial research.

1.3.1 Historical context

The evidence of a chemical interaction between transition metals and olefins has been known since the discovery of a platinum-ethylene complex by Zeise in 1827 [75]. In the 20th century, Berthelot was the first to observe that ethylene was absorbed by hydrochloric acid solutions of cuprous chloride [40]. The first known pilot scale demonstration of metal complexation for olefin recovery was performed by Horsley in the 1920's by using concentrated $AgNO_3$ to bind ethylene [47]. During the 1930's and 1940's, the patent and published literature reveals a plethora of olefin absorption data using liquid solutions or solid salts of either silver or copper to purify olefins [34][57][89][117]. While these pioneering works were not lacking in

experimental proof, a firm explanation of π-complexation theory was not provided until Dewar in 1951 [24]. By describing the interactions between the metal and olefin in terms of the donor-acceptor behavior of the respective atomic and molecular orbitals, Dewar set the framework for Chatt and Duncanson to schematically show the bonding nature of a hybridized platinum(II)-ethylene complex [13].

Meanwhile in the early 1950's olefin-transition metal complexes were first employed to produce stereoregular polymers. These Ziegler-Natta (ZN) catalysts containing transition metals such as titanium were a revolutionary discovery for ethylene and propylene polymerization because they allowed for much more control of molecular weight and tacticity than previous catalysts [86]. It is generally believed that the mechanism for the extremely fast polymerization reactions from ZN catalysts includes a π-complex between the metal and the olefin as an intermediate transition state for initiation and monomer addition. This mechanistic view proposed by Cossee and Arlman [18] has been supported by recent theoretical and experimental studies for both traditional ZN catalysts and novel metallocene-type catalysts [17][85].

Not only do π-complexes play an important role in separations and polymerization catalysis, but they are also the subject of considerable research in the field of biology. Ethylene is known to be "a plant hormone that causes seeds to sprout, flowers to bloom, fruit to ripen and fall off, and leaves and petals to shrivel and turn brown" [80]. Investigation of the role of copper(I) as an ethylene receptor site in plants has widened the understanding of many phases of plant development [108]. Biological systems also employ copper(I) for oxygen binding and transport via the proteins hemocyanin and tyrosinase in order to catalyze important reactions with biological substrates [98]. Another application of π-complexes is in photocatalysis and in the conversion and storage of solar energy where copper-olefin complexes were shown to undergo free radical transformations [31].

Certainly the research of olefin-metal π-complexes has a history of broad applications of which ethylene-ethane separations still plays an active part.

1.3.2 Focus of present research

While π-complexes with olefins have been shown to exist for Ag(I), Cu(I), Pd(II), Hg(II), Pt(II), and others, not all of these metals are practical for use in absorption applications [40]. This research focused on copper(I) complexes because they are comparatively more inexpensive, more easily reversible, and more stable than the other metals. Only non-aqueous solutions of copper(I) were studied for two reasons. First, cuprous salts generally have very poor solubility and stability in aqueous systems, so high capacity solutions are difficult to prepare. Second, volatilized water in the olefin stream must be removed prior to introduction into the polymerization reactor [27]. Even if preparation of a stable, high-copper(I) content aqueous solution were possible, the removal of water from the purified olefin stream would necessitate an additional drying step that would diminish the economic advantages of the reactive absorption process. As a result of the decision to use organic solvents, a decrease in olefin/paraffin absorption selectivity occurs because of the higher physical absorption capacity of organic solvents. This effect is more pronounced with higher molecular weight olefin/paraffin systems (e.g. the propylene/propane system would suffer from a lower selectivity than the ethylene/ethane system); therefore, in an effort to minimize the physical effects from the organic solvent, this research only examined the ethylene/ethane separation. A review of the applicable literature concerned with π-complexes for olefin/paraffin separation not limited to non-aqueous copper(I) for ethylene/ethane separation is given in Chapter 2.

In this work, the discussion is not limited to the choice of an appropriate reactive absorption solution, but considerable attention is given to the characteristics of the interaction between an ethylene-ethane mixture and the reactive absorption

solution. The absorption equilibrium and kinetics of the metal-olefin interaction are discussed, and models are developed that show a good fit to the acquired experimental data. In addition to the equilibrium and kinetic fundamentals, a continuous absorption/regeneration process was designed to test the separating ability and robustness of the reactive absorption solution. The results from the operation of this equipment are discussed along with several insights for an improved larger scale design of the process.

Chapter 2.
Literature Review

2.1 Olefin π-complexation theory and observations

In order to identify an effective olefin complexation system, many aspects of the transition metal must be considered. First, a thorough understanding of the nature of the π-complex bond is essential to predicting the interactions of the metal system and the olefin. The olefin complexing ability is dependent on the electronic interactions of the entire system; therefore, the choice of transition metal, anion, coordinating ligand, and physical state will each affect the olefin bond stability. In considering the different contributions to metal-olefin stability, it is important to look for those qualities that will lead to an optimized absorption system. Important qualities include a high capacity for ethylene, fast complexation kinetics, ease of reversibility (i.e. low heat of absorption), and stability to time and impurities (esp. reduction/oxidation reactions) [91].

The olefin complexing solution of choice for this research comprised of cuprous chloride coordinated by aniline ligands using either N,N-dimethylformamide or N-methyl-2-pyrrolidone as a solvent. Although the published literature does not contain any reference to this specific system, prior unpublished research at The University of Texas at Austin presented in section 2.4.1 supports this system over numerous other metal salt-ligand pairs. In addition, this chemical system is comprised of relatively inexpensive starting materials that are commercially available in bulk quantity as shown in section 5.1. By examining the literature for other olefin complexing systems across the various research fields, insight can be gained from discussion of the nature of the π-complex bond, anions and ligands used for metal coordination, and stability of the copper(I) ion.

2.1.1 Nature of the π-complex bond

The essence of the π-complex bond between an olefin and a transition metal as first described by Dewar consisted of a σ component and a π component representing contributions from each species [24]. The schematic description of the metal-olefin complex developed by Chatt and Duncanson shown in Figure 2-1 laid the framework for our basic understanding of metal-olefin interactions [13]. The σ component of the bond is due to overlap of the π electrons from the olefin double bond and the vacant outermost *s* orbital of the metal. For the case of Cu(I) or Ag(I), the outermost *s* orbital is empty because the single electron has been lost from ionization to the +1 valence state. This is usually as a result of an electronegative anion that removes the solitary electron to fill its outer shell (e.g. CuCl in solution ionizes to Cu^{+1} and Cl^{-1} because the chloride ion has a high electronegativity due to its outer shell lacking just one electron). For nonionizing metal species or crystal structures, the metal is bound to an electron-withdrawing group that substantially pulls the charge from the metal resulting in a partial positive charge equivalent to an empty outer *s* orbital [91]. The π component of the bond is due to overlap of the metal's filled *d* orbital and the olefin's empty π antibonding (i.e. π*) orbital. For the case of the platinum complex mentioned above, the π component of the bond is strengthened by hybridization of the filled *d* orbital with the empty outer *p* orbital to provide more overlap with the olefin's π* orbital [13].

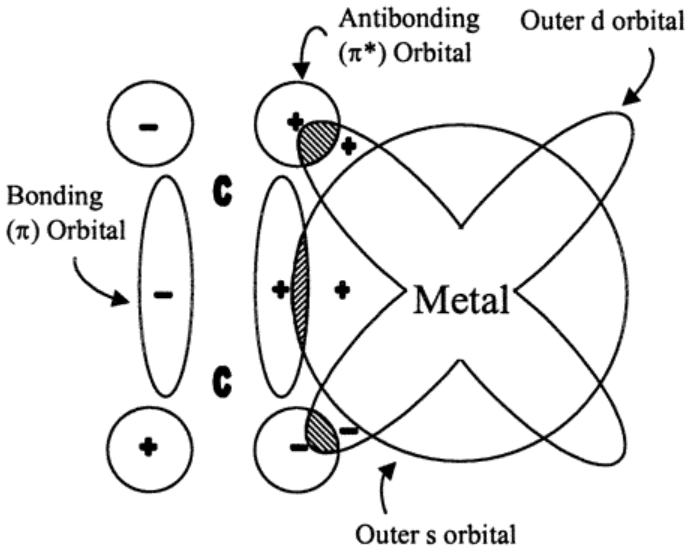

Figure 2-1. Dewar-Chatt model of metal-olefin π-complex (from [91])

The question of whether the σ component or the π component contributes more to the bond has been a topic of debate for some time. Hartley [39] first divided metal-olefin complexes into two classes, class S and class T, with the major difference being the extent of π back-donation from the metal. Class T compounds were identified as those with a greater π component (e.g. $[(Ph_3P)_2Pt(C_2H_4)]$) while class S compounds have a greater σ component (e.g. $[Pt(C_2H_4)Cl_3]^-$). Unfortunately, Hartley's classification system did not gain much popularity, and it has seldom been used in the literature. While Hartley's review was based mostly on experimental results, many authors have performed theoretical studies on the metal-olefin bonding. Ziegler and Rauk [122] performed a Hartree-Fock-Slater calculation on Cu^+, Ag^+, and Au^+ complexes with ethylene and found that the π component of the bond was more important for the Cu^+-C_2H_4 complex, but the σ component was the dominant factor in the Ag^+-C_2H_4 and Au^+-C_2H_4 complexes. This conclusion was rejected by Kelber et al. [60] who stated that the degree of π-backbonding in Cu^+-C_2H_4 complexes was negligible compared to the σ-bonding (ligand to metal charge donation). They claim

to have used a more accurate basis set than Ziegler and Rauk to explain the difference in their results. Kelber et al. support their conclusion with ultraviolet absorption and emission spectra of a solution of CuCl and polystyrene by showing that the excitation is due to ligand-to-metal rather than metal-to-ligand charge transfer.

A study by Chen and Yang [16] looked at the adsorption of ethylene onto $AgSO_3C_6H_5$, and the electron distributions were quantified into distinct molecular orbitals. For the metal-olefin complex bond, the contribution from σ donation accounts for 84% of the bond while the π component accounts for only 16%. This result was justified by examination of the highest occupied molecular orbital (HOMO) and lowest unoccupied molecular orbital (LUMO) of the two species. In general the smaller the gap between the HOMO and LUMO of two reacting species, the stronger the bond. For the σ component, which is donation from C_2H_4 to $AgSO_3C_6H_5$, the difference between the HOMO of the hydrocarbon and the LUMO of the adsorbent is 2.60 eV. For the π component, which is back-donation from $AgSO_3C_6H_5$ to C_2H_4, the difference between the HOMO of the adsorbent and the LUMO of the hydrocarbon is 4.29 eV. Since the σ component has a much smaller gap than the π component, they concluded that the majority of the π-complex bond is due to the donation from the olefin to the metal.

In agreement with the previous results, Merchan et al. [76] showed by a pseudopotential ab initio molecular orbital study that the back-bonding was negligible compared to the σ-bonding for a Cu^+-C_2H_4 complex. They also went on to suggest that the hydrogen-carbon bonds in the olefin deform to give the bent structure shown in Figure 2-2. Using a natural bond orbital calculation, Huang and coworkers [50] also found the optimized geometry of AgCl-C_2H_4 and CuCl-C_2H_4 complexes to have bending in the C-H bonds of 2.60º and 2.74º, respectively.

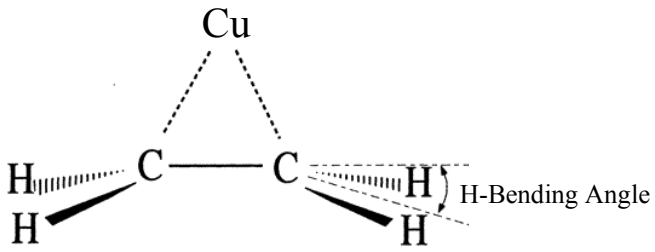

Figure 2-2. Proposed bent structure of Cu^{+}-C_2H_4 complex (from [50])

Huang et al. also reported that CuCl formed stronger olefin complexes than AgCl because the presence of the halide gave a partial positive charge on the copper of 0.644 versus 0.625 on the silver. The metal with a higher positive charge attracts more electrons from the olefin so that the σ donation from the olefin to the vacant *s* orbital is greater for Cu^{+}. The stronger σ donation leads to a shorter complex bond which in turn increases the overlap of the metal's *d* orbitals with the olefin's π^{*} orbitals giving a stronger π donation as well. In regards to the relative strengths of donation and back-donation, the CuCl-C_2H_4 was found to show a slightly greater degree of back-donation than σ donation, and the AgCl-C_2H_4 was opposite with σ donation slightly more than π donation [50]. For the case of CuCl-C_2H_4, it has been reported elsewhere that the back-donation constitutes more than half the electronic interaction energy whereas it is relatively minor when the halide is absent in the calculations [7].

Examination of the literature certainly suggests that the nature of the π-bond is a complex function of the electronic configuration of the metal system. Whether σ donations or π donations make up the majority of the bond depends on the metal itself as well as whether the metal is bound to any other species like halides or ligands. A more in depth discussion of the effects of anions and ligands is given next.

2.1.2 Halide anions for metal coordination

It has been shown that one of main factors affecting the olefin binding properties of a metal solution is the counter-ion associated with the metal. For copper(I) solutions, halides are typically compared in terms of their stabilizing effect on the copper-olefin complex. The degree which the halide affects olefin complexation is directly related to its own interactions with the metal as a ligand. The hard and soft acid and base (HSAB) theory predicts that soft acids, which include class B metals Cu^{+}, Ag^{+}, and Pt^{2+}, will have stronger interactions with softer or more polarizable bases. Since the atoms in each group become progressively softer with increasing atomic weight, the implications are that the stability of metal-halide complexes should increase in the following order, F < Cl < Br << I [84]. Experimental studies reported by Hartley [39] have suggested that olefin complexes with the metals Ir^{+}, Ag^{+}, and Pt^{2+} are stronger when the metals are coordinated to softer ligands. For example, the platinum(II)-olefin bond was stronger when bromide was used as a ligand instead of chloride. As another example, the ethylene complexation reaction (2-1) was shown to exhibit a much higher equilibrium constant when the halide anion, A, was iodide over chloride [113]. These results suggest that heavier halides lead to stronger metal-olefin complexes; however, this is not always the case.

$$\left[\mathrm{IrA(CO)(Ph_3P)_2}\right] + \mathrm{C_2H_4} \leftrightarrow \left[\mathrm{(C_2H_4)IrA(CO)(Ph_3P)_2}\right] \qquad (2\text{-}1)$$

This trend as well as the HSAB theory predicted order of metal-halide stability has been disputed by a number of researchers. Studies on complexes of typical class B metals rhodium(I) and iridium(I) by infrared and visible spectroscopy have shown the order of halide preference to be F > Cl > Br > I [5][6][28]. An X-ray structural analysis of fluoro- and chloro-rhodium(I) complexes with ethylene indicated that the Rh-C bond lengths in the fluoro complex (2.096 Å) were shorter than the chloro complex (2.116 Å); therefore, the lighter fluoride compound showed a

stronger metal-olefin bond than the heavier chloride. The C-C distance in the complexed ethylene was also longer for the fluoro complex (1.380 Å) than the chloro complex (1.319 Å) which was attributed to more back-bonding from the metal to the olefin in the fluoro complex. The researchers concluded that the metal coordinated with fluoride was a better π donor than the metal coordinated with chloride [35].

Returning to copper(I) chemistry, the experimental data in the literature supports class B behavior for most cases. In a study on the binding equilibrium of carbon monoxide, Kitagawa and Munakata [64] found the equilibrium constants of reaction (2-2) increase in the order Cl < Br < I where X is the halide and L is a bipyridine structure and acetone is the solvent. The complex was only reactive when present in a binuclear structure due to reasons which will be discussed later.

$$\left[Cu^{I}XL\right]_2 + CO \leftrightarrow \left[Cu^{I}{}_2X_2L_2(CO)\right] \qquad (2\text{-}2)$$

The affinity for CO binding by the heavier halide-copper complexes is supposedly because the copper(I) atom becomes more positively charged in the chloro derivatives than the iodo compounds. The authors claim that the more electronegative chloride anion decreases the electron density on the copper(I) atom which promotes the dissociation of CO [64]. Interestingly, it was because of the higher charge on the copper(I) over silver(I) as a result of the chloride bond that led Huang et al. [50] to attribute stronger olefin-metal interactions to CuCl over AgCl as discussed above. Huang et al. also examined CO complexation by molecular orbital calculations and adsorption experiments and found it to be analogous to ethylene adsorption. In a complementary report, Huang et al. [49] compared halide effects on ethylene complexation with copper(I) and silver(I). An extensive study of the bond lengths is shown in Table 2-1 where the C-C bond length in free ethylene (1.3340 Å) is found to increase for all cases of metal complexation. As the size of the halide decreases from iodide to fluoride, the C-C bond length increases (from 1.3473 Å to 1.3489 Å for Cu) and the M-C bond length decreases (from 2.4281 Å to 2.3342 Å for

Cu). Since the σ donation from the olefin to the metal and the π back-donation from the metal to the olefin will both serve to weaken the C-C double bond, a higher degree of C-C bond elongation in Table 2-1 represents stronger olefin adsorption. They concluded that an anion with a higher electronegativity would pull more electrons from the metal, which would give the metal more positive charge to form stronger olefin bonds [49].

Table 2-1. Geometries of Adsorption for MX-C_2H_4 (from [49])

M	X	r(C-C)	r(M-C)
Cu	F	1.3489	2.3342
Cu	Cl	1.3485	2.3864
Cu	Br	1.3478	2.4035
Cu	I	1.3473	2.4281
Ag	F	1.3479	2.6176
Ag	Cl	1.3470	2.6367
Ag	Br	1.3466	2.6783
Ag	I	1.3462	2.6969
free C_2H_4		1.3340	

On the other hand, a different study supporting the class B behavior of copper(I) looked at the kinetic stability of copper(I)-halides to oxidation [94]. Lighter halides were found to give lower stability constants than heavier halides so that the halide affinity for copper(I) is F << Cl < Br < I. Due its softer nature, iodide gave a more covalent bond with copper(I) than the chloride. It was also stated that Ag(I) forms stronger complexes than Cu(I) because as a softer metal ion, it displays more class B character. Clearly there is a lack of universal agreement on the stability effects of halides on metal complexes. While theoretical molecular orbital studies and quite a few experimental results suggest that lighter halides should form stronger metal complexes, there are an equal number of published reports stating the opposite trend.

2.1.3 Other ligands for metal coordination

One of the reasons inspection of the coordinating ability of different transition metals and metal-halide complexes appears so ambiguous is that a blind comparison as such neglects the effects of coordination ligands, olefin substituents, and solvent effects. These three factors are responsible for much of the variation on the electronic properties of the metal-olefin bond across literature systems. The main sources of data that have been discussed so far are crystal structure analysis of a solid complex, spectroscopic analysis of dilute liquid solutions, and theoretical modeling of molecular orbitals. Attempting to compare trends in electronic binding between a molecular orbital study of a simple metal-halide-olefin system with an actual solution-phase experiment has led to poor agreement. The lack of consideration of the complicated interactions encountered including ligand exchange reactions and interacting solvent molecules could be the source of some of these discrepancies.

Coordinating ligands, defined as electron rich compounds that form a complex with the metal, are necessary to stabilize transition metals for olefin reactivity. In a strict sense, both halide anions and complexed olefins are ligands. In a liquid solution, the halide anion is generally viewed as remaining in a complexed state with the metal instead of completely dissociating into the solution, but for other anions, complex formation is seldom observed. For solids, the anion is an integral part of the crystal structure; therefore, it is usually regarded as having complexing interactions with the metal. Occasionally, the metal complex in solution is prepared by using olefins as ligands so that other stabilizing compounds are not required [119]; however, this approach has little practical importance for separations because the olefin must eventually be released from the metal in a regeneration step which would yield a very destabilized metal. When coordinating ligands are discussed, it is usually in the context of nitrogen-containing compounds because of their electron donating properties.

While the simplest amine, ammonia, has been used to coordinate copper, it is disfavored due to high volatility [57]. More commonly used structures are aromatics like pyridine (py). Symmetric, tetrahedral coordinated copper(I)-pyridine complexes $[Cu(py)_4]^+$ were given by Lewin et al. [71] by X-ray crystallography. Tetra-coordinated copper(I)-pyridine complexes were also shown by Chen and Iwamoto [15] using polarography and infrared spectroscopy. Using propylene carbonate as a solvent for the electrochemistry experiments, they went on to show that aniline formed weaker complexes with copper(I) than pyridine due to a lower calculated equilibrium constant and a ligand coordination number of three for aniline. The anion in both of these studies was perchlorate, and it was not found to coordinate with the copper(I) atom. The copper(I)-pyridine system was also studied by Kitagawa and co-workers [65], except they found that when chloride was used instead of perchlorate, a different complex geometry resulted. In this new structure, two chlorides acting as ligands served to bridge the copper(I)-pyridine complexes as shown in Figure 2-3. Whereas the perchlorate structure $[Cu(py)_4]ClO_4$ was tetra-coordinated and unable to complex CO, the binuclear chloride bridged structure showed excellent binding with CO.

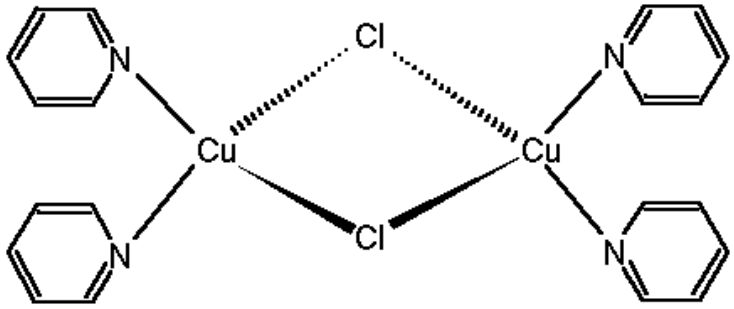

Figure 2-3. Binuclear structure of chloride bridged complex (from [65])

In a complementary study, Kitagawa and Munakata revealed that bonding of a similar chloride bridged copper(I)-bipyridine (bpy) complex to CO resulted in no

dissociation of either the bipyridine ligand or the chloride. The complex geometry was assumed to undergo distortion from a nearly tetrahedral shape around each copper(I) atom to a square-pyramidal configuration around the binding copper(I) as shown in Figure 2-4. In this study, the effect of using different solvents was also investigated, and it was determined that using ethanol instead of acetone led to a very stable mononuclear $[Cu(bpy)_2]Cl$ complex which lacked any reactivity towards CO complexation.

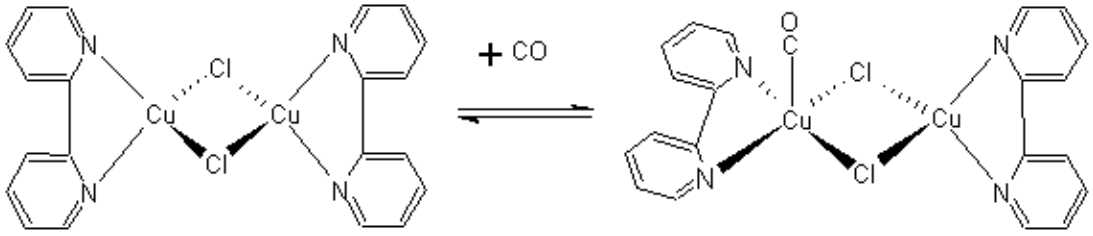

Figure 2-4. Geometrical change with CO addition (from [79])

Another example of a bridged halide species was given by Gil-Rubio et al. [35]. The $[\{Rh(\mu\text{-}F)(PPr^i_3)_2\}_2]$ complex (where Pr^i is an isopropyl group) was similar to Figure 2-3, but upon addition of ethylene, the bridge was ruptured at the fluoride linkages to give two nearly square planar *trans*-$[RhF(C_2H_4)(PPr^i_3)_2]$ complexes as shown in Figure 2-5.

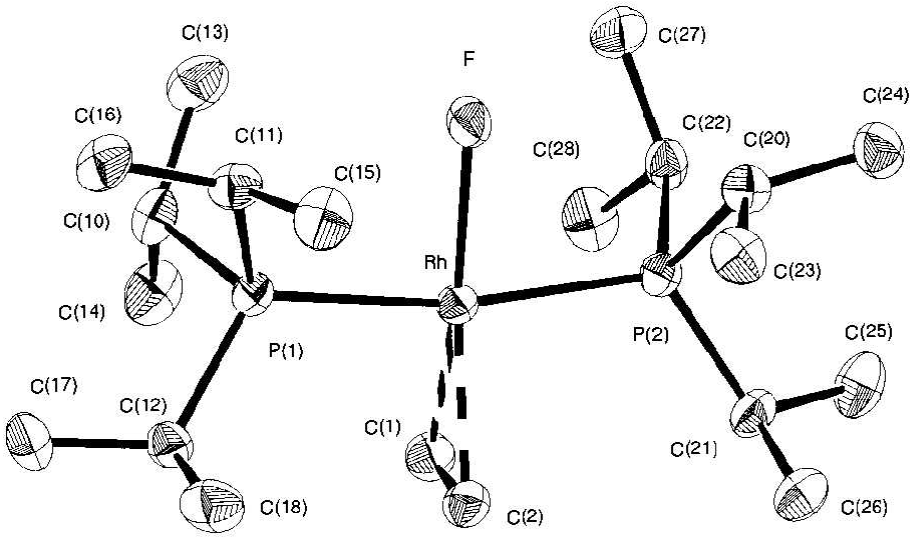

Figure 2-5. Structure of *trans*-[$RhF(C_2H_4)(PPr^i_3)_2$] (from [35])

While it has been shown that ethylene (and CO) complexation reactions can occur by addition and rearrangement of the complex to a new geometry, it is also common for the olefin to replace a ligand (L) already occupying a coordination site on the metal (M). Reaction (2-3) is called a ligand exchange or substitution reaction where the coordination number of olefin is *x* and those of the ligand before and after olefin complexation are *p* and *p-y*, respectively.

$$\left[ML_p\right] + x(\text{olefin}) \leftrightarrow \left[ML_{p\text{-}y}(\text{olefin})_x\right] + y\text{L} \tag{2-3}$$

$$K_{eq} = \frac{\left[ML_{p\text{-}y}(\text{olefin})_x\right][\text{L}]^y}{\left[ML_p\right][\text{olefin}]^x} \tag{2-4}$$

Equilibrium constants defined by (2-4) for the ligand substitution reaction were reported by Hartley [39] for Rh(I), Ni(0), Pd(II), Pt(0), Pt(II), and Cu(I). It is also possible for the solvent to interact with the metal and form weak complexes that will affect the olefin complexation equilibrium. Acetonitrile as a co-solvent with ethanol has been found to behave as a ligand such that higher concentrations of acetonitrile yielded lower values for the equilibrium constant [80]. Essentially, the

olefin was not able to displace the solvent ligand as easily at higher concentrations; therefore, the value of *y* in equation (2-4) was not a constant. When the ligand coordination number is not constant at different concentrations, the system is said to exhibit a strong ligand concentration effect meaning that higher concentrations of the ligand inhibit the olefin complexation reaction more than would be expected.

As far as the effect of the coordinating ligand on olefin complexation, it has been found that the basicity of the ligand strongly influences the olefin-metal complex. Munakata et al. [80] showed that the equilibrium constant for the olefin complexation addition reaction increases linearly with increasing pK_a of different derivatives of 2,2'-bipyridine and 1,10-phenanthroline (pK_a = 4.10-6.58). Continuing this idea, Suenaga et al. [100] compared the binding for tetramethylethylenediamine (tmen) (see Figure 2-6) with that observed from the aromatic N-ligands from the previous study. The higher basicity of the aliphatic N-ligand (pK_{a1} = 9.15, pK_{a2} = 5.91) correlated with larger ^{1}H NMR shifts of the olefinic protons. The researchers indicate that the σ donation from the tmen nitrogens is enhanced as the basicity increases and as a result the copper(I) can participate in more π back-bonding with the olefin. On the other hand, the aromatic nitrogens experience more π bonding with the copper(I), so the copper(I)-ethylene bond has less π back-bonding nature. Kamau and Jordan [58] note, however, that ^{1}H shifts are difficult to interpret in terms of the relative importance of the σ- and π-donation strengths.

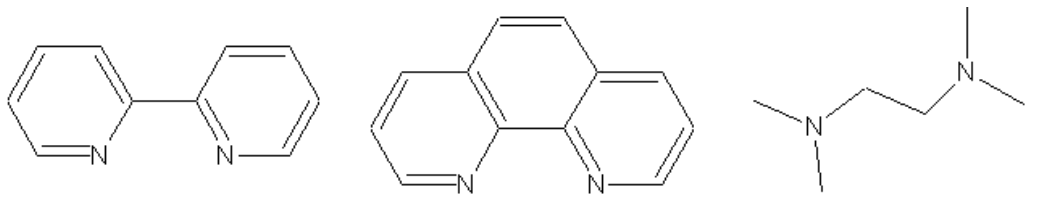

Figure 2-6. Structure of ligands for basicity trend (from [80][100])

The literature seems to dispute whether π interactions in copper(I)-olefin complexes are more important than σ interactions. An observation that is often used to support the π interaction hypothesis is that electron-withdrawing substituents on the olefin serve to decrease the stability of the copper(I)-olefin complex [39]. This result was reached by Thompson et. al. [108] from an X-ray structural analysis of copper(I)-ethylene complexes which is also claimed to be observed by a decrease in biological activity relative to ethylene for olefins with electron-withdrawing groups. While nickel(0) has been reported to give more stable olefin complexes with electron-withdrawing groups and silver(I) has been shown to be more destabilized with electron-withdrawing groups [39][58], copper(I) has been shown to be amphoteric in nature [80]. Olefins having CH_3, CHO, $COCH_3$, or $COOCH_3$ as substituents groups gave destabilized copper(I)-olefin complexes as before, but olefins with OC_2H_5, $OCOCH_3$, CN, or Cl groups actually gave more stabilized copper(I)-olefin complexes. It was concluded that the bonding of copper(I) is intermediate between that of nickel(0) and silver(I) by exhibiting olefin complex stabilization by σ donation and π back-donation [80].

2.1.4 Copper(I) stability

A significant cause for concern in reactive absorption systems is metal stability. Copper solutions are especially vulnerable to losing chemical activity due to degradation reactions. While the cuprous ion is capable of forming π-complexes with ethylene, other valences of copper do not participate in complexation reactions with olefins [9]. The oxidation of copper(I) by molecular oxygen is the most common means of copper degradation. Many copper(I) systems in the literature have admitted stability problems when exposed to air [21][25][31]. The reaction is usually very fast and can proceed through a number of intermediate structures as shown in Figure 2-7 [59]. Addition of dioxygen can be end-on or side-on, and the 1:1 Cu/O_2

(superoxo) is usually a precursor to the more stable 2:1 Cu/O_2 (peroxo) complex. While the structure of the oxidized complex can vary depending on the coordinating ligand, most copper(I) complexes with nitrogen-based ligands form the side-on binuclear copper geometry when oxidized [98].

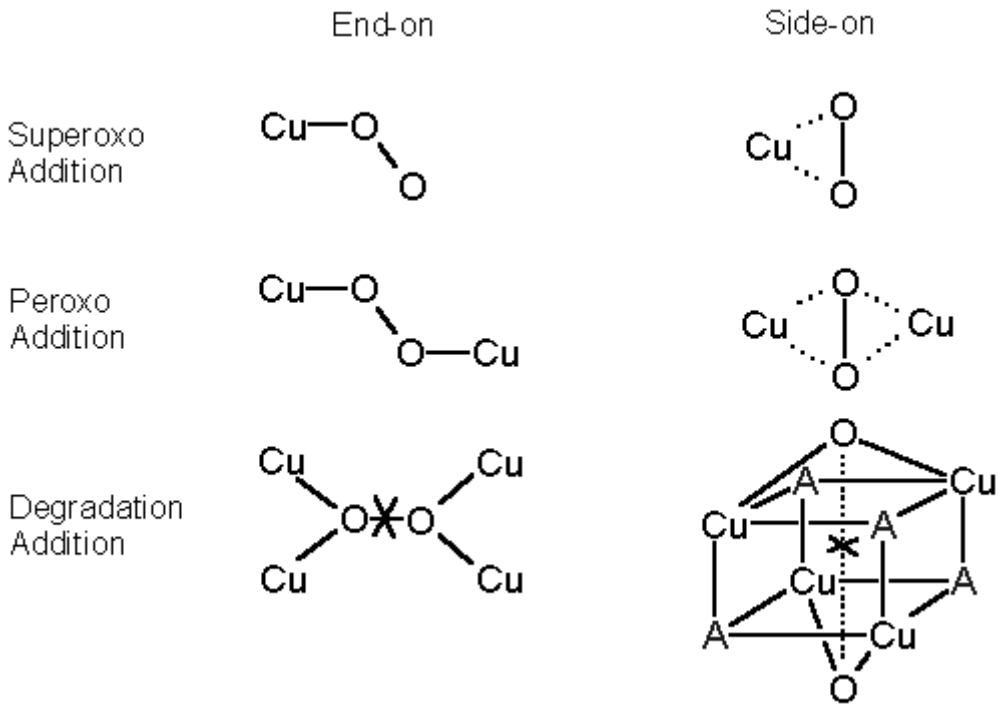

Figure 2-7. Copper(I)/dioxygen intermediates (ligands not shown) (from [59][10])

Reactions that lead to structures as those in Figure 2-7 are usually reversible; however, if not stabilized by proper ligands, these intermediate structures will usually undergo further addition of copper(I) followed by a cleavage of the O-O bond. The overall oxidation reaction (2-5) is the most common means of oxidative degradation of copper(I) complexes [92]. As suggested in Figure 2-7, the product of the degradation addition will be either two mono-oxygen cupric complexes or a cage-like cupric structure.

$$4\left[L_x Cu^{I}\right] + O_2 \rightarrow 2\left[L_{x\text{-}y} Cu^{II}_2 O\right] \quad or \quad \left[L_{x\text{-}y} Cu^{II}_4 (O)_2\right] + yL \tag{2-5}$$

In order to prevent oxidation, an inert atmosphere should be maintained at all times when handling copper(I) complexes. If oxidation (or reduction) should occur, for some systems the process has been shown to be reversible upon treatment with the appropriate agent. An industrial patent issued to Haase [38] addresses maintaining the stability of cuprous solutions. The Haase system consists of CuCl with an amine ligand such as benzylamine or 2-methylpentamethylenediamine that may or may not include an additional solvent. The proposed method to control the oxidation state of the copper ion relies on visual color detection. The particular system has an amber color in the preferred cuprous state, a greenish color when excessive cupric ions are present, and a reddish haze when excessive metallic copper is present. By contacting the copper solution with carbon monoxide when in the oxidized case and oxygen when in the reduced case, the process operator should be able to maintain the solution in the cuprous state by visually testing to decide whether the solution needs reduction or oxidization. By using high basicity amines to form strong complexes with copper(I), a high degree of reversibility of the oxidation (and reduction) reactions is realized. Exposure to oxygen is not disastrous to copper(I) complexes because the complex is so stabilized that permanent oxidation degradation reactions do not occur.

Another specific application of treating with specific reducing or oxidizing gases to maintain metal valence state is discussed by Jayaraman et al. [56] for Ag^{+}-exchanged Y zeolite. The ethylene adsorption capacity of the zeolite was first measured before treatment. To show the reversibility of the redox behavior of the silver(I) system, the adsorbent was contacted with hydrogen gas to reduce the silver(I) to its metallic form. Consequently, a significant decrease in ethylene complexation capacity was observed. Next, the adsorbent was treated with oxygen to restore the reactive Ag(I) state. The ethylene adsorption capacity for the oxygen treated adsorbent was 85% of the fresh state showing nearly complete recovery of complexation ability. These examples show that the redox properties of transition

metals can be reversible; however, maintaining stability in oxidizing or reducing environments can be a complicated task for copper(I) complexes.

Other than oxidation, disproportionation of the cuprous ion is a main cause of copper(I) instability problems. Disproportionation as shown in reaction (2-6) is when the cuprous ions exchange charge to form cupric ions and zerovalent copper metal. This is usually the result of improper solvent choice or coordinating ligands that do not provide enough stability [4]. Hirai et al. reported that the lack of alkyl groups on coordinating diamines led to complete and immediate disproportionation of CuCl in methanol [43].

$$2Cu^{+} \leftrightarrow Cu^{2+} + Cu(\text{solid metal}) \qquad (2\text{-}6)$$

The solvent and coordinating ligands play an important role in stabilizing the copper(I) ion such that Randles [88] observed that alcohol solvents with lower dielectric constants yielded better Cu(I) stability. In order to ensure the stability of Cu(I) complexes, Tyeklar et al. recommend the exclusive use of organonitrile solvents for the handling of Cu(I) complexes with tripodal tetradentate ligands [110]. As a means of stabilizing the cuprous ion, it is quite common to employ very large, polynuclear ligands as chelators to the central metal ion. While these ligands may provide excellent stability and protection from disproportionation and oxidation, they provide too much steric hindrance to approaching ethylene from the standpoint of a selecting a good absorption solution. The steric hindrance from the chelating molecules usually yields lower ethylene complexation equilibrium constants so that they are not practical for olefin absorption applications.

2.2 Practical applications of olefin complexation via absorption

Of all the practical applications of metal-olefin complexation systems, absorption is the most commonly studied approach. Of all reactive separation processes, absorption articles and patents have been cited over ten times more frequently than any other process (including reactive distillation, membranes, and

adsorption) from 1972 to 1997 [70]. The simplicity, availability, and scalability of gas-liquid contactors makes absorption an attractive separation technique. Examining the literature for olefin absorption shows that solutions of silver(I) and copper(I) salts receive nearly all the attention. There are a few important trade-offs to consider when comparing absorption systems. In general, higher olefin capacity is preferred because the more olefin absorbed per volume of solution, the lower the solution circulation rate that is required. More olefin capacity is realized by higher metal content in the solution, but the result of a higher metal loading is a higher solution viscosity that hinders mass transfer properties and causes pumping difficulties. Aqueous silver(I) solutions are more stable to oxidation than copper(I) systems, but the cost of silver is many times more than copper. Higher olefin/paraffin selectivity is a characteristic of aqueous systems, but water is easily volitilized in the regeneration step leading to wet olefin product streams. These trade-offs will be discussed in light of the observations of the significant research in silver and copper-based systems.

2.2.1 Silver-based systems

Aqueous silver nitrate is a common silver-based system which has a high metal solubility of up to 10 M concentration of silver(I). Early studies on silver nitrate systems to complex ethylene showed that the number of moles of ethylene absorbed per mole of silver(I), or absorption efficiency, decreases with increasing metal concentration [2]. For example, a 9 M silver nitrate system has a much higher capacity for ethylene than a similar 1 M silver nitrate system, but the absorption efficiency of the former is only 0.17 while it is 0.34 for the latter [19]. Baker [2] found that the addition of tetrafluoroboric acid (HBF_4) greatly increased the ethylene absorption capacity of a 2 M silver nitrate solution from an absorption efficiency of 0.28 to 0.58. Numerous metal tetrafluoroborate salts were shown to similarly increase the absorption efficiency of a 2 M $AgBF_4$ system. These effects were thought to be due to the hydration of the metal or hydrogen cations which lowers the

degree of hydration of the silver ion and facilitates olefin complexation. The use of nitric acid (HNO_3) only increased the efficiency of the 2 M silver nitrate from 0.28 to 0.32. Compared to the tetrafluoroborate ion, the nitrate anion associated strongly with the silver(I) ion which counterbalanced the presence of the highly hydrated hydrogen ion; therefore, the case with the added HNO_3 did not show the same degree of absorption benefit upon acid addition as the HBF_4 case [2]. While the addition of acid helped to shed light on the metal-anion-solvent interactions, practical application would further complicate the process by requiring an additional step to remove the acid. For example, acid removal would need to be performed stringently in ethylene oxide production in order to prevent poisoning of sensitive catalysts downstream [1].

Crookes and Woolf [19] extended the anion study to find that silver(I)-anion interactions decrease in the trend $NO_3^- > CF_3CO_2^- > ClO_4^- > BF_4^-$. Stronger interactions meant that the anion was more successful in competing with ethylene for the silver(I), but weaker anions showed little competition for the metal. As mentioned with $AgNO_3$ above, for some salts the absorption efficiency exhibited a negative concentration dependence (i.e. $Ag(MeSO_3)$ and $Ag(PhSO_3)$). Silver trifluoroacetate ($Ag(CF_3CO_2)$) ethylene absorption was nearly independent of metal concentration. Others salts actually showed a positive dependence (i.e. $AgClO_4$ and $AgBF_4$) on metal concentration such that higher metal loadings actually showed improved ethylene absorption per mole of metal. These results shown in Figure 2-8 suggest that silver(I)-anion and silver(I)-solvent interactions are quite important.

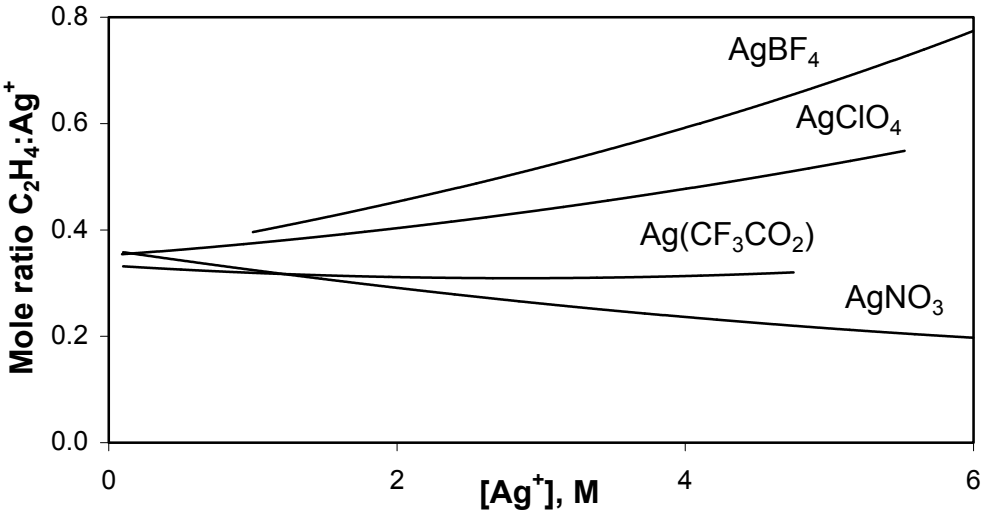

Figure 2-8. Absorption efficiency of silver(I) salt solutions (from [2][19])

Since these systems are in aqueous solution, the water molecules hydrate the silver(I) cation behaving as ligands. For the very weak anions, higher metal concentrations mean a lower overall water concentration, so ethylene has fewer water molecules to compete with to approach the silver(I); therefore, for weak anions, an increase in ethylene capacity was observed for higher metal concentrations. For the strong anions like nitrate, for example, the authors suggest that self-complexing of the silver nitrate occurs via linkages among nitrate groups, so the interactions between groups increase as the concentration of the groups increase [19].

A very thorough investigation of a silver nitrate system presenting both equilibrium data and pilot study results was given by Keller et al. [61]. Silver salt concentrations up to 8 M were studied, and the viscosity increased by over a factor of 2 going from pure water to the concentrated solution. This viscosity increase is relatively minor compared to the concentrated non-aqueous solution used in the present research. For the silver solution, it was noted that hydrogen sulfide (H_2S), hydrogen, and acetylene pose the greatest problems to the silver solution. Presence of H_2S was found to cause loss of silver by the formation of a metal sulfide, so a

conventional acid-gas unit was used upstream of the silver absorber. Hydrogen was found to gradually reduce the silver(I) to metallic silver, so hydrogen peroxide and nitric acid were added to stabilize the solution. Unfortunately, the presence of hydrogen peroxide was found to oxidize some ethylene to carbon monoxide and carbon dioxide, which showed up in trace amounts in the olefin product stream along with some oxygen from the H_2O_2 breakdown. These components may need to be removed from the olefin product by other processes downstream. The authors suggest copper oxide or metallic copper for CO and O_2 removal, caustic wash for CO_2 removal, and molecular sieves for water removal [61]. Acetylene was found to react irreversibly with silver(I) to form silver acetylide (Ag_2C_2) which has limited solubility and readily detonates under a shock. Not only does acetylene reduce the active silver(I) concentration, but it can present a significant safety hazard if allowed to accumulate. In order to limit the acetylene effects, a slip stream of the solution is treated with silver permanganate which oxidizes the acetylide complex freeing the silver(I) ion and producing carbon dioxide. The resulting manganese dioxide precipitates out of solution, and the slip stream is returned to the absorber feed stream.

Operation of the pilot plant with silver nitrate gave a 98% recovery of all ethylene fed to the absorber. The feed was a mixture of methane (37%), ethylene (36.5%), hydrogen (20%), ethane (5.6%), carbon monoxide (0.5%), and trace amounts of nitrogen, acetylene, and propylene. The absorber was a packed column operated at 240 psia and a mean temperature of 35ºC, and the desorber (stripper) was operated at 9 psia and 50ºC. Using only an absorber-stripper design proved to carry over too many components that were either physically absorbed or weakly complexed with silver(I) (i.e. carbon monoxide, ethane, methane, etc.). To overcome the absorption of these unwelcome components, a vent column was placed between the two primary columns as shown in Figure 2-9.

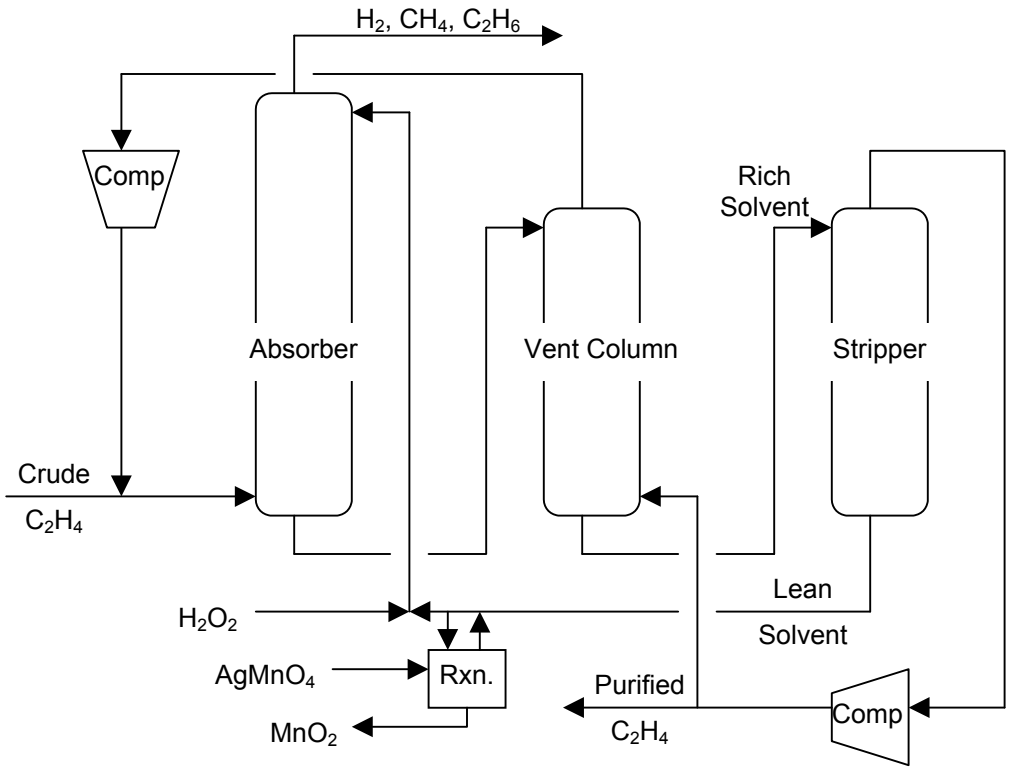

Figure 2-9. Pilot plant process using $AgNO_3$ (from [61])

The vent column was operated at a pressure slightly below the absorber, and a small fraction of the purified ethylene was fed into the bottom to strip the weakly absorbed components. Since the gas stream exiting the top of the vent column contains about 10% of the ethylene to the absorber feed, it is compressed and combined with the feed to the absorber for recovery. Clearly, design of an ethylene purification process using the silver nitrate solution was far more complicated than simply inserting a two-column absorber-stripper set-up. Additional processing details were required upstream, in the process, and downstream in order to successfully purify the olefin.

2.2.2 Copper-based systems

Copper(I) systems for olefin purification were recognized early as having the potential to serve as an alternative separation technique. In a patent filed in 1931, Watts [117] performed pilot scale work to show that ammoniacal cuprous salt solutions were capable of purifying a cracked pyrolysis gas stream to 95+% ethylene purity. By using a two-stage regeneration step, the non-olefin components were stripped first and recycled to the absorber (in a similar fashion to Figure 2-9), and the high purity olefins were recovered at a lower pressure from the second stage. Joshua and Stanley [57], however, were quick to point out in a patent issued in 1935 that such ammonia-based solutions suffer the disadvantage that large amounts of ammonia are lost in the regeneration of such solutions due to its high volatility. The use of alkylamines instead of ammonia was recommended, and the solutions were claimed to be stable in the absence of air and acetylenes. While the previous two examples were performed at 17 atm and 30 atm, Robey [90] claimed a cuprous solution that could effectively complex ethylene at much lower pressures by using a solution of pyridine, acetic acid, and cuprous oxide. In fact, the given ethylene solubility at atmospheric pressure was over four times larger than those reported previously. Robey also claimed that a system composed of pyridine, hydrochloric acid, and cuprous chloride would be stable enough to produce pure olefins in the presence of up to 0.1% acetylene. Ray [89] pointed out that the use of hydrochloric acid produces very corrosive environments for vessel metallurgy. A non-aqueous system of cuprous chloride in orthophenetidine was claimed to be able to absorb 0.4 moles of ethylene per mole of copper(I). A comparison of the different systems and their ethylene capacity is given in Table 2-2.

Table 2-2. Ethylene capacity at STP of literature systems

System	Ethylene Absorption L gas/L soln	Year	Ref.
NH_3, CH_2O_2 (formic acid), Cu^+, CO_2	3.0	1934	[117]
H2O, C_2H_7NO (MEA), CuCl, HCl	8.4*	1935	[57]
C_5H_5N (pyridine), $C_2H_4O_2$ (acetic acid), Cu_2O	17.5	1941	[90]
$C_8H_{11}NO$ (o-phenetidine), CuCl	26.4	1952	[89]
$C_2H_4O_2$ (acetic acid), $CuBF_4$	63.4	1970	[111]
C_7H_8 (toluene), $CuAlCl_4$	120	1971	[74]
$C_5H_{14}N_2$ (N,N,N'-trimethylethylene-diamine), CH_4O (methanol), CuCl	79.3	1989	[67]

*Given as L gas/kg soln (no soln density reported)

In 1968 Dunlop and Blytas [25] stated that exposure to water and air should be absolutely avoided to maintain solution stability for their chemical system of cuprous trifluoroacetate (CuTFA) in propionitrile. Instability of the cuprous ion leads either to oxidation to the cupric state (Cu(II)) or disproportionation to the cupric ion and metallic copper (Cu(0)) as mentioned earlier. The importance of maintaining the copper in the cuprous state is the loss of π-bond complexation ability, which leads to very poor olefin absorption and solid precipitates. The practice of adding ammonia or other amines to the solution to maintain copper(I) stability is claimed to be unsatisfactory because the amine-copper(I) complexes are so strong that they inhibit olefin complexation. The trifluoroacetate anion is a weak ligand compared to

ammonia or chloride; therefore, it is more easily replaced by olefins giving solutions with larger olefin capacity.

Due to the success of weak anions for olefin complexation, Uebele et al. [111] prepared $CuBF_4$ solutions and demonstrated selective ethylene removal from a mixed gas stream. Ethylene to copper(I) 1:1 stoichiometry was found for acetic acid solutions of up to 2 M $CuBF_4$. Cymbaluk et al. [20] prepared a similar system of copper(I) acetate in xylene and bubbled BF_3 through the system to form weak complexes with the copper(I). The ethylene to copper(I) stoichiometry of this system was reported as 2:1. Moving down one row in the periodic table, the use of $AlCl_4^-$ instead of BF_4^- with the solvent toluene was also found to give complexes with 2:1 stoichiometry [74]. With these complexes, ligand exchange reactions were shown to be able to separate complexible gases based on their complex strength. The order of decreasing complex strength is propylene > ethylene > acetylene > carbon monoxide. Note that for this system, acetylene does not irreversibly bind to copper(I), but it was shown to be displaced by contacting acetylene-complexed solutions with ethylene or propylene. The main drawback to $CuAlCl_4$ and $CuBF_4$ systems is that they have been observed to catalyze polymerization of the olefin and alkylation of the aromatic solvent by the olefin [46]. Due to such side reactions, these cuprous salts did not find immediate applications for olefin separation; however, Haase and Walker [36] implemented the $CuAlCl_4$-toluene solution for carbon monoxide absorption in what is called the COSORB process. The process is essentially the same as the one claimed by Long et al. [74], except the only complexible ligand allowed in the process gas stream (typically a synthesis gas stream from a natural gas plant) is carbon monoxide. The degree of alkylation and polymerization side reactions in olefin applications were later reduced by incorporating additives like pyridine-aluminum chloride to scavenge acidic compounds [37].

Horowitz and Tyler [46] employed CuTFA salts to primarily examine the use of different solvents for the copper system. Two main criteria that were set forth for

choosing an appropriate solvent were to maximize cuprous salt solubility and to have a low volatility to avoid solvent losses in the olefin decomplexing step (either increased temperature or decreased pressure). There was also a considerable effort to choose a salt-solvent system that minimized alkylation of the solvent and polymerization of the olefin. The patent called for the combination of a salt like CuTFA and an aromatic solvent that is a mixture of monoisopropyl biphenyl isomers. One of the main problems with this system was the high crystallization temperatures from 70 to 100ºC associated with these solutions.

Using nitrile solvents with CuTFA, Blytas [4] went on to show an important trade-off between olefin-paraffin selectivity versus olefin capacity as a function of pressure. Figure 2-10 shows that as the capacity for olefin absorption for a solution of CuTFA in propionitrile and xylene increases with increasing pressure, the selectivity of the solution for olefin decreases. The higher selectivity at a lower capacity suggests that chemical interactions, i.e. π-bonding, dominate at low loadings, but as the capacity of the system increases, physical solubility of the paraffin becomes more important. The trade-off observed is that higher equilibrium pressures give a higher olefin capacity at the expense of a decrease in olefin-paraffin selectivity. Also from Figure 2-10, a higher copper concentration is preferred since a much higher selectivity is realized for the 1 CuTFA/Xylene solution compared to the 0.67 CuTFA/Xylene solution especially at low loadings.

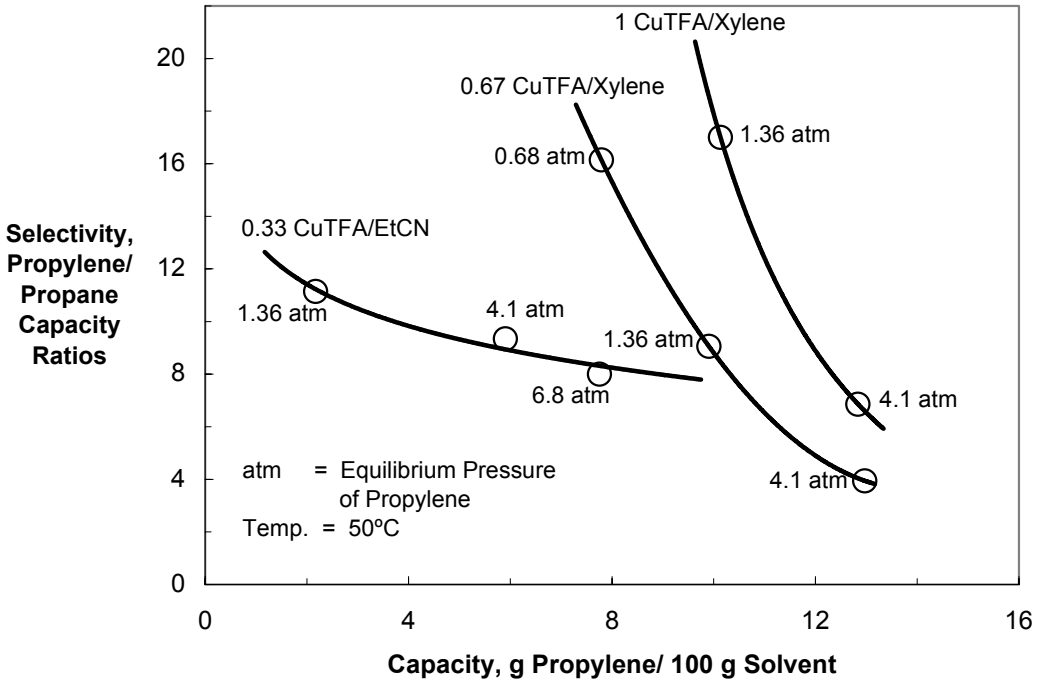

Figure 2-10. Propylene/propane system with CuTFA (from [4])

Blytas [4] also stated that the high cost of CuTFA salt reduces its attractiveness for large-scale separations. Solubility and absorption data were compared for some more attractive salts such as $CuNO_3$, Cu_2SO_4, and CuCl. CuCl was found to be the most soluble salt in propionitrile with solutions up to 40 wt% of copper(I), over double the solubility of any of the other salts. Ethylene absorption was found to be somewhat higher for the CuTFA over the $CuNO_3$ case. The sulfate system showed relatively poor ethylene uptake, and the chloride system was not compared directly. Generally, the cuprous salts of organic acids like TFA^- and acetate were observed to have higher olefin and paraffin absorption capacity, but those anions that do not have an organic nature like nitrate and chloride showed less capacity with higher olefin selectivity.

For most of the preceding work, propionitrile was the preferred solvent, but the use of propionitrile as a solvent is disfavored in ethylene/ethane separations due to its high volatility. Blytas was primarily concerned with higher olefins for use in extractive distillation applications where the solvent could provide boilup vapor (so that high solvent volatility is desirable) [4], but extractive distillation is not attractive for C_2 separations because refrigeration and high compression would be needed to reflux the light hydrocarbon. Furthermore, in order to remove propionitrile from the olefin stream, extraction with sulpholane is typically performed (because water produces an azeotropic mixture) thus complicating the process [83]. Alternative solvents that are sufficiently non-volatile, maintain copper(I) stability through ligand interactions, and allow easy displacement in the presence of olefins have been claimed in the form of N-alkyl substituted amides including N-methyl-2-pyrrolidone, which is the solvent of choice in the current research [83].

A copper solution described by Cymbaluk et al. [21] uses cuprous 2-ethyl hexanoate in the presence of a high molecular weight olefin like propylene tetramer or neodene in an aromatic solvent like xylene. One purpose of the high molecular weight olefin was to solubilize an olefin-complexing solution that existed as a slurry. Most likely, the high molecular weight olefin formed a weak complex with the cuprous ion in the same manner previously observed. Since the carboxylate anion resembles a saturated chain, it is likely that this system will experience a large amount paraffin solubility. The patent states the desire to have as much copper as possible in solution but not at the expense of a solution viscosity so great that pumping and fluid handling become difficult. An upper limit of tolerable viscosity was found for solutions of about 2 M copper(I) salt.

In one of the few academic journal articles on olefin-paraffin separation by reactive absorption, Ho et al. [45] present a copper based solution with data exhibiting high absorption capacities at low ethylene pressures. The absorption system comprised of cuprous hexafluoroacetylacetonate (diketonate) with α-methyl

styrene as a weakly complexing solvent. The weakly complexing solvent helped prevent disproportionation of the cuprous ion to maintain solution stability. The interaction between the copper(I) diketonate, solvent, and olefin are represented by Figure 2-11. The absorption of different olefins was measured in a stirred cell, and substituent groups on the olefin producing greater steric hindrance were found to display the least stable complexes as mentioned in section 2.1.3. In the same manner, the weakly complexing solvents were all α-olefins with varying degrees of substituent groups. The α-olefin with the least steric effect next to the double bond (i.e. 4,4-dimethyl-1-hexene) was found to display the poorest ethylene absorption, but the solvent α-methyl styrene showed the highest ethylene absorption because the phenyl group gave the largest steric effect. The preferred system showed an ethylene-ethane selectivity of about 17, but the salt is not commercially available which will lead to a higher solution cost.

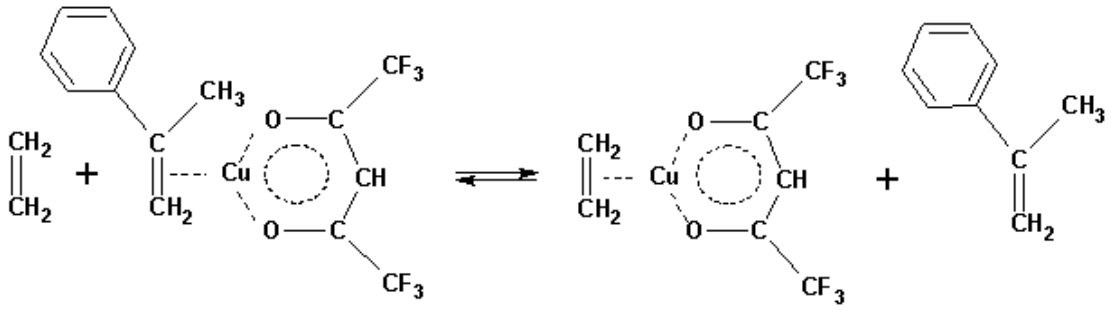

Figure 2-11. Ethylene complexation to cuprous diketonate (from [45])

An ethylene absorption study on CuCl with aliphatic diamines in methanol also compared the steric effects of coordinating species [43][67]. In this study, diamines with two ethyl groups on each nitrogen gave substantially lower ethylene absorption than diamines with two methyl groups. However, when the methyl groups were not present at all, the copper(I) was observed to experience significant disproportionation to metallic copper and a cupric state. For this case, the copper(I) is

stabilized by the chelating ability of the diamine like the case of the diketonate in Figure 2-11, but these ligands cannot be completely replaced or else the copper(I) is no longer stabilized. Some substituents on the nitrogen were required for stability, but excessive side groups inhibited the olefin's ability to approach the copper(I) center.

Figure 2-12 shows a comparison of the ethylene absorption equilibrium of some of the literature sources discussed. Note that the Cymbaluk et al. and Ho et al. systems are comprised of much more complicated anions and/or solvents than the other systems. Although these systems show maximum ethylene capacity at much lower pressures, they are much more costly to prepare than commercially available metal salts.

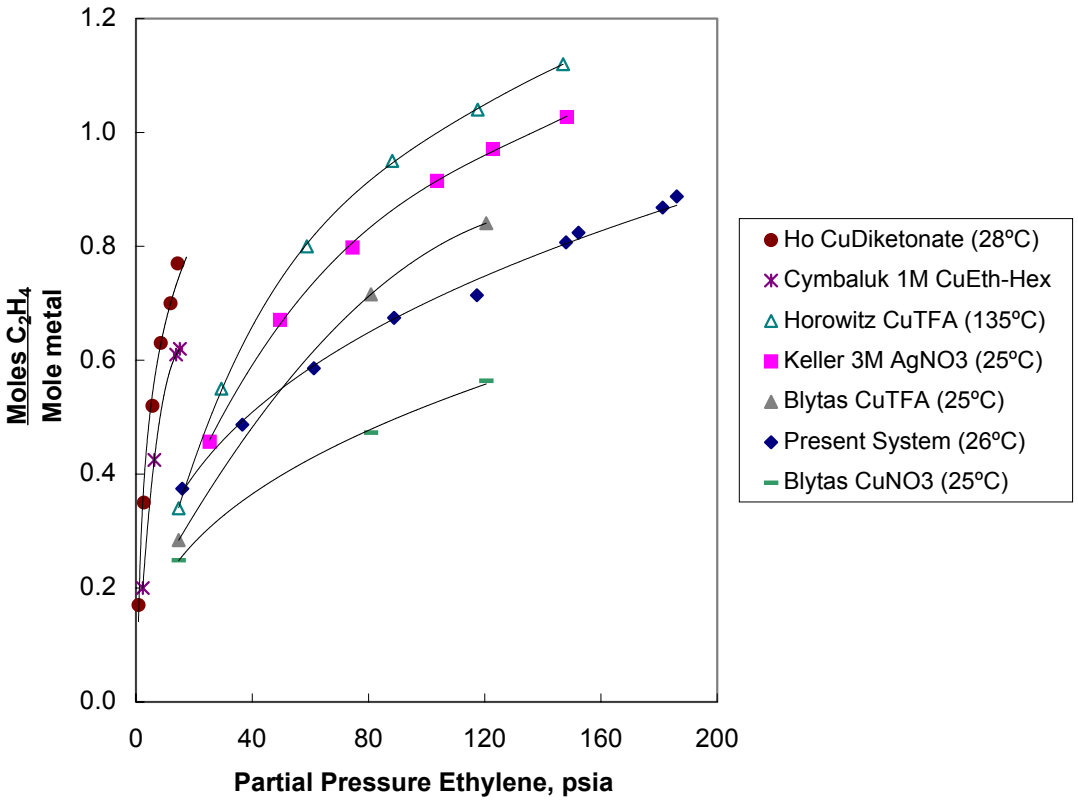

Figure 2-12. Equilibrium uptake of several documented systems

2.2.3 Summary of absorption systems

The primary areas of concern for copper and silver systems are capacity, stability, safety, and cost. Examples from both copper and silver-based systems have shown that a 1:1 ethylene-to-metal complex is the most common while in a few cases a 2:1 ratio was found. Aqueous silver solutions have been prepared with very high metal loadings at nominal increases in viscosity. For example, the viscosity of a 7.7 M $AgNO_3$ is only twice that for pure water [61]. Non-aqueous copper solutions have been found to increase in viscosity to a prohibitively high level at copper(I) concentrations of around 2 M [21]. Most copper-based systems are in non-aqueous solutions because hydrogen atoms have a high solvating power with respect to the cupric ion driving the disproportion reaction (2-6) to the right [83]. This usually results in very low copper(I) solubility unless a strong ligand or anion is used to stabilize the copper(I). To achieve substantial levels of copper(I) solubility, organic solvents are employed, but these usually suffer from higher degrees of paraffin solubility. The other cause of copper(I) instability, oxidation, was left unsolved in a each of the literature examples. Every case referred to preparation and storage of copper(I) solutions in an inert atmosphere, and none gave any indication of stability to oxidation. Unlike copper(I) systems where oxidation is a primary concern, with silver solutions reduction to metallic silver is a main problem especially if the olefin-paraffin feed has a significant amount of hydrogen or other reducing component. Both silver and copper suffer instability when exposed to impurities such as hydrogen sulfide and acetylene. Although specific examples were given where stability to these compounds was demonstrated, both metals can react irreversibly with impurities to produce insoluble and/or shock sensitive compounds. Finally, the main drawback of silver solutions is their high cost. Relative to copper, a silver solution may be as much as 60 times more expensive [91]. Both copper and silver have their advantages and disadvantages, but in light of their comparable ethylene capacity,

stability to impurities, and safety concerns, the deciding factor to further investigate copper systems for ethylene absorption was their low cost.

2.3 Other practical applications of olefin complexation

This section of the literature review continues the investigation of practical applications of metal complexes for olefin/paraffin separation. A brief overview of some of the key research in each specific field is presented with implications to the present research. The main areas of focus are solid adsorbents and facilitated transport membranes due to the bulk of existing literature, and some attention is also given to the electrochemically modulated system due to its novelty.

2.3.1 Solid systems for olefin adsorption

Historically, solid adsorption systems were first studied along the same time frame as liquid absorption systems, but they have not experienced the same breadth of research as their liquid counterparts. The important copper(I) adsorption research includes some early work with copper(I) salts and more recent studies using supported copper(I) covering industrial applications for adsorbents.

Some of the first research using solid salts for olefin complexation compared the stability of ethylene and propylene adsorption onto CuCl [34]. Both olefins were found to form 1:1 complexes with CuCl. There was very little difference between the equilibrium pressure curves of all olefins investigated (including isobutylene). Ethylene on CuBr was also studied and found to show a 1:1 complex ratio, but the complex was much less stable than CuCl. The preparation of the adsorbent included mixing the powdered cuprous salt with small mesh pumice. One of the drawbacks of this system was that the olefin-copper complexes were relatively unstable. None of the olefins formed complexes at ambient conditions, and only ethylene was stable enough to form complexes as room temperature (requiring a pressure of nearly 8 atm for CuCl and 50+ atm for CuBr). Long [75] has confirmed the 1:1 stoichiometry for

monoolefins and CuCl or CuBr complexes and shown that CuCl complexes are more stable than CuBr complexes. The main drawback to using CuCl salt is the lack adsorption capacity due to the low surface area of the salt.

One of first studies with experimental proof of the ethylene/ethane selectivity of copper(I) adsorbents was given by Hirai et al. [44]. Using copper(I) chloride and polystyrene resins having amino groups, they found the pure gas selectivity (defined as amount ethylene adsorbed to ethane) as 7.9 at high copper loadings. Without the copper(I) chloride, the ethylene selectivity on the polystyrene resin was only 0.79; therefore, the presence of the copper(I) chloride greatly improved the selectivity of the resin. While these resins showed high selectivity, they suffered from a low ethylene capacity like their predecessors. Higher ethylene adsorption capacity has been shown on Cu(I) Y zeolites [11][48]; however, these zeolite structures also exhibit a high capacity for paraffin reducing the ethylene selectivity of the separation. Preparation of an adsorbent that showed both high capacity and selectivity was shown by Yang and Kikkinides [121]. By dispersing a monolayer of CuCl on γ-Al_2O_3, a pure gas selectivity of over 8 was obtained with an ethylene capacity of 0.73 mmol/g which was over double the highest capacity previously reported in the literature. This capacity corresponded to a molar ratio C_2H_4/Cu^+ of 0.22, which the authors attributed to steric and energetic properties of the CuCl monolayer coverage on the activated alumina. This system proved to be very sensitive to oxygen with CuCl being converted to CuO upon exposure to even a small amount of air [73].

2.3.2 Membrane systems for olefin/paraffin separation

Membranes containing silver(I) or copper(I) salts can be used to separate olefin/paraffin mixtures. Facilitated transport through supported liquid membranes containing silver nitrate have demonstrated permeability ratios for ethylene over ethane as high as 1000 [106]. Teramoto et al. report that the selectivity is dependent on $AgNO_3$ concentration, which was observed to vary during the course of the

experiments due to evaporation of the water solvent. Thus, to maintain membrane stability, it was necessary to presaturate the feed gas with water; however, the issue of a wet olefin product stream that must be dried before processing still persisted. To overcome the membrane instability from drying, an alternative processing technique is to use a flowing liquid membrane. The process consists of continuously circulating the silver solution over the permeate side of the membrane to selectively pick up olefins and transporting the solution to a flash pot where the solution is degassed and recirculated back to the membrane module [109]. Nymeijer et al. [81] used a flowing liquid process with a hollow-fiber membrane with a hydrophilic polymer to achieve high selectivity and flux without drying out the membrane. The presence of silver nitrate served to reduce the physical solubility of both ethylene and ethane due to the salting-out effect while enhancing the facilitated transport of the olefin by silver complexation. They reported comparable flux productivities to previous work (~ $1x10^{-5}$ $cm^3/cm^2 \cdot s \cdot cmHg$) and an ethylene/ethane permeability selectivity of 165, which was independent of the liquid flow rate.

The main drawbacks of facilitated transport membranes for industrial applications have been given as (1) poor mechanical stability, (2) the difficulty in preparing thin, high-flux composite structures, (3) the need for a wet feed to maintain mobility of the olefin-selective carrier, (4) poor chemical stability due to carrier poisoning [78]. In an attempt to overcome the first three problems, many researchers have pursued solid reactive polymers that do not require a liquid solvent. One such successful attempt was given by Sungpet et al. [104] with their composite silver-form Nafion-poly(pyrrole). By using oxidized poly(pyrrole) polymer, the silver(I) ions were weakly coordinated so that ethylene complexes could form without the necessity of weakly coordinating water ligands. This hypothesis was backed by the observation that silver-form Nafion and proton-form Nafion-poly(pyrrole) membranes showed no evidence of ethylene complexation by FTIR spectroscopy, but the silver-form Nafion-poly(pyrrole) membranes showed a large shift in the C=C stretching frequency.

These novel membranes had an ethylene/ethane selectivity of about 15 and relatively low ethylene fluxes (~ $1x10^{-7}$ $cm^3/cm^2 \cdot s \cdot cmHg$).

Another work of particular interest to the present research is the study by Su et al. [99] using poly(*N*-vinylpyrrolidone) (PVP) and SiO_2 composite membranes with silver salt ($AgNO_3$, $AgClO_4$, or $AgBF_4$). Before the silver salt was added, IR spectra showed that the carbonyl group of the PVP hydrogen bonded to the silanol group as shown in the first reaction in Figure 2-13. Upon addition of $AgBF_4$, the carbonyl stretching shifted back considerably to its original position due to the formation of a weak complex between the silver(I) ions and the nitrogen atoms of PVP as shown in the second reaction in Figure 2-13.

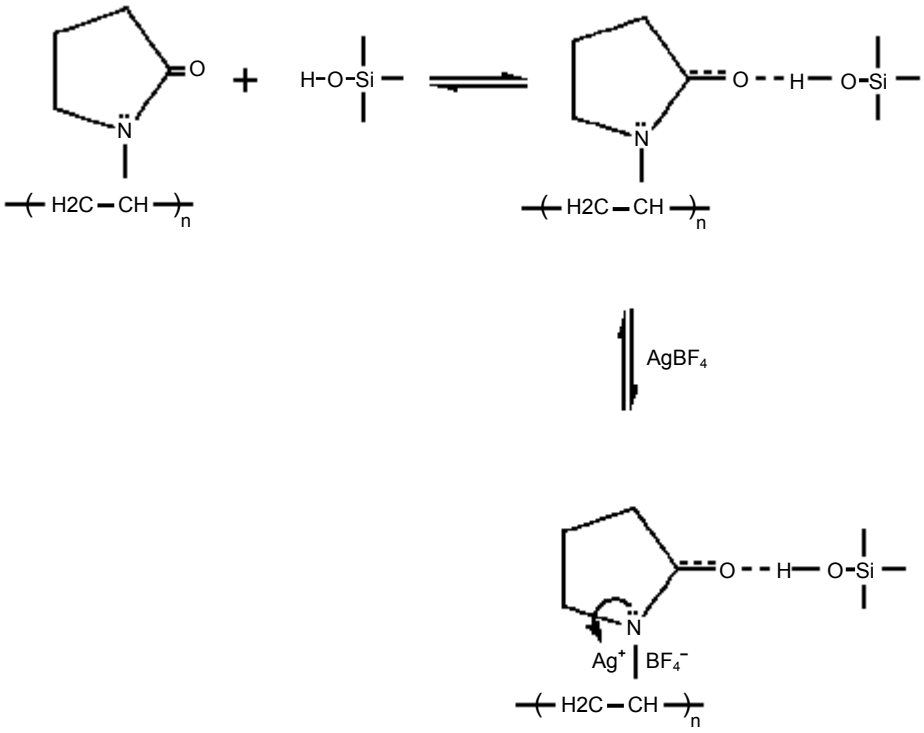

Figure 2-13. Interactions of SiO_2-PVP hybrid with $AgBF_4$ (from [99])

The authors suggested that "the free electron pair of nitrogen and the two electrons of the π-bond of carbonyl group in PVP are delocalized and shared by the three atoms of N, C and O" [99]. On the other hand, the perchlorate and nitrate salts did not show any back-shifting of the carbonyl group and showed poorer permeabilities to ethylene than the $AgBF_4$ case. The rationale for this observation of anion effect was tied to steric and electronic effects. A more thorough analysis of anion effects on olefin complexation was given by Sunderrajan et al. [102]. From a solution study of silver salts with 1-hexene, the highest olefin complexation from different anions was best characterized by larger anions with lower anion donor electron density. In general, stronger olefin-metal complexes are formed from anions that exhibit weak interactions with the metal ion, whether from steric effects due to large anion size or electronic effects due to weak donor-acceptor behavior.

The Su et al. [99] study was not the only one to demonstrate the superiority of the BF_4^- anion in comparison to others. For propylene/propane separation, $AgBF_4$ was found to outperform $AgCF_3SO_3$, $AgCF_3CO_3$, and $AgNO_3$ for olefin uptake [103]. In one of the few studies with solid polymer membranes containing cuprous salts, Kim et al. [63] found membranes prepared with BF_4^- to show much better olefin/paraffin separation performance than the anions ClO_4^- and $SO_3CF_3^-$. This study also used the polymer PVP to stabilize the copper(I) ions along with trimethyl phosphite ($P(OMe)_3$) to reduce the initial cupric salt to the active state. The ethylene/ethane selectivity was found to be dependent on the presence of both species exhibiting an optimum value of 7 with an average flux of $2x10^{-5}$ $cm^3/cm^2 \cdot s \cdot cmHg$. By applying the key findings from these membrane systems, a reactive absorption system should consist of an active metal ion with anions and ligands strong enough to prevent oxidation/disproportionation yet weak enough to allow facile complexation of the olefin.

2.4 Electrochemical applications of olefin complexation

A unique aspect of using metals for olefin/paraffin separations is that the electrochemical properties of the metal can be manipulated to change the interactions with the olefin. As noted earlier for copper systems, only copper(I) is active to π-complexation with olefins, and copper(II) and copper(0) show no binding activity to olefins. In an electrochemical process, electrons can be either added or removed from the system to tailor the valence state of the metal. Terry et al. [107] were the first to take advantage of the electrochemical properties of the metal and demonstrate a novel olefin/paraffin separation process. Since Cu(I) will selectively bind ethylene but Cu(II) does not, the process consisted of contacting a mixed ethylene/ethane stream with a Cu(I) solution via a hollow-fiber membrane then passing the solution through a porous carbon electrode to oxidize the metal to Cu(II). The oxidized copper will release the complexed ethylene, which is concentrated through contact with a second hollow-fiber membrane. After the gas is removed, the Cu(II) solution is passed through the other side of the electrochemical cell to reduce the metal back to Cu(I) completing the process loop as shown in Figure 2-14.

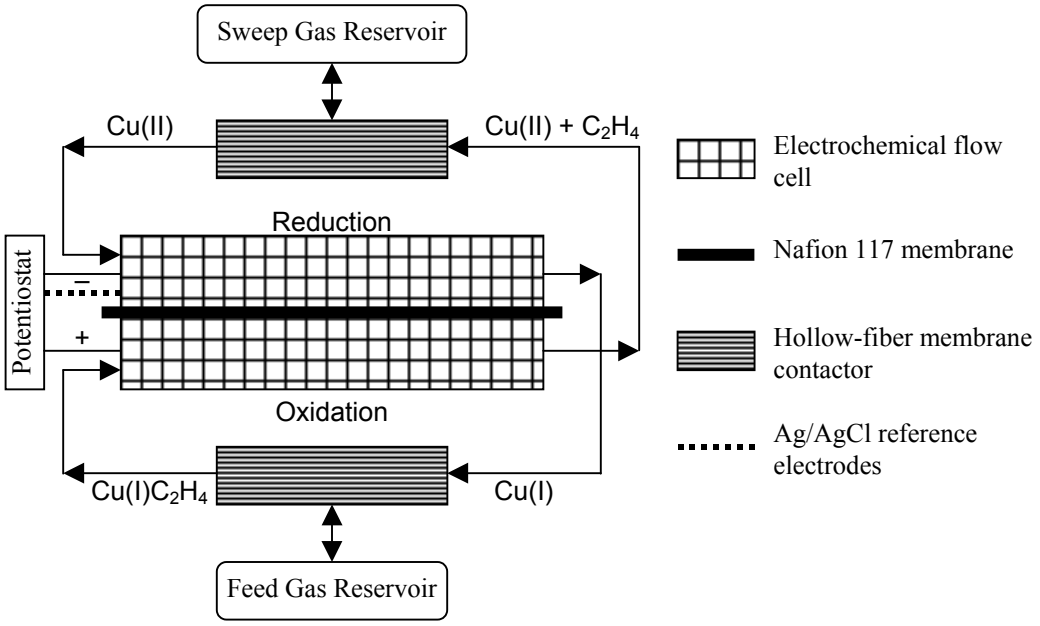

Figure 2-14. Electrochemically modulated complexation process (from [107])

For the experiments the feed gas was nearly 50%/50% ethylene/ethane that after two hours of operation produced a product gas of 99% ethylene purity. The copper concentration was relatively low (0.05 M) due to limited solubility, so the absorption equilibrium did not yield very high selectivities for ethylene over ethane. However, the complexation reaction was found to be quite fast, so the process was optimized based on differences in kinetic uptake rates of the two gases. Since this system prepared using CuCl with KCl and HCl experienced limited solubility and ethylene capacity, Suzuki et al. [105] found that using the weaker triflate ($CF_3SO_3^-$) anion with an additional weakly coordinating ligand, vinyl sulfonate, allowed copper concentrations up to 0.09 M and showed nearly 4 times higher ethylene solubility. This result is consistent with the previous literature that weaker counter-anions allow

for more ethylene competition for binding sites which gives higher equilibrium constants.

Another proposed electrochemical process to separate ethylene/ethane mixtues that is quite unique uses a nickel dithiolene complex ($Ni[S_2C_2(CF_3)_2]_2$) to selectively bind the olefin [116]. A very peculiar aspect of this system is that the olefin actually binds to the S ligands rather than the metal center as shown in Figure 2-15.

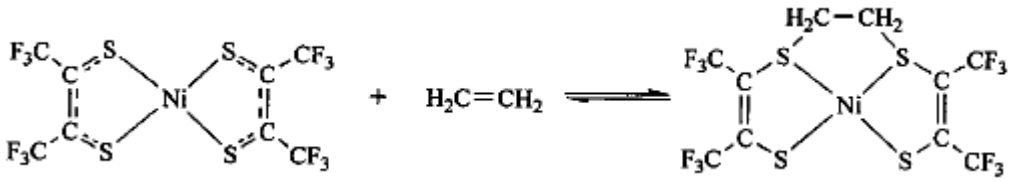

Figure 2-15. Ethylene binding by nickel dithiolene complex (from [116])

One very appealing characteristic of this system is that it was shown to be inert to treatment with H_2, CO, C_2H_2, and H_2S, typical poisons to other metal-based systems. This system was claimed to easily release ethylene when electrochemically reduced thus presenting the possibility of a more robust separation process. However, a further look into the reduction reaction suggested that the olefin-free reduced complex $Ni[S_2C_2(CF_3)_2]_2^-$ actually is further reduced irreversibly to the dianion $Ni[S_2C_2(CF_3)_2]_2^{2-}$ [32]. Processing instabilities such as forming irreversible byproducts as well as low ethylene capacities have hindered the fast adoption of electrochemical systems as seen by the examples above.

2.4.1 Cyclic voltammetry as an olefin capacity screening technique

Many researchers have used electrochemical techniques as analytical tools to quantify olefin complexation with metals [32][105][116]. This section will review work performed by Wang et al. [115] at The University of Texas at Austin to compare the ethylene absorption capacities of numerous aqueous and non-aqueous

silver and copper reactive absorption solutions by cyclic voltammetry. While the review by Wang et al. covered over 50 metal salt-ligand pairs, only selected systems to be compared with experimental results (see section 6.2) will be discussed in detail here.

Cyclic voltammetry (CV) was utilized to examine the qualitative changes in the redox properties of the Cu(II)/Cu(I) and Cu(I)/Cu couple in equilibrium with 1 atm N_2 and with 1 atm C_2H_4 by bubbling the appropriate gas through the solution containing the metal ion for 30 minutes. Electrochemical measurements were carried out using an EG&G Princeton Applied Research (PAR) Potentiostat/Galvanostat (Model 273A) controlled with the PAR 270 software package and a three-electrode cell at room temperature. The experimental setup shown in Figure 2-16 consists of a platinum disk as the working electrode, a platinum wire as the counter electrode, and a silver wire as the reference electrode.

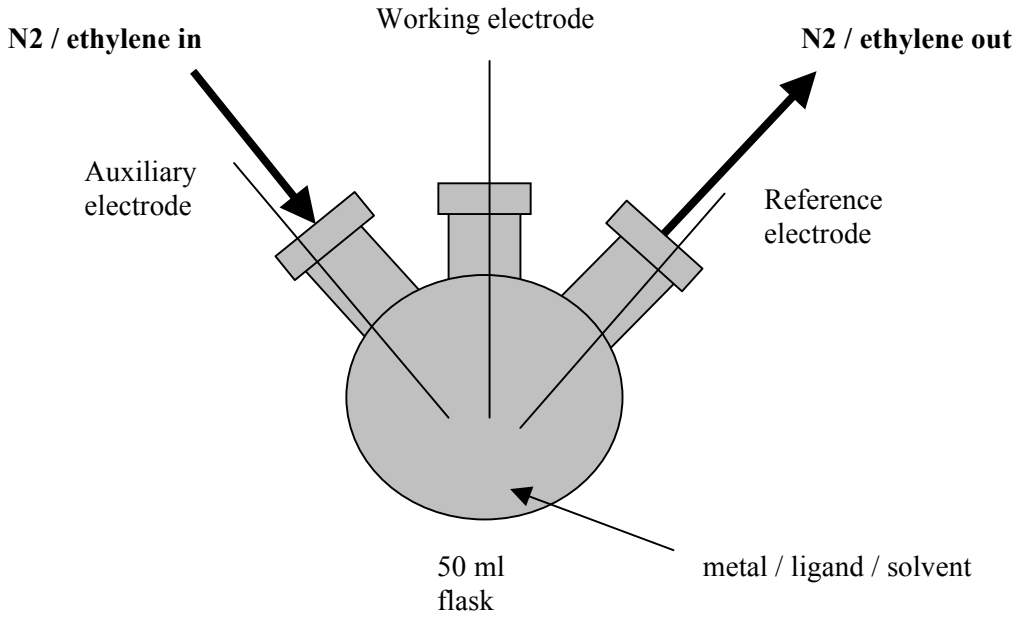

Figure 2-16. Cyclic voltammetry experimental setup (from [115])

The general experimental protocol involved establishing the CV curve for the copper ion in a given environment by first saturating the environment with oxygen-free nitrogen, which was produced by passing the research grade gas (assay, 99.9999%) over a column of BASF catalyst. After establishing the base voltammogram in the nitrogen saturated environment, the gas flow through the system was switched to ethylene, and complexes between the metal ion and the ethylene were observed by a shift in the half-wave potential. The difference between the CVs under these conditions reflects the capacity of the environment to form olefin complexes. The magnitude of the shift of the half-wave potential corresponds to the environment's capacity to absorb ethylene.

For all cyclic voltammetry (CV) experiments, a metal salt concentration of 0.01 M was used. Using large metal concentrations is not appropriate for CV because the success of the experiment depends on the local depletion of the particular metal ion around the electrode. On the other hand, a large metal concentration is desired for practical ethylene absorption applications, so it is worth noting that these exact CV systems are not useful unless the results can be applied to concentrated metal solutions as well. Metal salt-ligand pairs included combinations of cuprous chloride and cuprous bromide salts with pyridine, benzylamine, and aniline. The cyclic voltammetry experiments at 0.01M copper concentration included multiple ligand concentrations over a range of scan rates to identify trends in ethylene complexation. The supporting electrolyte necessary for the success of the technique was tetrabutylammonium perchlorate at 0.1M, and the solvent used for dilution where appropriate was dimethylformamide (DMF).

2.4.1.1 Cyclic voltammetry theory

The change in half-wave potential $\Delta E_{1/2}$ as a result of complexation can be described by the following equilibrium reactions. For any metal complexation reaction, the half-wave potential is shifted due to the creation of the new complex

bonds requiring a fraction of the electrons from the metal cation. Given a different electron density on the central cation, a different amount of energy is needed to reduce the metal before and after the olefin complexation [77]. For the monovalent metal ion (Cu(I)/Cu(0) couple), the reduction reaction is

$$\mathrm{Cu}^{+} + e^{-} \leftrightarrow \mathrm{Cu} \tag{2-7}$$

The Nernst equation for this reaction is given by

$$E = E^{O} + \frac{RT}{nF}\ln\frac{\mathrm{a}\left(\mathrm{Cu}^{+}\right)}{\mathrm{a}\left(\mathrm{Cu}\right)} = E^{O} + \frac{RT}{nF}\ln \mathrm{a}\left(\mathrm{Cu}^{+}\right) \tag{2-8}$$

where a(x) denotes the activity of species x and a(Cu) is taken as unity. The complexation reaction of ethylene is

$$\mathrm{Cu}^{+} + x\left(\mathrm{C_2H_4}\right) \leftrightarrow \mathrm{Cu}^{+}\left(\mathrm{C_2H_4}\right)_x \tag{2-9}$$

where the equilibrium expression is

$$\mathrm{K_{eq}} = \frac{\mathrm{a}\left(\mathrm{Cu}^{+}\left(\mathrm{C_2H_4}\right)_x\right)}{\mathrm{a}\left(\mathrm{Cu}^{+}\right)\mathrm{a}\left(\mathrm{C_2H_4}\right)^{x}} \tag{2-10}$$

Combining reactions (2-7) and (2-9) gives the reduction reaction for the complex ion

$$\mathrm{Cu}^{+}\left(\mathrm{C_2H_4}\right)_x + e^{-} \leftrightarrow \mathrm{Cu} + x\left(\mathrm{C_2H_4}\right) \tag{2-11}$$

The Nernst equation for this reaction is obtained by combining equations (2-8) and (2-10).

$$E = E^{O} + \frac{RT}{nF}\ln\frac{\mathrm{a}\left(\mathrm{Cu}^{+}\left(\mathrm{C_2H_4}\right)_x\right)}{\mathrm{a}\left(\mathrm{Cu}\right)\mathrm{a}\left(\mathrm{C_2H_4}\right)^{x}\mathrm{K_{eq}}} \tag{2-12}$$

By assuming a large concentration of ethylene compared to metal ions and equivalent diffusion coefficients for the metal ion and its complex with ethylene, equation (2-12) can be shown to give the shift in half-wave potential $\Delta E_{1/2}$, equation (2-13) [30].

$$\Delta E_{1/2} = E^{k}_{1/2} - E_{1/2} = -\frac{RT}{nF}\ln \mathrm{K_{eq}} - \frac{xRT}{nF}\ln \mathrm{a}\left(\mathrm{C_2H_4}\right) \tag{2-13}$$

From the cyclic voltammetry experiment, the half-wave potential in equation (2-13) is the midpoint between the peak anodic and cathodic currents of a particular scan.

$$E_{1/2} = \frac{E_{pa} + E_{pc}}{2} \tag{2-14}$$

For example, Figure 2-17 shows a CV scan of a CuCl system with the anodic and cathodic peaks labeled for nitrogen and ethylene gases. $E_{1/2}{}^{k}$ for the ethylene case is shifted right from $E_{1/2}$ for the nitrogen case. The magnitude of this shift is denoted by $\Delta E_{1/2}$ in Figure 2-17. For a one-electron (n=1) reversible process at room temperature equation (2-13) becomes

$$\Delta E_{1/2} = -0.0591 \cdot \log \mathrm{K_{eq}} - 0.0591 \cdot x \cdot \log \mathrm{a}\left(\mathrm{C_2H_4}\right) \tag{2-15}$$

From the observed value of the shift in half-wave potential $\Delta E_{1/2}$ (also called formal potential difference), the value of K_{eq} can be estimated for the complexation of ethylene in solution. For $K_{eq}>1$, larger negative values of $\Delta E_{1/2}$ mean the system has a larger ability to absorb ethylene.

For the divalent copper (corresponding to the Cu(II)/Cu(I) couple), the direction of electron transfer from the cuprous ion is opposite from the previous derivation. This leads to a shift in half-wave potential given by

$$\Delta E_{1/2} = E_{1/2}^{k} - E_{1/2} = \frac{RT}{nF} \ln \mathrm{K_{eq}} + \frac{xRT}{nF} \ln \mathrm{a}\left(\mathrm{C_2H_4}\right) \tag{2-16}$$

For a one-electron (n=1) reversible process at room temperature,

$$\Delta E_{1/2} = 0.0591 \cdot \log \mathrm{K_{eq}} + 0.0591 \cdot x \cdot \log \mathrm{a}\left(\mathrm{C_2H_4}\right) \tag{2-17}$$

When $K_{eq}>1$, a shift of the formal potential difference greater than zero ($\Delta E_{1/2}>0$) corresponds to an increase in the absorptivity of ethylene by this chemical system.

For these non-aqueous solutions, coordinating ligands were used to stabilize and solvate the metal ions. The equilibrium reactions contain additional exchange reactions due to the competition between the ligands and the olefin for the metal ion. Generally, *p* ligands are required to coordinate the copper ion given by

$$Cu^{+} + pL \leftrightarrow Cu^{+}L_{p} \tag{2-18}$$

where *L* is either the anion or an organic ligand. Reaction (2-18) is assumed to occur quickly and completely so that essentially all metal ions are coordinated. When an ethylene molecule is introduced into the system, it can either add to the metal-ligand complex or replace an existing ligand. If the ethylene adds to the complex, the coordination number of the metal will increase and a new geometry will arise, but the estimation of the corresponding K_{eq} from equation (2-15) is the same.

$$Cu^{+}L_{p} + x(C_2H_4) \leftrightarrow Cu^{+}L_{p}(C_2H_4)_{x} \tag{2-19}$$

If the ethylene replaces an existing ligand, the complex can retain its original structure with the cleavage of a metal-ligand bond and the formation of the metal-olefin bond.

$$Cu^{+}L_{p} + x(C_2H_4) \leftrightarrow Cu^{+}L_{p-x}(C_2H_4)_{x} + xL \tag{2-20}$$

The displaced ligand creates a different form of the equilibrium equation that changes the calculation of K_{eq} for the Cu(I)/Cu(0) couple.

$$\Delta E_{1/2} = -0.0591 \cdot \log K_{eq} - 0.0591 \cdot x \cdot \log \frac{a(C_2H_4)}{a(L)} \tag{2-21}$$

The additional term in equation (2-21) makes the calculation of K_{eq} much more difficult without prior knowledge of the interaction between the anion and other ligands with the metal ion. The coordination number (including whether or not the anion behaves as a coordinating ligand) and structure of the complex would be necessary to proceed without direct measurement of the ligand concentration. Relatively weak ligands are easily replaced by incoming ethylene, but stronger ligands or ligands present in high enough concentrations create competition with ethylene for coordination sites. This competition for the metal can lead to reduced capacity when solvent molecules can act as ligands or when ligands are too strong for ethylene to compete.

2.4.1.2 Cyclic voltammetry results

The change in potential due to ethylene treatment was recorded over a range of scan rates. The results as formal shifts in half-wave potential ($\Delta E_{1/2}$) are presented in Table 2-3 at the range of scan rates used. The system with the best capacity for ethylene absorption was comprised of cuprous chloride with aniline with DMF as the CV solvent. The CV curve for CuCl with aniline is shown in Figure 2-17 where the shift in formal potential is seen as the difference between the peaks for the ethylene (dashed line) over the nitrogen (solid line) where both the cathodic and anodic peaks for the Cu(I)/Cu(0) couple exhibit large shifts. At low ligand concentrations, both chloride and bromide systems exhibit a two-step redox process meaning that the Cu(II)/Cu(I) couple and Cu(I)/Cu(0) couple are distinguishable in the voltammogram as in Figure 2-17. For these cases, only the Cu(I)/Cu(0) data is shown in Table 2-3.

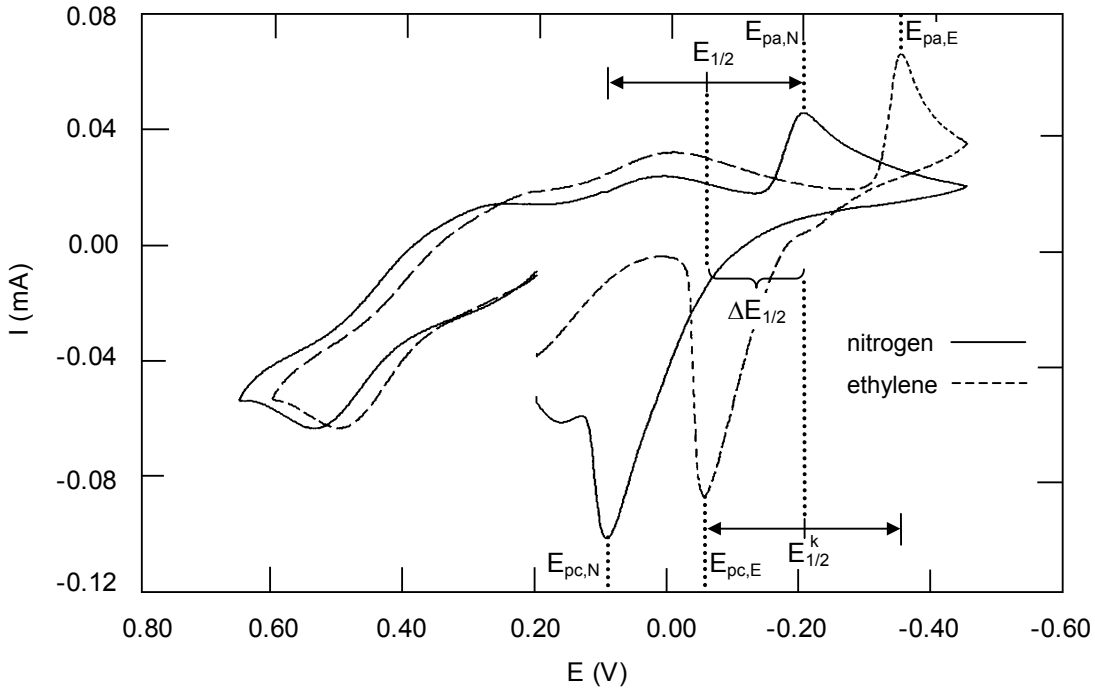

Figure 2-17. CV curve of non-aqueous 0.01M CuCl with 0.4M aniline at 100 mV/s. The features on the left at about 0.40V correspond to the Cu(II)/Cu(I) couple while those on the right between 0.20 and -0.50V correspond to the Cu(I)/Cu(0) couple (from [115])

Table 2-3. CV data at given scan rates and ligand conc. for Cu(I)/Cu(0) couple (from [115])

Ligand	Scan rate, mV/s	$\Delta E_{1/2}$ (mV, ±2)			
		CuCl		CuBr	
		0.05M py	0.40M py	0.05M py	0.40M py
Pyridine	20	-58	-30	-23	-32
	50	-60	-33	-31	-35
	100	-63	-35	-30	-34
	200	-64	-30	-28	-30
	1000	-58	-24	-23	-31
		0.05M bza	0.40M bza	0.05M bza	0.40M bza
Benzylamine	20		-32		-16
	50	-63	-30	-44	-14
	100	-57	-26	-38	-11
	200	-50	-29	-30	-8
	1000	-52	-67	-39	-6
		0.40M an	4.0M an	0.40M an	4.0M an
Aniline	20		-150		
	50	-147	-139	-152	10
	100	-147	-148	-143	-5
	200	-147	-146	-136	-11
	1000	-141	-154	-129	-16

From the CV data, the coordinating ability of the ligands studied increases in the following order: aniline << pyridine < benzylamine. If the cuprous ion coordinates with a stronger ligand such as benzylamine, ethylene molecules show a lesser degree of complexation as seen by the smaller negative shifts in the formal potential. By examining both the chloride and bromide cases for a ligand concentration of 0.4M, the shifts in formal potential increase from benzylamine to pyridine to aniline following the coordination strength from greatest to least. If a ligand is strongly coordinating, then it will show its greatest ethylene capacity at the concentration nearest its coordination ratio with the metal ion. However, increases in ligand concentration show reduced ethylene capacity due to binding tendency of the

ligand making it difficult for the olefin to compete for the metal. This trend is significant for benzylamine with the shift in the formal potential decreased (from -57 to -26 mV for CuCl and from -38 to -11 mV for CuBr at 100mV/s scan rate) when the ligand concentration is increased from 0.05M to 0.4M. If a ligand is weakly coordinating like aniline, it will not show the reduction in ethylene capacity at ligand concentrations over its coordination number. For example, the cuprous chloride and aniline case shows essentially no change in shift in the formal potential (given as -147 and -148 mV at 100mV/s scan rate) from 0.4M to 4.0M corresponding to ligand to metal ratios of 40:1 and 400:1 which are well in excess of the normal range of coordination number (2 to 5) for copper(I) complexes in solution [79]. The strong ligand concentration effect is important because a large concentration of a strong ligand can impede the absorption process. Determining the best ligand can be difficult because if the ligand is too strong it will hinder the ethylene substitution reaction (equation (2-20) above). If the ligand is too weak, the ligand will not fully complex the metal ion leading to a more destabilized copper, which will likely have poor solubility and hence yield a solvent with poor olefin capacity.

The effect of anion is similar to that of the coordinating ligand. The chloride ion was observed to be a weaker anion than the bromide ion. By examining the 0.05M pyridine systems for the two anions, the chloride case shows over double the shift in formal potential as the bromide case. Another example of the anion exhibiting the same type of behavior as ligands can be seen in the aniline systems. Since aniline is a weak ligand, the coordinating effect of the counter-ion becomes more significant. With the weak chloride ion, the ethylene capacity is nearly independent of the aniline concentration. As a result, even a high concentration of weak ligand does not reduce the copper's complexing ability because the chloride ion is easily replaced, and incoming ethylene molecules have no problem exchanging with the weak aniline ligands. For the opposite case, a strong anion does not surrender as easily which is evident by the cuprous bromide system's remarkable

drop in shift in formal potential for the more concentrated aniline case. Therefore, the inhibitory effect seen with strong ligands is also present even with weak ligands because one of the coordinating sites on the copper ion is lost to the stronger bromide ion.

With stronger ligands, it is more difficult to observe this anion effect since the behavior can be attributed to the ligand strength as mentioned above. In fact this concentration/anion effect argument does not hold true for the pyridine-cuprous bromide system. This system surprisingly retains its ethylene-binding ability at 0.4M pyridine over 0.05M pyridine. An additional experiment was performed with cuprous bromide using excess pyridine as the solvent which still showed considerable shift in formal potentials up to -28mV for the highest scan rate. It is unclear why the pyridine-CuBr system does not show decreased capacity for higher ligand concentrations especially since the trend is observed with the chloride case.

The trend that the chloride anion formed weaker complexes than the bromide complexes is consistent with the hard and soft acid and base prediction for stability of metal-halide complexes ($F < Cl < Br << I$) [84]. This order has been confirmed for ethylene adsorption on solid CuCl and CuBr both experimentally [34][75] and theoretically (for a mono-coordinated surface) [16]. However, solution studies with other metals such as rhodium and iridium suggest the opposite trend [5][6][28].

The cyclic voltammetry bench-top electrochemistry technique was used to study six chemically different olefin absorption systems at two concentrations. By using the Nernst equation, the shift in formal potential was directly correlated to the system's equilibrium or capacity to absorb ethylene. This study confirmed that weak ligands with weak anions exhibit the greatest olefin capacity, and these systems should be the focus of further study as potential reactive absorption solvents.

Chapter 3.
Experimental Equipment and Procedures

3.1 Copper solution preparation

Due to the instability inherent in copper(I) systems to oxidation discussed in section 2.1.4, it was necessary to prepare and store all copper(I) solutions in an inert atmosphere glove box as shown in Figure 3-1. The equipment and procedures used in solution preparation are briefly discussed here. The main steps for solution preparation include accurately measuring the chemical ingredients, mixing in the salt at appropriate conditions for ligand complexation, filtering any insolubles, contacting with carbon monoxide to reduce any oxidized copper, measuring solution density and viscosity, and transferring to the autoclave via a small sample bomb.

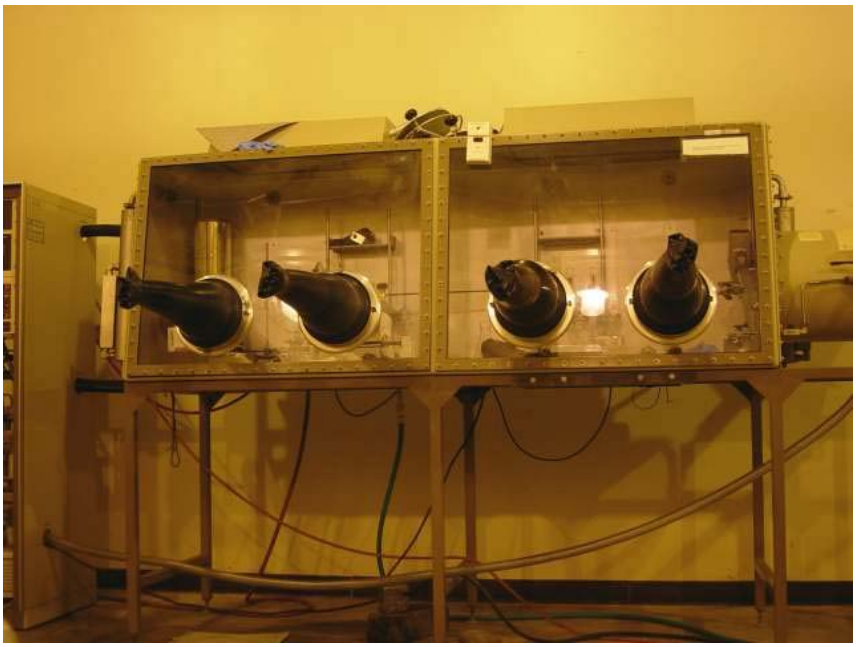

Figure 3-1. Photograph of glove box system

3.1.1 Equipment for solution preparation

An inert atmosphere for solution preparation was provided by a VAC Dri-Train glove box system. The VAC Dri-Train glove box system contained a moisture and oxygen-free atmosphere by recirculating an inert gas as shown in Figure 3-2. The inert gas used for the glove box atmosphere was nitrogen provided by the PRC Bldg. 133 house line from a cryogenic tank. The purity of this gas was greater than 99.995%. The glove box was a hermetically sealed system by which materials must be introduced and removed via the side antechamber. The Dri-Train system was equipped with two purifier beds capable of removing small amounts of water and oxygen from the circulating inert gas. Each purifier bed was capable of removing approximately 10 standard liters of oxygen and 225 grams of water. The determination of when a purifier bed became saturated could be confirmed with additional monitoring equipment. For oxygen level testing, a 25W electric lightbulb with a hole filed through the glass was passed into the glove box. When the lightbulb was screwed into a socket, it burned out quickly in the presence of excess oxygen. For oxygen levels less than 5 ppm, the bulb will burn for 6 hours or more. The system was designed so the circulating gas always flowed through one of the purifier beds allowing the other bed to be regenerated. Purifier bed regeneration was an automatically controlled 12-hour cycle that was performed when the bed became saturated with oxygen or water. The bed regeneration cycle consisted of heating the bed, flowing a reducing gas mixture of 3 to 10% hydrogen in nitrogen through the bed, pulling a vacuum across the bed, and refilling the bed with inert gas. In addition, activated carbon and molecular sieve traps were present between the glove box and purifier beds to remove trace organic vapors and excess water vapor. Since there was no integrated oxygen or water level detection in the Dri-Train system, the frequency of regeneration was determined by the user.

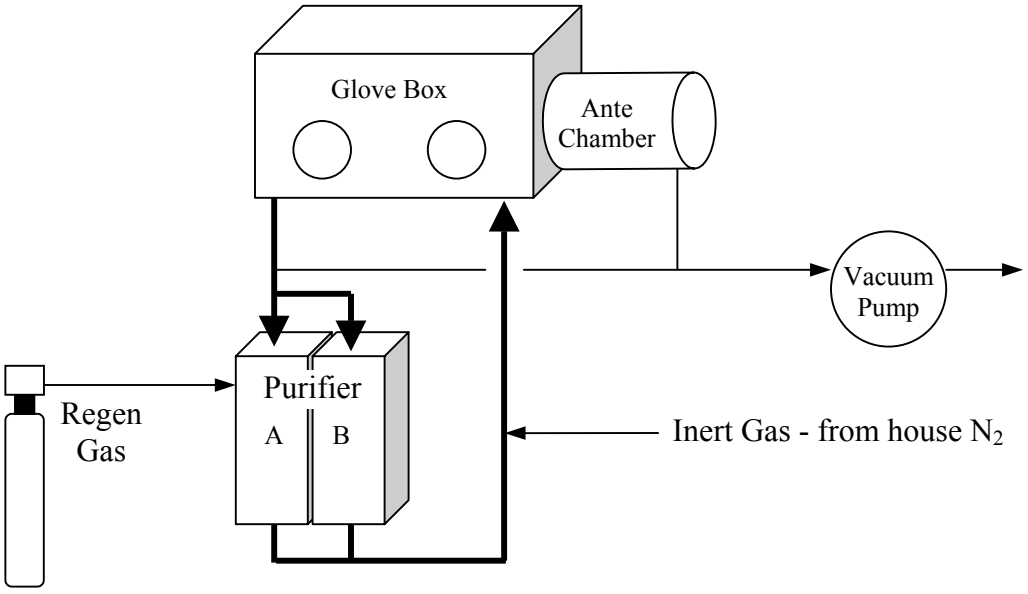

Figure 3-2. Flow diagram of VAC Dri-Train glove box system

For startup of the glove box or following periods of prolonged inactivity, it was necessary to purge the gas contents by flowing eight to ten glove box volumes of inert gas. Purging required at least six hours of inert gas flow with adequate circulation in the glove box (based on a flowrate of 1 CFM). Once startup was completed, the Dri-Train system was designed for continuous operation, and an inert atmosphere was maintained automatically. Care was taken to avoid using chemicals which could poison the purifier beds such as sulfur compounds (H_2S, RSH, COS, SO_2, SO_3, etc.), halides, chlorides, halogens, alcohols, hydrazine, phosphene, arsine, arsinate, mercury, and large amounts of water.

For solution preparation, chemical raw materials were obtained and used as received without further purification or treatment. Most chemicals were obtained from Fisher Scientific Company or the UT Chemistry Stockroom. Table 3-1 gives a

complete listing of the chemical used along with the supplier, purity, and primary impurities.

Table 3-1. Chemical raw materials used

Chemical	Supplier	Purity	Primary impurities
CuCl	Acros Organics	97%	SO_4 0.05%; Pb 0.02%; Fe 0.005%
CuBr	Acros Org.	98%	Not listed
Aniline	Fisher Scientific	99.9%	C_6H_5Cl 0.003%
Benzylamine	Acros Org.	99%	Not listed
Pyridine	Fisher Sci.	99.9%	H_2O 0.02%; NH_3 0.0008%
DMF	Fisher Sci.	99.9%	H_2O 0.02%
NMP	BASF	99.9%	H_2O 0.008%

DMF: N,N-dimethylformamide; NMP: N-methyl-2-pyrrolidone

For solution mixing and filtration, standard Pyrex glassware equipment was used. For taking solid and liquid weights, a three-beam sliding mechanical balance by O'haus was kept inside the glove box for convenient measurement. A Thermolyne heat/stir plate was also kept inside the glove box for solution preparation. The filtration assembly for removal of insolubles was a simple water aspirator with a buchner funnel as shown in Figure 3-3. A water line was routed into the glove box, passed through the aspirator, and piped to an external drain to avoid contaminating the inert atmosphere with water vapor. The trap flask shown in Figure 3-3 was used to prevent any accidental back-flow of water into the filter flask. Medium porosity filter paper by Fisher Scientific was used for all filtrations.

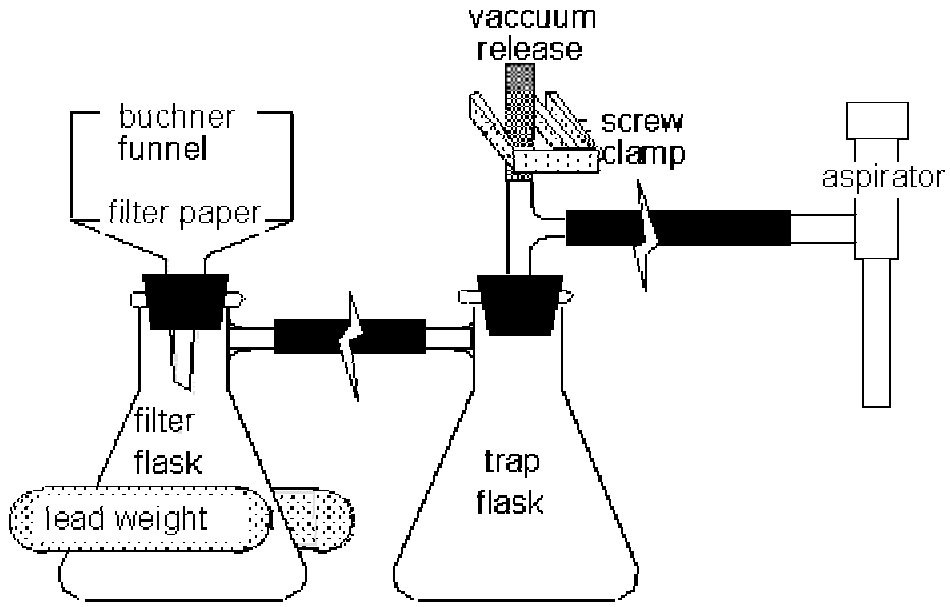

Figure 3-3. Filtration assembly for removal of insolubles

For density measurements, standard volumetric flasks of 50 mL and 100 mL were used. The density was found at a given temperature by filling the volumetric flask to the full mark with the solution. The difference in weight of the filled flask from the empty flask is used to find the density. For viscosity measurements, a Fann Model 35 Couette coaxial cylinder rotational viscometer as shown in Figure 3-4 was used. The viscometer measures the torsion on a bob due to viscous drag exerted by the fluid on the annular region between the bob and a rotating outer sleeve. The viscometer had appropriate dimensions to fit through the antechamber, so the viscosity measurements on the copper solutions were performed in the glove box. Successful operation of the viscometer consisted of filling the stainless steel cup with the liquid solution and raising the cup and platform up to a pre-specified level of the bob and sleeve apparatus. With the standard device spring and rotor speed of 300 rpm, the instrument is designed to give viscosity in cP through the dial read-out.

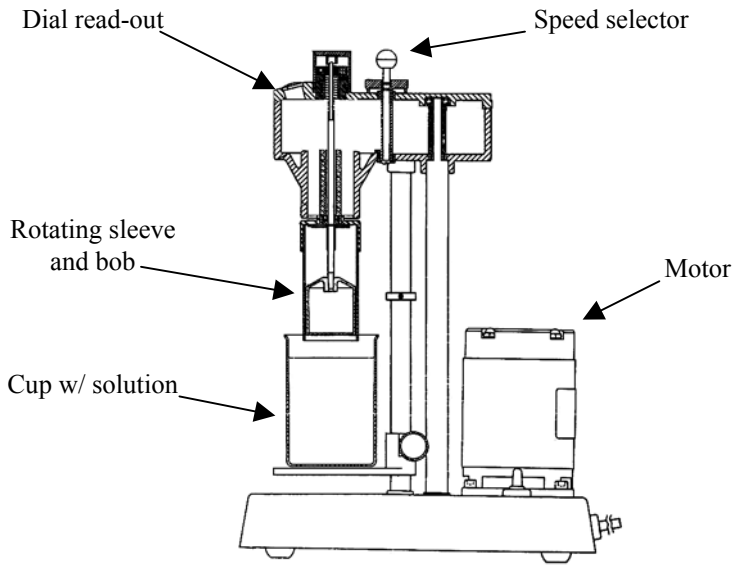

Figure 3-4. Fann Model 35 rotational viscometer

During solution preparation or for preparation for analytical experiments, it was sometimes necessary to contact the prepared solution in the glove box with either carbon monoxide (CO) or ethylene gas. Contacting with CO was done to reduce any reversibly oxidized copper in the solution, and contacting with ethylene was done to prepare ethylene loaded solutions for the analytical techniques discussed in Chapter 4. The experimental setup for the gas contacting experiments shown in Figure 3-5 consisted of a three-neck flat bottom flask on the heat/stir plate with a small, lecture-size bottle of either pure CO (from Praxair at 99.5%) or ethylene (from Air Liquide at 99.5%). The gas was introduced into the liquid via a glass gas sparging tube of medium porosity from Ace Glass, Inc. The pressure for these experiments was maintained at atmospheric by keeping the vent line open to a line through the back of the glove box to the exhaust hood.

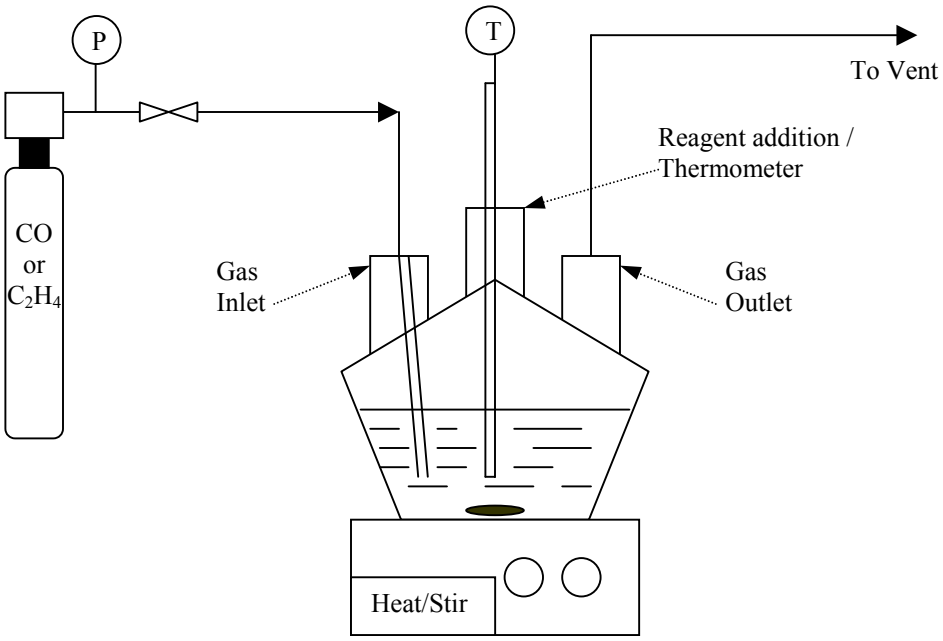

Figure 3-5. Gas contacting experimental setup

Once the prepared solution was ready to be removed from the glove box, special equipment was used to avoid exposure of the solution to air. For solutions to be introduced into the autoclave, a 300 mL stainless steel sample bomb equipped with Nupro valves and Swagelok quick-connect fittings was used to transfer the solution from the glove box to the autoclave. The sample bomb was equipped with quick-connects on both ends shown in Figure 3-6(a), and nitrogen gas was used to pressurize the solution to facilitate transfer from the sample bomb into the autoclave. For solutions to be introduced into the continuous flow process, a high-pressure stainless steel tank was used to transfer the solution from the autoclave to the flow process.

The tank shown in Figure 3-6(b) was equipped with Swagelok quick-connect fittings, a Nupro spring pressure-relief valve (with blue spring rated for 50-350 psig), a pressure gauge from US Gauge (200 psig), and a removable top opening for easy filling and pouring inside the glove box.

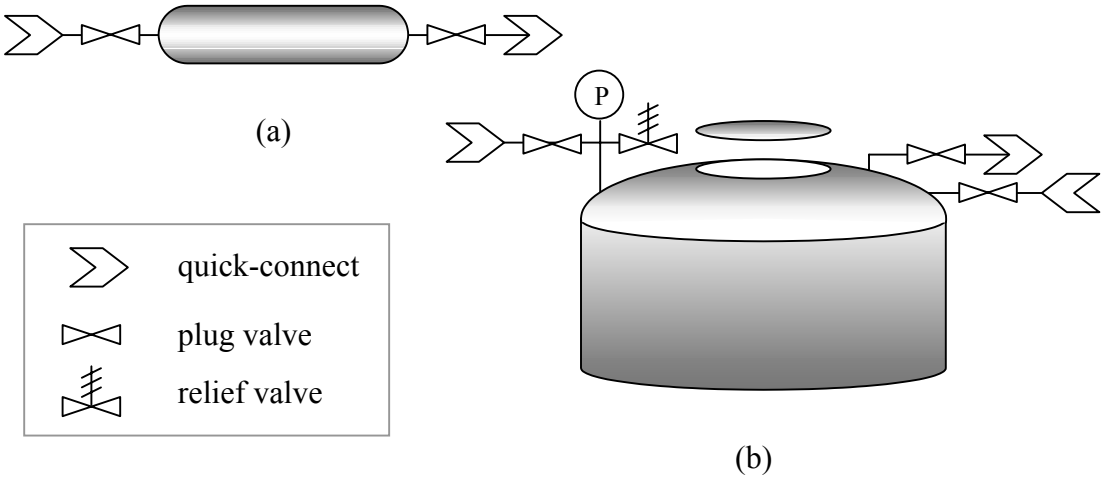

Figure 3-6. Solution transfer vessels

3.1.2 Procedure to prepare a copper(I) solution

The starting materials to prepare a new solution are a copper salt (such as CuCl), a coordinating ligand (such as aniline), and a solvent (such as NMP). To prepare a solution from starting materials, with a funnel the desired amount of ligand was poured into an Erlenmeyer flask, a small stirring bar added, then an equivalent volume of the solvent was poured into the flask. The stirring plate was on at a low setting at this point, and the hot plate was turned on. The flask was covered to prevent excess vaporization and the temperature was brought to 70ºC. Next the desired amount of copper salt was added with a dry funnel to prevent adhesion to walls. For all experiments a ligand to copper molar ratio of 4.1:1 was used following the recommendation by Haase [38] for optimum coordination of cuprous halides with

nitrogen-containing ligands. Upon addition of the salt, the color of the flask contents changed from clear, golden amber (ligand-solvent only) to reflective, lustrous black (copper salt-ligand-solvent). After salt addition, the solution temperature rose sharply due to ligand complexation of the copper(I). Once the temperature began to fall, additional solvent was added to bring the solution to the desired copper molarity.

If no additional solvent was added, the solution precipitated crystals as it cooled due to saturation of the ligand-copper complex. The diluted solution was stirred and allowed to cool to room temperature without the precipitation of crystals. After stirring for an hour, a small amount of undissolved powder remained in the bottom of the flask. It is unknown whether this powder was uncomplexed copper salt, oxidized cupric insolubles, or impurities in the salt. The powder was not likely a precipitated ligand-copper complex because the powder did not scatter light like the precipitated crystals, and it was present to some degree at low copper loadings and also at high temperatures.

In order to remove the powder from the copper solution, vacuum filtration was performed using the setup in Figure 3-3. The total weight of wet filtered powder was less than 6% of the mass of dry salt added for all experiments. For CuCl systems, the filtered residue was usually a dark green powder suggesting that it contained cupric chloride (a green solid). It is supposed that the powder is mostly undissolved, uncomplexed cupric chloride impurity thought to be originally present in the reagent salt. The appearance of the cuprous chloride reagent in the bottle was white when first purchased, but over a period of months it gradually acquired a faint green tint. The green color was believed to be due to some minor amount of oxidized cupric chloride. As shown in Table 3-1, the copper salts were not of extremely high purity because it was desirable for the solution to be inexpensive and commercially available.

In early preparation attempts, instead of simply filtering the powder, the solution was contacted with CO to reduce the oxidized cupric state to the desired

cuprous state. It was hoped that the cupric substance would reversibly release the oxygen upon contact with CO to demonstrate that the state of the copper solution could be manipulated by treatment with oxidizing or reducing gases as mentioned earlier in the work by Haase [38]. According to the setup in Figure 3-5, the experiment was set up such that the volumetric level of the solution was at least half of the flask volume. A thermometer was inserted into the open neck to seal the system and monitor the temperature of the experiment. The CO inlet tube and the thermometer were completely submerged yet not interfering with the stir bar. The simple gas contacting experiment consisted of slightly opening the regulator valve on the gas cylinder until a low flow of bubbles evolved from the sparging tube submerged in the copper solution. The stirrer was started and gas-liquid contact maintained until the gas flow was stopped after an arbitrarily chosen contact time of 15 minutes.

While the degree of reduction was not analytically quantified, the solution was evaluated visually to compare the effects of the CO treatment. At ambient contacting temperatures, the solution remained unchanged and the powder residue maintained a green hue. At contacting temperatures near 70ºC, the stirred solution showed an obvious color change from the dark green tint observed previously to a reddish brown color. Upon cooling and filtering this solution, the solid residue was found to be a metallic reddish brown solid that was thought to be mostly reduced copper metal. While conditions were not found that effectively reduced the cupric powder to the soluble cuprous state, likely a more carefully controlled experiment at an intermediate temperature could have produced the desired cuprous state. Nevertheless, it was confirmed that treatment with CO reduced the copper solution at higher temperatures.

In order to drive off the complexed CO, the solution was heated and stirred to a temperature of 95-105ºC for a period of about an hour until gas bubbles no longer evolved from the solution. The decomplexed solution was then drawn into the evacuated sample bomb shown in Figure 3-6 to be introduced into the autoclave. It

was not necessary for the solution to undergo CO or ethylene complexation before being transferred from the glove box to the autoclave. In fact, for most solutions no additional treatment was done beyond filtration of insolubles followed by a density measurement.

3.2 Autoclave absorption apparatus

The majority of the experimental data obtained was found using the autoclave absorption apparatus shown in Figure 3-7. Also called the stirred equilibrium cell, the autoclave was a very versatile piece of equipment. It was used for measuring absorption equilibrium data for pure gases and mixtures of ethylene and ethane in addition to kinetics of pure ethylene absorption.

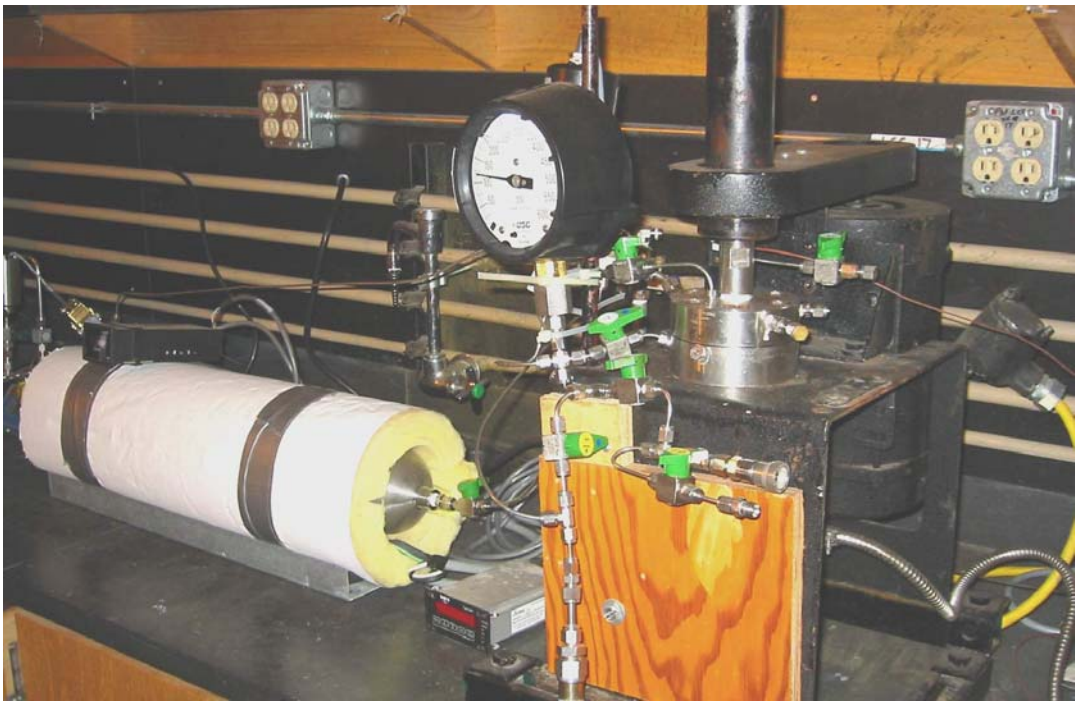

Figure 3-7. Photograph of autoclave experimental setup

3.2.1 Equipment for autoclave apparatus

The setup for the autoclave experiments is shown in Figure 3-8 following absorption experimental techniques common in the literature [55][62]. The basic equipment was a high pressure vessel with an autoclave for gas-liquid equilibrium. The autoclave was a 500 cm^3 316 stainless steel model manufactured by Autoclave Engineers. A belt driven magnetic stirrer and ceramic band heater were custom fitted to the autoclave. Plumbing on the autoclave allowed for a MKS pressure transducer, a pressure gauge by US Gauge (600 psig), a thermocouple well with a J-type Omega thermocouple, a Nupro safety relief valve (with yellow spring rated for 350-750 psig), a gas feed line from the high pressure vessel, a vent line, a vacuum line, an auxiliary gas feed line, and a liquid sample line. The high pressure vessel used to transfer a known amount of gas into the autoclave was a 1 gallon, stainless steel bomb equipped with a MKS pressure transducer, a pressure gauge from Weksler Instruments (1000 psig), a Nupro safety relief valve (with yellow spring rated for 350-750 psig), and an internal type-K Omega thermocouple. The gases used in the autoclave experiments were chemically pure grade ethylene and ethane from Air Liquide. The purity of the ethylene was listed as 99.5% with impurities listed as ethane, 0.10%; methane, 500 ppm; nitrogen, 100 ppm; oxygen, 50 ppm; carbon dioxide, 5 ppm; carbon monoxide, 5 ppm. The purity of the ethane was listed as 99.0% with impurities given as ethylene, 0.40%; propylene, 0.10%; propane, 400 ppm; other C3+, 0.15%; methane, 50 ppm.

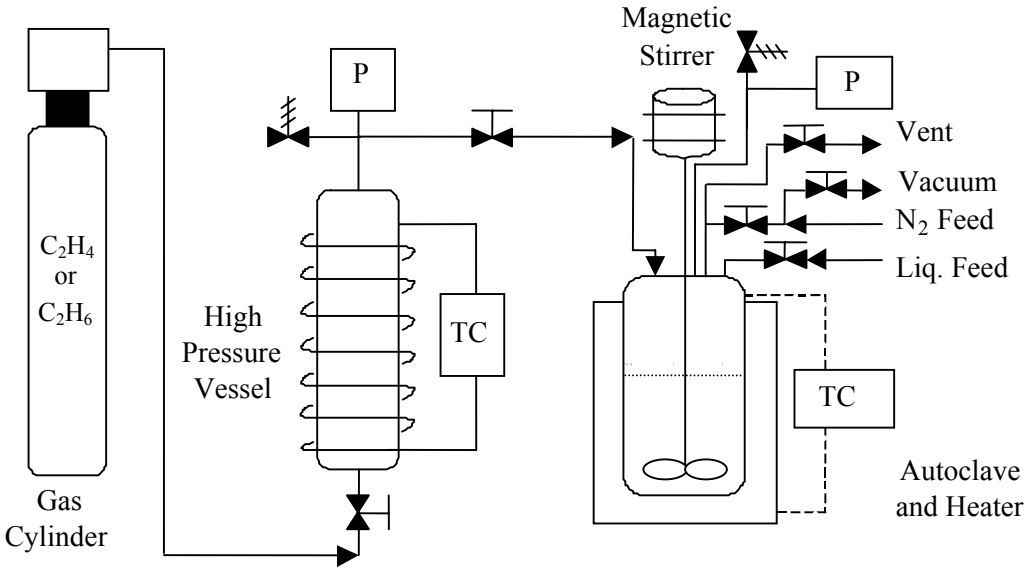

Figure 3-8. Autoclave apparatus experimental setup

The dimensions of the internals of the autoclave are shown in Figure 3-9. The total depth of the autoclave was $11^{7}/_{8}$", and the diameter was $1^{13}/_{16}$". The stirrer had a diameter of $1^{1}/_{4}$" with six vertical baffles joined by two horizontal discs, and it was positioned $^{7}/_{8}$" from the bottom of the autoclave. The thermocouple well was positioned $6^{3}/_{8}$" from the bottom, so it was always in the gas phase because liquid volume never exceeded 250 mL. The positioning of the liquid feed line was below the usual liquid level at $1^{7}/_{8}$" from the bottom allowing for the liquid feed line to be used as a liquid sample line, too.

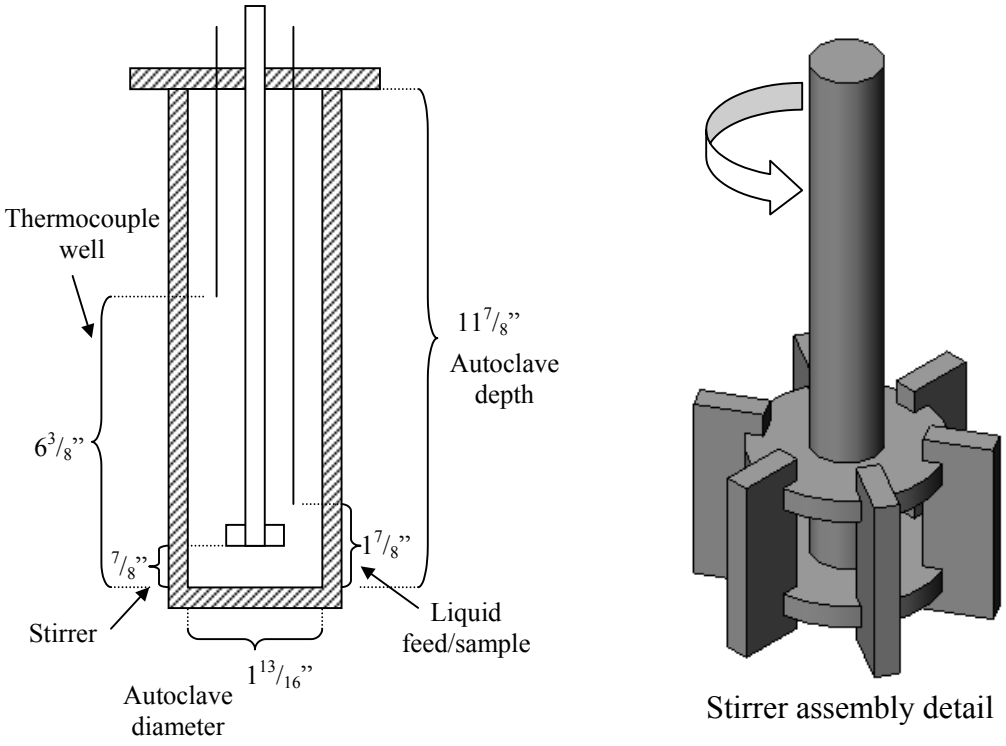

Figure 3-9. Internal dimensions of autoclave with stirrer detail

Before performing autoclave experiments, the instruments and vessel volumes were calibrated. First, the high pressure vessel volume was calculated by water volume, and then the pressure transducers were checked by comparison with gauge readings over a pressure range from 0 to 300 psig. The MKS transducer on the autoclave was found to have a significant slope error and it was returned to the manufacturer for repair and recalibration. The pressure transducer check before and after recalibration is given in Appendix A.1. The accuracy of the thermocouples was checked by measurement in ice water and boiling water, and both were found to exhibit acceptable accuracy to ±0.2 ºC. The total autoclave volume including not only the vessel itself but also the connecting tubing to the transfer lines and instruments was calculated before adding the liquid solution. The total volume of the

empty autoclave was calculated by a series of nitrogen gas charges over pressures from 90 psia to 285 psia. In order to calculate the autoclave volume, a simple mass balance around the system showed the initial and final conditions of both vessels can be used by equating the number of moles of gas transferred to the autoclave.

$$n_{\text{bomb, initial}} - n_{\text{bomb, final}} = \Delta n = n_{\text{autoclave, final}} - n_{\text{autoclave, initial}} \tag{3-1}$$

A generalized correlation for gases that is an alternative form of the Redlich/Kwong equation as described in Smith et al. [97] was used to calculate the autoclave volume (a more rigorous approach is developed later).

$$\frac{V_{\text{bomb}}}{R}\left(\left(\frac{P}{ZT}\right)_{\text{bomb},i} - \left(\frac{P}{ZT}\right)_{\text{bomb},f}\right) = \frac{V_{\text{autoclave}}}{R}\left(\left(\frac{P}{ZT}\right)_{\text{autoclave},f} - \left(\frac{P}{ZT}\right)_{\text{autoclave},i}\right) \tag{3-2}$$

The compressibility factor Z was defined as

$$Z = \frac{1}{1-h} - \frac{4.9340}{T_r^{1.5}}\left(\frac{h}{1+h}\right) \tag{3-3}$$

where h is given by

$$h = \frac{0.08664 \cdot P_r}{ZT_r} \tag{3-4}$$

where $T_r = T/T_c$ and $P_r = P/P_c$. The value of h was first guessed to solve for Z in equation (3-3), and then h was calculated by equation (3-4) and iteratively adjusted until the convergence was acceptable. Rearrangement of equation (3-2) with the solved value of Z for each condition yields the expression for the autoclave volume.

$$V_{\text{autoclave}} = V_{\text{bomb}} \frac{\left(\left(\frac{P}{ZT}\right)_{\text{bomb},i} - \left(\frac{P}{ZT}\right)_{\text{bomb},f}\right)}{\left(\left(\frac{P}{ZT}\right)_{\text{autoclave},f} - \left(\frac{P}{ZT}\right)_{\text{autoclave},i}\right)} \tag{3-5}$$

The autoclave volume from equation (3-5) was calculated for 26 different experiments, and the average empty autoclave volume was 533 mL with a standard deviation of 6 mL corresponding to a %RSD of 1.2%. The vapor volume for a

particular set of autoclave experiments was found by subtracting the volume of liquid added to the autoclave from the empty autoclave volume.

3.2.2 Procedure for absorption equilibrium experiment

The basic principle behind the operation of the autoclave was to allow gas-liquid contact for a long enough period of time such that each component's overall rate of mass transfer tended toward zero. By choosing appropriate conditions and making some key assumptions, the equilibrium condition was observed fairly easily. One primary assumption was that the absorption liquid is nonvolatile at the absorption conditions. Examination of the vapor pressure curves of aniline, NMP, and DMF in Figure 3-10 shows that at ambient temperature the total vapor pressure contribution of the liquids is less than 0.01 psi for equimolar mixtures of NMP and aniline. At 40ºC the total vapor pressure of this mixture is less than 0.1 psi.

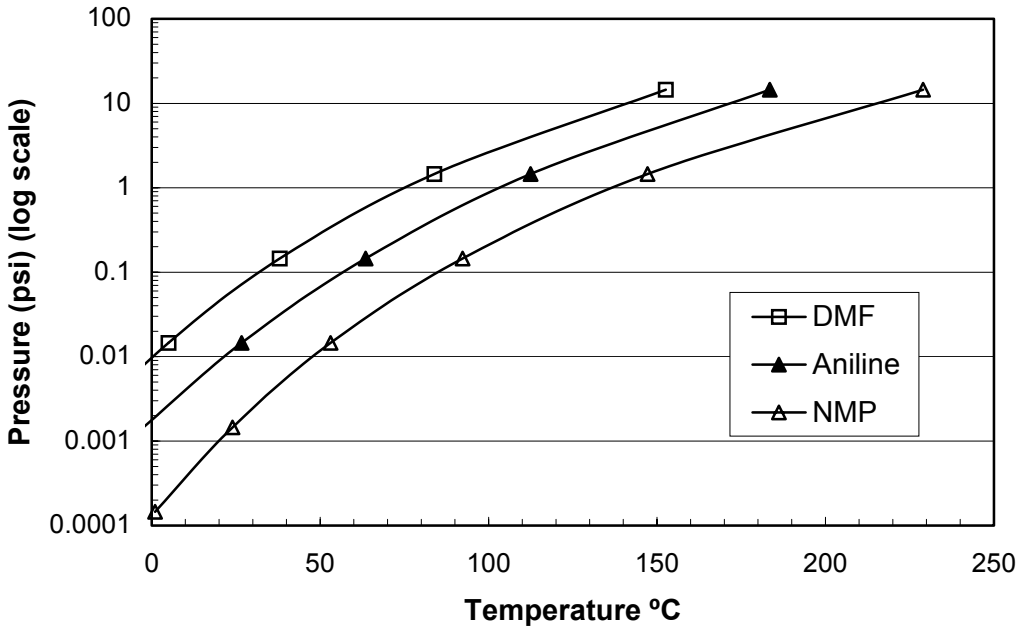

Figure 3-10. Vapor pressure curve of aniline, NMP, DMF (data from [72])

Before introducing a prepared absorption solution into the autoclave, it was necessary to disassemble and thoroughly clean the vessel and all associated tubing with solvent (NMP or DMF, whichever would be used in the succeeding experiment). High pressure nitrogen was used to flush out and dry all tubing and connections before the autoclave was reassembled for the experiment. Upon reassembly the autoclave was pressure tested with nitrogen to ensure that there were no significant pressure leaks. The maximum tolerance for the pressure test was 0.4 psi per hour at an autoclave pressure of 100 psia. Since most experiments required less than an hour to complete and the longest experiments were no longer than 2.5 hours, this degree of leak tolerance was insignificant compared to the total pressure change due to absorption.

After the leak test, which also effectively purged the air from the autoclave with nitrogen, the autoclave was evacuated with an Edwards model RV3 rotary vane vacuum pump. The autoclave was then isolated via a shutoff valve from the vacuum pump and tested once more to make sure that air was not able to leak into the system. The evacuated autoclave was now ready for the absorption solution. The solution contained in the sample bomb that was filled in the glove box was connected via a quick connect fitting to the liquid feed line and held in a vertical position such that gravity would assist flow out of the sample bomb into the autoclave. In addition, nitrogen was connected to the opposite (top) side of the sample bomb via the other quick connect fitting to help pressurize the liquid into the autoclave.

For most of the absorption equilibrium experiments, nitrogen remained in the autoclave to keep an inert atmosphere and a positive pressure on the system. Another key assumption was that nitrogen is not significantly absorbed by the liquid solution. Since both liquid components were nitrogen-containing compounds, this assumption was tested and found that at high nitrogen pressures, the degree of absorption could be significant; however, at atmospheric pressure, the nitrogen solubility was low enough to be considered insignificant (<0.01 M) compared to the capacity of the

solution for ethylene and ethane. For this reason, at the beginning of an absorption experiment, the excess nitrogen pressure was vented to atmospheric pressure before the absorption gas was introduced. The resulting implication of this procedure was that the gas phase in the autoclave was a two-component mixture made up of primarily the charged absorption gas but still containing 1 atm of nitrogen.

To begin an absorption equilibrium experiment, the initial pressure and temperature of both the gas bomb and the autoclave were recorded. The shutoff valve separating the two vessels was then opened to allow the desired amount of gas into the autoclave vapor space, and the valve was immediately closed again. Due to the sharp increase in pressure of the autoclave vapor space, the temperature was observed to show a sharp increase (usually ~2ºC) immediately after charging the gas which made an accurate temperature reading difficult. The autoclave gas temperature then gradually decreased as the system returned to thermal equilibrium. Up until this point, the liquid stirrer was still off, so it was assumed that the amount of gas absorbed into the liquid until the stirrer was turned on was negligible. Following about a one-minute delay after charging the gas, the autoclave temperature had stabilized enough to record an accurate value, and the charged autoclave conditions for calculations were recorded at this point.

After recording the charged autoclave pressure and temperature, the stirrer was turned on, and the conditions were recorded periodically. The stirrer speed was set to a high enough value to reach absorption equilibrium within an hour or two. The actual speed of the stirrer was recorded periodically with a Fisher digital tachometer that measured the rpm of the outer magnetic rotor of the stirrer assembly with a strip of reflective tape. The precision of the digital tachometer was ± 1 rpm at lower speeds (50 – 300 rpm) and ± 5 rpm at higher speeds (> 600 rpm). By examining the pressure data with time, the approach to equilibrium was observed when the rate of pressure change became very slow. Eventually, a steady condition was obtained where the pressure no longer changed as seen in Figure 3-11 for the

pressure reading with time. Once the final equilibrium conditions were recorded, the stirrer was stopped and the solution either regenerated or kept for a subsequent absorption experiment.

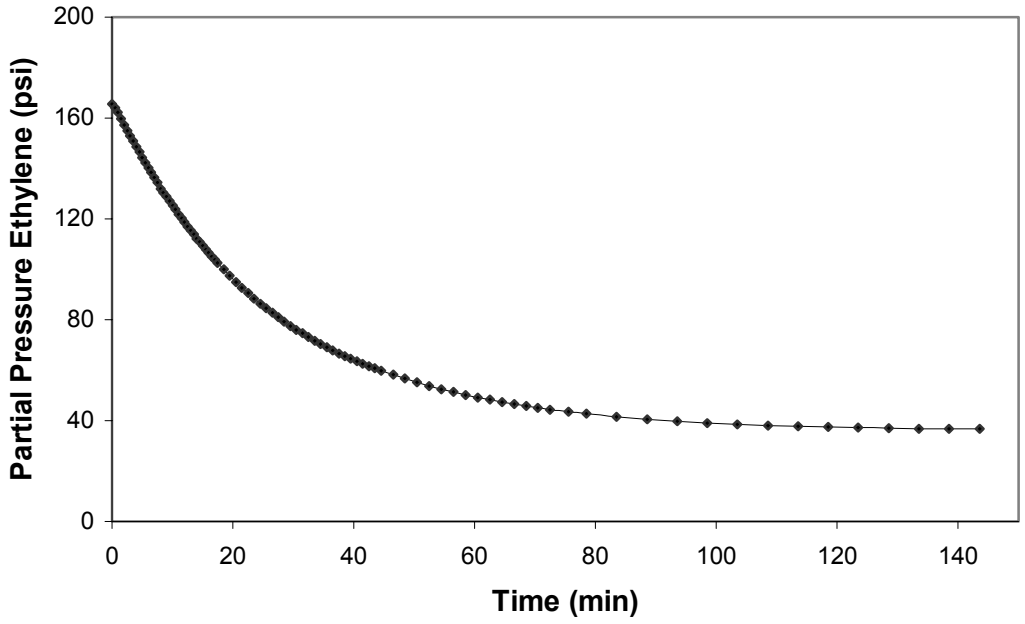

Figure 3-11. Pressure profile of a typical ethylene absorption experiment

To calculate the amount of absorbed gas at equilibrium or at any time during the experiment, a mass balance was used to relate initial moles of gas in the charged autoclave with moles of gas in the vapor space at the final conditions.

$$n_{\text{absorbed}} = n_{\text{autoclave, charged}} - n_{\text{autoclave, time}} \tag{3-6}$$

$$n_{\text{absorbed}} = \frac{V_{\text{autoclave}}}{R}\left(\left(\frac{P}{ZT}\right)_{\text{autoclave, charged}} - \left(\frac{P}{ZT}\right)_{\text{autoclave, time}}\right) \tag{3-7}$$

where the autoclave volume can be found by equation (3-5) using the initial and charged conditions of the experiment or by subtraction of the liquid volume from the value calculated from the empty autoclave (533 mL). The first method was preferred

because it was able to account for changes in liquid volume due to losses from liquid sample withdrawal or vaporization losses during regeneration. The agreement between the two methods of calculating the autoclave vapor volume was within 3% for nearly all cases without liquid loss. Since it was not sufficiently accurate to assume the gas was ideal, the compressibility, *Z*, was calculated for each condition by the three-parameter Prausnitz and Pitzer correlation as developed by Smith, Van Ness, and Abbott [97].

$$Z = 1 + \frac{B \cdot P}{R \cdot T} \tag{3-8}$$

where *B* for a binary mixture is defined by the following equation.

$$B = y_1^2 B_{11} + 2 y_1 y_2 B_{12} + y_2^2 B_{22} \tag{3-9}$$

The virial coefficient B_{ij} characterizes a bimolecular interaction between molecule *i* and molecule *j*, and *y* represents the mole fraction in the gas mixture. The coefficients B_{ij} can be found by the following equation

$$B_{ij} = \frac{RT_{cij}}{P_{cij}} \left(B^0 + \omega_{ij} B^1 \right) \tag{3-10}$$

with the *ij* terms defined as follows

$$T_{cij} = \left(T_{ci} T_{cj} \right)^{1/2} \left(1 - k_{ij} \right) \tag{3-11}$$

$$P_{cij} = \frac{Z_{cij} R T_{cij}}{V_{cij}} \tag{3-12}$$

$$Z_{cij} = \frac{Z_{ci} + Z_{cj}}{2} \tag{3-13}$$

$$V_{cij} = \left(\frac{V_{ci}^{1/3} + V_{cj}^{1/3}}{2} \right)^3 \tag{3-14}$$

$$\omega_{ij} = \frac{\omega_i + \omega_j}{2} \tag{3-15}$$

where the subscript c denotes critical values from a physical property database, ω is the acentric factor of the gas, and k_{ij} is the binary interaction parameter specific to each binary pair. Since k_{ij} was not found for nitrogen/ethylene, nitrogen/ethane, or ethylene/ethane, it was set to 0. Expressions for B^0 and B^1 which are functions of the reduced temperature, $T_r = T/T_c$ are given here for a specific component.

$$B^0 = 0.083 - \frac{0.422}{T_r^{1.6}} \tag{3-16}$$

$$B^1 = 0.139 - \frac{0.172}{T_r^{4.2}} \tag{3-17}$$

Calculating Z by the preceding equations is straightforward for the state when the autoclave was first charged. Since the pre-charged autoclave was assumed to contain only nitrogen gas in the vapor space and the gas bomb contained a gas of known composition, the number of moles of each species was known for the charged state. The mole fraction for the beginning of the experiment is easily calculated.

$$y_i = \frac{n_i}{n_{total}} \tag{3-18}$$

However, once gas begins to be absorbed into the liquid, the number of moles of absorbed gas is no longer known. By making the assumption that the nitrogen is not absorbed, the mole fraction of each component can be solved by iterations in an Excel spreadsheet. To converge on the solution, the mole fraction of absorbed gas is adjusted until the calculated number of moles by the compressibility factor is equal to the value obtained by the mass balance. A sample iteration for the mole fraction of gas in the vapor phase is given in Appendix A.2. Thus each pressure reading during the course of an experiment will have a different value of Z and mole fraction corresponding to the amount of gas absorbed at that particular point in the experiment.

For the absorption equilibrium experiments where the bomb was filled with a mixture of ethylene and ethane instead of a pure gas, it was not possible to

differentiate mathematically the quantity of each gas absorbed. These experiments required additional information from analytical results of either the gas or liquid phase composition as described in section 4.5.2. These results combined with the above mass balance convergence technique proved useful for quantifying the equilibrium absorption of mixtures.

3.2.3 Procedure for absorption kinetics experiment

The procedure for an absorption kinetics experiment was nearly identical to that for an equilibrium experiment. The two main differences between the kinetic and equilibrium experiments were the initial autoclave composition and the stirrer speed. For the equilibrium experiments, 1 atm of nitrogen was present in the autoclave upon charging the absorption gas; however, in order to avoid any gas phase mass transfer resistance, the kinetic experiments were performed with only the absorption gas. By beginning the experiment with the same gas that was to be charged, the calculation of gas phase composition was greatly simplified because the gas consisted of only a single component. The drawback to starting with the absorption gas already in contact with the liquid solution is that the system has a significant absorption capacity at atmospheric pressure. To minimize the possibility of pre-absorbed gas in the liquid solution, the regeneration step was performed immediately before the kinetic experiment. By fully regenerating the solution such that the amount of absorbed gas in the liquid was assumed to be approximately zero, the kinetic experiment was performed with pure absorption gas and no gas phase mass transfer resistance.

Before charging the absorption gas to the autoclave, the stirrer speed was adjusted and set to the desired value. After the gas was charged and the one-minute delay for the charged gas reading, the stirrer was turned on and measurements were taken at very short intervals. For the beginning of the experiment, pressure and temperature readings were recorded every 10 to 15 seconds. The stirrer speed was also checked frequently to ensure that the motor was not drifting from the initial

speed. Typical stirrer speeds for the kinetic experiments (between 100 and 300 rpm) were much lower than the equilibrium experiments (between 600 and 800 rpm) because higher stirrer speeds caused distortions in the flatness of the liquid interfacial area. Results confirming the flatness of the gas-liquid interface are given in section 7.2.

As the change in autoclave pressure with time decreased due to the system approaching equilibrium, the pressure and temperature readings were taken less frequently. Eventually, the pressure change with time became very small, and the kinetic experiment was completed by increasing the stirrer speed to quickly reach the equilibrium condition. Calculation of the amount of gas absorbed at any given time was done by equation (3-7), and this data was used to compare different kinetic models as detailed in section 7.3.

3.2.4 Procedure for regeneration of absorption solution

Once a liquid solution has absorbed ethylene (or ethane), it can be regenerated for a subsequent experiment by driving off the absorbed gas. Conditions favorable for solution regeneration are increased temperature and/or reduced pressure. A different procedure for each of these two regeneration conditions was used throughout the experimental research. The high temperature regeneration consisted of venting the vapor space of the autoclave through a water-filled flask in the fume hood, turning on the stirrer, and turning on the autoclave heater to slowly increase the temperature. Since the autoclave thermocouple was in the vapor space and not the liquid, the usual practice was to supply power to the autoclave heater over short time intervals and allow the system to approach thermal equilibrium before supplying additional heat. With this technique, accidental flashing of the liquid solution, which could lead to excessive solution losses, was avoided. As the temperature of the system increased, the rate of gas bubbles emerging from the vent tube in the water-filled flask could be monitored. Gas bubbles were produced mainly from desorbing

gas, but a small fraction of bubbles were due to the gas expansion caused by the heating of the autoclave vessel. Quantification of the total gas volume that escaped was unsuccessful due to limitations in gas flowrate measuring equipment on hand.

Once the temperature of the autoclave reached around 70ºC, the amount of gas escaping as bubbles in the water-filled flask had greatly decreased. The autoclave was further heated to near 90ºC where gas no longer evolved from the autoclave. The vent valve was then closed, and the heater and stirrer were turned off. Immediately afterwards, the autoclave was filled with 100 psig of nitrogen and vented. This nitrogen fill/vent step was repeated two more times to purge the ethylene gas, so when the system cooled back down, there would be no possibility of re-absorption of ethylene. After purging with nitrogen, the autoclave was allowed to cool back to room temperature. Since accelerated cooling capabilities were not available, the heating regeneration technique limited the number of absorption experiments able to be performed to one per day. Strictly speaking, some degree of absorbed gas was still in the liquid corresponding to the solubility at 90ºC, but this capacity was beyond the quantitative capability of the autoclave experiment. In fact, a comparison of the absorption capacity of the regenerated solution was equivalent to that of the freshly prepared solution.

The other regeneration technique did not involve heating the solution but instead consisted of successive evacuation steps. By opening the valve to the vacuum pump, the pressure on the system was pumped down to the vapor pressure of the system. The shutoff valve to the vacuum pump was closed immediately after the pressure had decreased to the minimum, and the stirrer was turned on. Stirring facilitated gas desorption until a new equilibrium condition was reached. Once the new equilibrium condition was reached, the stirrer was stopped, and the vacuum line was re-opened. The procedure was repeated until the increase in pressure upon mixing was negligible. The total number of required evacuation cycles was usually between 5 and 10 for ethylene and between 3 and 5 for ethane. One advantage of this

technique was that an additional experiment could be performed immediately without waiting for the autoclave system to cool to room temperature. Like the heating technique, the evacuation technique still resulted in a liquid solution containing the amount of gas corresponding to the equilibrium pressure obtained in the evacuation. The amount of gas remaining in solution (<0.01 M) was too small to be accurately measured by the autoclave technique; therefore, it was negligible compared to the amount of gas absorbed in the successive absorption experiments.

The heating method of regeneration was usually used between absorption equilibrium experiments with ethylene. Since absorbed ethane was solely due to physical solubility (no chemical complexation), heating the solution was not preferred because the heating method required much more time and attention than the evacuation technique. For kinetic experiments, it was undesirable for the autoclave to contain nitrogen as previously discussed, so for ethylene and ethane regeneration during kinetic studies, the evacuation method was preferred. When the evacuation method was used to regenerate solutions treated with ethylene gas, the amount of time and number of cycles required was far greater than the ethane cases due to the additional difficulty of breaking the π-complex over physical solubility alone. Both techniques suffer the possibility of solvent or ligand losses due to vaporization at the regeneration conditions. By calculating the autoclave volume using equation (3-5) for successive absorption experiments, the magnitude of losses for each technique can be quantified. As shown in Figure 3-12, neither technique showed an obvious trend in liquid loss. In order to smooth out the inherent ± 3% error in the autoclave volume calculation, an average volume was used once all experiments for a given liquid system were completed.

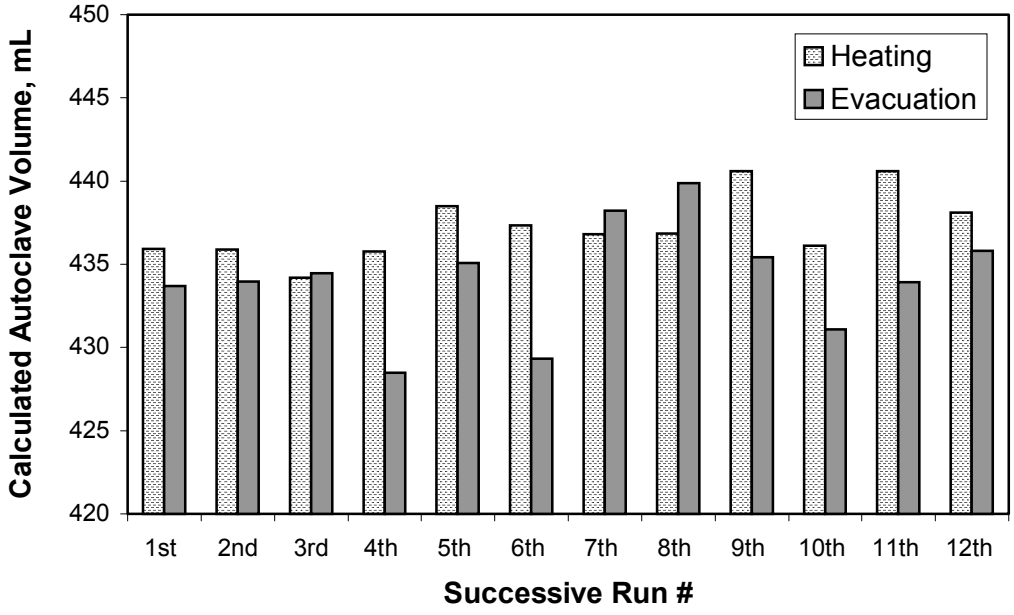

Figure 3-12. Liquid volume losses for successive regenerations

3.3 Continuous absorption/regeneration process

In order to investigate the ethylene/ethane separation capability of the absorption solution, an experiment was designed for continuous operation by means of a small-scale process. The setup shown in Figure 3-13 consisted of a gas absorption side and a solution regeneration side. The experimental equipment and procedures for the continuous process are described here.

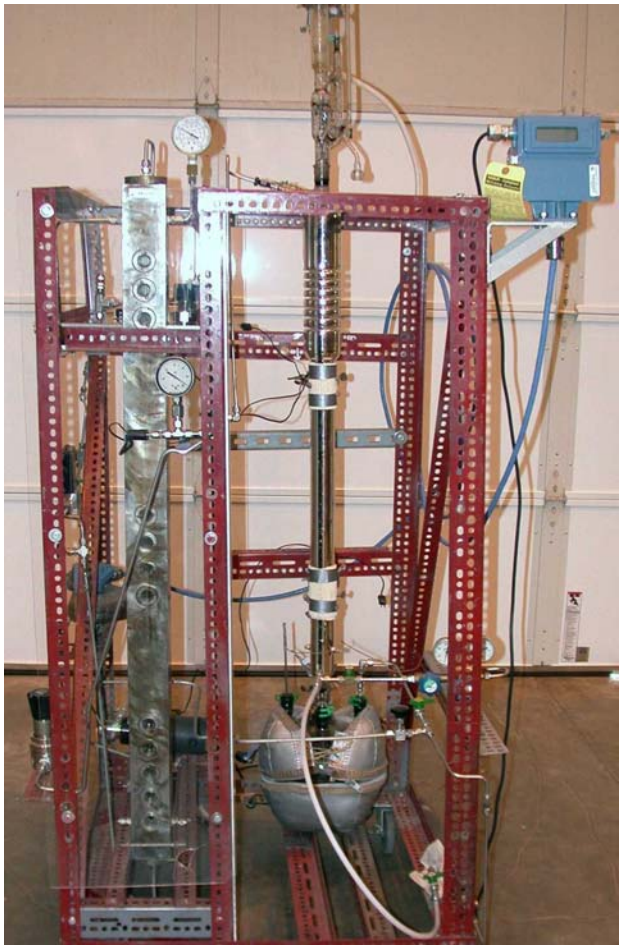

Figure 3-13. Photograph of continuous absorption/regeneration process

3.3.1 Equipment for continuous absorption/regeneration process

A complete flow sheet of the continuous process is shown in Figure 3-14. The absorption section on the left consisted of feed gas cylinders, gas and liquid flowmeters, absorption column, back pressure regulator, and all associated valves and tubing. The regeneration section on the right consisted of back pressure regulator, regeneration column, condenser, heated holding flask, concentric tube heat exchanger, liquid pump, and all associated valves and tubing.

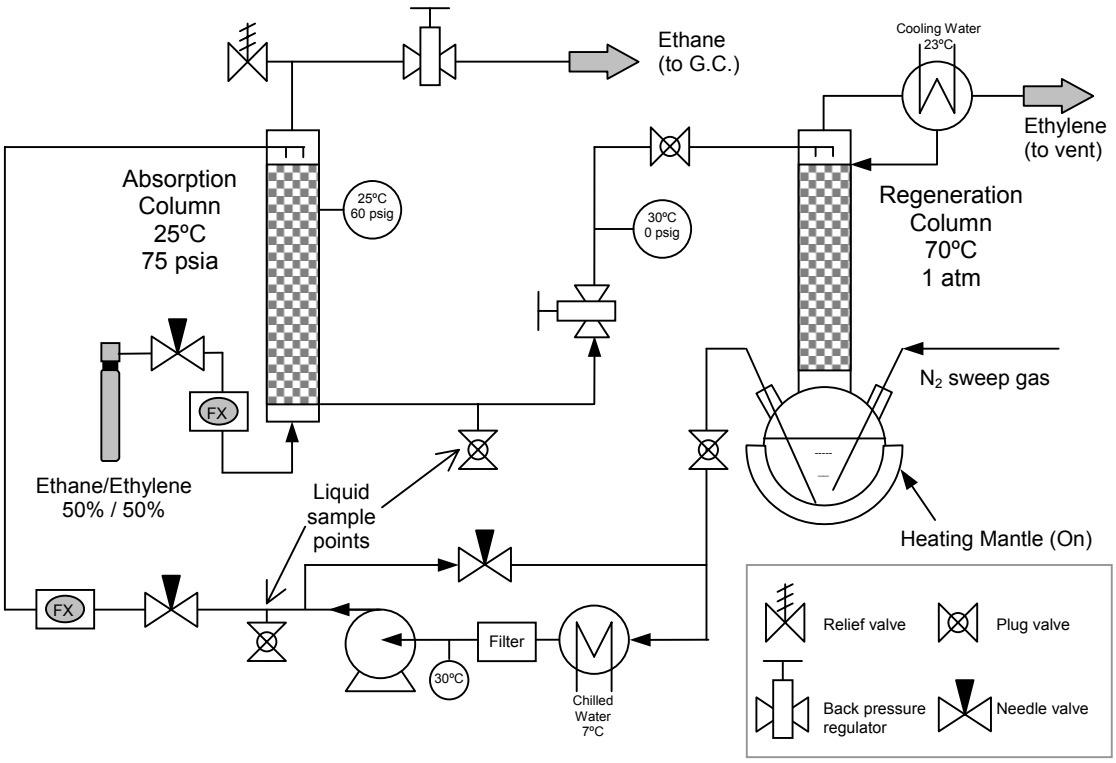

Figure 3-14. Flowsheet of the continuous process

For the continuous absorption/regeneration experiments, two different feed gases from Air Liquide were used: a 30/70 molar mixture of ethylene/nitrogen and a 50/50 molar mixture of ethylene/ethane. Impurities in these gases were not listed. The gas flowmeter was a MKS model 258C thermal conductivity mass flowmeter with a maximum flowrate of 50 SLPM (standard liters per minute) of nitrogen and a maximum operating pressure of 150 psi. The accuracy of the meter was given as 0.8% of full-scale range (or 0.4 SLPM). In order to use the flowmeter with gases other than nitrogen, calibrations were performed with a soap bubble flow meter (1000 mL capacity). The setup and results of these calibrations are given in Appendix A.3. The liquid flowmeter was a Micro Motion model CMF010 elite coriolis sensor with a maximum flowrate of 4 lb/min and a maximum operating

pressure of 400 psi. The accuracy of the liquid flowmeter was given as 0.10% of the rate. Since the coriolis meter measures actual mass flow, calibration for use with the absorption liquid was not necessary. The accuracy of the meter was checked before the experiments were begun by timing a given volume of NMP, and the results were satisfactory.

The absorption column was a specially made piece of equipment designed for high pressure use in a previous research project. It was a solid 3.5" x 3" x 50.5" stainless steel bar with a one inch hole bored through the center. According to original design specifications, the absorption column could withstand pressures up to 2000 psi; however, for this application, the column was operated at a pressure of 60 psig for all experiments. The top and bottom were fitted with a threaded screw assembly and rubber o-rings as shown in Figure 3-15(a). The gas inlet was a welded perforated steel bulb to which a cut section of a sieve plate was attached as shown in Figure 3-15(b) that also served as the packing support. The packing used in both columns was dumped ¼" perforated stainless steel rings as shown in Figure 3-16. The total height of the packing in the absorption column was 30". For the liquid inlet, ¼" stainless steel tubing was centered over the top of the packing, and no special efforts were made for liquid distribution since the inner diameter of the column was only 1". At the top of the column, a pressure gauge from US Gauge (200 psig) and the gas product were withdrawn via NPT threaded side ports. After exiting the column, the gas product was connected to a safety relief valve (with blue spring rated for 50-350 psig) and passed through a Tescom 500 psi back pressure regulator before the gas was released to the vent hood. The vent line was equipped with a tee fitting with a septum for gas sampling. The front and back of the absorption column contained 12 ports spaced in groupings of 3, 4, and 5 at the top, middle, and bottom of the column, respectively. These versatile ports were used for quartz sight glass windows, a type-J thermocouple, steel plugs (shown in Figure 3-17), and liquid withdrawal at the bottom.

(a) (b)

Figure 3-15. End plugs for absorption column

Figure 3-16. Packing used in absorption and regeneration columns

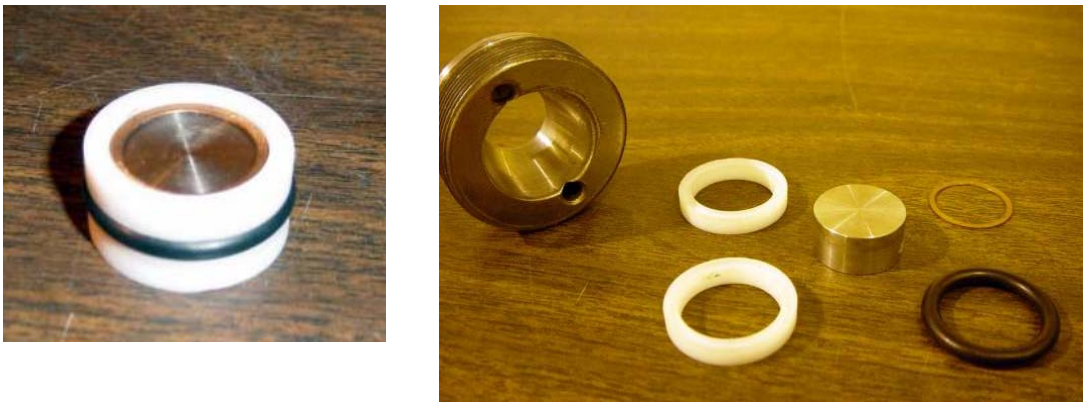

Figure 3-17. Components for port in absorption column (steel plug shown)

After exiting the bottom of the column, the absorption liquid was passed through a tee fitting where a liquid sample could be withdrawn (sampling technique is fully discussed in 3.3.2). Then the liquid line was passed through a Tescom 500 psi back pressure regulator before entering the regeneration column. Also along the feed line to the regeneration column were a pressure gauge from US Gauge (60 psig) and a type-J thermocouple. The regeneration column was a silver-coated (exterior), vacuum-jacketed glass column from Ace Glass. The column had a one-inch inner diameter, and it was packed with 33.5" of the same random packing as the absorption column. The top and bottom of the column were size 29/42 ground glass joints. At the top of the column, the liquid inlet was a custom made take-off adapter with the feed entering at 15º above the horizontal plane as shown in Figure 3-18. Above the liquid feed, a condenser with flowing cooling water (at 23ºC) was in place to condense any vaporized absorption solution. Due to the low vapor pressures of NMP and aniline as mentioned earlier, no condensed material was ever observed; therefore, in retrospect the condenser was not a necessary piece of equipment. The gas outlet from the condenser was routed to the vent hood, so the regeneration section was maintained at atmospheric pressure.

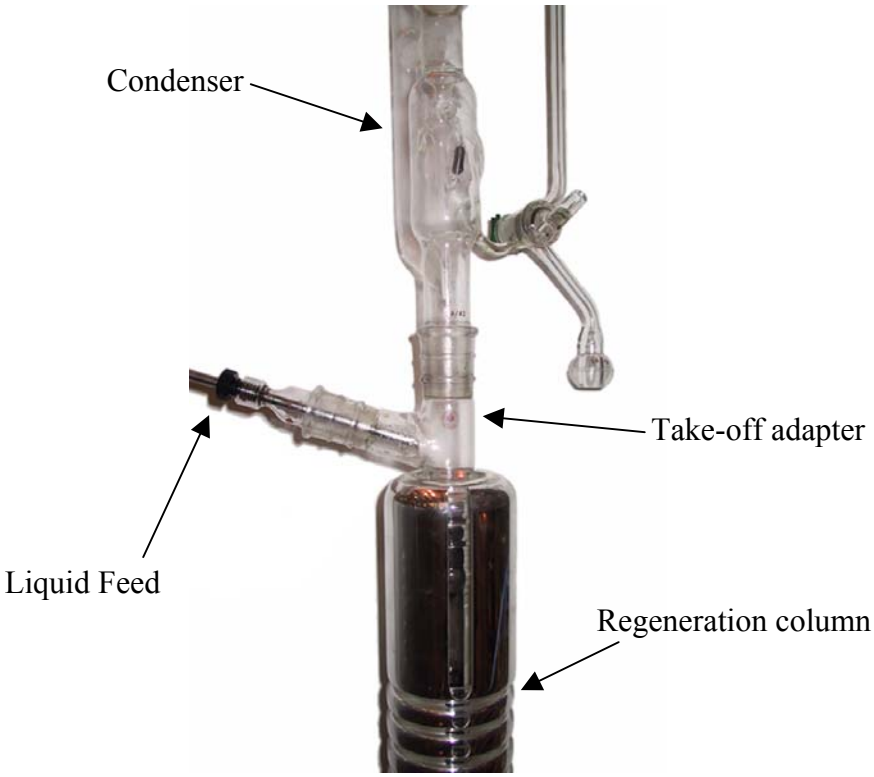

Figure 3-18. Liquid feed configuration in regeneration column

At the bottom of the regeneration column, a four-neck 4L round bottom glass flask was used as a holding tank for the solution. The flask was enclosed in a heating mantle where heat was supplied to release any non-flashed ethylene (or ethane). A type-J thermocouple was inserted through one of the necks of the flask into the liquid phase, and the temperature readout was wired to a Love controller that cycled the heating mantle to keep the flask contents at a specified temperature. Another neck of the flask was connected to a nitrogen line regulated from the PRC Bldg. 133 house supply line. This gas was introduced below the liquid level in order to help strip the complexed ethylene and to provide a continuous sweep gas so that no air diffused into the system from the open vent line. The liquid solution was removed via a dip tube into the bottom of the flask and passed through a concentric tube heat exchanger like

that shown in Figure 3-19. The heat exchanger was a homemade shell and tube type with the hot absorption liquid passing through the inner ¼" stainless steel tube while chilled water (at 7ºC) passed through the annular ½" stainless steel tube. The design of the exchanger called for a length of 6 feet and the calculations are given in Appendix A.4.

Figure 3-19. Concentric tube heat exchanger prototype

After the heat exchanger, the liquid was passed through a Nupro filter (140 micron mesh size) to remove any solids and avoid attrition damage to the pump gears. The filter was checked frequently, but no evidence of trapped solids was ever observed. Another type-J thermocouple was in place after the filter to monitor the heat exchanger's effectiveness. Next the liquid was pumped up to absorption pressures by a Tuthill D-series variable speed gear pump. Due to chemical compatibility issues, the pump was fitted with polyphenylene sulfide gears and bearings and ethylene-propylene o-rings and seals. The maximum flowrate of the 1/10 hp motor was given as 378 mL/min at 3500 rpm, and the pump speed could be varied from 40 to 3600 rpm. The pump effluent was passed through a tee fitting where the flow could bypass the absorption and regeneration columns and pass through a needle valve back through the heat exchanger. This bypass allowed for shutting off or reducing the absorption column feed without the need to stop the pump or greatly reduce its speed. The regenerated liquid solution fed to the absorption column was passed through another tee fitting where a liquid sample could be withdrawn for analysis.

3.3.2 Procedure for continuous absorption/regeneration experiment

To begin the experiment, the entire apparatus was thoroughly purged with nitrogen for 8 hours, and flows of chilled and cooling water were started. After the nitrogen purge, the 4-neck glass flask was filled with the absorption solution by filling the solvent tank (from Figure 3-6(b)) in the glove box, pressurizing it with nitrogen to 40 psig, and using this pressure to expel the solvent from the tank into the glass flask. The solvent was then heated to the desired temperature of either 60 or 70ºC. After this temperature was reached the pump was turned on and the variable speed controller was used to adjust the liquid flow rate as needed for each experiment. The liquid flowrate was chosen based on the packed absorber design rule-of-thumb for a maximum flow of 10 GPM/ft^2, which is equivalent to 30 lb/hr. Most experiments were performed at liquid flowrates below this value at 20 lb/hr. The gas flowrate was chosen by experimentally measuring the flood point over a range of liquid flows and setting the vapor rate to 80% of the flood value. Some liberty was taken to adjust the conditions based on run results, and an effort was made to include combinations of the minimum, design, and maximum flowrates. Table 3-2 shows the full range of flow rates studied for each gas.

Table 3-2. Flow conditions studied

30% ethylene, 70% nitrogen				50% ethylene, 50% ethane			
Date	Liquid rate, lb/hr	Gas rate, SLPM	Regen. temp., ºC	Date	Liquid rate, lb/hr	Gas rate, SLPM	Regen. temp., ºC
6/18/03	20	5	60	8/6/03	15	3	60
6/18/03	30	5	60	8/6/03	20	3	60
6/20/03	20	5	60	8/7/03	20	5	59
6/20/03	20	5	60	8/7/03	20	1	60
6/25/03	20	5	60	8/7/03	20	2	59
7/16/03	2	5	70	9/16/03	15	3	60
7/16/03	5	5	70				
7/17/03	5	5	71				
7/17/03	30	5	66				
7/18/03	20	1	70				
7/23/03	5	5	70				
7/23/03	20	5	60				
7/25/03	20	5	60				
8/1/03	20	2	60				

The absorption gas flow and pressure were manipulated to maintain the desired gas flow rate and a column pressure of 60 psig. The column pressure was chosen based on equilibrium results suggesting that the maximum extent of chemical effects were observed around an ethylene partial pressure of 50 psia while the highest ethylene:ethane selectivity was realized at the sub-atmospheric pressures; therefore, for the 50% ethylene feed gas mixture at 75 psia, an ethylene partial pressure of 37 psia was nearly optimal based on the tradeoff for ethylene capacity and ethylene:ethane selectivity (see section 6.3.6 for details). Adjusting the cylinder regulator set the column pressure, and the gas flow rate was set by adjusting the back-pressure regulator on the vapor outlet.

The liquid flowrate out of the bottom of the absorption column was controlled by the back-pressure regulator on the liquid line between the two columns. In order to maintain a constant liquid level at the bottom of the absorption column, the level

was monitored closely by the sight glass windows at the bottom. Care was taken to maintain the liquid level within lower and upper limits. If the level decreased as low as the liquid outlet port, the absorption gas would escape into the regeneration column. If the level rose over the vapor inlet, then column flooding would begin to occur. Both of these scenarios were undesirable, so the liquid level was monitored at all times to maintain stable operation.

In the regeneration section, the nitrogen purge was set a low rate (approx. 1 SLPM) during the first experiments; however, results analysis (see section 8.2) showed that the regeneration of the solution was very inefficient. Improvements in ethylene recovery in the regeneration section were obtained with higher nitrogen rates (approx. 5 SLPM). After realizing that the nitrogen gas rate had a much larger effect on the ethylene concentration of the liquid feed than originally expected, the rate was set to just below the level that resulted in regeneration column flooding. This was accomplished by visual observation of the flood point at the top of the column. The lack of a flowmeter to quantify the nitrogen flow rate turned out to be a significant drawback when trying to explain run to run variations in liquid feed concentrations coming from the regeneration column. Additional column hydraulic experiments with the MKS flowmeter on the nitrogen feed line to the regeneration column showed a linear relationship between absorption solution flowrate and nitrogen gas flowrate. From Figure 3-20, the approximate value of the nitrogen gas flowrate could be found based on the known liquid flowrate and the fact that the column was operated right at the flood point. However, this correlation did not consider the volume of gas that was desorbing from the liquid solution in the actual experiment, so these values were only used for estimation purposes and not in any calculations of the material balance.

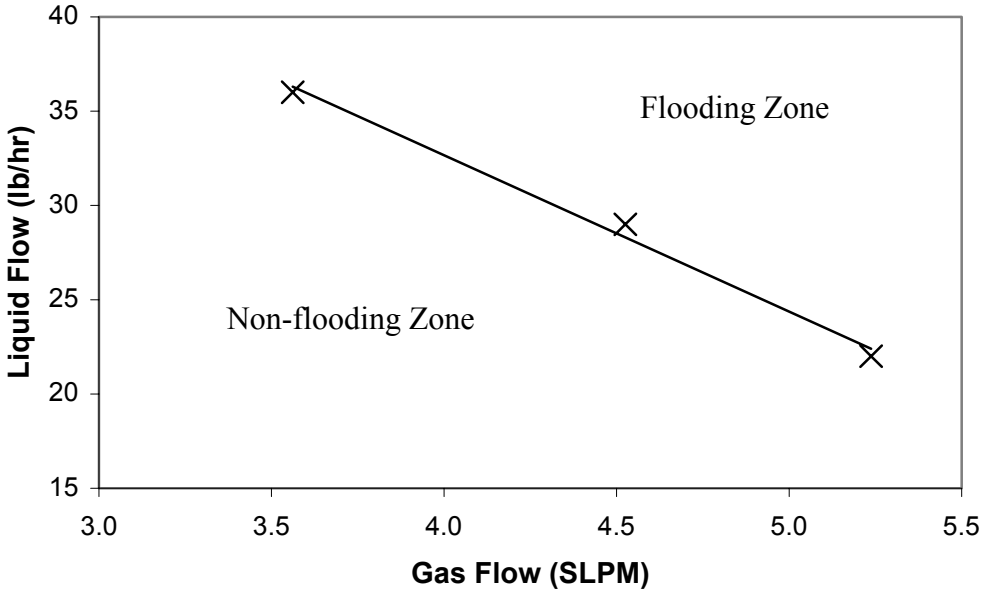

Figure 3-20. Regeneration column flooding with nitrogen gas

The continuous absorption/regeneration process was operated for approximately five times the liquid residence time in order to reach steady-state operation. The liquid residence time is simply the time required for circulation of the entire quantity of liquid in the system.

$$t_{\text{steady-state}} = 5 \cdot \left(\frac{\text{Volume}_{\text{total liquid}}}{\text{Q}_{\text{liquid}}} \right) \left[\frac{\text{cm}^3}{\text{cm}^3 / \text{min}} \right] \tag{3-19}$$

After steady operation for the specified time, samples were taken for analysis from the absorption column gas product, the liquid product, and the liquid feed. An exception to the five times liquid residence time procedure was made for the lowest liquid flow rate because the gas consumption was too great for the required five hours of operation. This case was run for 1.5 hours before a round of samples was taken, and an additional round of samples was taken afterwards to verify steady-state

operation. Before drawing the samples, all sample vials were crimped in the glove box and evacuated for five minutes by an 18-gauge needle attached to a vacuum line. The evacuated sample vials were then labeled and weighed on an analytical balance.

For the gas sample, a 10mL gas-tight syringe was used to pull an 8 mL gas sample from the gas outlet and inject it into a vial. The gas sample was always taken first because its withdrawal imposed no disturbance on the process. The liquid feed sample imposed the greatest disturbance on the absorption column, so this sample was always taken last. To pull a liquid sample, the dead space from the sample valve to the tee fitting was purged by opening the sample valve allowing the liquid to flow through a high-pressure drop tubing (40" of 0.030" ID PEEK tubing) for 8-10 seconds. The purpose of the high-pressure drop tubing was to prevent any absorbed gases from flashing out of solution across the valve. The quantity of removed liquid was measured to be approx. 5 mL of liquid, while the total volume of dead space in the sample line was less than 1 mL. The high-pressure drop tubing was then quickly removed and replaced with a clean 18-gauge needle. An evacuated vial was placed on this needle, and the sample valve was quickly opened and closed causing a small amount of liquid to enter this vial. This procedure is shown graphically in Figure 3-21. The filled vials were then reweighed on the analytical balance, and the samples were stored overnight in a refrigerator before being taken to Sasol's analytical laboratory for analysis the next day.

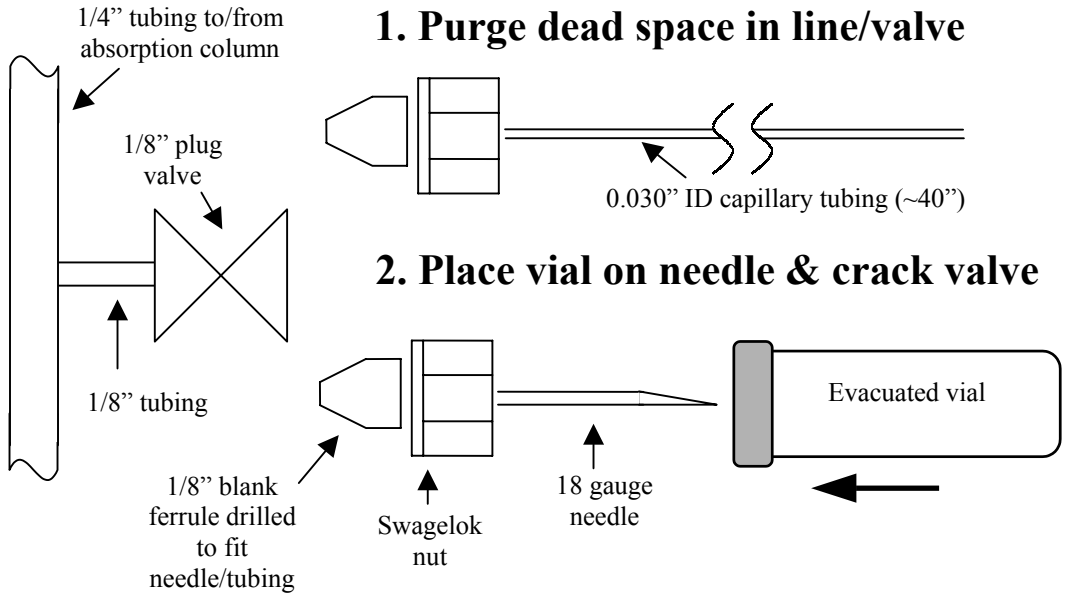

Figure 3-21. Liquid sample procedure

Once the sampling of the absorption section was complete, the gas flow to the absorption column was switched to nitrogen and the regeneration flask heater was turned off. Circulation of the solution was continued until the flask temperature decreased below 40ºC for ease in handling. The pump was then stopped and the nitrogen pressure was used to empty all liquid lines to the regeneration flask. The contents of the regeneration flask were then pumped back into the metal solvent tank via a connection to the liquid feed sample valve. The solvent was stored back in the glove box in the metal solvent tank when not in use to prevent its degradation by oxidation.

Chapter 4.
Analytical Techniques

4.1 Analytical requirements

Analytical support was needed in instances where the information present was insufficient to accurately find results. The first useful application of analytical support was in validation of copper molarity in prepared solutions. Since solutions prepared in the glove box were mixed and heated in an open environment (for instance, when adding the copper salt) and later filtered for solids removal, the exact molarity of copper in the solution could not be precisely stated from the measured weights and density. In order to more accurately quantify the amount of copper in a given volume of solution, flame atomic absorption (flame AA) was performed on the prepared solution. The other obvious requisite for analytical support was in measuring the quantity of absorbed gas in solution. For closed systems like the autoclave equilibrium experiments, the ethylene concentration in the liquid could usually be calculated from a mass balance; however, with open systems like the continuous absorption/regeneration process, the knowledge of the ethylene concentration in the liquid could not be calculated from other variables. Three different techniques were investigated to find a reliable way to quantify ethylene absorbed in the liquid phase. Fourier transform infrared spectroscopy (FTIR), ultraviolet-visible spectroscopy (UV-Vis), and headspace gas chromatography (HS-GC) were all studied, but successful application was only found with HS-GC. These analytical techniques will be discussed along with the reasons for choosing one over the others. Traditional gas chromatography (GC) was sufficient for vapor analysis, and since it is a universally familiar and straightforward technique, the discussion of GC will only be mentioned as it applies to other techniques.

4.2 Flame AA

To verify the total copper concentration of an absorption solution, flame AA experiments were conducted in the analytical chemistry laboratory in Welch Hall. With flame AA, no differentiation is possible among different ionic valences of copper, so the reported metal concentrations include all Cu^0, Cu^+, and Cu^{2+} present in solution. Due to the experimental simplicity of the technique, no problems were encountered in acquiring accurate and reliable results.

4.2.1 Experimental setup

The instrument was a Perkin-Elmer 3110 Atomic Absorption Spectrophotometer with an air-acetylene flame (~2300ºC). The light source for this experiment was a constant current hollow cathode copper lamp. Vaporized sample atoms in the flame absorbed light, which was then passed into a monochromator set at 325.2 nm, the strongest absorption line for copper. A photomultiplier detector that measured light intensity quantified the amount of absorbed light. The slit width was set to 0.7 mm, the slit height to high, the lamp current to 15 mA, and the integration time to 3 sec. The nebulizer uptake was set to approx. 3-4 mL/min in order to adequately aspirate the samples. For each data point, the instrument collected three replicate readings and reported the values, the average, and standard deviation of the readings.

4.2.2 Results

The degree of absorption is directly proportional to the amount of copper in solution, so a calibration curve was constructed with a standard solution. The standard copper solution was prepared in the glove box beforehand by simply mixing the ingredients in a 50 mL volumetric flask. The molarity of the standard solution was 0.0119 M copper chloride and 0.0498 M aniline diluted with NMP. Since this solution was 100 times more dilute than the normally prepared solution, it contained

no solids and did not require heating or filtration. The standard was diluted with additional NMP to varying degrees such that the concentration of the diluted unknown was within the range of the standard dilutions. The estimated value of the unknown concentration was calculated by the solution preparation procedure to be approximately 1.16 M copper chloride. This unknown solution was diluted 10^4 times in order for the atomic absorption reading to be within an appropriate scale. In addition to the standard dilutions and the unknown solution, a blank solution was prepared by diluting the same quantity of aniline with NMP without the copper salt. By running this blank solution, any absorption resulting from species other than the added copper would be observable.

At the beginning and at the end of the flame AA experiment, the blank solution was run showing zero absorbance for each case; therefore, there were no copper contaminants in the solvent/ligand system that would lead to inaccurate results. The standard dilutions were run in order of increasing copper concentration from most dilute to most concentrated with the unknown also placed in order at the estimated concentration. The calibration curve of the standard dilutions and the absorbance of the unknown are shown in Figure 4-1. From the calibration curve, the molarity of the diluted copper unknown was 1.13×10^{-4} M, so the copper molarity of the prepared absorption solution was 1.13 M with an uncertainty of ± 0.03 M. Comparing the concentration found with flame AA with the approximate value from the solution preparation (1.16 M), very good agreement was found with the expected value. Additional flame AA experiments were performed on solutions withdrawn from the autoclave after a series of equilibrium experiments. For another CuCl:aniline:NMP solution and a CuCl:aniline:DMF solution, the agreement between flame AA and expected copper concentration was within 10%.

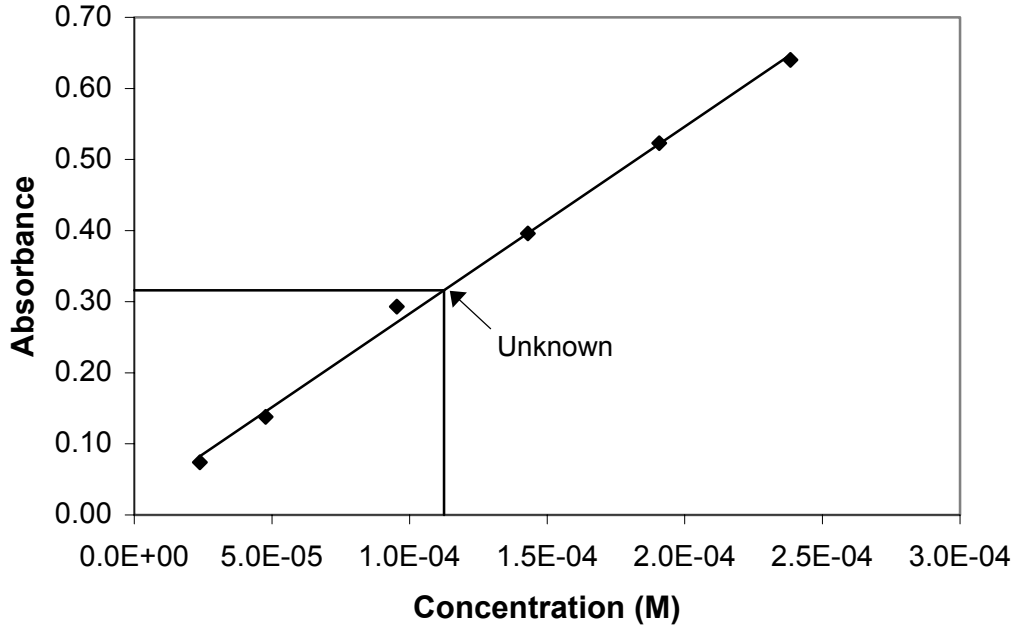

Figure 4-1. Flame AA results for copper molarity

4.3 FTIR

An early attempt to quantify ethylene in the liquid phase was made with FTIR. Literature results for silver-based systems suggested that the amount of complexed ethylene could be quantified by the peak area of the carbon-carbon double bond stretching frequency [102]. Due to the observation that the complexed ethylene exhibited a shift to a lower frequency than non-complexed ethylene [87], it was also expected that the ratio of physically absorbed to chemically absorbed ethylene could be quantified. However, operational difficulties were encountered when liquid analysis of a DMF based solution proved to be chemically incompatible with the ZnSe FTIR crystal. While these problems could very likely have been overcome with additional resources, the decision was made to find a technique that would not require purchasing costly replacement crystals for the FTIR analysis.

4.4 UV-Vis

The next analytical technique utilized to try to quantify ethylene in the liquid phase was UV-Vis. Traditional UV-Vis has the advantage of operational simplicity and a wide library of spectra for different species. Experimentally, the copper solution only contacted the quartz sample cuvet, so there was no concern about the chemical compatibility issue present with FTIR. Support for UV-Vis to observe copper-ethylene complexes is ambiguous in the literature. The existence of a copper(I)-ethylene complex in aqueous solution was shown to have a large absorption band at 228 nm and a smaller peak at 270 nm [9]. Geiger and Ferraudi [31] showed that in methanol solutions, copper(I)-ethylene complexes showed absorption bands at 220 nm and 276 nm that decreased in area as the concentration of complexed ethylene decreased. These copper(I) complexes were not stabilized by coordinating ligands but were prepared by vigorously mixing a solution of $Cu(CF_3SO_3^-)_2$ and copper powder in an ethylene atmosphere for several hours. On the other hand, Munakata et al. showed that copper(I) complexes with macrocyclic coordinating ligands like those shown in Figure 2-6 yielded a featureless spectrum when complexed with ethylene [80] or CO [64]. They also stated that copper(I) complexes generally provide no absorption bands in the visible spectrum. Likewise, Jacobson et al. [54] found that CO complexation with copper(I) polydentate ligands produced a featureless UV-Vis spectrum. The present copper(I)-ethylene solution was not exactly like any studied previously, so it was unknown beforehand whether the complex would show absorption bands or not.

4.4.1 Experimental setup

UV-Vis experiments were performed on two different spectrophotometers, Cary 300 and Hewlett-Packard 8453, and spectral data from the two instruments showed excellent consistency. The Cary 300 instrument passed light of a controllable wavelength through a sample and measured the transmission of the light over a range

of wavelengths from 800 to 200 nm. At 350 nm the light source was automatically changed from a tungsten (visible region) lamp to a deuterium (ultra violet region) lamp. The HP 8453 instrument subjected the sample to the entire range of wavelengths simultaneously and used a linear photodiode array detector to measure the absorption data much faster than the monochromatic method. This instrument also used a tungsten lamp and a deuterium lamp as the light sources. The sample setup usually consisted of a rectangular 1 cm quartz cuvet. In a later effort to reduce the absorbance scale without further diluting the solution, a 0.1 cm path length quartz cuvet was used where noted.

Solutions were prepared in the glove box at the Pickle Research Center and diluted to the desired concentration before being transported to the UV-Vis experiment at the UT Austin main campus. The dilution solvent was initially chosen as NMP in order to avoid complicating the mixture; however, methanol was later used as a better alternative as discussed below. For ethylene complexed solutions, the pre-diluted solution was contacted with ethylene gas at 1 atm as shown in Figure 3-5. A portion of this complexed solution was diluted and placed in a sealed bottle until the UV-Vis experiment. The remainder of complexed solution was heated until the ethylene complexed solution was observed to produce bubbles from 50ºC to 80ºC. The portion of solution not contacted with ethylene showed no evidence of gas desorption under similar conditions. A series of experiments was also performed with CO complexed solution to compare to literature results. The procedure for sample preparation was the same as that for ethylene.

4.4.2 Results

Absorption spectra for pure NMP and pure methanol are shown in Figure 4-2. Pure NMP was found to absorb strongly in the region from 300 to 200 nm. Since this was thought to be a key region for the copper-ethylene complex, the solvent was changed to methanol. Fortunately, the copper solution was miscible in methanol at

the concentrations studied, and pure methanol showed very little absorption at wavelengths over 200 nm. With the Cary spectrophotometer, the spectrum for methanol was displayed without any data processing to other spectra. With the HP instrument, the methanol was treated as the blank run, and the absorbance for the other runs were corrected for the solvent absorbance. Recognizing this fact is helpful in interpreting the following results.

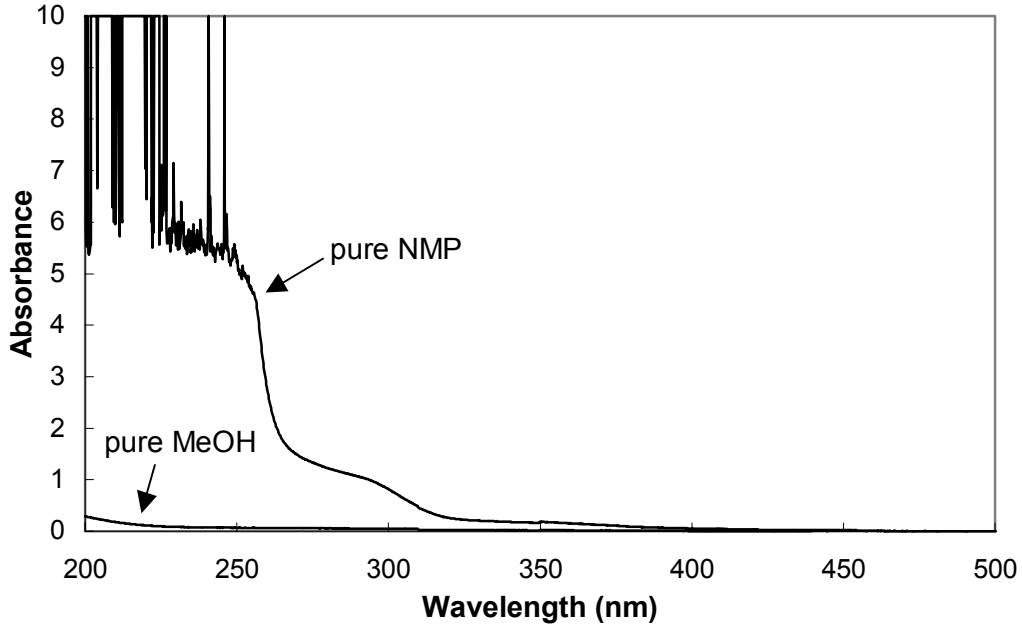

Figure 4-2. Solvent comparison. 1 cm cell, Cary 300

Both complexed and uncomplexed copper solutions were diluted with methanol at dilution factors of 100, 500, $1x10^3$, $5x10^3$, and $2.5x10^4$. The absorbance was off-scale for lower dilution factors, and not until the $2.5x10^4$ dilution were all of the peaks resolved. Comparison of the spectra for the different solutions is given in Figure 4-3. The solution that was complexed with ethylene (curve b.) showed no difference from the uncomplexed solution (curve a.). The uncomplexed solution showed slightly larger peaks than the ethylene complexed solution around 285 nm,

235 nm, and 206 nm probably due to minor experimental variations in the degree of dilution. In addition to these solutions, a copper-free solution (curve c.) was analyzed that contained aniline and NMP in the same ratio as the copper solutions. The same dilution in methanol was applied to this solution, and the spectrum was identical to the copper-containing solutions. The UV-Vis spectra was found to give no indication of copper(I) in solution much less the copper-ethylene complex. As a check on the reliability of the observed spectral data, the spectrum of aniline in methanol calculated from absorbance data is also shown in Figure 4-3 (curve d.) [69]. The literature values of absorbance, A, were given as a function of the cell path length, b, and the concentration of aniline, c, so that the molar absorptivity (or extinction coefficient), ε, could be calculated for each wavelength by equation (4-1) known as Beer's law, usually valid for c less than 0.01 M.

$$A = \varepsilon bc \tag{4-1}$$

Using the calculated values of ε and the concentration of aniline in solutions a.-c. (0.00018 M), values of A were calculated for each wavelength. The size and position of the peaks for aniline from the literature suggest that the experimental peaks at 285 nm and 235 nm are solely due to aniline. Comparison of curves c. and d. suggested that the peak at 206 nm is made up of contributions of aniline and NMP since aniline alone did not absorb as strongly as the mixture with NMP.

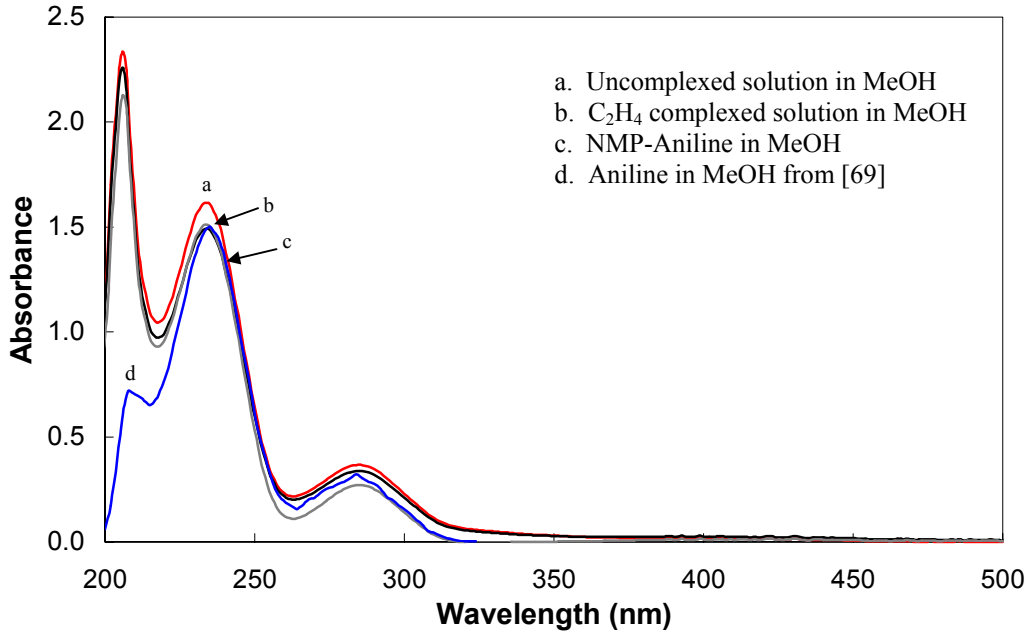

Figure 4-3. Ethylene complexation at $2.5x10^4$ dilution. 1 cm cell, HP 8453

A possible explanation for the lack of evidence of the copper-ethylene complex is because aniline and NMP are such strong absorbers that the copper-ethylene effects were hidden. Recall that literature results suggested the complex to absorb around 220 nm and 276 nm, but in these same regions, the aniline-NMP mixture showed strong absorbance. In order to resolve the peaks in this region, a high dilution factor was necessary. Possibly at lower dilutions, the complex contributed significantly to the total absorbance, but once the solution was diluted by a factor of $2.5x10^4$ the complex contribution was effectively washed out. To examine whether less dilution could be more effective, a cuvet cell with a shorter path length was used to reduce the absorbance with a lower dilution factor according to equation (4-1). This experiment was performed on solutions complexed with CO, uncomplexed copper solutions, and copper-free solutions of aniline and NMP all

diluted by a factor of $2.5x10^3$. Comparison of identical solutions with a 1 cm path length cuvet and a 1 mm path length cuvet is shown in Figure 4-4.

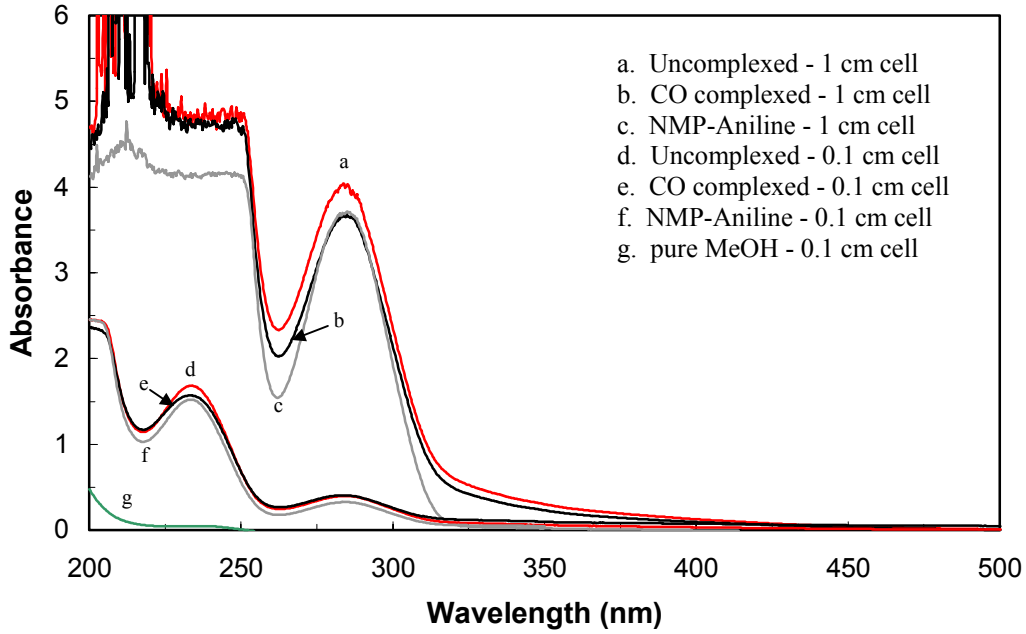

Figure 4-4. CO complexation at $2.5x10^3$ methanol dilution. Cary 300

Analysis of the spectra with the 1 cm path length cuvet showed that the absorbance was too strong especially for wavelengths less than 250 nm. The peak at 280 nm did not show as much interference, but there was no difference among the CO complexed (curve b.), uncomplexed (curve a.), and the aniline-NMP (curve c.) solutions. As noted earlier, this peak at 280 nm was likely solely due to aniline. By using the 0.1 cm path length cuvet, the absorbance for the peak at 280 nm was reduced by roughly a factor of 10 as expected from equation (4-1). The information at wavelengths less than 250 nm was greatly clarified with the shorter path length cell; however, the spectra were nearly identical to those from Figure 4-3. Since the solutions in Figure 4-3 are an order of magnitude more dilute and the path length an order of magnitude longer than those in Figure 4-4, the spectra should produce

equivalent values of absorbance. With the shorter path length, no difference was observed between the CO complexed case (curve e.), the uncomplexed case (curve d.), and the aniline-NMP case (curve f.). The only observable difference between the 0.1 cm cell spectra (with HP 8453) in Figure 4-4 and the 1 cm cell experimental spectra (with Cary 300) in Figure 4-3 was the behavior at the far left region. As mentioned earlier, the HP 8453 spectrophotometer subtracted the pure methanol absorbance from the later runs, but the Cary 300 did not perform any such data processing. From the pure methanol spectrum (curve g.) in Figure 4-4, the absorbance increased approaching the 200 nm wavelength. When this absorbance was subtracted from the values of the particular solutions in Figure 4-4, the results from the two instruments showed excellent agreement.

The lack of evidence for the copper-CO complex was not likely due to absorbance shielding from the aniline and NMP in the solution because the use of the 0.1 cm cuvet did not produce any more information than results at lower concentrations. If the shorter path length cell had shown the existence of peaks (or significantly larger peaks) for the complexed solutions over the aniline-NMP case, then it could be said that further dilutions may have shielded the complex peaks by the strongly absorbing aniline and NMP. Since this was not the case, the uncomplexed copper solution and the copper-ethylene and copper-CO complexes likely produce featureless spectra in the UV-Vis range as noted in references [80], [64], and [54]. Therefore, the use of UV-Vis as an analytical technique for complexed ethylene was appropriately abandoned.

4.5 HS-GC

Since the spectroscopic techniques proved difficult to implement effectively, a more straightforward approach was sought to analyze the liquid. Headspace gas chromatography was found to be the most effective technique for measuring ethylene absorbed in the liquid phase. HS-GC is generally preferred over traditional GC when

it is undesirable to inject the liquid directly onto the chromatography column because the liquid phase contains substantially non-volatile components. In the present chemical absorption solution, the copper ions are effectively non-volatile, and the ligand and solvent both have high boiling points that would require high GC temperatures and long elution times. In HS-GC practice, a small aliquot of liquid with volume V_S is placed in a large enough sample vial to allow for a significant volume of gas V_G to be in the headspace over the liquid as shown in Figure 4-5. The phase ratio β is given as the ratio of the volumes of the two phases present.

$$\beta = \frac{V_G}{V_S} \tag{4-2}$$

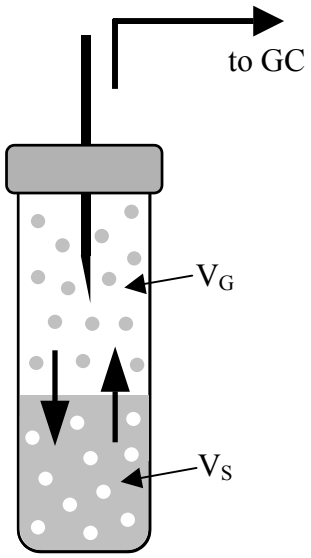

Figure 4-5. Headspace sample vial with analyte in VLE

The key principle behind the effectiveness of HS-GC is vapor-liquid equilibrium (VLE). By maintaining the sample vial at certain conditions for a long enough period of time, equilibrium is attained for the two phases. The volume of analyte transferred to the gas phase during equilibration is not considered to result in

an appreciable change in V_S [66]. At equilibrium, the concentrations of analyte in the liquid and gas phases, C_G and C_S respectively, are related by the thermodynamic equilibrium constant K, also called the partition (distribution) coefficient in chromatography (ignoring activities for the present discussion).

$$K = \frac{C_S}{C_G} \tag{4-3}$$

A material balance on the analyte can be used to relate C_G to the original concentration of analyte in the liquid sample C_o.

$$C_G = \frac{C_o}{K + \beta} \tag{4-4}$$

For a given system at constant equilibrium conditions, both K and β are constants.

$$C_G = (\text{const}_1) \cdot C_o \tag{4-5}$$

In traditional GC, the peak area A of an analyte is proportional to its concentration in the injected sample. In HS-GC, an aliquot from the vapor phase of the sample vial is withdrawn and injected onto the GC column, so that the concentration of the analyte C_G is related to the peak area by

$$A = (\text{const}_2) \cdot C_G \tag{4-6}$$

where the constant here is a function of the detector response factor and other parameters specific to the particular operation of the GC. Combining equation (4-5) and (4-6) yields a linear relationship between the original analyte concentration in the liquid and the peak area

$$A = (\text{const}_3) \cdot C_o \tag{4-7}$$

where the combined constant incorporates the GC parameters and the headspace constants. In order to acquire reproducible results in HS-GC analysis, the operating conditions contributing to the constant in equation (4-7) must be carefully controlled, especially the factors that determine the VLE in the sample vial [66]. A description

of the experimental setup and results obtained in quantification of ethylene and ethane in the copper absorption solution is discussed below.

4.5.1 Experimental setup

The experimental setup for HS-GC analysis was in place at Sasol's Austin Laboratory. The headspace autosampler was a Tekmar 7050 with rotating sample vial carousel. Each sample was equilibrated for 10 minutes at 90ºC before the vial was pressurized with carrier gas and a sample withdrawn into the 100 μL sample loop for injection into the GC. The GC was a Hewlett Packard 5890A with a flame ionization detector (FID) and a GS-Q, 30 m x 0.53 mm column. The column temperature was maintained at an isothermal temperature of 50ºC, and the helium carrier gas flow was automatically controlled so that the flowrate to the FID was maintained at 8.5 mL/min. When performing analysis at the Sasol lab, gas and liquid samples were analyzed at identical autosampler and GC conditions. In verification of the HS-GC technique, occasionally GC gas analysis was performed at the Pickle Research Campus on a GOW-MAC 550 with a thermal conductivity detector and a HayeSep A, 5' x 1/8" column. The sample loop volume was 0.5 mL; the detector and column were both set at 50ºC; and the bridge current to the detector was set at 115 mA.

The procedure for filling a vial with a liquid sample was discussed in section 3.3.2. The sample vial was a 22.4 mL glass container with a lip at the top for crimping with a PTFE coated butyl septum encompassed in an aluminum cap. After the filled sample vials' weights were recorded, the vials were placed in a refrigerator for storage until the next morning. The overnight storage was necessary because the only time of day that the HS-GC instruments were available was during the early morning hours. To begin the HS-GC analysis, the liquid sample vials were arranged on the autosampler carousel in order of increasing ethylene concentration. Following the liquid samples, the gas samples were arranged in the carousel in order of

increasing ethylene concentration until the very end where the gas standards were placed. The gas standards were prepared by inserting a tube into the bottom of a vial and delivering cylinder gas (either pure ethylene or the 50%/50% ethylene/ethane mixture) into the tube at a high flowrate (~10 SLPM) for about 60 seconds to purge air from the vial and fill with the cylinder gas. The tube was quickly removed and the vial sealed and crimped closed. Kolb and Ettre [66] report this method for gas sampling to be sufficiently accurate for HS-GC calibration.

Once the vials are placed in the autosampler, the equilibration, injection, and rotation of the sample were completely automatic; however, the range (which is the degree of signal processing from FID to amplifier) of the GC required manual adjustment for large variations in ethylene concentration in the sample. Samples run at too low a range value yielded peaks that climbed off-scale and resulted in a lost data point since a vial could not be accurately analyzed more than once. Samples run at too high a range value gave peaks that were too small for accurate analysis. Operating experience enabled the appropriate range setting to be used for each sample.

4.5.2 Results

For the application of HS-GC in determining the amount of ethylene in the copper solution, conditions were designed such that the ethylene was completely degassed into the headspace. The benefit of driving all the ethylene from the liquid phase is that no separate standard or calibration was necessary. If a significant partition of ethylene in the liquid still existed at analysis conditions, then the constant in equation (4-7) would need to be found by analyzing a sample with known C_o; however, producing such liquid standards were tedious and impractical especially when operating the continuous absorption regeneration process, for example. In order to accomplish complete volatilization, the values of K and β were manipulated independently. To drive the equilibrium constant down, the autosampler equilibration

temperature was set at 90ºC. From previous autoclave equilibrium regeneration cycles (as mentioned in section 3.2.4), this temperature was a high enough to decomplex and desorb nearly all ethylene. To keep the phase ratio large, the sample valve to inject the liquid sample into the vial was cracked and closed very rapidly. The average weight of liquid sample injected to the vial was 560 mg; therefore, the average phase ratio was 44. By keeping β large and *K* small, the amount of ethylene in the liquid phase becomes very small compared to the amount of ethylene in the gas phase as shown by rearrangement of equation (4-3)

$$K = \frac{n_S}{V_S} \Big/ \frac{n_G}{V_G} = \frac{n_S}{n_G} \cdot \beta \quad \therefore \quad \frac{K}{\beta} = \frac{n_S}{n_G} \tag{4-8}$$

where n_S and n_G are the number of moles in the liquid and vapor sample, respectively.

By assuming that substantially all of the ethylene in the vial is in the vapor phase, the quantification becomes analogous to gas analysis, and calculation of the constant in equation (4-6) by the gas standard sample area is sufficient. In order to test this assumption and validate HS-GC as an accurate analytical technique, an autoclave absorption experiment was performed with the 50%/50% ethylene/ethane gas mixture. After the liquid solution in the autoclave was contacted with the gas mixture and stirred to equilibrium, gas samples were withdrawn from the vapor space of the autoclave, and liquid samples were withdrawn via a liquid sample line submerged below the vapor-liquid interface as shown in Figure 3-9. The liquid sampling procedure was identical to that for taking samples from the continuous absorption regeneration process, except that the purge step in Figure 3-21 was operated for a longer time due to the higher volume of dead space between the bulk liquid and the sample valve. The samples from the gas phase were analyzed on both GCs (at Sasol and PRC), and the resulting gas composition allowed for calculation of an equilibrium point for the system. The liquid phase HS-GC analysis results gave an independent calculation of the equilibrium of the system. Figure 4-6 shows a comparison of the resulting equilibrium data from the gas phase calculation and the

liquid phase calculation. The relative compositions of ethylene and ethane were used to complete the mass balance and calculate the concentration of each gas in solution (y-axis) as a function of the partial pressure of each species (x-axis).

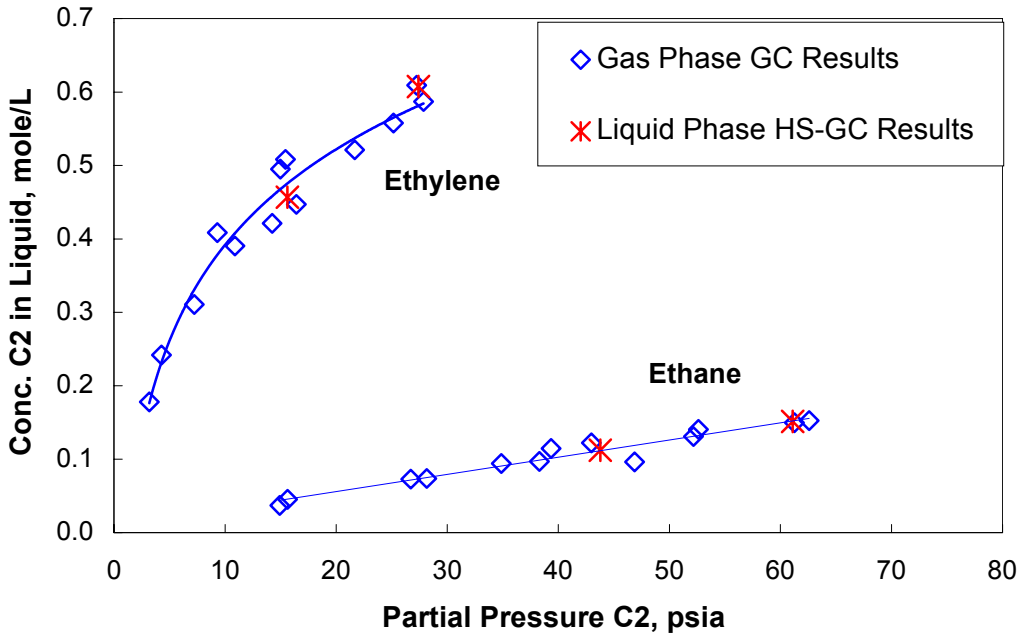

Figure 4-6. Autoclave equilibrium results of gas phase and liquid phase analysis

The HS-GC analysis on the liquid phase proved to give nearly identical equilibrium results as the vapor phase calculation, so the assumption of completely volatile ethylene sufficed to the accuracy of the equilibrium comparison. The precision of the HS-GC technique for the relative composition of the absorbed gas was good as well with replicate samples showing a relative standard deviation (RSD) of less than 2%. The quantitative direct calculation of gas concentration based on the sample weight in the vial showed excellent agreement with the autoclave calculated value even though the RSD was not as good. For the lower loading of the two HS-GC data points shown in Figure 4-6, the average ethylene and ethane concentrations from the direct HS-GC analysis were 0.454 M and 0.112 M respectively with a RSD

of 7%, and the autoclave calculated values (shown on Figure 4-6) were 0.457 M and 0.112 M. The vapor phase replicate samples from the Sasol GC had a RSD of less than 2% in this study. Replicate samples from the PRC instrument were found to have a RSD of less than 5%. Due to the good precision of the technique and the excellent agreement of the liquid phase HS-GC results with the gas phase results, HS-GC was the preferred analytical technique for quantifying ethylene and/or ethane in the liquid phase.

Chapter 5.
Solution properties and stability

5.1 Raw material properties

The exact chemical solutions used in this research were all novel solutions in the sense that no evidence of their prior use existed in the open literature. For this reason, much experimental work was necessary for the evaluation of physical properties. Results for copper loading, ligand concentration, solution density, and solution viscosity are presented in this section. Qualitative comparisons for the behavior of different ligand-salt pairs are also presented by the heat of complexation of the ligand and the relative stability of the system in an oxidizing environment. Results for solutions in DMF are presented for the same ligand-salt pairs that were used in the CV experiment (see section 2.4.1). Selected systems were also investigated with NMP instead of DMF as the solvent. The chemical structure, molecular weight, acid dissociation constant (pKa), and normal boiling point for the raw materials used are given in Table 5-1.

Table 5-1. Structure and physical properties of raw materials (from [72][120])

Substance	Structure	M.W.	pK_a	Density @ 25°C g/cc	Normal boiling point °C
DMF	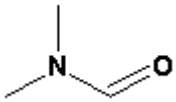	73.09	-	0.944	153
NMP	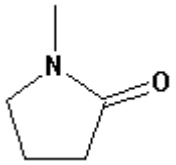	99.13	-	1.0230	202
aniline	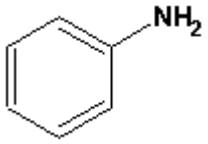	93.13	4.87	1.0217	184.1
pyridine	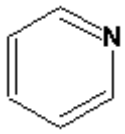	79.10	5.23	0.9819	185
benzylamine	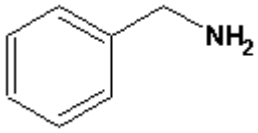	107.16	9.34	0.9813	115.2
CuCl	Cu—Cl	98.999	-	4.14	-
CuBr	Cu—Br	143.45	-	4.98	-

As far as safety considerations while handling the solutions, comparison of the MSDS (material safety data sheet) information in Table 5-2 for these chemicals shows the health and environmental risks. Aniline was especially harmful with a severe warning of its carcinogenic nature. DMF was also stated as a known carcinogen, yet NMP was only listed as an irritant although not enough data had been collected on NMP to be certain of the risk of long-term exposure. For this and other reasons to be discussed later, the use of NMP as a solvent was preferred over DMF

considering the large quantities of solvent used to clean the solution vessels and operational equipment. In addition to health and safety information, also shown in Table 5-2 is the average market price for bulk quantities of each chemical. This data was important for consideration of large-scale implementation of the olefin-paraffin reactive absorption process.

Table 5-2. Health and cost information for raw materials

Substance	Hazard symbols	Exposure limits TWA*	Bulk cost per pound
DMF	toxic	10 ppm	\$0.75 [b]
NMP	irritant	100 ppm	\$1.97 [a]
aniline	toxic & harmful to environment	2 ppm	\$0.38 [a]
pyridine	harmful & flammable	5 ppm	\$3.88 [a]
benzylamine	corrosive	N/A	\$1.60 [b]
CuCl	harmful & harmful to environment	1 mg(Cu)/m^3 (dust)	\$9.80 [b]
CuBr	irritant	1 mg(Cu)/m^3 (dust)	\$7.82 [b]

*time-weighted average for a 10-hr workday in a 40-hr workweek
[a] from reference [14] [b] from vender quotations

5.2 Copper loading and solution density

For the chemical systems used in the comparison to CV experiments, all six ligand-salt combinations of aniline, pyridine, and benzylamine with CuCl and CuBr were prepared as discussed in section 3.1.2. It was originally planned to prepare all systems to a copper molarity of ~1.1 M; however, for two cases, the solubility limit was reached before a solution with this copper concentration was possible. For the aniline-CuBr and the benzylamine-CuBr solutions, crystals were observed to precipitate as the solution cooled after the salt addition step. Stirring was continued

on these solutions until room temperature was reached, and additional DMF solvent was added until just past the point where all of the crystals dissolved. By measuring the amount of DMF added, the copper molarity of the diluted solution was calculated. The target molarity of ~1.1 M was chosen based on the recommendations by Haase [38] and Cymbaluk et al. [21] that a copper molarity around 1 M was sufficient for high olefin capacity yet usually low enough to prevent very viscous solutions. Preparation of the solutions at the copper solubility limit was thought to be somewhat undesirable because small solvent losses would lead to a super-saturated solution that could precipitate solids unexpectedly. The presence of solids or a slurry solution was especially undesirable in the continuous absorption regeneration process where pump gear attrition and plugged flow passages would be detrimental.

The results from the calculation of solution molarity and density are given in Table 5-3. For the diluted solutions of aniline-CuBr-DMF and benzylamine-CuBr-DMF, the calculated copper molarity corresponded to just below the saturation limit at 25ºC; however, the saturation limit of the other solutions was not reached, and the calculated molarity was close to or just above the target value of 1.1 M. As mentioned previously, the ligand concentration in solution was desired to be 4.1 times the copper concentration for optimum coordination. For the undiluted cases, the ligand molarity was calculated to be between 4.62 M and 4.75 M. The DMF diluted solutions were at a lower concentration corresponding to the degree of dilution required to dissolve the crystallized complex. Density measurements were performed at 25ºC in the glove box with volumetric flasks as described earlier. Triplicate measurements were taken for each solution, and the maximum standard deviation was 0.001 g/mL. In addition to the DMF-based solutions, NMP-based solutions were prepared with aniline-CuCl and benzylamine-CuCl for additional autoclave experiments.

Table 5-3. Copper solution properties

Solution composition	Copper molarity M	Ligand molarity M	Density @ 25°C g/mL
aniline-CuCl-DMF	1.12	4.62	1.066
aniline-CuBr-DMF	0.93	3.83	1.088
pyridine-CuCl-DMF	1.10	4.70	1.053
pyridine-CuBr-DMF	1.18	4.75	1.107
benzylamine-CuCl-DMF	1.12	4.66	1.060
benzylamine-CuBr-DMF	0.57	2.42	1.029
aniline-CuCl-NMP	1.16	4.62	1.111
benzylamine-CuCl-NMP	1.09	4.65	1.100

In discussion of the low copper solubility of the aniline-CuBr-DMF and benzylamine-CuBr-DMF solutions, a brief consideration of the bromide versus chloride ions and their interaction with copper complexes is helpful. The observed lower solubility of the two bromide cases suggested the solvent solvated the coordinating ligands in the complex and not necessarily the copper ion. The solutions with low solubility were bromide systems with both a strong ligand (benzylamine) and a weak ligand (aniline). The pyridine-CuBr system was not observed to show any reduction in solubility from the chloride cases. Therefore, solubility was not likely a function of ligand strength but the degree that the ligand was able to fully coordinate the copper-ligand complex without being obstructed by strong anions. If the bromide ions are more likely to hold tightly to the copper cation than their chloride counterparts, then it is not surprising that the CV results indicated that bromide systems exhibited poorer ethylene complexation. By occupying a coordination site that otherwise would hold a ligand, the bromide ion would disable a potential ethylene-ligand exchange site and lead to poorer solvation of the complex due to fewer ligand molecules surrounding the copper(I) ion.

5.3 Solution viscosity

In order to accurately model the kinetics of olefin absorption, it was necessary to know the viscosity of the absorption solution. Experimental results of solution viscosity measured with the Fann viscometer as described previously (see section 3.1.1) are shown in Figure 5-1. The viscosity of the aniline-CuCl-NMP solution was found over a range of temperatures from 25ºC to 45ºC. The molarity of this solution was very similar to that shown in Table 5-3 above. At 25ºC the viscosity was found to be nearly 8 cP and it decreased nearly linearly to a value close to 4 cP at 45ºC. Viscosity data were also collected for a copper-free solution of aniline and NMP at the same molar ratio used in the CuCl experiment. The corresponding molarity of aniline in this solution was 4.75 M. By comparison with the copper-free solution, the presence of the CuCl salt nearly doubled the solution viscosity over the entire temperature range. Also shown in Figure 5-1 is the viscosity behavior of pure liquids aniline and NMP from reference [72]. The mole fraction of aniline in the copper-free solution was 0.44, and the solution showed an identical viscosity trend to pure aniline.

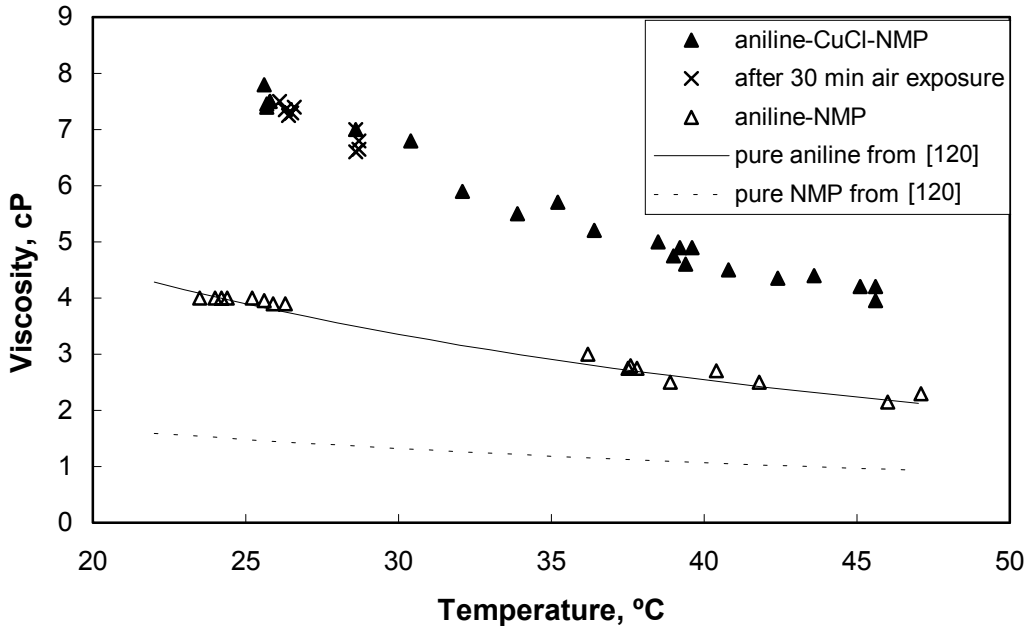

Figure 5-1. Viscosity of aniline-CuCl-NMP and aniline-NMP solutions

As a test to how exposure to oxygen affects the solution viscosity, the copper-containing solution was removed from the glove box and stirred in the fume hood for 30 minutes. After this air exposure time, the solution was noticed to have darkened somewhat and seemed to "stick" to contacting surfaces more, which were taken to be the visual signs of solution oxidation. However, further testing of the viscosity of this oxidized solution showed that the viscosity did not increase significantly after air exposure. According to Figure 5-1, the air-exposed solution did not deviate at all from the fresh solution. The margin of error in a particular viscosity reading was ±0.3 cP, so the degree of scatter in the data points in Figure 5-1 was well within this error.

5.4 Heats of complexation with ligands

While preparing the different ligand-salt solutions in the glove box, the aniline solutions were observed to exhibit at least 10ºC less temperature rise shortly after adding the salt than the pyridine and benzylamine solutions. The temperature of the solution before and after salt addition is shown in Table 5-4. In order to account for effects of the different heat capacities of the various ligands and salts used, an estimate of the heat released is also presented for comparative purposes. The thermal energy change for each component was calculated as follows

$$q = nC_p\Delta T \tag{5-1}$$

where n is the moles of the ligand, solvent, or salt, C_p is the heat capacity of the species at the average temperature, and ΔT is the temperature change. ΔT for the ligand and solvent was the difference in the temperatures in Table 5-4, and ΔT for the salt was the post-salt addition temperature minus 25ºC. The values of C_p were obtained from reference [120]. The heat of complexation of the ligand-copper complex given in Table 5-4 was estimated by the sum of the change in thermal energy of each component.

$$\Delta H = \frac{q_{\text{ligand}} + q_{\text{solvent}} + q_{\text{salt}}}{n_{\text{complex}}} \tag{5-2}$$

Table 5-4. Heat effects during solution preparation

System	Pre-salt temperature ºC	Post-salt temperature ºC	Heat released, kcal/mol
Pyridine-CuCl	72	95	6.2
Pyridine-CuBr	72	95	6.2
Benzylamine-CuCl	71	89	7.0
Benzylamine-CuBr	73, 72	97, 94	8.9
Aniline-CuCl	73	81	3.3
Aniline-CuBr	72, 72	80, 79	3.2

This estimation of the heat of complexation neglects the heat losses to the glove box, which was probably rather significant since the mixing flask was not insulated. However, before salt addition the heat loss to the glove box was compensated by the heating plate that maintained a constant solution temperature. For comparison purposes, the heat loss was assumed to be similar in each case and was not considered even though the magnitude of the reported heats of complexation certainly must contain significant error compared to the unknown actual value. Examination of the data in Table 5-4 suggested that the heat of complexation was directly related to the ligand but unrelated to the anion. The benzylamine systems showed the highest heat of complexation at an average of 8.3 kcal/mol, and the pyridine systems were next at 6.2 kcal/mol. The aniline systems were somewhat lower at 3.2 kcal/mol. Higher heats of complexation correspond to stronger ligands and a stronger ligand-copper interaction; therefore, the observed order of ligand strength increased from aniline to pyridine to benzylamine. In comparison with the CV results, this observation validates the ligand strength trend during complexation as: aniline < pyridine < benzylamine.

5.5 Solution stability

From the preparation of absorption solutions in the glove box to removal from the autoclave, the effects of different ligand-salt pairs were observed and qualitatively compared. The aniline-CuCl-DMF and aniline-CuCl-NMP solutions were both immediately black upon salt addition in the preparation step. Although the solutions were black, swirling the liquid in a flask showed that a thin film of liquid on the flask wall had a yellow-green tint and no residue was left behind from the falling film. Upon air exposure, these solutions showed an immediate change by loss of the yellow-green tint and a very black film that tended to stick to flask walls upon swirling. Despite this visual darkening, the solutions remained liquid indefinitely in air. While analysis of the ratio of cuprous to cupric species was not successfully

attempted, it was thought that the color change was due to partial oxidation of the cuprous ions.

During preparation of the aniline-CuBr-DMF solution, the color was initially the same as the aniline-CuCl-DMF solution until the solution began to cool whereby reddish crystals were observed to precipitate. Filtration of this product yielded a red-purple crystal. When a portion of this crystal was added to a beaker of pure DMF, the crystals dissolved immediately and the solution took on a light green color. This crystal was thought to be aniline-copper(I)-bromide complex whose solubility in DMF was rather low, which was why the solid easily dissolved when mixed with excess solvent. When the remainder of the red-purple crystal were removed from the glove box, the solid appeared to "melt" turning more purple and then eventually black. Analysis of this precipitate and its oxidation products was not attempted. Like the solid, the diluted aniline-CuBr-DMF solution removed from the autoclave turned black immediately following air exposure, but like the chloride solution, it remained a liquid.

As with the aniline solutions, the pyridine-CuCl-DMF solution turned black upon mixing the salt; however, the pyridine-CuBr-DMF solution turned a dark green color instead of black. While in the glove box, neither of the pyridine solutions precipitated crystals up to the ~1.1 M concentration studied. Once exposed to air, the pyridine-CuCl-DMF solution was very unstable solidifying completely within 30 minutes. This was the only solution to solidify as a result of oxidation, and the explanation of this instability is not completely understood. The pyridine-CuBr-DMF solution was more stable upon air exposure turning black as the others while remaining a liquid.

The benzylamine solutions were the most colorful with both the chloride and bromide solutions turning light turquoise upon addition of the salt. The benzylamine-CuCl solutions with DMF and NMP showed acceptable solubility, and upon air exposure both became increasingly blue until eventually darkening to a black liquid.

The benzylamine-CuBr-DMF was initially a light turquoise color, but after cooling the solution precipitated white crystals yielding a clear yellow solution. Filtration of the solid showed the crystals to be perfectly square, around ~1 mm, which dissolved immediately in excess solvent. Upon air exposure the dry white solid turned to a deep royal blue color and "melted" to a slushy consistency. Like the aniline complex, this white crystal was suspected to be a benzylamine-copper(I)-bromide complex with poor solubility in the solvent. Oxidation of the copper disrupted the ligand-copper complex and the wetness observed was likely some sort of cupric complex. While an in depth examination of these crystals and oxidation products would be an interesting study, such effort was not undertaken because it was not directly beneficial to the design of an olefin purification process.

5.6 Conclusion

When choosing an olefin absorption solution, it was desirable to have a solution with a high copper capacity in order to potentially absorb more ethylene. Since the presence of the copper salt nearly doubled the viscosity of the aniline-CuCl-NMP solution, a tradeoff worth consideration may be that there is a maximum tolerable solution viscosity. Higher pumping costs as well as decreased mass transfer coefficients are generally associated with high viscosity fluids, so some degree of copper capacity may need to be sacrificed for optimum process design. As far as the cost of the absorption solution, all solutions studied were relatively inexpensive to prepare; furthermore, minor variations in solution cost are not significant factors compared to the operating cost of the process. Solution stability though is of great concern because if the entire solution inventory is easily ruined, the process will not be economically feasible regardless of how cheap the raw materials may be. Due to immediate formation of a solid upon air exposure, the pyridine-CuCl-DMF should definitely be avoided. The aniline solutions showed the least visual change upon air

exposure while the benzylamine solutions showed stark color changes apparently due to copper(I) oxidation.

Chapter 6.
Absorption equilibrium

6.1 Introduction

For autoclave absorption experiments, the number of moles of gas absorbed at equilibrium was calculated as described in section 3.2.2. This absorption was not limited to chemical complexation but included gas physically dissolved in the solution as well. Typically in the olefin absorption literature, equilibrium data is presented either as moles of gas absorbed per liter of solution or moles of gas absorbed per mole of metal versus partial pressure of the absorbing gas. The first method is preferred when the absorption solution has a significant physical solubility for the gas because the chemical effects cannot be isolated without special data manipulation (as in section 6.3.4). If the total number of moles of gas absorbed were divided by the moles of copper in the solution, the resulting information could be potentially misleading since not all gas in solution chemically complexed the copper. Hence, in the following sections, the absorption equilibrium data for ethylene is presented as moles per liter of solution unless otherwise noted. The temperature of the absorption equilibrium data obtained was between 23ºC and 26ºC for all cases and the heat of complexation of ethylene was unnoticeable in the autoclave experiments.

6.2 Equilibrium results with cyclic voltammetry systems

In order to validate cyclic voltammetry as an accurate comparative tool for predicting of olefin absorption, the equilibrium capacity of the six systems described previously was found by autoclave experiments. Each experiment produced one value of equilibrium concentration of ethylene in the liquid and partial pressure ethylene in the gas, which yielded one equilibrium point on the plot of pressure

versus ethylene concentration in liquid. A combination of multiple absorption experiments at different gas charges produced the curve observed in Figure 6-1 for a given system. A total compilation of the equilibrium data is given in Appendix A.5. From Figure 6-1 the aniline systems were observed to show the highest ethylene absorption followed by a close grouping of benzylamine and pyridine systems at lower ethylene absorption.

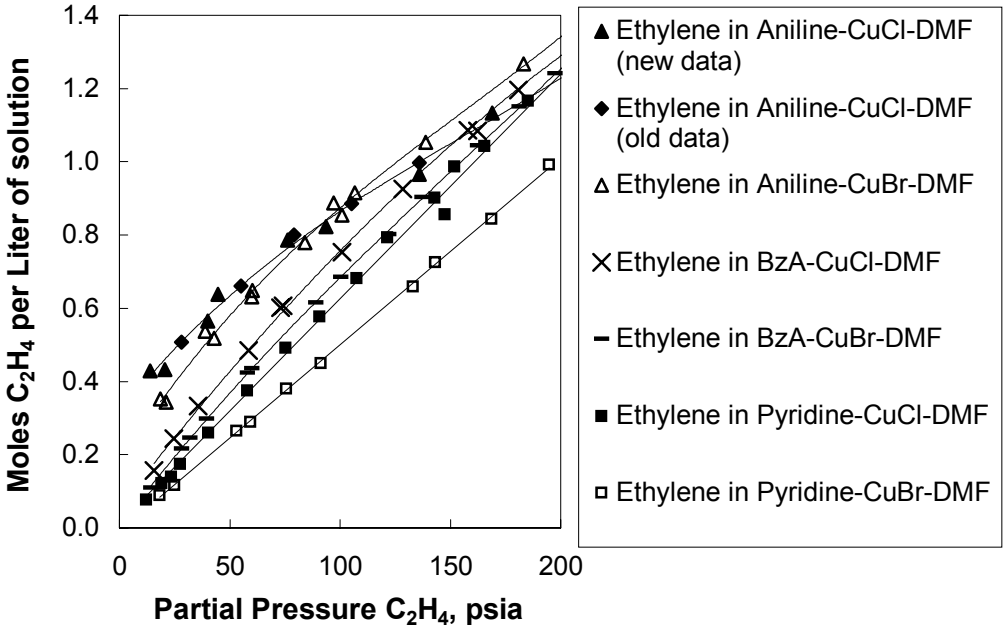

Figure 6-1. Ethylene absorption equilibrium for all six CV systems

To confirm the experimental reliability of the results, the aniline-CuCl-DMF results were compared to earlier data from a system prepared identically except with about 2.5 times the liquid volume in the autoclave. Since the system for CV comparison (new data) lined up exactly with the previous results (old data) shown in Figure 6-1, the experiment did not contain any unique error. The error involved with producing repeatable equilibrium points at a given ethylene partial pressure was found to be less than 5% for these autoclave experiments.

6.2.1 Ligand and anion trends

The autoclave and CV techniques consistently showed that aniline far out-performed the systems of pyridine and benzylamine. Another commonality with CV was the fact that the copper chloride systems showed higher absorption than the copper bromide systems for all autoclave cases. The shape of the equilibrium lines for the different solutions in Figure 6-1 was seen to increase in curvature from bottom (low ethylene capacity solution) to top (high ethylene capacity solution). While these autoclave experiments with CV solutions did not collect data below ~1 atm ethylene partial pressure, the equilibrium curve should pass through the origin as long as the complexation is reversible. The pyridine systems showed a linear dependence on pressure suggesting a strong physical solubility effect of the solvent. The benzylamine equilibrium curves also appeared to be nearly linear with pressure exhibiting only a small deviation from passing through the origin.

Both aniline-CuCl-DMF and aniline-CuBr-DMF equilibrium curves displayed high ethylene absorption at low ethylene partial pressures. Extrapolation of the aniline curves would show high curvature at sub-atmospheric ethylene partial pressures before becoming linear at higher ethylene pressures (i.e. > 50 psia). This curvature in the aniline systems was due to the chemical effects that dominated physical solubility effects at low pressures. Of the three ligands studied, the aniline systems showed the most favorable capacity for absorbing ethylene, which agreed excellently with results from the CV experiments.

The relative strength of the ligands observed in the CV results carries over to the discussion of the autoclave equilibrium results. Since the ligand-copper complex bond has a significant σ character from donation by nitrogen's lone pair, the basicity of the ligand is good indicator of ligand strength. Of course prediction of the strength of the ligand-copper complex is more complicated than the value of the pK_a, but examination of these values can yield comparative information. The order of pK_a

from Table 5-1 confirms that aniline should form the weakest copper complex since it is the weakest base and is not expected to donate electrons as easily as benzylamine and pyridine. Stronger ligands, like benzylamine and pyridine, should allow more electronic overlap with copper and are more likely to form stronger copper-ligand complexes creating more competition for the incoming ethylene. Aniline is a relatively weak ligand so its replacement by ethylene is more facile. Optimizing the ligand can be difficult because if the ligand is too strong it will have more competition with ethylene and hinder complexation. On the other hand, if the ligand is too weak, the ligand will not effectively stabilize the metal ion, which can lead to insoluble, uncomplexed copper in the preparation process.

In addition to comparing coordinating ligands in Figure 6-1, the trend of the different anions can also be discussed. Since all of the CuBr systems were slightly lower on the equilibrium plot than the corresponding CuCl systems, the Br^- ion was thought to associate more strongly to the copper cation than the Cl^- ion as mentioned in the CV discussion in section 2.4.1.2. Further examination of the equilibrium data revealed that the lower absorption of the CuBr solutions was mostly due to the differences in copper molarity. Two of the three CuBr solutions had lower copper solubility, so the lower equilibrium absorption for these cases could be reconciled by plotting the absorption on a per mole of copper basis. Since the procedure for this calculation is thoroughly discussed in section 6.3.4, the discussion of the results is deferred until then.

6.2.2 Physical solubility and salting-out effect

Unlike the CV experiments where the observed complexation was strictly chemical, the observed absorption from the autoclave equilibrium was a combination of chemical effects and physical effects. To further examine the role of physical solubility in the absorption equilibrium curves, a new solution was prepared with an equivalent molar ratio of pyridine and DMF without the copper salt. Equilibrium

curves for ethylene and ethane gases generated with this copper-free solution found both gases to exhibit ideal Henry's law behavior (evident by their linear slope and intersection with the origin) as shown in Figure 6-2. The equilibrium line for ethane had a lower slope than ethylene due to the pyridine-DMF solution's natural affinity for the olefin (i.e. intermolecular forces). For ethylene the equilibrium curve of the pyridine-DMF solution was nearly identical to the pyridine-CuCl-DMF solution and quite a bit greater than the pyridine-CuBr-DMF solution (same data as in Figure 6-1). Since the pyridine-CuBr-DMF system experienced less absorption than the pyridine-DMF, the solutions were observed to experience the salting-out effect – changes in physical solubility after the addition of a salt. The salt effect was best demonstrated by an additional series of experiments with ethane gas for the pyridine-CuCl-DMF system and the pyridine-DMF system. Since ethane was a non-reactive gas, the only absorption was due to physical solubility. The equilibrium curve of pyridine-CuCl-DMF with ethane was considerably lower than the curve of the pyridine-DMF solution as shown in Figure 6-2. The equilibrium curve of pyridine-CuCl-DMF with ethylene did not appear to demonstrate salting out because that line was nearly the same as the line produced from pyridine-DMF with ethylene.

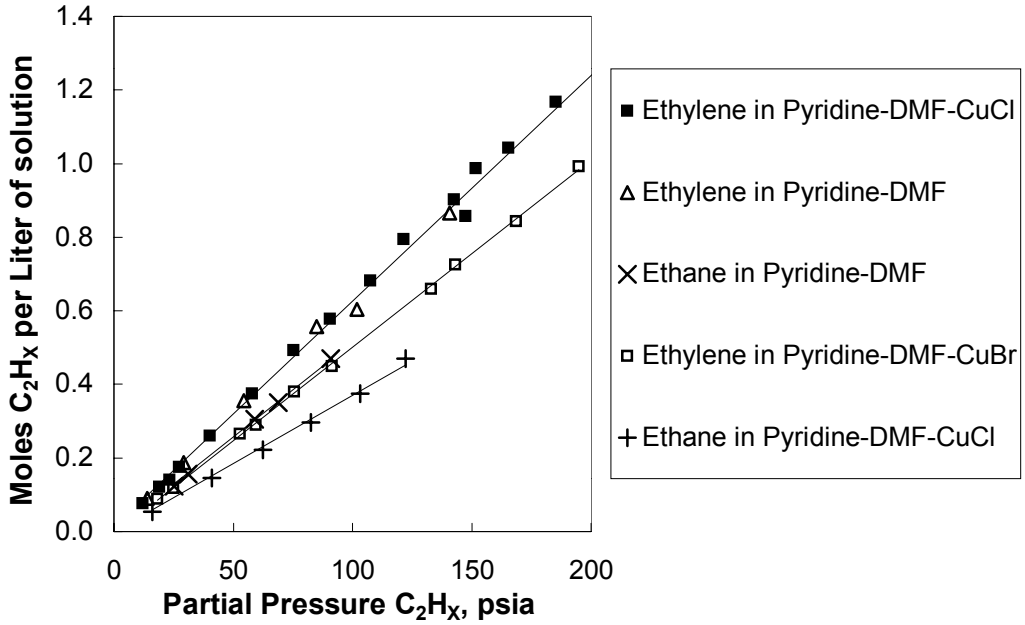

Figure 6-2. Physical solubility and salt effect

The pyridine-CuCl-DMF system should have experienced a similar effect as the pyridine-CuBr-DMF system, but since the pyridine-CuCl-DMF line showed greater absorption than the pyridine-CuBr-DMF line, the argument could be made that the chloride system experienced more chemical effects than bromide system. The chemical effects may have compensated for the loss of physical solubility raising the pyridine-CuCl-DMF line, which incidentally was in the same position as the copper-free pyridine-DMF line. For future work, the salt effect hypothesis should be tested with a solution of a non-reacting salt. A possibility would be to prepare a solution identical to the pyridine-CuCl-DMF solution except to use NaCl (or KCl) instead of CuCl. The new salt should not participate in any chemical absorption, so the resulting equilibrium curve should show the pure salt effects on the physical absorption. Ideally, this new solution should exhibit an ethylene capacity slightly lower than the pyridine-CuBr case.

6.2.3 Comparison with CV data

One of the main goals of this work was to determine whether the absorption capacities of concentrated systems could be qualitatively defined from dilute solutions in a bench scale electrochemical experiment. If the total uptake from the autoclave for each absorption solution at atmospheric ethylene partial pressure is compared to the shift in half-wave potential from the CV experiments, a parity plot suggesting a good fit is obtained in Figure 6-3. However, from all of the preceding discussion of the large amount of physical solubility and possible salt effects inherent in the autoclave, such a comparison may be potentially misleading. For example, the pyridine-CuBr absorption equilibrium curve was linear with a zero intercept implying practically no chemical effects. The pyridine-CuCl system showed some chemical effects if the salt effect was assumed similar. However, it is not likely that the chemical effects would persist to high ethylene loadings as suggested by the fact that the equilibrium line had the same slope at very high pressures that it had at low pressures. The different slopes of the equilibrium line for the chloride and bromide cases especially at higher loadings were also seen with aniline (except in this case the bromide had the greater slope). Possibly the chloride ion had some interaction that would cause a different degree of salting out than the bromide ion. Regardless of the explanation, the pyridine-CuCl like the bromide system was also linear with a zero intercept. When compared to the CV results, these two pyridine systems may be more accurately represented by zero chemical effects.

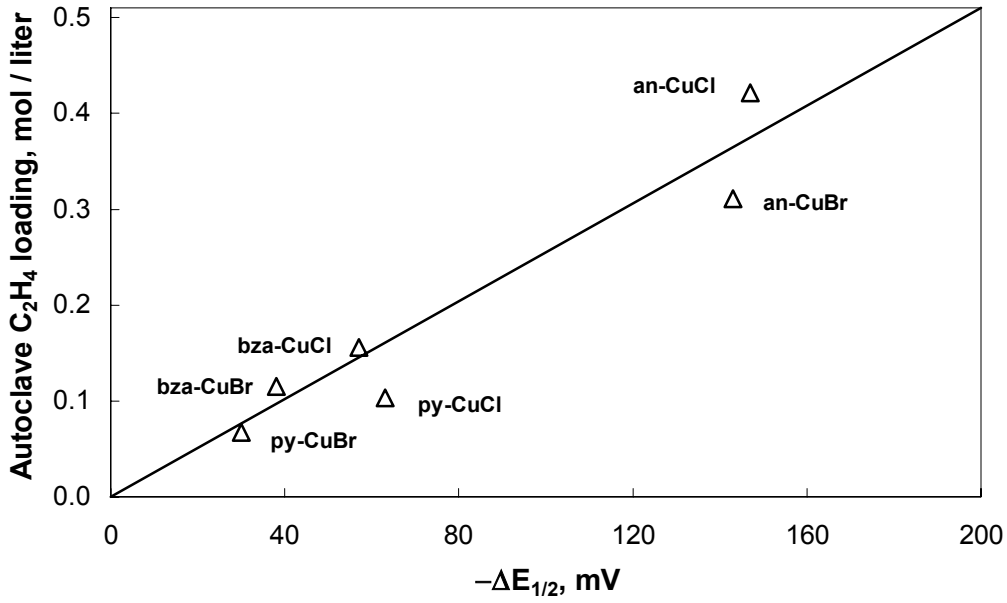

Figure 6-3. Parity plot of autoclave equilibrium and CV results

It is apparent the autoclave equilibrium data contains a large dependency on the physical solubility of the different ligands and their concentration. For example, in both pyridine systems, a large portion of a system's total absorption capacity was due to physical solubility, so a system that has slightly more or less ligand compared to solvent will show a different capacity even though the chemical effects remain unchanged. Because the ligand and solvent have different physical solubilities for ethylene, a change in their ratio will change the degree of absorption of the solution. Varying these factors would cause the corresponding points on the parity plot in Figure 6-3 to fluctuate accordingly.

One possible explanation for the poor chemical absorption of the strong ligand systems (pyridine especially) was the strong ligand concentration effect that was observed in the CV results. Even though the ligand to copper ratio in the autoclave was around 4.1:1 while the CV experiments were at 5:1 and 40:1, the higher overall

concentration of the autoclave solution could account for the difference. Simple solution thermodynamics can be used to show that the dilute 0.01M copper solution will not encounter as many ligand molecules at 5:1 ratio as the 1.1M copper solution at a 4.1:1 ratio. In addition, the actual coordination number of the metal-ligand complex could be less than the assumed value. Pyridine-CuCl complexes have been shown to have a binuclear structure with halide bridges so that each copper ion is four coordinated but only at a ligand to metal ratio of two as shown earlier in Figure 2-3 [65]. If the actual ligand to metal ratio for the complex were two instead of four as previously assumed, then the excess ligand concentration for the concentrated copper case would impede ethylene complexation as observed for the CV cases with higher strong ligand concentrations.

6.3 Aniline:CuCl solutions

Since both the CV technique and the autoclave equilibrium experiments showed aniline-CuCl systems to exhibit the greatest ethylene capacity of the systems studied, further in depth equilibrium and kinetic studies focused on this aniline-CuCl solution. Autoclave equilibrium experiments were performed with the solvents DMF and NMP to determine if the choice of solvent had much effect on the ethylene absorption. For the olefin-paraffin selectivity at equilibrium, experiments were performed with pure gases ethylene and ethane and with a 50%/50% molar mixture. To investigate the dual effects of physical solubility and chemical complexation, equilibrium experiments were performed with ethylene and ethane and a copper-free solution. Tabulated data from these experiments is given in Appendix A.5.

6.3.1 Solvent comparison

As shown in Table 5-1, the normal boiling point of DMF is 153ºC making it considerably more volatile than aniline, which boils at 184ºC. The solvent was a necessary ingredient in the solution because solutions of CuCl in aniline formed a

solid at room temperature. For a practical application of the olefin/paraffin reactive absorption process, in order to regenerate the absorption solution and break the ethylene-copper complex, the solution will need to be heated to temperatures around 80ºC resulting in considerably more loss of the DMF than aniline. To minimize additional processing steps to remove the solvent carried over with the olefin, a solvent with similar complex solubility yet with a lower volatility was desired. NMP has a normal boiling point of 202ºC, and at 80ºC the vapor pressure of NMP is a full order of magnitude below DMF as shown in Figure 3-10. Since it is structurally similar to DMF, there were no problems achieving similar copper solubility using NMP as the solvent. For the present research, it was seen as an additional benefit that NMP was less toxic than DMF since large quantities of the solvent were used to clean and prepare equipment between experiments. As far as cost, Table 5-1 shows that NMP is slightly more expensive when purchased in bulk quantity; however, since the inventory of solvent should not diminish very rapidly, this difference is likely to have minimal impact on the cost of the total process.

To examine whether the choice of solvent affected the ethylene absorption capacity, equilibrium data from solutions of aniline-CuCl-DMF and aniline-CuCl-NMP is shown in Figure 6-4. The calculated copper molarity for these solutions was 1.12 M for the DMF solution and 1.16 M for the NMP solution as shown in Table 5-3. Whether the equilibrium data was plotted on a per liter of solution or a per mole of copper basis was immaterial for this case since the copper concentrations were similar. The equilibrium data for the two cases was indistinguishable at low partial pressures while the DMF solution showed slightly more absorption at very high ethylene pressures. Since most chemical effects were observed at low pressures, the difference at high pressures was likely due to slightly higher physical solubility of ethylene in DMF over NMP. The effect of the solvent on the chemical absorption was negligible for these two cases, so NMP was considered the solvent of choice

primarily because it had a lower volatility than DMF while also maintaining a comparable ethylene absorption to similar DMF solutions.

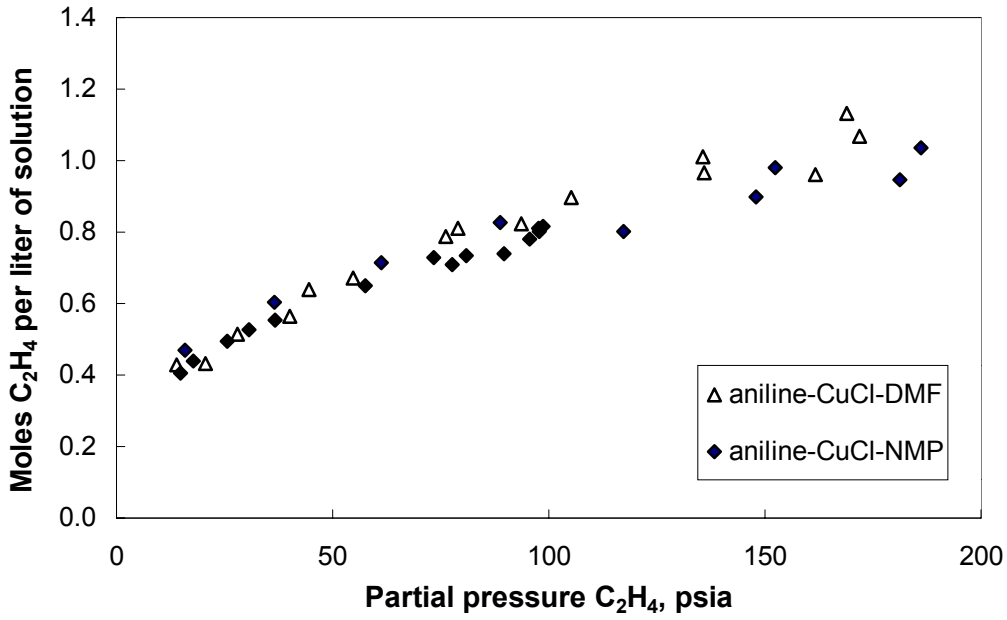

Figure 6-4. Comparison of DMF and NMP solvents

6.3.2 Pure gas

For the aniline-CuCl-NMP solution described previously, autoclave equilibrium experiments were performed with ethylene and ethane. Figure 6-5 shows that the absorption solution has much higher capacity for ethylene than ethane. The trendline through the ethane equilibrium data was fit with a y-intercept of zero, and the R^2 value of the line was 0.996 with a slope of 0.00201 mol·(L psia)$^{-1}$. For physical solubility, the Henry's law constant can be defined as

$$m = \frac{c^*}{P^*} \tag{6-1}$$

where c is concentration of the gas in the liquid phase, P is the partial pressure of the gas, and the * superscript refers to the equilibrium condition. The ethylene equilibrium data was definitely not described by Henry's law; in fact, the solution still had an ethylene capacity over 0.45 M at atmospheric pressure.

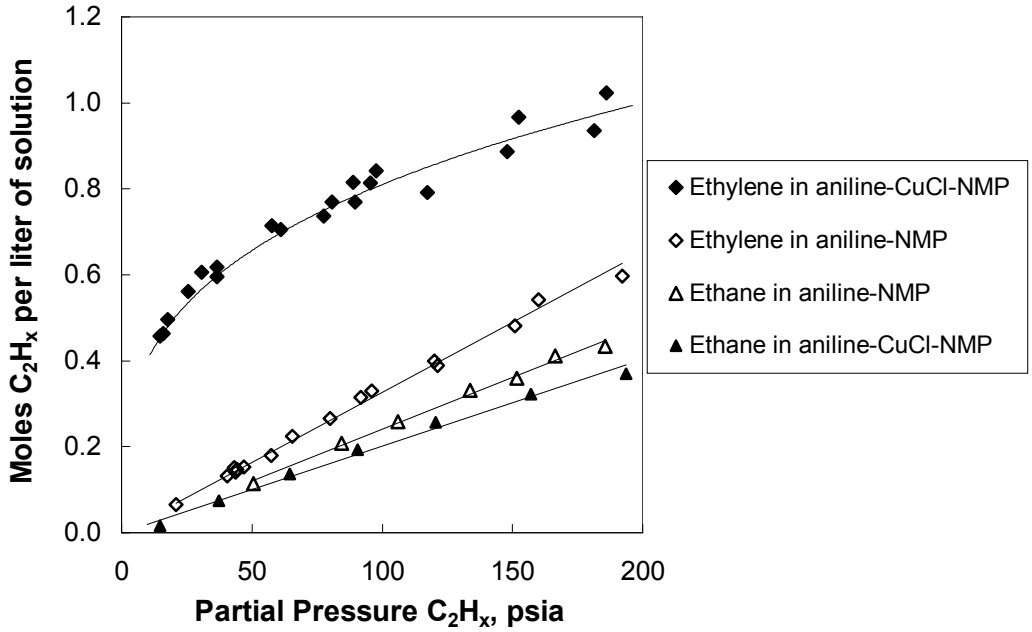

Figure 6-5. Ethylene and ethane equilibrium with copper and copper-free solutions

In order to determine how much of the ethylene absorption was due to physical solubility in the liquid, a copper-free solution of aniline and NMP was prepared with the liquids in the same molar ratio as in the CuCl case. Comparison of equilibrium data obtained for this solution with ethylene and ethane in Figure 6-5 showed that the aniline-NMP solution had higher capacity for ethylene over ethane. The ethylene capacity of the aniline-NMP solution was much lower than the copper case suggesting that chemical effects were indeed important. Like ethane in aniline-CuCl-NMP, both ethylene and ethane with the aniline-NMP solution showed absorption equilibrium following Henry's law. For ethylene, the R^2 value of the line

was 0.993 with a slope of 0.00322 mol·(L psia)$^{-1}$. For ethane, R^2 value of the line was 0.997 with a slope of 0.00245 mol·(L psia)$^{-1}$.

With ethane, the aniline-NMP solution demonstrated higher solubility than the aniline-CuCl-NMP; therefore, like the pyridine-CuBr-DMF case, a salting-out effect was observed. Unlike the pyridine system from before, since this aniline solution exhibited a very high olefin capacity, the decrease in paraffin solubility due to the presence of the CuCl resulted in a greater improvement in selectivity than if the salting-out had not occurred. Because the presence of the salt decreased the gas solubility, it would not be correct to assume that the physical solubility of the ethylene in the aniline-CuCl-NMP solution was the same as the copper-free solution.

6.3.3 Mixed gas

In order to examine the absorption equilibrium of an olefin/paraffin gas mixture in the aniline-CuCl-NMP solution, autoclave experiments were carried out with a 50/50 ethylene/ethane molar mixture. These experiments were performed identically to pure gas experiments, except that after the autoclave reached equilibrium, the stirrer was turned off and a gas sample was withdrawn for GC analysis. GC analysis yielded the mole fraction of the vapor in the autoclave, and since the total pressure was known, the partial pressure of each gas was determined. The mass balance allowed straightforward calculation of the number of moles of each gas in the liquid phase. The resulting equilibrium data is shown in Figure 6-6 along with the pure gas data presented previously. Since the initial autoclave vapor phase mole fraction immediately after charging the gas mixture was 0.50 for each gas and the solution absorbed considerably more ethylene than ethane, a single experiment gave higher equilibrium partial pressures of ethane than ethylene. From comparison with the pure gas data, the ethylene absorption in the mixture was nearly identical to the pure gas. The ethane gas seemed to show slightly higher solubility when ethylene was present rather than as a pure gas. A linear fit to the mixed gas equilibrium data

for ethane gave an R^2 value of 0.910 with a slope of 0.00254 mol·(L psia)$^{-1}$. The poorer fit to this data was likely due to the additional experimental error involved with the GC analysis.

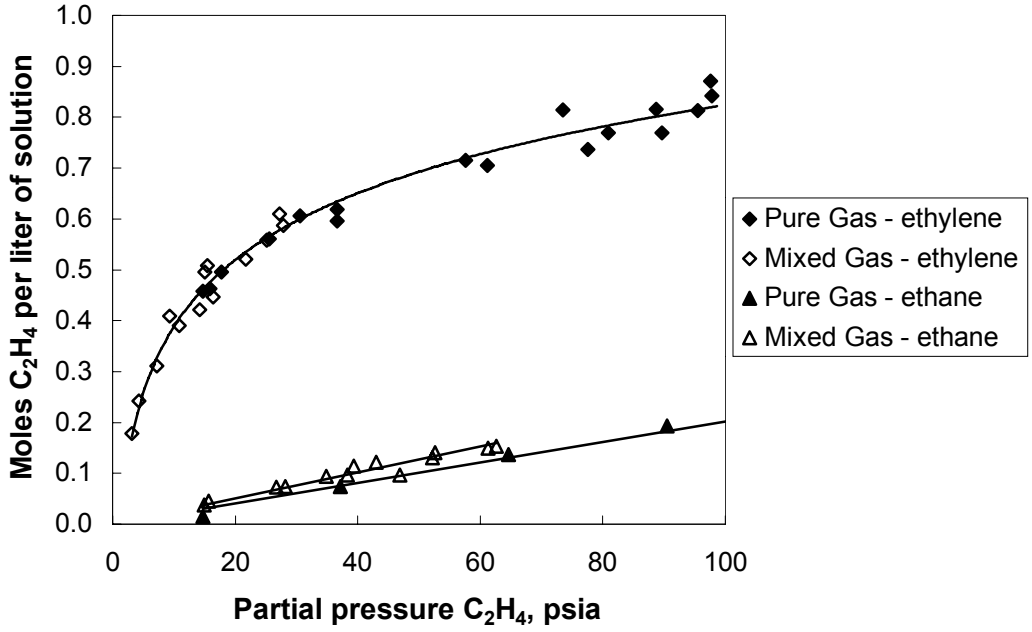

Figure 6-6. Mixed and pure gas absorption equilibrium

A possible explanation why the mixed gas ethane showed greater absorption than the pure gas ethane is that the solution was more highly loaded with light hydrocarbon gas. The high concentration of absorbed ethylene created a more favorable environment for the physically dissolved ethane even though most of the ethylene at these equilibrium conditions was chemically complexed to copper. The enhancement to solubility was rather small due to the fact that ethylene's olefinic nature is quite different than the saturated paraffin; however, some enhancement to solubility still occurred. An increased absorption as such was not observed for the mixed gas ethylene because the pure gas ethylene equilibrium already contained the synergistic effect. By analogy to the mixed gas ethane absorption, the physical

solubility of the pure gas ethylene was enhanced as a result of the high concentration of complexed ethylene. As a result, the presence of the CuCl in the absorption solution contributed two opposite effects to the physical solubility. The first effect was the decrease in solubility due to the salting-out effect, and the second effect was the increase in solubility due to the more ethylenic nature of the solution, commonly referred to as the "like dissolves like" rule for solubility.

6.3.4 Chemical and physical effects

Since the mixed gas equilibrium data showed excellent agreement with the pure gas data, especially for ethylene, combining this data gave a full description of ethylene behavior with the aniline-CuCl-NMP solution at ethylene partial pressures as low as 3.2 psia. In order to account for CuCl effects and estimate the degree of physical solubility of ethylene with the copper solution, an analogy with the non-reactive cases was used. This technique called the N_2O analogy in CO_2 absorption is commonly employed to find the solubility of CO_2 in an amine solution [68]. Usually the CO_2 solubility is found by assuming that the ratio of the solubility of the reactive gas (CO_2) to the non-reactive gas (N_2O) in a non-reactive liquid (water) is the same as the ratio of the solubility of these gases in the reactive liquid (amine solution). In our case, the physical solubility of ethylene in the aniline-CuCl-NMP solution was corrected for the presence of the CuCl by using the pure gas value for ethane solubility in the reactive solution because the data covered a larger pressure range and there was less experimental error in this technique than the mixed gas value. The copper-free solution referred to with *non-Cu* subscript in the following equation was the non-reactive solution in the analogy.

$$m_{\text{ethylene Cu}} = \frac{m_{\text{ethylene non-Cu}} \cdot m_{\text{ethane Cu}}}{m_{\text{ethane non-Cu}}} \tag{6-2}$$

$$m_{\text{ethylene Cu}} = \frac{(0.00322)(0.00201)}{0.00245} = 0.00264 \frac{\text{mol}}{\text{L} \cdot \text{psia}} \tag{6-3}$$

With the calculated physical solubility of ethylene, the chemical and physical effects were able to be isolated from one another. In order to estimate the degree of chemical complexation versus physical solubility, the calculated physical solubility from equation (6-3) was subtracted from the total ethylene concentration in the liquid for each equilibrium point. The resulting ethylene absorption was entirely due to chemical complexation with copper.

$$c^*_{\text{chemical}} = c^*_{\text{total}} - P^* m_{\text{ethylene Cu}} \tag{6-4}$$

A comparison of the physical and chemical effects is shown in Figure 6-7. Examining the total ethylene at pressures over ~40 psia revealed that the slope of the equilibrium data was nearly the same as the calculated physical solubility. As a result, the calculated chemical absorption plateaued around 40 psia at an ethylene concentration around 0.58 M in the liquid. Since the slope of the total ethylene absorption line at high pressures matches the slope of the calculated physical solubility, the copper solution is fully loaded chemically. Since the copper concentration was 1.16 M, this would lead to the assumption that about half of the copper in solution participates in a 1:1 complex with ethylene. This could be a result of ligand strength that inhibits the ethylene exchange equilibrium or a result of partial degradation of the copper(I) state due to oxidation. Another possibility is that all of the copper(I) is active and forms a 2:1 complex with ethylene.

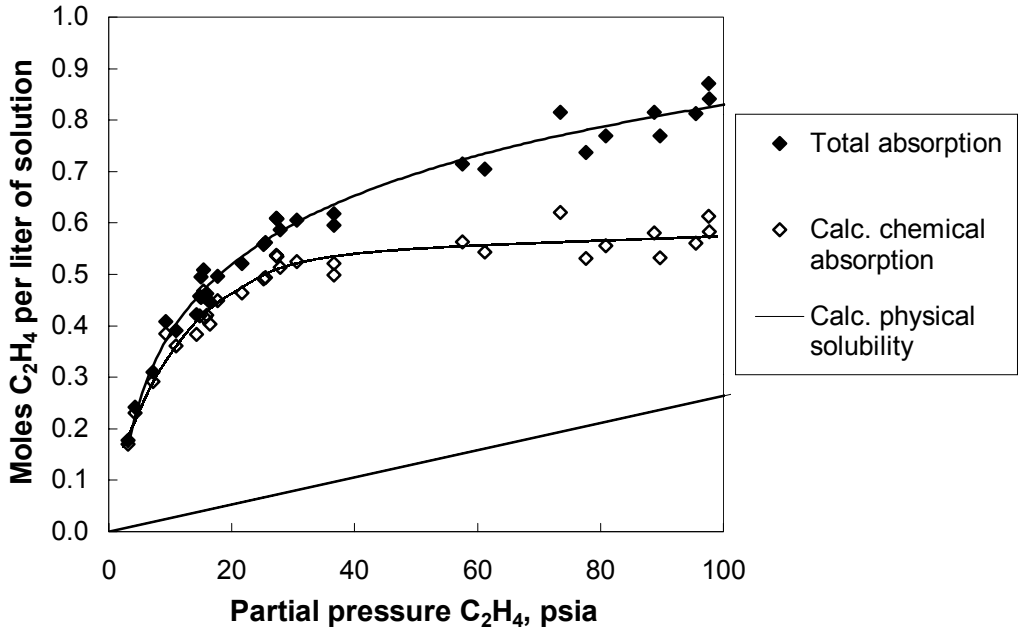

Figure 6-7. Calculated chemical and physical equilibrium

Returning to the previous discussion of the comparison of CuCl and CuBr in the CV comparison solutions, similar data analysis can be performed. According to Figure 6-7, the slope of the total ethylene absorption at high pressures can be assumed to be the same as the slope due to physical solubility. By estimating the slope of the equilibrium curves in Figure 6-1 at partial pressures in the range of 70 psia to 150 psia, the chemical effects were calculated by equation (6-4). Since the copper concentration was so different for the CuCl and CuBr solutions, the calculated chemically complexed ethylene concentration was divided by the copper molarity to show equilibrium data on a per mole of copper basis in Figure 6-8. Presenting the absorption equilibrium in this way shows that for aniline there was only a slightly greater absorption capacity for the CuCl solution and for benzylamine there was no difference between the CuCl and CuBr solutions.

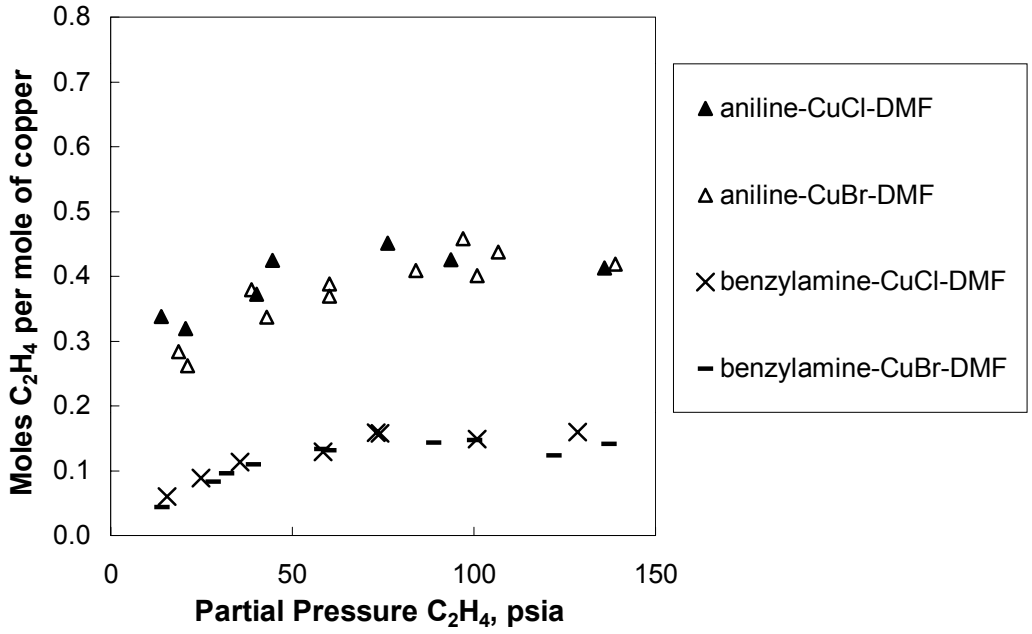

Figure 6-8. Calculated chemical equilibrium of CuCl and CuBr solutions

Like the aniline-CuCl-NMP solution shown in Figure 6-7, both aniline solutions in Figure 6-8 show a maximum ethylene capacity of about 0.5 moles of ethylene per mole of copper (i.e. a 2:1 copper:ethylene ratio). For the benzylamine solutions, the maximum ethylene capacity was around 0.16 moles of ethylene per mole of copper (i.e. a 6:1 copper:ethylene ratio). While bridged 2:1 metal:ligand complexes have been shown to exist for special literature systems [29], it is not likely that the complex would take on a 6:1 metal:ligand structure. Instead of pointing to the complex structure, the calculated ethylene capacity more likely is a function of the ligand strength. As mentioned earlier, strong ligands compete more for the copper site, so as the ligands are replaced with ethylene, the concentration of free ligands will increase to shift the equilibrium back to the left in equation (2-20). Contrary to the initial conclusion that the bromide ion contributed to inferior absorption solutions for aniline and benzylamine, these results suggest that the anion choice was nearly

irrelevant when compared to the ligand choice. Note that the lower copper solubility of the two CuBr cases is the factor that makes these solutions inferior not the anion's effect on the ethylene absorption.

6.3.5 Equilibrium modeling

Until this point, the equilibrium data of ethylene with the aniline-CuCl-NMP solution has been presented as data points with a fitted trendline to connect the equilibrium points; however, in order to successfully describe the absorption process, an equilibrium model should exist that sufficiently explains the reactions and phenomena that occur. For the simple case, the interaction between the complex and the ligand were ignored, and the equilibrium reaction is as shown before.

$$\mathrm{Cu}^{+} + x\left(\mathrm{C_2H_4}\right) \leftrightarrow \mathrm{Cu}^{+}\left(\mathrm{C_2H_4}\right)_x \tag{6-5}$$

For the case of a 1:1 copper:ethylene complex, the coefficient x is 1, and the equilibrium constant is defined by

$$\mathrm{K_{eq}} = \frac{\left[\mathrm{Cu}^{+}\left(\mathrm{C_2H_4}\right)\right]}{\left[\mathrm{Cu}^{+}\right]\left[\mathrm{C_2H_4}\right]} \tag{6-6}$$

where the activity coefficients are neglected here for simplification. In fact, for concentrated reactive absorption systems, Danckwerts [23] suggests that the use of activity coefficients is generally superfluous and can lead to substantial errors when calculating equilibrium and rate constants for different solution compositions.

The concentration of dissolved ethylene in equation (6-6) is given by equation (6-1) and the concentration of copper:ethylene complex is given by equation (6-4). The concentration of free copper can be found by a total copper balance and equation (6-6) becomes

$$\mathrm{K_{eq}} = \frac{c^{*}_{\mathrm{total}} - mP^{*}}{\left(c_{\mathrm{Cu\ total}} - c^{*}_{\mathrm{total}} + mP^{*}\right)\left(mP^{*}\right)} \tag{6-7}$$

where $c_{\text{Cu total}}$ is the total copper concentration, and m is the calculated Henry's law constant for the ethylene in copper case, 0.00264 mol·(L psia)$^{-1}$. Even though $c_{\text{Cu total}}$ is known as 1.16 M, in order to compare viable models, the total copper concentration will be treated as an unknown and calculated. Rearrangement of equation (6-7) in order to find the unknowns K_{eq} and $c_{\text{Cu total}}$ yields the following linear equation

$$\frac{c^*_{\text{total}}}{mP^*} = -K_{eq}\left(c^*_{\text{total}} - mP^*\right) + \left(1 + K_{eq} \cdot c_{\text{Cu total}}\right) \tag{6-8}$$

where the slope is $-K_{eq}$ and the y-intercept is $1+ K_{eq}\cdot c_{\text{Cu total}}$. Figure 6-9 shows the linear fit to this equation of the equilibrium data points below 100 psia. The R^2 value of the linear fit was 0.888 and the value of K_{eq} from the slope of the line was 45.2 L/mol. The calculated value of the total copper concentration was 0.65 M, which was 56% of the actual value of 1.16 M.

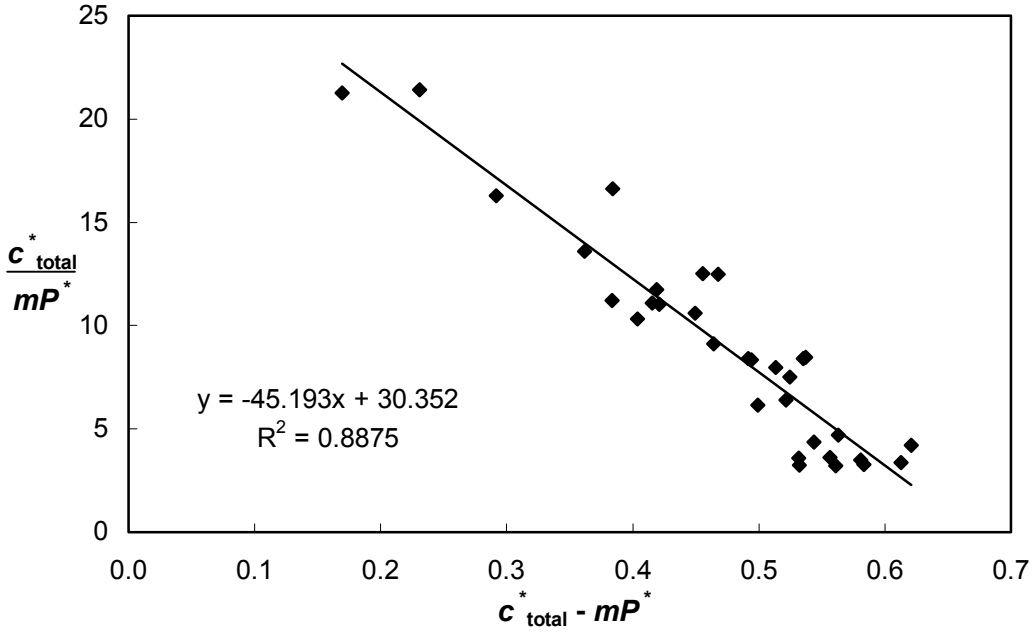

Figure 6-9. Linear fit for first-order equilibrium model

The low calculated copper concentration was expected from the simple first-order model due to the asymptotic limit observed in Figure 6-7 for the calculated chemical absorption. The explanation for this behavior using the first-order model is that only 56% of the copper in solution was available for ethylene complexation. The remaining 44% of the copper was inactive and did not participate in the reaction. The first-order equilibrium model satisfactorily matched the observed data for the total ethylene absorption as shown in Figure 6-10.

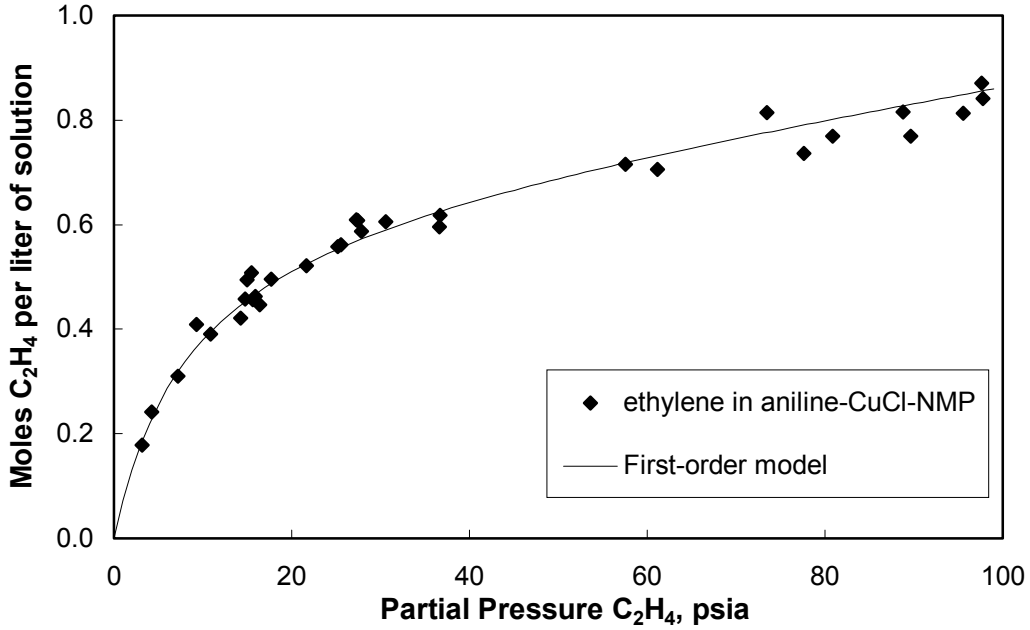

Figure 6-10. First-order model with equilibrium data

In order to test the hypothesis that the copper formed a 2:1 complex with ethylene, an equilibrium model that is second-order in copper was derived in the same manner as before. The reaction and equilibrium were defined as follows

$$2Cu^{+} + C_2H_4 \leftrightarrow \left(Cu^{+}\right)_2 C_2H_4 \qquad (6\text{-}9)$$

$$K_{eq} = \frac{\left[\left(Cu^{+}\right)_2 C_2H_4\right]}{\left[Cu^{+}\right]^2\left[C_2H_4\right]} \tag{6-10}$$

where the concentration of free copper now accounts for ions per complex formed. The mathematical expression for K_{eq} becomes

$$K_{eq} = \frac{c^*_{total} - mP^*}{\left(c_{Cu\ total} - 2\left(c^*_{total} + mP^*\right)\right)^2\left(mP^*\right)} \tag{6-11}$$

Linearization of equation (6-11) is much more difficult than equation (6-7) due to the unknown total copper concentration under the squared term. However, with the use of the Solver tool in MS Excel, partial linearization was sufficient to iteratively solve for both K_{eq} and $c_{Cu\ total}$ simultaneously. Rearrangement of equation (6-11) gives an expression with K_{eq} still in the *y* term on the left-hand side.

$$\left[\frac{c^*_{total}}{mP^*} - 1 - 4K_{eq}\left(c^*_{total} - mP^*\right)^2\right] = 4K_{eq}\cdot c_{Cu\ total}\left(mP^* - c^*_{total}\right) + K_{eq}\left(c_{Cu\ total}\right)^2 \tag{6-12}$$

By iteratively forcing the guessed value of K_{eq} in the *y* term to equal the calculated value from the slope and intercept, the best-fit line was found to have a K_{eq} of 13.0 M^{-2} and a total copper concentration of 1.70 M. The trendline fit of the equilibrium data for the second-order in copper case shown in Figure 6-11 had an R^2 value of 0.959. Even though the trendline fit for this model was somewhat improved over the first-order model, the total copper concentration result makes this model unreasonable. When the calculated copper concentration was lower than the actual value in the first-order model, at least a physical explanation was possible; however, when the copper concentration is calculated to be higher than the actual value, this result is not reconcilable with a logical physical argument. The complex was not believed to have a 2:1 copper:ethylene structure due to the fact that the second-order equilibrium model was inferior to the first-order model.

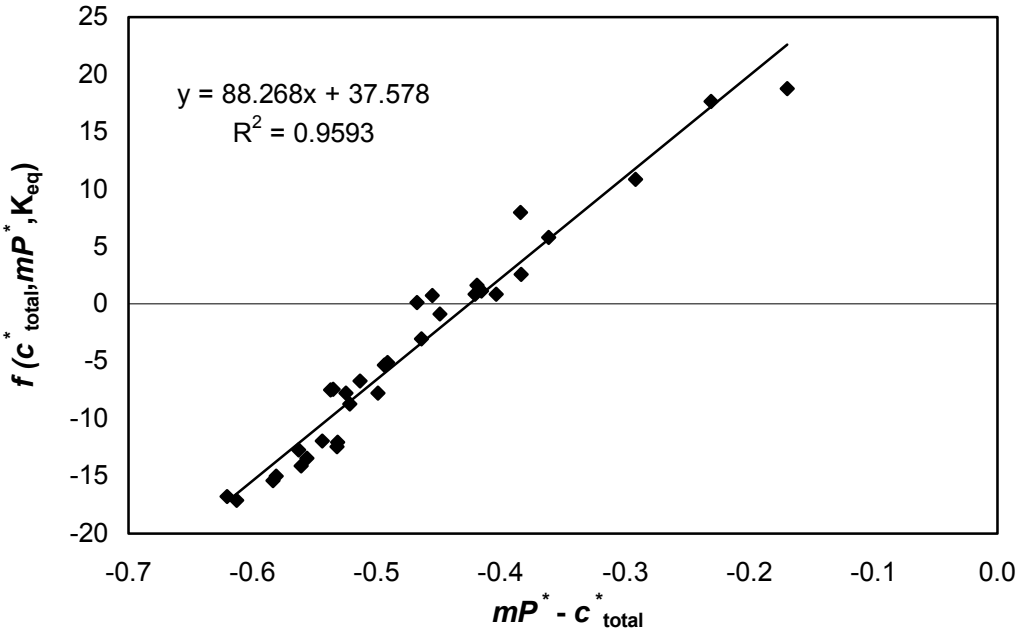

Figure 6-11. Second-order model with equilibrium data

As a further attempt to explain the equilibrium behavior of the ethylene complexation, the ligand substitution reaction was considered. The reaction and equilibrium expressions for the substitution of a ligand molecule with an ethylene molecule on the copper site is given by

$$\mathrm{Cu^{+}L}_{p} + \mathrm{C_2H_4} \leftrightarrow \mathrm{Cu^{+}L}_{p-1}\left(\mathrm{C_2H_4}\right) + \mathrm{L} \tag{6-13}$$

$$\mathrm{K_{eq}} = \frac{\left[\mathrm{Cu^{+}L}_{p-1}\left(\mathrm{C_2H_4}\right)\right]\left[\mathrm{L}\right]}{\left[\mathrm{Cu^{+}L}_{p}\right]\left[\mathrm{C_2H_4}\right]} \tag{6-14}$$

The concentrations of the dissolved ethylene, ligand complexed copper, and ethylene complexed copper were identical to the simple first-order model. The concentration of the ligand was found by a mass balance around the ligand

$$\mathrm{K_{eq}} = \frac{\left(c^{*}_{\text{total}} - mP^{*}\right)\left(c_{\text{anil total}} - p\left(c_{\text{Cu total}} - c^{*}_{\text{total}} + mP^{*}\right) - \left(p-1\right)\left(c^{*}_{\text{total}} - mP^{*}\right)\right)}{\left(c_{\text{Cu total}} - c^{*}_{\text{total}} + mP^{*}\right)\left(mP^{*}\right)} \tag{6-15}$$

where $c_{\text{anil total}}$ is the total concentration of aniline in solution, 4.62 M. For this model, the two unknowns are K_{eq} and p, the coordination number of the aniline-copper complex. The actual total copper concentration is used because the simple first-order model already sufficiently fits the data without using the actual copper concentration. Linearization of equation (6-15) was straightforward to yield the following expression.

$$c^*_{\text{total}} - mP^* = \mathrm{K}_{\text{eq}} \frac{\left(c_{\text{Cu total}} - c^*_{\text{total}} + mP^*\right)\left(mP^*\right)}{\left(c^*_{\text{total}} - mP^*\right)} + \left(p \cdot c_{\text{Cu total}} - c_{\text{anil total}}\right) \qquad (6\text{-}16)$$

The linear fit to this expression was very poor as shown in Figure 6-12 with an R^2 value of only 0.482. For the low pressure (< 30 psia) data corresponding to data points on the left of the plot, the points appear to line up with nearly a zero y-intercept (0.042), which would yield a ligand coordination number of 4. The value of K_{eq} for these low pressure points in 5.2 (unitless) but the R^2 value is still unacceptably low at 0.626. For the higher pressures, the y-intercept was 0.558 and the slope (K_{eq}) was 0.029 with an R^2 value of 0.002.

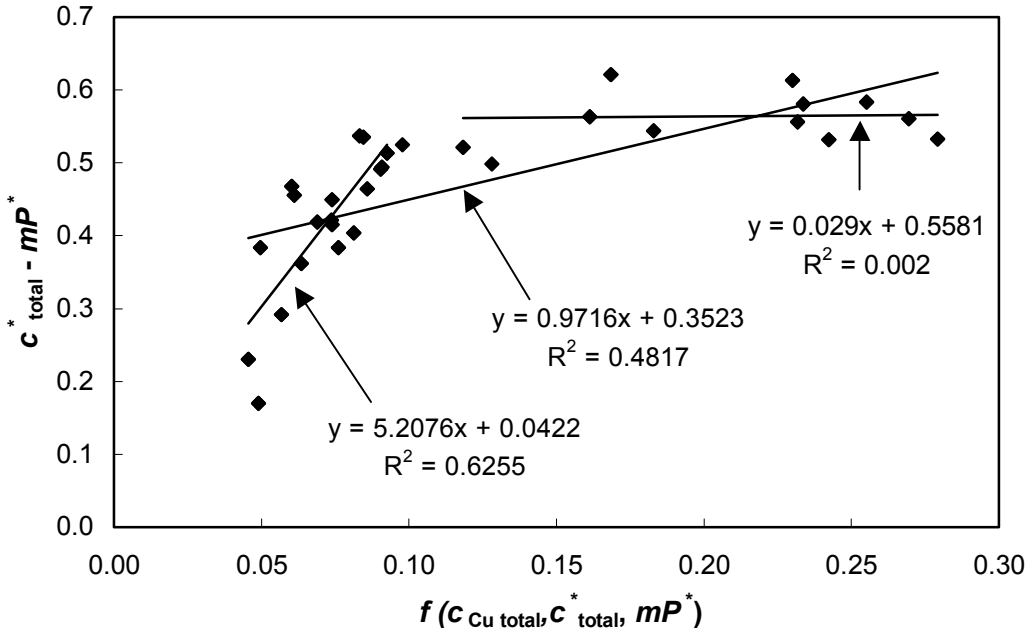

Figure 6-12. Ligand substitution model with equilibrium data

Even though the ligand substitution model showed a poor fit to the data, Figure 6-12 raises some interesting points to consider. If the ligand coordination number at low ethylene loadings is 4, then the aniline to copper ratio in solution is appropriate for ethylene absorption. At higher ethylene loadings, the concentration of free ligand is higher, and the equilibrium data predicts a lower equilibrium constant and a higher y-intercept corresponding to a coordination number of about 4.5. In order to fit the entire range data, the ligand coordination of the copper ion would need to vary depending on the free ligand concentration. This is probably not a reasonable assumption; however, it may possible that some fraction of the copper(I) ions are 4-coordinated and another fraction are 5-coordinated. Munakata and Kitagawa [79] note that although copper(I) complexes favor a four-coordinated tetrahedral geometry, three- or five-coordinate complexes frequently appear. It could be postulated that the ethylene will have an easier time replacing a ligand on the 4-

coordinated copper complexes due to approachability of the metal ion. For the 5-coordinated copper complex, the ligands effectively shield the metal ion such that the ethylene cannot approach as easily leading to a lower equilibrium constant. At lower ethylene loadings the equilibrium behavior would exhibit more of the 4-coordinated behavior increasing the concentration of free ligand driving reaction (6-18) to the right. The consumption of the 4-coordinated ethylene-free complex would effectively limit the amount of ethylene complexed because reaction (6-19) is less favorable.

$$Cu^{+}L_4 + C_2H_4 \leftrightarrow Cu^{+}L_3(C_2H_4) + L \tag{6-17}$$

$$Cu^{+}L_4 + L \leftrightarrow Cu^{+}L_5 \tag{6-18}$$

$$Cu^{+}L_5 + C_2H_4 \leftrightarrow Cu^{+}L_4(C_2H_4) + L \tag{6-19}$$

This phenomenon could explain the observed effects, but not enough information was available from the autoclave experiments to check its validity. Accordingly, these issues were not pursued further, and the simple first-order model was used in all subsequent equilibrium calculations.

6.3.6 Equilibrium selectivity

With the equilibrium model for ethylene absorption into the aniline-CuCl-NMP solution and the experimental physical solubilities of the non-reactive cases, the equilibrium selectivity was calculated. Selectivity at a given pressure was defined by the ratio of absorption (in mol/L) of ethylene to ethane. For the copper solution, the absorption of ethylene was calculated by the simple first-order model, and the absorption of ethane was the physical solubility.

$$s = \frac{c^{*}_{\text{total}}\left\{K_{\text{eq}}, c_{\text{Cu total}}, m_{\text{ethylene}}, P^{*}\right\}}{m_{\text{ethane}} P^{*}} \tag{6-20}$$

For the aniline-NMP solution, both gas concentrations in the liquid were calculated by the Henry's law constant. The calculated equilibrium selectivity is shown in Figure 6-13. For the copper solution, the selectivity was highest at the lowest gas

pressures because the physical solubility effects were dominated by the chemical complexation effects. The mixed gas selectivity was slightly lower than the pure gas because of the higher solubility of ethane when ethylene was present. At atmospheric pressure, the pure gas selectivity was about 15, and the mixed gas selectivity was about 12. At partial pressures over about 50 psia, the selectivity starts to level out due to the fact that the copper sites were becoming saturated while the physically solubility remains unchanged. For the copper-free solution, the ratio of the solubilities of the gases was 1.3, which was independent of pressure. Taken to much higher pressures, the liquid will eventually become saturated with the gas, but for the pressure range studied, no deviation from Henry's law was found.

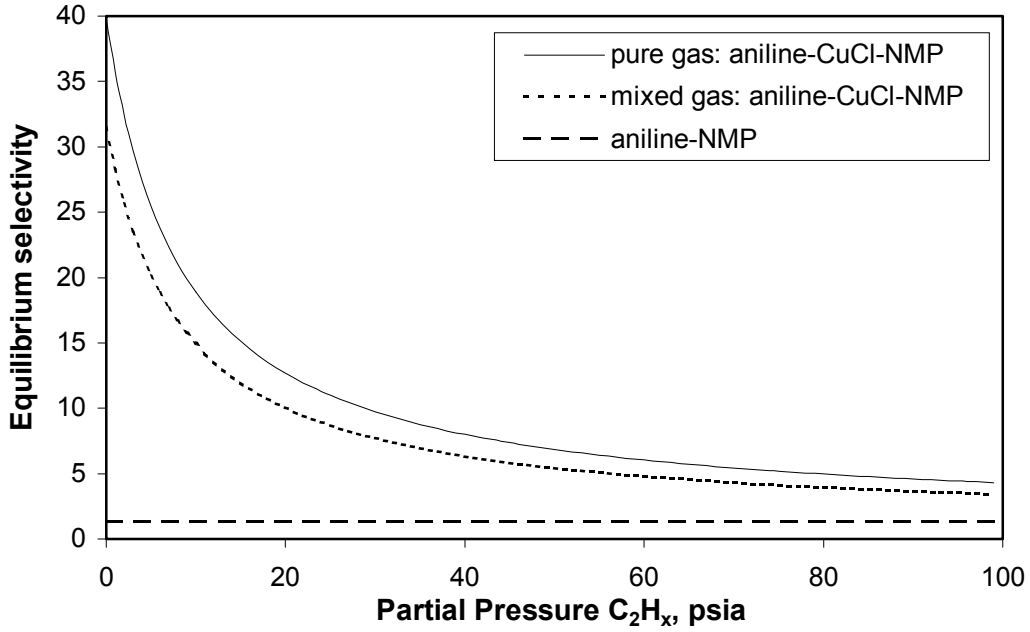

Figure 6-13. Equilibrium selectivity

A tradeoff existed for ethylene absorption and operating pressure such that higher pressures led to higher capacity but lower selectivity and lower pressures led to higher selectivity and lower capacity. Even though the maximum ethylene/ethane

selectivity was found at vacuum pressures, the low ethylene capacity would be prohibitory to optimum process design. An optimum range can be found by examining the calculated chemical effects in Figure 6-7. Since the extent of the chemical effects was observed to be around 40 psia, this ethylene pressure should be the maximum operating partial pressure. Below around 15 psia the chemical effects show the sharpest decrease, so this should be around the minimum operating pressure in order to not compromise capacity. Based on the stated operating range from about 15 psia to 40 psia, the mixed gas ethylene/ethane equilibrium selectivity for optimum process design should be between 7 and 12 from Figure 6-13.

6.4 Conclusion

The autoclave experiments provided a wealth of equilibrium data that was heretofore nonexistent for the chemical systems of interest. By comparison to the trends observed from the CV study, the total absorption of the copper solutions matched up very well; however, the autoclave absorption data included a significant amount of physical solubility built into the results. By manipulating the data based on the linear slope of the equilibrium curves at high pressures, the chemical effects were estimated for the aniline and benzylamine systems. The pyridine systems were found to contain negligible evidence of chemical absorption when compared to a copper-free solution. This study showed that the ligand choice was the most prevalent factor in absorption equilibrium. A comparison of NMP and DMF solvents showed that the absorption was not significantly different for these two solvents even though NMP was considered superior due to its lower volatility. A detailed equilibrium study of the aniline-CuCl-NMP solution provided information into the physical solubility, salting out effect, mixed gas ethane solubility enhancement, model development, and selectivity. The simple first-order reaction model was found to sufficiently fit the equilibrium data while predicting that a fraction of the copper was inactive for ethylene complexation. With the use of the equilibrium model, the

ethylene/ethane selectivity of the solution helped to find the optimum pressure range for an ethylene absorption process considering the tradeoff between selectivity and ethylene capacity.

Chapter 7.
Kinetics of absorption

7.1 Introduction

The kinetics of ethylene absorption were measured in the autoclave following the procedure described in section 3.2.3. Stirred cells have been used frequently in the literature for gas absorption; however, the amount of published work on the kinetics of ethylene absorption using transition metals has been nonexistent. The experimental technique of operating the gas and liquid batchwise to obtain kinetic information has been demonstrated by Jamal and Meisen [55] and Xu et al. [118]. By charging pure absorption gas and recording the pressure decrease, reaction coefficients were calculated for appropriate models to fit the experimental data. In a similar manner, this present study compared the fitting capability of five different kinetic models to determine which model best described the experimental data. The experimental data and calculated ethylene absorption rate for the kinetic experiments is given in Appendix A.6.

In developing a kinetic expression for ethylene absorption, several assumptions were made to simplify the calculations. The first assumption is that the film theory is valid for the system. Danckwerts [23] has shown that for most cases of gas absorption with chemical reaction and equal diffusivities of reacting species, the simple film theory provides equivalent accuracy to other more complicated models like penetration theory and surface renewal theory. In order to use kinetic expressions based on the film theory for stirred cells with cases where the diffusivities of the reactants are not equivalent, the diffusivity ratio of the reacting species must be replaced with the square root of the diffusivity ratio following Chang and Rochelle [12]. In order to maintain the reaction in the film, the liquid was not

stirred at high stirrer rates, which would lead to a distorted gas-liquid interface. A flat gas-liquid interface was necessary in the film theory so that the film thickness was uniform across the cross-section of the autoclave. Another key assumption is that the solution begins with negligible complexed and dissolved ethylene. The regeneration technique was found to effectively produce ethylene-free solutions in that successive absorption experiments gave repeatable equilibrium points, and HS-GC analysis on a regenerated solution sample showed negligible remaining ethylene. The next assumption is that mass transfer resistance in the gas phase is negligible. Since the ethylene was the only gas introduced into the autoclave and the ligand and solvent have a very small vapor pressure at the experimental temperature, the vapor phase consisted of pure ethylene. Stated another way, the assumption is that the components in the liquid phase are non-volatile. Not only should the ligand and solvent be non-volatile, but the copper-ligand and copper-ethylene complexes remain completely in the liquid phase.

In order to solve for the unknown concentrations in the liquid phase, some key assumptions about the interfacial and bulk concentrations were necessary as shown schematically in Figure 7-1. In the following discussion, the reversible, finite reaction rate model is used because it is the most complicated of the models considered. For other models to be discussed later, simplifications are noted.

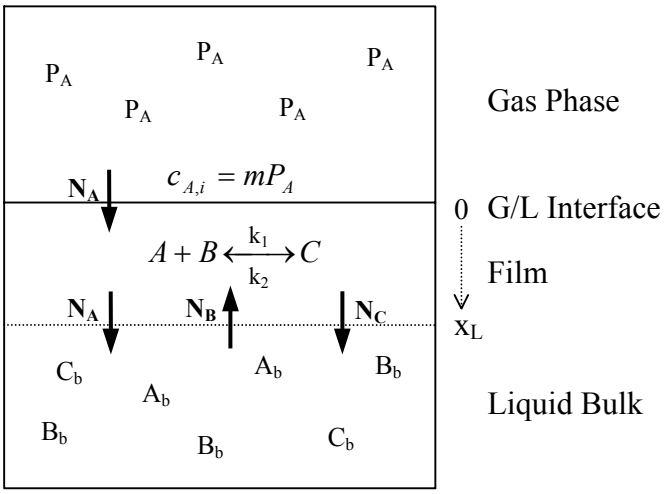

Figure 7-1. Schematic of gas-liquid concentrations

The interfacial concentration of ethylene in the liquid is given by the physical solubility of ethylene in equilibrium with the gas phase partial pressure. From the calculated Henry's law constant in equation (6-3), the uncomplexed ethylene concentration at the interface is given by

$$c_{A,i} = m_{\text{ethylene Cu}} P \tag{7-1}$$

where P is the measured pressure, which is a function of time. For simplicity, the complexation reaction (6-5) is rewritten as

$$A + B \xleftrightarrow{k_1, k_2} C \tag{7-2}$$

where k_1 and k_2 are forward and reverse reaction rate coefficients, respectively, A is uncomplexed ethylene, B is copper not complexed to ethylene, and C is the copper-ethylene complex (ligand interactions are ignored here). The reaction is assumed to occur exclusively in the film of thickness x_L, so that in the bulk of the liquid there is no more reaction proceeding. This assumption leads to the requirement that the bulk liquid is in equilibrium. For the kinetic experiment, the measured value as a function time was the total concentration of ethylene in the liquid, given previously as c_{total}.

Since a model describing the equilibrium for reaction (7-2) has already been established, equation (6-7) can be rearranged for the bulk pseudo-equilibrium pressure, P_b. This pressure is called the bulk pseudo-equilibrium pressure because the vapor-liquid system is not actually at equilibrium, but the bulk liquid is at an equilibrium state due to the assumption that the entire reaction occurs in the film. After solving the quadratic equation for P_b from equation (6-7), the bulk concentration of A, B, C are given by

$$c_{A,b} = m_{\text{ethylene Cu}} P_b \tag{7-3}$$

$$c_{B,b} = c_{\text{Cu total}} - c_{C,b} \tag{7-4}$$

$$c_{C,b} = c_{\text{total}} - c_{A,b} \tag{7-5}$$

where $c_{\text{Cu total}}$ is the calculated copper concentration to fit the equilibrium data and not the actual copper concentration.

7.2 Mass transfer coefficient

Before the kinetics of the reaction can be calculated, the mass transfer coefficient of the absorption must be known. Since absorption of ethylene into the copper solution is a reactive process, it is not possible to determine the mass transfer coefficient without additional information. The absorption rate for a system without reaction effects is given by

$$R_A = k_L^* a\left(c_{A,i} - c_{A,b}\right) \tag{7-6}$$

where k_L^* is the physical mass transfer coefficient and a is the interfacial area, which is constant 16.65 cm^2 from the cross-sectional area of the autoclave. The concentrations in the driving force in the right-hand side of equation (7-6) are calculated as described earlier, and R_A is measured experimentally from the total moles of gas absorbed per time. The calculated data for moles of gas in the vapor and $a(c_{A,i} - c_{A,b})$ versus time were fitted to polynomial functions in order to smooth out experimental inconsistencies for each kinetic experiment as shown in Figure 7-2. The

function for moles of gas in the vapor was differentiated to get the change in moles per time as a function of time.

$$R_A = -\frac{dn_A}{dt} \tag{7-7}$$

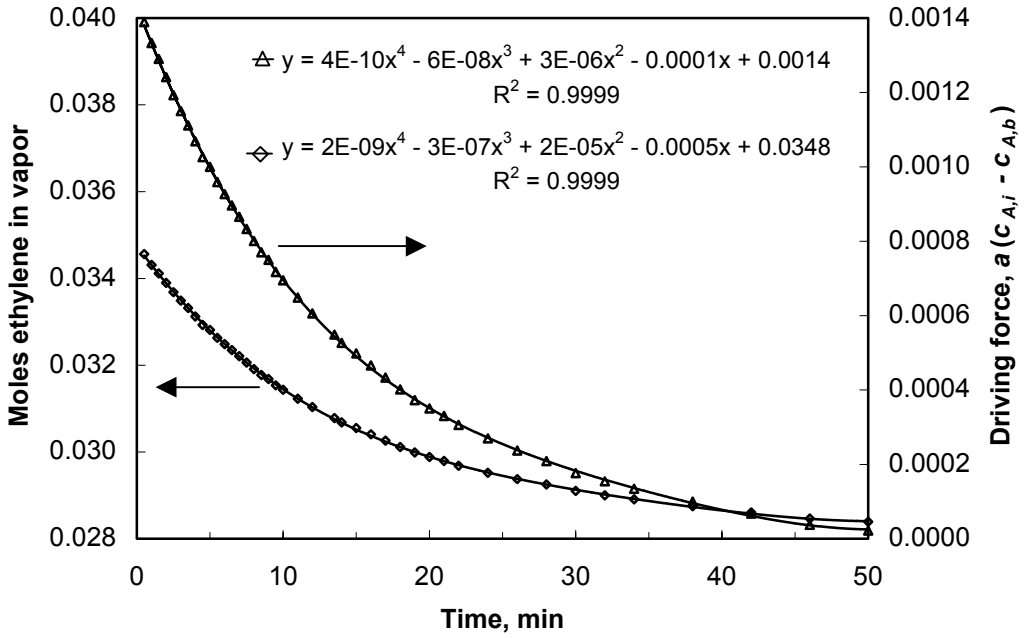

Figure 7-2. Experimental data for mass transfer coefficient

The non-reactive systems were ethylene in a copper-free solution of aniline and NMP as mentioned earlier, ethane in the copper-free solution, and ethane in the aniline-CuCl-NMP. Each experiment with these non-reactive systems at a different gas charge or different stirrer rate exhibited curves with shapes like those in Figure 7-2. A fourth-order polynomial fit was usually sufficient to fit the experimental data to an R^2 value of at least 0.999. In no case was the polynomial fit ever used to extrapolate the data beyond the fitted range. When the absorption rate from the derivative of the fit for moles of ethylene in the vapor was plotted versus the driving

force, a linear relationship with zero intercept was obtained as shown in Figure 7-3. The slope of this line was the mass transfer coefficient (0.00538 cm/s for the data shown). Also shown in Figure 7-3 is the experimental data without the polynomial fitting function. The absorption rate was found by a simple difference formula between successive points.

$$R_A = -\frac{\left(n_{A,2} - n_{A,1}\right)}{\left(t_2 - t_1\right)} \tag{7-8}$$

Even though the experimental data in Figure 7-2 showed a very regular fit to the polynomial trendline, the experimental error in the data is exaggerated when the algebraic difference absorption rate is plotted versus the driving force as shown by the "data points" in Figure 7-3. Most of the non-fitted data points fall within ± 20% of the trendline fitted values. The trendline fitted values showed a very good linear fit with an R^2 value of 0.998 in the example given and better than 0.99 for every other mass transfer experiment. There was usually a slight deviation very close to the origin corresponding to long reaction times and the approach to equilibrium. This deviation existed because at very low driving forces, the error between the experimental condition and the equilibrium point becomes somewhat significant. The experimental error inherent in finding an equilibrium point best reflects this observation.

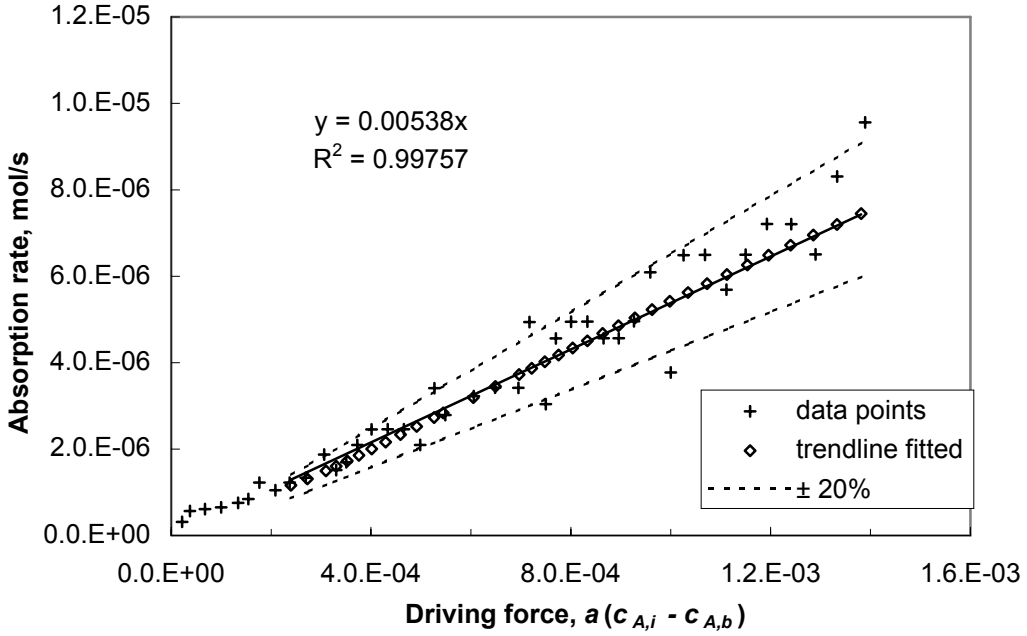

Figure 7-3. Linear fit for mass transfer coefficient

For each non-reactive system, the aforementioned experiment was repeated over a range of stirrer rates and gas charges. The range of gas charges studied was from 18 psia to 50 psia, and the magnitude of the gas charge was found to have no effect on the mass transfer coefficient. The range of stirrer rates studied varied depending on the gas-liquid system. Ethylene in aniline-NMP was the first system studied, so it covered the largest range of stirrer speeds. With stirrer rates from 120 rpm up to 260 rpm, a log-log plot of the mass transfer coefficient versus the stirrer rate as shown in Figure 7-4 was found to be very linear with an R^2 value of 0.994 and a maximum point deviation from linearity of 3%. The slope of this line was 0.84, which is close to the range of reported literature values. Hikita et al. [41] report a value of 0.7 for CO_2 absorption in water with stirrer speeds from 100 to 240 rpm; Versteeg et al. [114] give 0.72 for CO_2 and N_2O absorption in water and amine solutions with stirrer speeds from 18 to 90 rpm; and Jamal and Meisen [55]

give 0.77 for N_2 absorption in an amine solution with stirrer speeds of 1035 and 1550 rpm. Considerably fewer mass transfer experiments were performed with ethane and aniline-NMP than with ethylene. Due to fewer experiments, the R^2 value was slightly lower at 0.88, but the slope is the same as the ethylene case. The ethane in CuCl-aniline-NMP system showed the most scatter with an R^2 value of 0.58 and a maximum point deviation from linearity of 17%; however, with eight experimental data points, the slope of the points is nearly the same as the other cases.

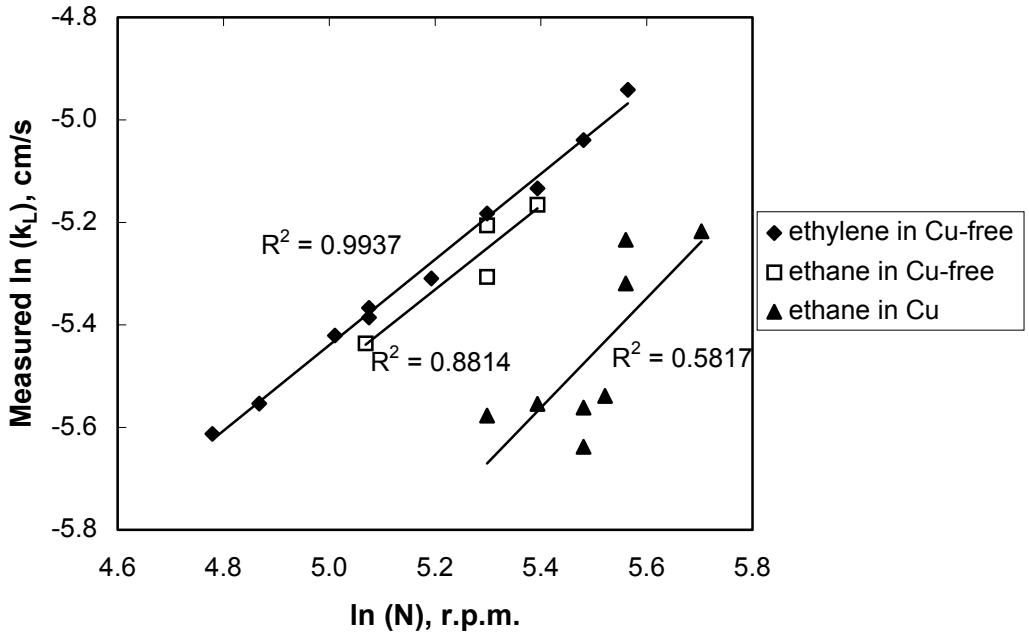

Figure 7-4. Mass transfer coefficient as a function of stirrer rate

The slope of the different systems in Figure 7-4 was expected to be a strong function of the stirrer position and setup of the contacting device and independent of the gas-liquid system [114]. In order to ensure that the depth of liquid from the gas-liquid interface to the stirrer was the same in the copper-free and CuCl solutions, the volume of the copper solution was carefully measured to be the same as the volume of the copper-free solution. The flatness of the gas-liquid interface in the region of

interest was confirmed by the linearity of data in Figure 7-4. According to Shrier and Danckwerts [96], such a log-log plot of k_L^* versus N will curve upwards showing significant deviation from linearity when the gas-liquid interface begins to be distorted. This behavior was observed at stirrer rates greater than 400 rpm (not shown) for the copper-free solution, but not over the range of stirrer rates used in the kinetic study.

The relationship between the stirrer rate and the mass transfer coefficient has been given in terms of dimensionless numbers to take the hydrodynamics of the entire process into consideration. In general, the correlation to fit mass transfer data is given by

$$\mathrm{Sh} = c1 \cdot \mathrm{Re}^{c2}\,\mathrm{Sc}^{c3} \tag{7-9}$$

where the dimensionless groups are defined by

$$\mathrm{Sh} = k_L^* d_{st} / D_A \tag{7-10}$$

$$\mathrm{Re} = d_{st}^2 N \rho_L / \mu_L \tag{7-11}$$

$$\mathrm{Sc} = \mu_L / \rho_L D_A \tag{7-12}$$

where d_{st} is the stirrer diameter (1¼"), D_A is the diffusivity of the gas in the liquid, N is the stirrer rate, ρ_L is the liquid density, μ_L is the liquid viscosity, and *c1*, *c2*, *c3* are constants to fit the data. The diffusivity estimated by the Wilke-Chang correlation was found to be 6.1×10^{-6} cm^2/s for ethylene in aniline-NMP. The mass transfer data for the ethylene in aniline-NMP system was regressed to fit equation (7-9). Literature systems typically assign *c3* as 0.33 or 0.5, and 0.5 was found to give satisfactory results for this study. The value of *c2* is the same as the slope of the log-log plot in Figure 7-4 given as 0.84. The value of *c1* was 1.74 from linear regression of the data. With these fitting parameters, the mass transfer coefficient for ethane in aniline-NMP was predicted and compared to the measured values as shown in Figure 7-5.

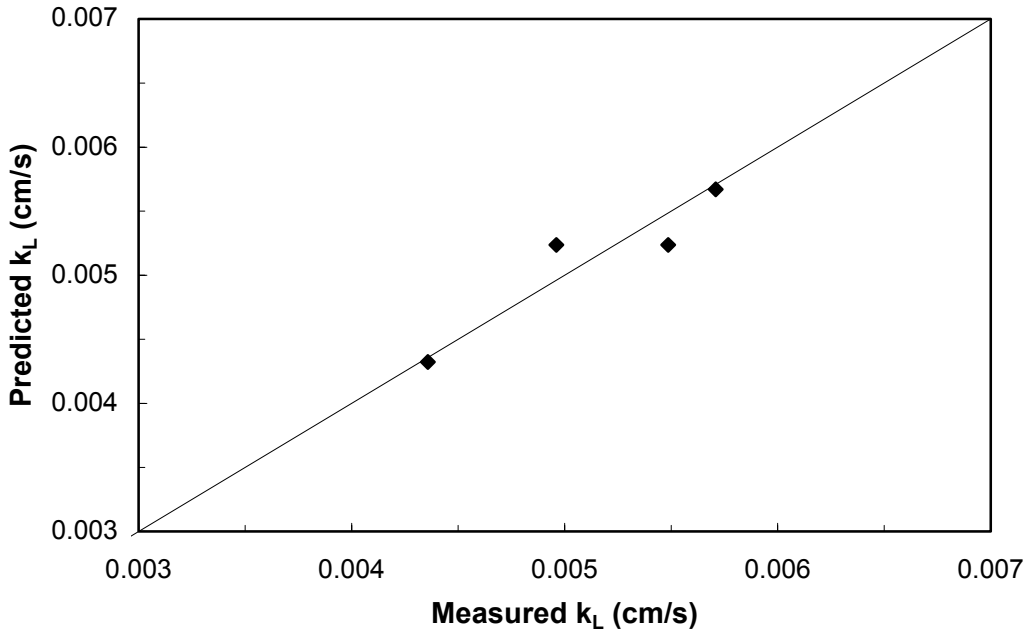

Figure 7-5. Experimental versus predicted k_L for ethane in aniline-NMP

Since the liquid was the same for the predicted values of the mass transfer coefficient as the regressed data, the only parameter in equation (7-9) that was different for the ethylene and ethane cases was the diffusivity. Due to the good fit with the predicted values, the ratio of ethylene to ethane diffusivities was correctly predicted by the Wilke-Chang correlation. Even though the ratio of diffusivities is accurate, there still may be quite a bit of error in the quantitative value of the diffusivity from the Wilke-Chang correlation. By rearranging equation (7-9) for the constant *c1*, the ratio terms for ethylene to ethane with the CuCl and the copper-free case can be related.

$$\frac{\left(\frac{k_L^* d_{st}}{\mathrm{Re}^{0.84}\,\mathrm{Sc}^{0.5} D_A}\right)_{\text{ethylene CuCl}}}{\left(\frac{k_L^* d_{st}}{\mathrm{Re}^{0.84}\,\mathrm{Sc}^{0.5} D_B}\right)_{\text{ethane CuCl}}} = \frac{\left(\frac{k_L^* d_{st}}{\mathrm{Re}^{0.84}\,\mathrm{Sc}^{0.5} D_A}\right)_{\text{ethylene Cu-free}}}{\left(\frac{k_L^* d_{st}}{\mathrm{Re}^{0.84}\,\mathrm{Sc}^{0.5} D_B}\right)_{\text{ethane Cu-free}}} \tag{7-13}$$

To simplify equation (7-13), the stirrer impeller was the same for all experiments, and the liquid density and viscosity were the same for a given solution.

$$\frac{\left(\frac{k_L^*}{N^{0.84} D_A^{0.5}}\right)_{\text{ethylene CuCl}}}{\left(\frac{k_L^*}{N^{0.84} D_B^{0.5}}\right)_{\text{ethane CuCl}}} = \frac{\left(\frac{k_L^*}{N^{0.84} D_A^{0.5}}\right)_{\text{ethylene Cu-free}}}{\left(\frac{k_L^*}{N^{0.84} D_B^{0.5}}\right)_{\text{ethane Cu-free}}} \tag{7-14}$$

For different solutes in the same solution, the only term in the Wilke-Chang correlation in equation (7-15) that remains in the ratio of diffusivities is the molar free volume of the solute V_A, which is 0.0444 m^3/kgmole for ethylene and 0.0518 m^3/kgmole for ethane [42].

$$D_A = \frac{1.17\text{x}10^{-9}\left(\xi_B M_B\right)^{0.5} T}{V_A^{0.6}\,\mu} \tag{7-15}$$

where D_A is given in cm^2/s, ξ_B is the association factor of the solvent 1.0, M_B is the molecular weight of the solvent, T is the temperature in Kelvin. After substitution is made for diffusivity in equation (7-14), the solvent dependent terms in the Wilke-Chang equation cancel; moreover, the ratio of the molar free volume of the solute on both sides of equation (7-14) is equivalent, so these terms cancel also. An equal ratio of mass transfer coefficients is obtained for equivalent stirrer rates for each solution, and the mass transfer of ethylene in the CuCl is simply

$$\left(k_L^*\right)_{\text{ethylene CuCl}} = \frac{\left(k_L^*\right)_{\text{ethylene Cu-free}}}{\left(k_L^*\right)_{\text{ethane Cu-free}}} \cdot \left(k_L^*\right)_{\text{ethane CuCl}} \tag{7-16}$$

where the stirrer rate at which k_L^* for ethylene in CuCl-aniline-NMP is found must be the same as the stirrer rate for ethane in CuCl-aniline-NMP. The copper-free systems

do not necessarily have to be at the same stirrer rate as the CuCl solutions as long as the stirrer rate which k_L^* is evaluated is the same for ethylene and ethane. For the copper-free solutions, k_L^* values at 200 rpm were used, and for the CuCl solutions 260 rpm and 300 rpm were used. This analogy for the mass transfer coefficient has been used previously in the literature for reactive absorption processes by Ebrahimi et al. [26] for H_2S absorption using the analogous case of N_2O in water and in ferric sulfate solutions. The mass transfer coefficient for ethylene in aniline-CuCl-NMP at 300 rpm was calculated from trendline values of k_L^* for each non-reactive system in Figure 7-4.

$$\left(k_L^*\right)_{\text{ethylene CuCl}} = \frac{0.00557_{@\,200\,\text{rpm}}}{0.00524_{@\,200\,\text{rpm}}} \cdot 0.00531_{@\,300\,\text{rpm}} = 0.00565\,\text{cm/s} \tag{7-17}$$

The reactive absorption kinetic experiments were performed at 300 rpm, so this value of the mass transfer coefficient was used in the following calculations.

7.3 Reaction kinetic models

In order to determine the kinetic effects due to chemical reaction, the enhancement factor is defined as the ratio of the actual rate of ethylene absorption to the rate for strictly physical absorption.

$$\Phi = \frac{R_{\text{observed}}}{R_{\text{physical}}} = \frac{R_{\text{observed}}}{k_L^* a\left(c_{A,i} - c_{A,b}\right)} \tag{7-18}$$

The observed rate of absorption was calculated at all points throughout the experiment based on change in moles in the gas phase, and the interfacial and bulk ethylene concentrations were found as described previously.

7.3.1 Finite, reversible model

In comparison of the different models used to describe the kinetic behavior, the reversible finite rate model is discussed first, and the simplifications associated with the other models will be developed in order. For reaction (7-2), Onda et al. [82]

have shown that material balances on each species give the following equations where *A* is uncomplexed ethylene, *B* is copper not complexed to ethylene, and *C* is the copper-ethylene complex

$$D_A \frac{d^2 c_A}{dx^2} = k_1 c_A c_B - k_2 c_C \tag{7-19}$$

$$D_B \frac{d^2 c_B}{dx^2} = k_1 c_A c_B - k_2 c_C \tag{7-20}$$

$$D_C \frac{d^2 c_C}{dx^2} = -\left(k_1 c_A c_B - k_2 c_C\right) \tag{7-21}$$

with the boundary conditions defining the interfacial and bulk concentrations and stating that the flux of the components other than ethylene is zero across the gas-liquid interface.

$$\text{at } x = 0: \quad \begin{array}{l} c_A = c_{A,i}\,;\, c_B = c_{B,i}\,;\, c_C = c_{C,i} \\ \dfrac{dc_B}{dx} = 0\,;\, \dfrac{dc_C}{dx} = 0 \end{array} \tag{7-22}$$

$$\text{at } x = x_L: \quad c_A = c_{A,b}\,;\, c_B = c_{B,b}\,;\, c_C = c_{C,b} \tag{7-23}$$

Solving equations (7-19) and (7-20) with the boundary conditions gives the relationship between free ethylene and the copper-ethylene complex in the film

$$c_C = c_{C,b} + \frac{N_A}{D_C}\left(x_L - x\right) - \frac{D_A}{D_C}\left(c_A - c_{A,b}\right) \tag{7-24}$$

where N_A is the molar flux of ethylene. In order to express the enhancement factor in terms of the interfacial and bulk concentrations, equation (7-24) was substituted back into equation (7-19) and an approximation was made by replacing c_B with $c_{B,i}$. This approximate solution by Onda et al. was shown to compare to within 1% to exact numerical solutions [82]. The resulting expression for the enhancement factor with the substitution for the diffusivity ratios following [12] is given as

$$\Phi = \frac{\left(c_{A,i} - c_{A,b}\right)\left(1 + \frac{1}{T}\sqrt{\frac{D_C}{D_A}}\right) + \sqrt{\frac{D_C}{D_A}}\left(\frac{c_{A,b}}{T} - c_{C,b}\right)\left(1 - \operatorname{sech}\sqrt{M_2}\right)}{\left(c_{A,i} - c_{A,b}\right)\left(1 + \frac{1}{T}\sqrt{\frac{D_C}{D_A}}\frac{\tanh\sqrt{M_2}}{\sqrt{M_2}}\right)} \tag{7-25}$$

where

$$M = \frac{k_1 c_{B,b}}{D_A} x_L^2 \tag{7-26}$$

$$M_2 = M\left(\frac{c_{B,i}}{c_{B,b}}\right)\left(1 + T\sqrt{\frac{D_A}{D_C}}\right) \tag{7-27}$$

$$T = \frac{K_2 c_{A,i}}{c_{B,i}} \tag{7-28}$$

$$K_2 = \frac{k_2}{c_{A,i} k_1} \tag{7-29}$$

$$c_{B,i} = c_{B,b} - \sqrt{\frac{D_C}{D_B}}\left(c_{C,i} - c_{C,b}\right) \tag{7-30}$$

where k_1 and k_2 are the forward and reverse rate coefficients, respectively. The solution to this set of equations requires iteration equation (7-25) while using equation (7-30) to solve the following equation for the enhancement factor at the interface.

$$\Phi = 1 + \sqrt{\frac{D_C}{D_A}}\frac{\left(c_{C,i} - c_{C,b}\right)}{\left(c_{A,i} - c_{A,b}\right)} \tag{7-31}$$

By guessing values of $c_{C,i}$ and solving equations (7-25) and (7-31) for Φ, the value of $c_{C,i}$ was adjusted until the difference in Φ for each point was minimal.

For the reversible kinetic models, the first-order equilibrium model from section 6.3.5 was used to calculate equilibrium concentrations. While the equilibrium model was found to show a good fit to the data, a small deviation from the model was

found to have a significant effect on the calculated concentrations in the kinetic experiment. Figure 7-6 shows a comparison of the actual ethylene uptake versus the absorption predicted from the first-order model. The equilibrium absorption data from the two kinetic experiments deviated from the predicted values. As a result, the equilibrium constant for the specific kinetic experiment was calculated from equation (6-7) and used for the model calculations.

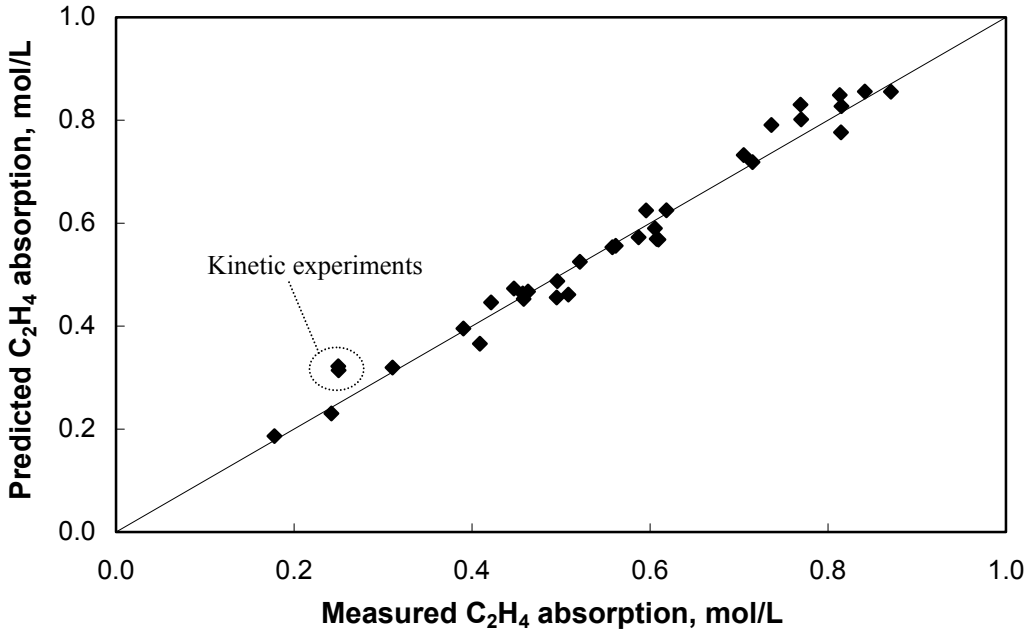

Figure 7-6. Measured and predicted ethylene absorption equilibrium

In order to determine whether the kinetic model accurately fit the data, the calculated rate of absorption from the model was set equal to the observed rate of absorption at the start of the kinetic experiment. The unknown parameters were adjusted until this fit was obtained. For the reversible, finite rate model, the unknown parameters were the forward reaction rate coefficient and the ratio of diffusivities D_A/D_B and D_A/D_C. The relative diffusivities of the copper-ethylene complex and the uncomplexed copper were assumed to be equivalent. An estimation of the reactant

diffusivities was made with equation (7-15) giving D_A = 3.0x10^{-6}cm^2/s and D_B = 7.5x10^{-7}cm^2/s. The ratio of diffusion coefficients D_A/D_B by the Wilke-Chang correlation was 4. The reaction rate coefficient was found to counteract the diffusivity ratio such that a decrease in the diffusivity ratio required an increase in the reaction rate coefficient and vice versa in order to fit the data at the initial condition. This relationship is intuitive because the diffusion of material into and out of the reaction film must be balanced by the rate which material reacts in the film. Figure 7-7 shows the effects of diffusivity ratios of 4, 2, and 1 on the fitted reaction rate coefficient (with units of L/mol·s) and the resulting fit to the actual data. The actual pressure versus time data and experimental conditions for the kinetic experiments are given in Appendix A.6.

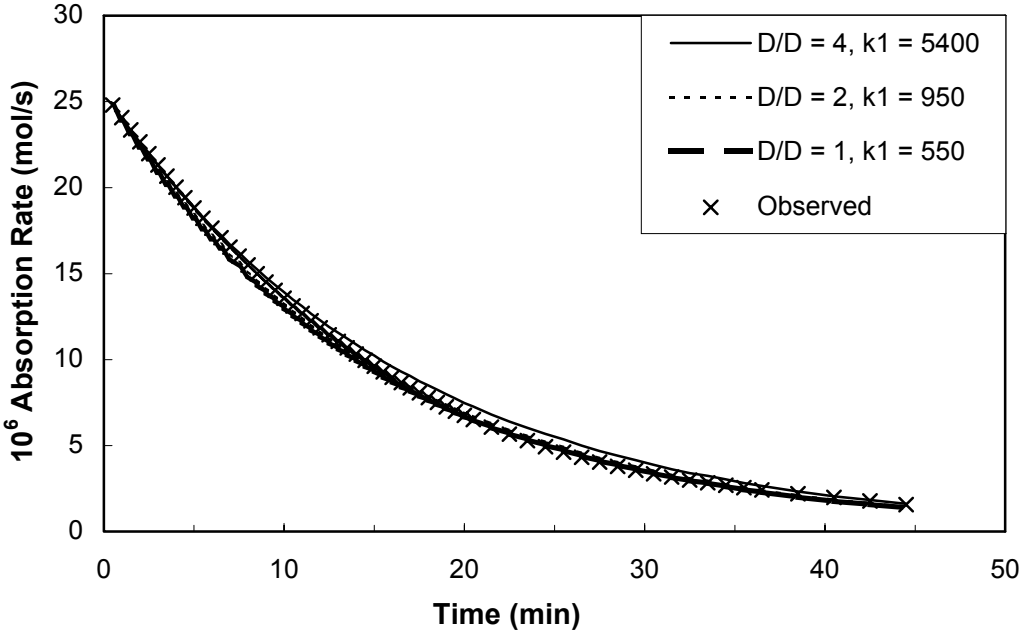

Figure 7-7. Finite, reversible model fitting parameters

Overall, the three different combinations of diffusivity and reaction rate in Figure 7-7 match the data very well. The case with equal diffusion coefficients

required the lowest value of k_1 (550 L/mol·s) to fit the data. As the diffusion coefficient of the copper reactant species was decreased, the model required increasingly higher reaction rates. With a D_A/D_B of 4 corresponding to the Wilke-Chang prediction, the reaction rate coefficient was 5400 L/mol·s. Since the copper reactant with coordinating aniline ligands attached would not be expected to diffuse as quickly as dissolved ethylene, this fit is preferred over the nearly equivalent fits to the data with lower D_A/D_B ratios. More insight into the counter-acting effects of diffusivity and reaction can be obtained by examining the concentrations of the reacting species at the interface and in the bulk using the finite, reversible model. The interfacial free ethylene was calculated based on the gas pressure as described earlier, and the dissolved gas in the bulk was found from the equilibrium condition. These concentrations are shown in Figure 7-8 for the duration of the kinetic experiment.

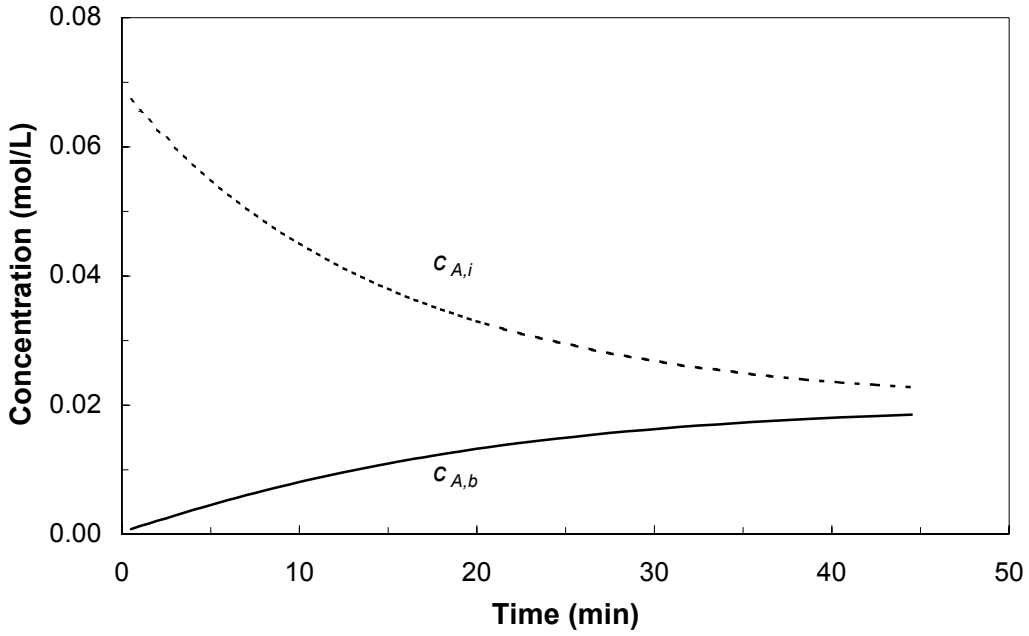

Figure 7-8. Interfacial and bulk concentrations of dissolved ethylene

The interfacial concentration of uncomplexed copper was found from equation (7-30) and the iterative solution of the model equations was used to find the interfacial concentration of the copper-ethylene complex. The bulk concentrations were determined from the equilibrium condition throughout the experiment. Results of these calculations are shown in Figure 7-9 and Figure 7-10 with diffusivity ratios of 1 and 4, respectively. Examination of these concentration profiles confirm that for each reacting species, the interfacial and bulk concentrations tend toward one another as the experiment proceeds to equilibrium at long times.

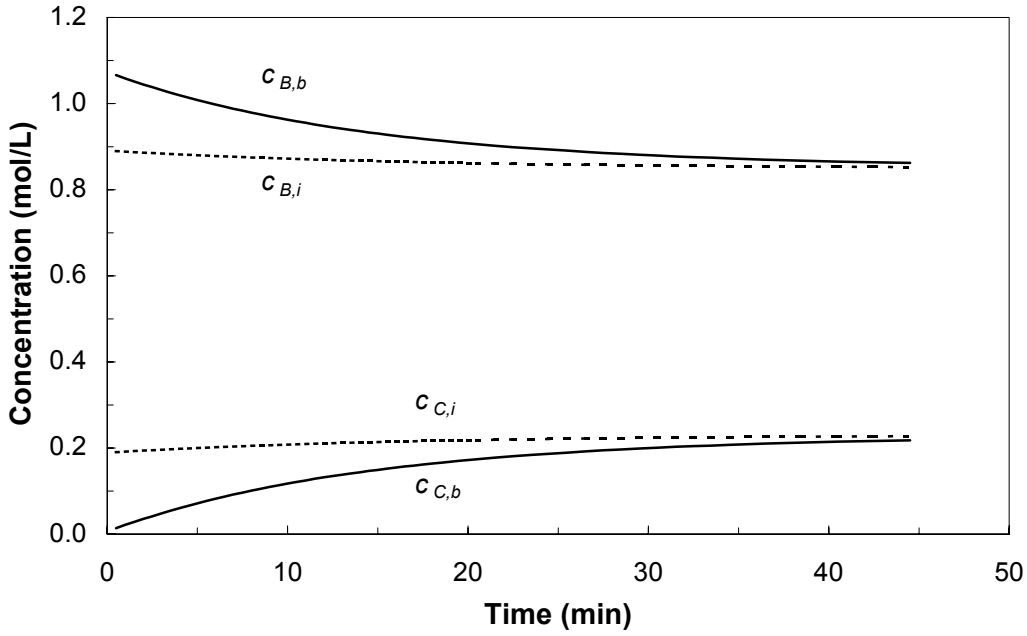

Figure 7-9. Interfacial and bulk concentrations of B and C at $D_A/D_B = 1$

For the case of equal diffusivities in Figure 7-9, the interfacial concentrations were rather close to the bulk concentrations throughout the length of the experiment. Since the diffusion of copper species is faster than in other cases, the products and reactants move into and out of the film more quickly. With less inhibition to the equilibrium reaction proceeding, the reaction rate does not have to be as high to fit the

data. Since the interfacial concentrations approach the bulk concentrations rather quickly, this case gives the shortest time to approach the bulk equilibrium condition.

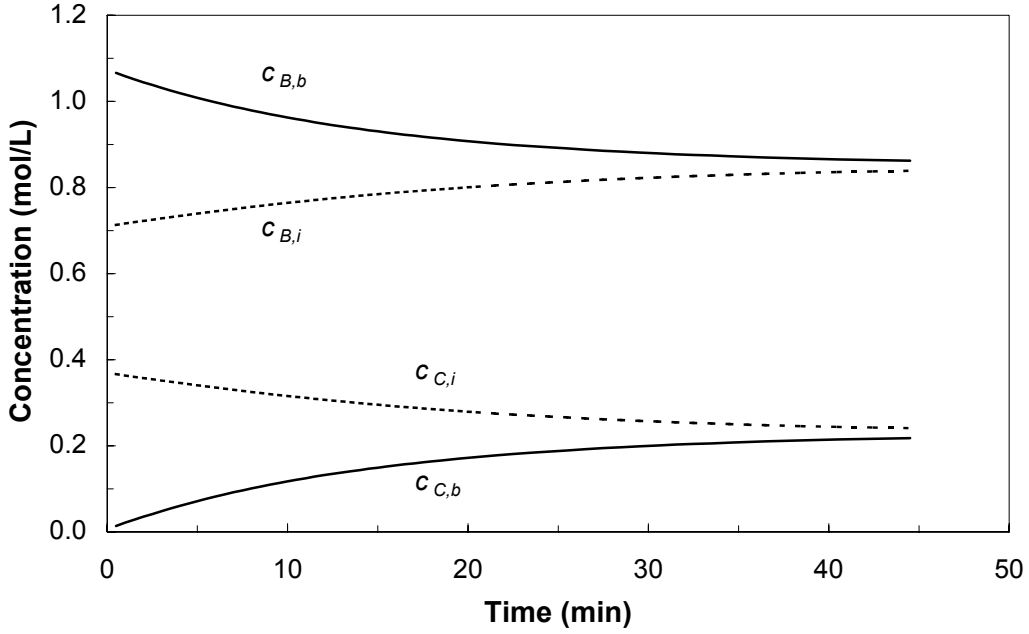

Figure 7-10. Interfacial and bulk concentrations of B and C at $D_A/D_B = 4$

For a diffusivity ratio of 4, the reaction rate coefficient was nearly an order of magnitude greater than with a diffusivity ratio of 1. Since the reaction in the film is occurring much faster than in the previous case, the model predicts that the interfacial concentration of the copper-ethylene complex will decrease with time. This behavior is opposite from the previous case because with the faster reaction, the products are building up at the interface faster than diffusion can carry them back into the bulk. In addition, the reactants are being consumed more quickly leading to lower interfacial concentrations of uncomplexed copper. These effects serve to inhibit the reaction driving force, so the approach to the bulk equilibrium condition is not as close as the previous case at long times.

While the counter-acting effects of diffusion and reaction serve to produce equivalent fits to the data in Figure 7-7, the case with a diffusivity ratio of 4 was most appropriate from a physical argument. The copper complex with coordinating ligands attached will likely diffuse many times slower than a simple dissolved ethylene molecule.

7.3.2 Instantaneous, reversible model

When the reaction rate coefficient is extremely large, the finite, reversible model is simplified to become the instantaneous, reversible model. Equations (7-19) through (7-21) are reduced to the following

$$D_A \frac{d^2 c_A}{dx^2} + D_C \frac{d^2 c_C}{dx^2} = 0 \tag{7-32}$$

$$D_B \frac{d^2 c_B}{dx^2} + D_C \frac{d^2 c_C}{dx^2} = 0 \tag{7-33}$$

with the boundary conditions given by equations (7-22) and (7-23). Danckwerts [23] has shown that the solution to these equations for the reaction rate is given by

$$R_A = k_L^* \left(c_{A,i} - c_{A,b}\right)\left[1 + \frac{D_B D_C \mathrm{K}_{\mathrm{eq}} c_{B,b}}{D_A\left(\mathrm{K}_{\mathrm{eq}} c_{A,i} D_C + D_B\right)}\right] \tag{7-34}$$

By making the assumption again that the diffusivities of the uncomplexed copper and the copper-ethylene complex are equal and using square roots as before, equation (7-34) can be simplified and written as the enhancement factor.

$$\Phi = 1 + \sqrt{\frac{D_B}{D_A}} \frac{\mathrm{K}_{\mathrm{eq}} c_{B,b}}{\left(\mathrm{K}_{\mathrm{eq}} c_{A,i} + 1\right)} \tag{7-35}$$

The diffusivity ratio is the unknown parameter in equation (7-34) that was adjusted until the calculated rate of absorption matched the experimentally measured rate of absorption. Unlike the finite rate model where the diffusivity ratio could be assigned any value and the reaction rate coefficient solved, the instantaneous model considers the reaction rate to be infinite; therefore, the diffusivity ratio can only have

one value that gives a fit to the experimental rate data at the beginning of the experiment. Optimization of D_A/D_B resulted in a value of about 5, which was slightly higher than the values tried with the finite, reversible model. In fact, by using a diffusivity ratio of 5 with the finite, reversible model an extremely high reaction rate coefficient of over $1x10^7$ L/mol·s was required to fit the data at time = 0. A comparison of the predicted absorption rates with the instantaneous and finite, reversible reaction models in Figure 7-11 confirms that with the high reaction rate coefficient required to fit the data, the finite model produces equivalent results to the instantaneous model.

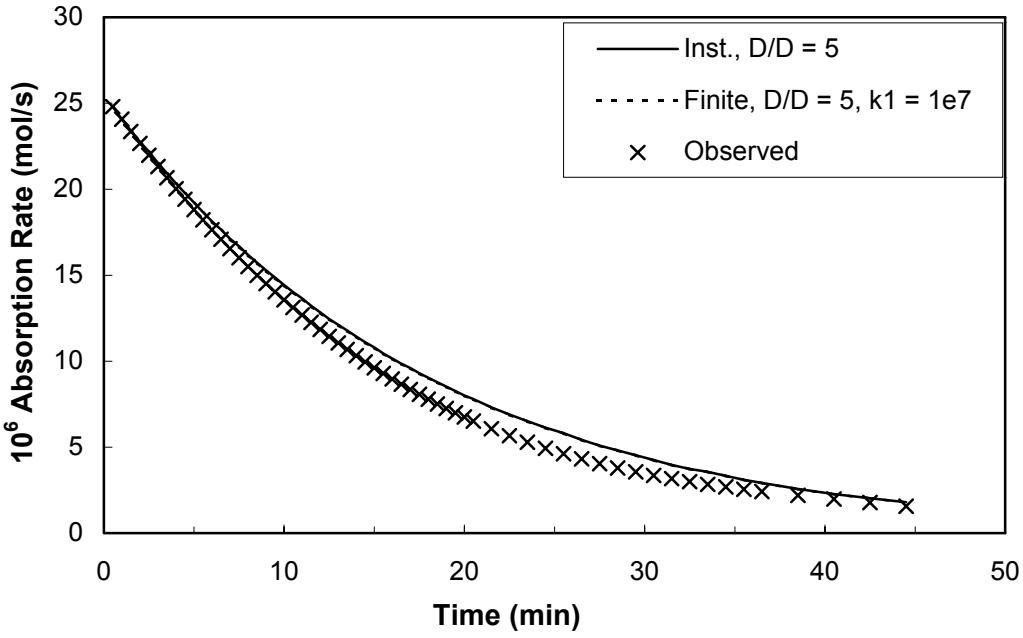

Figure 7-11. Comparison of finite and instantaneous, reversible models

The match with the experimental data with the instantaneous, reversible model was just as good as the finite, reversible model. The calculated diffusivity ratio of 5 is very reasonable when compared to the Wilke-Chang prediction. Given

the extremely high reaction rates required by the finite rate model, the ethylene complexation reaction was accurately approximated as an instantaneous reaction.

7.3.3 Finite, irreversible model

While equilibrium data and desorption experiments have confirmed that ethylene absorption in the copper solution is reversible, the irreversible model was investigated to determine whether an approximation could be found to accurately model the reaction over a specific range (i.e. short reaction times). A simplification of reaction (7-2) is found by neglecting the reversibility such that the reaction is given by

$$A + B \xrightarrow{k} C \tag{7-36}$$

The film model process is described by

$$D_A \frac{d^2 c_A}{dx^2} - k c_A c_B = 0 \tag{7-37}$$

$$D_B \frac{d^2 c_B}{dx^2} - k c_A c_B = 0 \tag{7-38}$$

with the boundary conditions given by equations (7-22) and (7-23). These equations can be solved numerically, but an approximation is available [112] for the case where $c_{A,b} = 0$, which is true at early times in the experiment. The enhancement factor is given by

$$\Phi = \frac{\sqrt{M \frac{\Phi_i - \Phi}{\Phi_i - 1}}}{\tanh \sqrt{M \frac{\Phi_i - \Phi}{\Phi_i - 1}}} \tag{7-39}$$

where M and Φ_i are given by

$$M = \frac{D_A k c_{B,b}}{\left(k_L^*\right)^2} \tag{7-40}$$

$$\Phi_i = 1 + \sqrt{\frac{D_B}{D_A}} \frac{c_{B,b}}{c_{A,i}} \tag{7-41}$$

The solution of equation (7-39) is iterative and the unknown parameters in the model are the diffusivity ratio and the reaction rate coefficient. The behavior of these two parameters was similar to the finite, reversible model in that a decrease in the diffusivity ratio required an increase in the rate coefficient. However, the effect of varying the diffusivity ratio on the absorption rate as a function of reaction time was minimal as shown in Figure 7-12. The fit to the experimental data for this model was obtained at $D_A/D_B = 1$ with $k = 178$ L/mol·s and at $D_A/D_B = 4$ with $k = 222$ L/mol·s. Overall the prediction of the experimental absorption rate was poor for the finite, irreversible model.

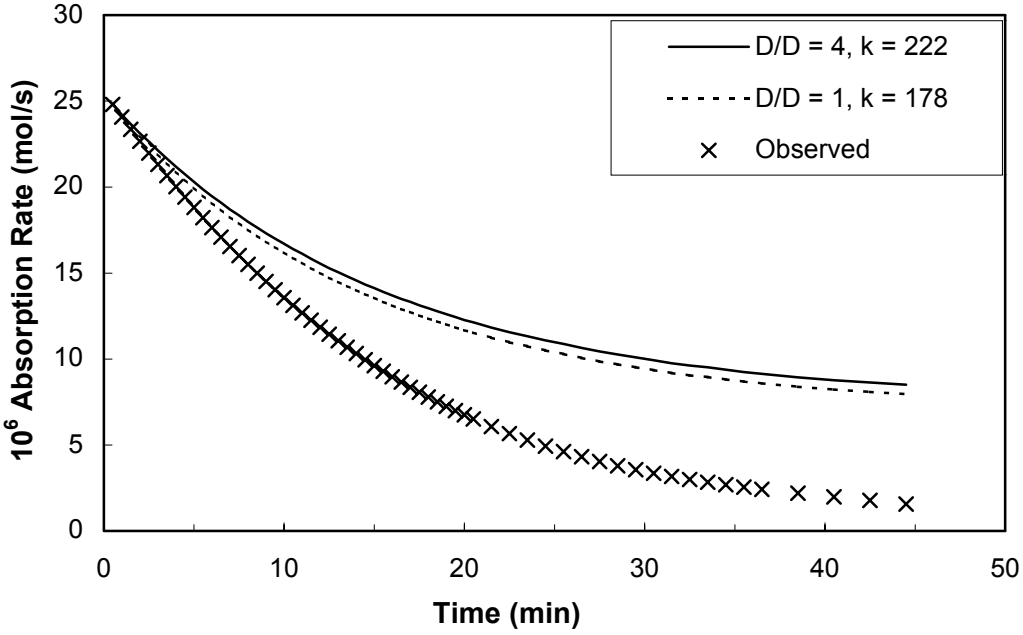

Figure 7-12. Diffusivity and reaction rate coeff. in finite, irreversible model

7.3.4 *Pseudo-first order model*

A simplification of the finite, irreversible second order model is found by assuming that the concentration of *B* does not change much during the reaction so that the concentration of *B* can be treated as a constant.

$$A \xrightarrow{k_1 B} C \tag{7-42}$$

The film model process is described by

$$D_A \frac{d^2 c_A}{dx^2} - k' c_A = 0 \tag{7-43}$$

where *k'* is $k_1 \cdot c_B$ and boundary conditions are given in equation (7-22) and (7-23) where applicable. An analytical solution for the enhancement factor has been reported in the literature [23]

$$\Phi = \frac{\left(c_{A,i} - \frac{c_{A,b}}{\cosh\sqrt{M'}} \right) \frac{\sqrt{M'}}{\tanh\sqrt{M'}}}{\left(c_{A,i} - c_{A,b} \right)} \tag{7-44}$$

where *M'* is given by

$$M' = \frac{D_A k'}{\left(k_L^* \right)^2} \tag{7-45}$$

The only unknown parameter to fit in the pseudo-first order model was the reaction rate coefficient that was determined as $k' = 159\ s^{-1}$. The predicted absorption rate with this model is shown in Figure 7-13. The model is nearly equivalent to the finite, irreversible model, thus the fit to the experimental data was also poor.

7.3.5 *Instantaneous, irreversible model*

Another way to simplify the reaction model is to assume that the reaction is very fast and irreversible. For this model, the bulk concentration of ethylene must be zero at all times. Solution of equations (7-32) and (7-33) with $c_{A,b} = 0$ gives the following expression for the enhancement factor.

$$\Phi = 1 + \sqrt{\frac{D_B}{D_A}} \frac{c_{B,b}}{c_{A,i}} \tag{7-46}$$

By fitting the model to the data at time = 0, the unknown diffusivity ratio D_A/D_B was calculated to be 6. Examination of the predicted reaction rate in Figure 7-13 shows that this model produced the worst fit to the experimental data. Since the finite, irreversible model was found to show a poor fit, it is not surprising that the instantaneous version of this model showed a bad fit also.

7.3.6 Reaction model summary

From Figure 7-13, all three irreversible models deviated from the experimental data to a greater extent at longer reaction times. At short times the finite, irreversible and pseudo-first order models were relatively close to the experimental data, so these models may have limited use for applications with a large driving force where the equilibrium condition is not approached. However, only the reversible models followed the appropriate shape of the experimental data throughout the entire data range. Table 7-1 gives the form and values of the fitting parameters used for each model in Figure 7-13.

Table 7-1. Reaction model form and parameters

Type	Form	D_A/D_B	k
Inst., irrev.	$A + B \rightarrow C$	6	NA
Pseudo-1st	$A \xrightarrow{k_1 B} C$	NA	159 s^{-1}
Finite, irrev.	$A + B \xrightarrow{k_1} C$	4	222 L/mol·s
Inst., rev.	$A + B \leftrightarrow C$	5	NA
Finite, rev.	$A + B \xleftarrow{k_1, k_2} C$	4	5400 L/mol·s

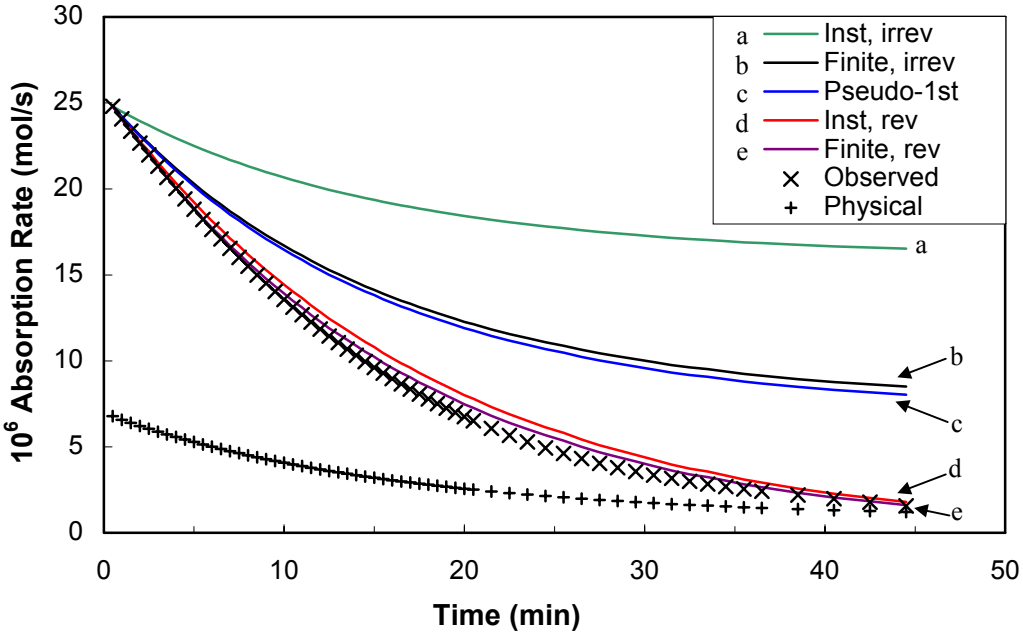

Figure 7-13. Comparison of reaction kinetic models

In comparison to the observed data and the reaction models, the calculated rate of physical absorption from equation (7-6) is also shown in Figure 7-13. At the beginning of the experiment the observed absorption rate was much higher than the calculated physical absorption rate with an enhancement factor of 3.66. Near the end of the experiment, the observed absorption rate approached the physical absorption rate leading to enhancement factors near unity for times over about 40 minutes. At the low stirrer rate used for the kinetic experiments, equilibrium was found to require very long times evident by the very slow approach of the experimental absorption rate to zero. After the rate slowed considerably (at times over about 40 minutes in Figure 7-13), the stirrer rate was increased to accelerate vapor-liquid equilibrium.

7.4 Conclusion

The determination of reaction kinetics is critical for the design of a reactive absorption process. If the chemical reaction rate were slow, absorption process design would require more mass transfer area or longer residence times in order to achieve sufficient olefin capacity. However, the kinetic experiments suggested that the ethylene complexation reaction was instantaneous. For instantaneous reactions, absorption equipment would be designed for high mass transfer coefficients with short contact times to selectively absorb more olefin than paraffin. In this way, equilibrium solubility of the paraffin would be avoided in order to increase the selectivity of the solution for the reacting gas.

The diffusivity ratio (D_A/D_B) calculated for the instantaneous, reversible model was 5, which compared well to the roughly estimated Wilke-Chang value of 4. Since a more accurate prediction of the diffusion coefficient for the concentrated metal-ligand complex was not found in the literature, an experimental investigation into this property would be helpful to confidently state the value of the diffusion coefficient.

Chapter 8.
Continuous absorption/regeneration process

8.1 Introduction

In order to evaluate the ethylene absorption solution in a flow environment, experiments were performed with the continuous absorption/regeneration process described in detail in section 3.3. Compared to the autoclave experiments, the mass transfer properties in this experiment more closely resemble those encountered in an industrial absorption process. While the mass transfer in the autoclave experiments was sufficient for the kinetic study, the gas-liquid contacting scheme in a packed absorption tower is much more favorable for gas absorption. A further goal of this study was to apply the equilibrium and kinetic findings to the operation of the packed absorption and regeneration contactors.

For all experiments in the continuous absorption/regeneration process, a prepared solution of aniline-CuCl-NMP was used with calculated molarities of 1.05 M, 4.64 M and 5.80 M respectively. The same solution whose total volume was about 1.8 L was used throughout the entirety of the experiments. One set of experiments was run for a period of five continuous weeks using the 30/70 ethylene/nitrogen blend as the feed gas, and another set of experiments was run for about one week with the 50/50 ethylene/ethane blend. The cylinder charge of the ethylene/nitrogen blend was much larger than that for the ethylene/ethane blend allowing for a larger variety of operating conditions and longer operation including the repetition of pertinent conditions on different days. The significant results for each gas feed are presented below.

8.2 30% Ethylene / 70% Nitrogen

The purpose of the experiments with the ethylene/nitrogen blend was to evaluate the operating conditions of the process as well as to determine if accurate results were obtainable. The carrier gas nitrogen was assumed to remain in the gas phase completely, so for the material balance around the absorber, ethylene was the only component transferred to the liquid. The absorption solution was assumed to be nonvolatile such that no solvent was lost to the gas phase. Several experiments were conducted with similar gas and liquid flowrates over the duration of the study to check the repeatability of the process and to examine the stability of the absorption solution. In addition, the two pinch conditions were examined where the solution was completely loaded with ethylene and where the ethylene was completely removed from the feed gas.

8.2.1 Material balance

A complete list of the flow conditions studied with the ethylene/nitrogen blend was given in Table 3-2. The compositions of ethylene in the gas product and liquid feed and product streams were found by analytical HS-GC results as described earlier. A material balance on the absorber shown schematically in Figure 8-1 was used to check the accuracy of the results. The overall mass balance is simply

$$V_f - V_p = L_p - L_f \tag{8-1}$$

where V refers to the total molar flowrate of vapor, L is the total molar flowrate of liquid, and f and p subscripts refer to the feed and product streams respectively. V_f and L_f are directly measured in the experiment by the mass flowmeters and converted to molar flowrates. A component balance on the carrier gas solves for V_p.

$$V_p = \frac{V_f\left(1 - y_f\right)}{\left(1 - y_p\right)} \tag{8-2}$$

The overall mass balance on ethylene relates the change in moles of the vapor and liquid streams.

$$V_f y_f - V_p y_p = L_p x_p - L_f x_f \tag{8-3}$$

For the initial experiments, the feed sampling procedure was not in place, so the material balance was used to calculate the ethylene composition in the feed x_f.

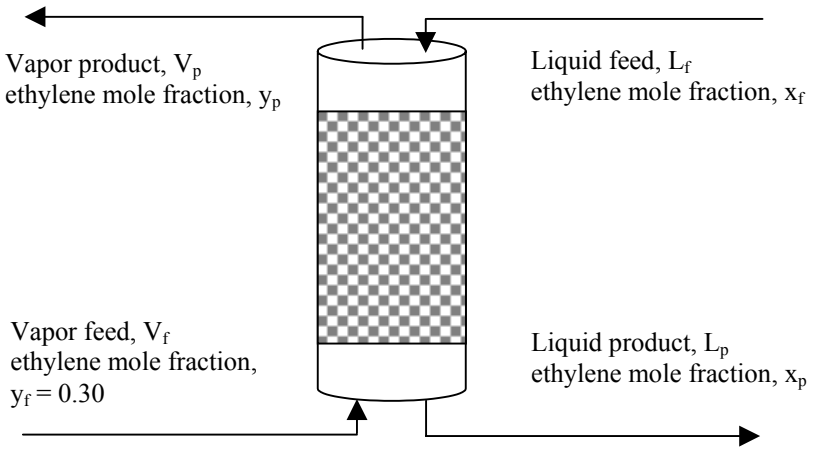

Figure 8-1. Schematic of absorber material balance

Of these different experiments, several were run at liquid flow rates of 20 lb/hr and gas flow rates around 5 SLPM corresponding to a molar flow ratio of ethylene-free liquid to carrier gas of about 10. Table 8-1 gives a summary of the analytical results from these experiments. The absorber temperatures were relatively constant for these experiments between 21ºC and 23ºC, and the temperature of the regeneration flask was maintained at 60ºC for these experiments. The initial experiments performed on 6/20 showed liquid product ethylene mole fractions of 0.025 and 0.024 while the final experiments performed over a month later (with the same solution) showed x_p of 0.029 to 0.023. The solution proved to be very robust showing no observable decrease in ethylene absorption over the duration of the experiment. The mole fraction of ethylene leaving the absorption column in the

vapor was relatively constant for all experiments around 0.16 except for the experiment on 7/23. For this experiment, the mole fraction ethylene in the liquid feed was at the highest value of 0.010. In fact, the regeneration section only removed about 66% of the absorbed ethylene for this case compared to around 74% for the other cases on 6/25 and 7/25. (Comparison with the values from the initial experiment on 6/20 was avoided because these were not analytical results but calculated from the mass balance.)

Table 8-1. Results from ethylene/nitrogen experiments at L/G = 10

Date	Absorber Temp (ºC)	Gas Flow (SLPM)	Liquid Flow (lb/hr)	y_p	x_p	x_f	Ethylene Recovery
6/20	23.0	4.87	19.8	0.16	0.025	0.002*	0.56
6/20	23.0	4.87	19.8	0.16	0.024	0.002*	0.55
6/25	23.3	4.94	19.7	0.16	0.027	0.007	0.57
7/23	20.8	4.94	19.9	0.21	0.029	0.010	0.37
7/25	22.7	4.94	20.0	0.15	0.023	0.006	0.58
* Calculated from mass balance							

The most probable cause of the high liquid feed concentration was the inefficient design of the regeneration step. The heat for the process was applied to the liquid that had already exited the packed column instead of preheating the liquid before entering the regeneration column. In addition, the flowrate of nitrogen that was used as a stripping gas was not monitored, so it likely varied over a wide range from one experiment to the next. Variations in the stripping gas flowrate likely contributed to the inconstancy of x_f, leading to a lower overall recovery of the feed gas in some cases. The recovery of ethylene R is defined as the ratio of moles of ethylene absorbed on a vapor basis to the total vapor feed ethylene.

$$R = \frac{V_f y_f - V_p y_p}{V_f y_f} \tag{8-4}$$

When the liquid feed entered the absorber with more ethylene, the driving force for mass transfer was lower, and the column was more inefficient at recovering ethylene from the vapor feed as seen by low value of R for the experiment on 7/23. After the high liquid feed concentration on the 7/23 experiment, the nitrogen stripping gas flowrate was increased to a rate just below what would cause flooding in the regeneration column. The liquid feed ethylene concentrations for all subsequent experiments were significantly decreased as a result of this adjustment.

Replicate analytical samples were taken for nearly every experiment with the ethylene/nitrogen blend. For the samples of x_p by HS-GC, the average relative standard deviation of replicate measurements was 2.3% with the maximum deviation for a single experiment 4.7%. The precision of the feed samples was not as good with an average RSD of 25%. While the quantity of ethylene in the feed samples was much smaller on the order of 0.005 mole fraction, the absolute error is about the same as the liquid product samples, which are on the order of 0.025 mole fraction. The total error involved with a liquid sample was approximately ±0.001 mole fraction ethylene. For the gas analysis, the average RSD of replicate samples was 8%. Since standard gas samples were analyzed with the sample from nearly every experiment, the results of these standards give another estimate of the precision of the gas sampling technique. Table 8-2 gives the results of standard gas samples that were withdrawn from the cylinder feed gas via a bypass around the absorption column. Quantification was performed with pure ethylene as described in section 4.5. The average of these values is 29.7 mole% ethylene with a standard deviation of ±0.9 mole% (an RSD of less than 3%) confirming that the sampling technique has sufficient accuracy and precision. It is not known why the gas product samples showed a higher RSD than the gas feed samples. One possible reason for the discrepancy is that while pulling the samples with the gas-tight syringe, the flowrate of the product samples was not high enough to ensure complete filling of the 8 mL

space. Since the feed sample was withdrawn from a bypass around the column, the actual flowrate was likely higher than experimental flowrates of the product gas.

Table 8-2. Results from feed samples

Date	Calculated mole% ethylene
6/20	29.24
6/25	29.84
7/16	28.75
7/18	28.88
7/25	31.02
8/1	30.26

Considering the error associated with the liquid and gas sample results, the material balance converges for most experiments as shown in Table 8-3. Convergence of the material balance was determined by rearranging equation (8-3) for the absolute difference between the calculated moles of ethylene transferred.

$$Error = \left|\left(V_f y_f - V_p y_p\right) - \left(L_p x_p - L_f x_f\right)\right| \tag{8-5}$$

The experiments where the material balance converged easily are denoted by an error of 0 in Table 8-3. The uncertainties in the analytical results for y_p, x_p, and x_f were included in the calculation of the error. Typically between 1 and 2 moles of ethylene were transferred, so the experiments in cases 6 – 8 and 13 contained a considerable magnitude of error. Cases 1 – 4 were not included because the liquid feed was not sampled in these experiments, so a material balance check was not possible. The low liquid rate experiments showed poor convergence of the material balance possibly due to operating times that were shorter than required from equation (3-19). For the experiment on 7/23 with a liquid rate of 5 lb/hr, the process was operated for 5 hours before the samples were taken, and the error in the material balance was considerably lower than the previous experiments with similar flow conditions. The experiments on 7/16 and 7/17 were only operated for 1 and 1.5 hours before sampling giving errors of 0.33 and 0.41 moles of ethylene, respectively. The experiment that showed

the worst convergence was only run for 1 hour while the required time was over 11 hours.

Table 8-3. Material balance results from ethylene/nitrogen experiments

Case	Gas Flow (SLPM)	Liquid Flow (lb/hr)	y_p ±0.009	x_p ±0.001	x_f ±0.001	Req'd time, hr	Act. time, hr	Error, mol
5	4.94	19.7	0.16	0.027	0.007	1.1	2.5	0.03
6	4.95	2.2	0.24	0.027	0.003	11	1	0.59
7	4.89	5.0	0.23	0.032	0.006	4.4	1	0.33
8	4.99	5.2	0.22	0.032	0.002	4.4	1.5	0.41
9	4.87	29.9	0.16	0.022	0.006	0.73	1	0
10	0.95	20.1	0.005	0.011	0.003	1.1	1.5	0
11	4.97	5.0	0.25	0.033	0.010	4.4	5	0.10
12	4.94	19.9	0.21	0.029	0.010	1.1	1.5	0.01
13	4.94	20.0	0.15	0.023	0.006	1.1	2.5	0.36
14	1.63	20.0	0.014	0.015	0.003	1.1	2	0

8.2.2 Equilibrium pinch

In order find the ethylene loading capacity of the copper solution in the absorption column, operating conditions were chosen to approach absorption equilibrium. By using low liquid flows with adequate gas flows, the gas-liquid contact was maximized. Three experiments were conducted at total gas feed rates around 5 SLPM and total liquid feed rates around 5 lb/hr. The liquid product of each had an ethylene mole fraction of 0.032 – 0.033 as shown in Table 8-3. From the equilibrium results in section 6.3, the absorbed ethylene concentration in equilibrium with a gas feed at a partial pressure of 22.5 psia (i.e. 0.3 * 75 psia) was estimated to be around 0.54 mol/L corresponding to a mole fraction of 0.046. The vapor product mole fractions for these flow experiments were in the range from 0.22 to 0.25. For the low end of this range, the equilibrium ethylene concentration at 16.5 psia

(0.22 * 75 psia) was about 0.50 mol/L corresponding to a liquid mole fraction of 0.043. With the liquid flowrate of 5 lb/hr, the ethylene loading was still about 70% of the equilibrium value for the partial pressure at the bottom of the column. The reaction was not limited by the ethylene in vapor phase because even at the top of the column, the equilibrium concentration was considerably higher than the liquid product.

In an attempt to achieve a closer approach to equilibrium in the liquid product, the liquid flowrate was further lowered to 2 lb/hr. At such a low flowrate, the liquid entering the regeneration column had decreased to a slow trickle. Instead of increasing the ethylene concentration in the liquid product, this flowrate actually resulted in a lower ethylene mole fraction of 0.027. This result was not clearly understood; however, the analytical value is based on only a single liquid sample decreasing the confidence in the measured value where the other experiments had replicate samples. It is also noteworthy that this experiment produced the poorest convergence of the mass balance from Table 8-3 suggesting that perhaps one of the concentrations was incorrect.

Two possible explanations are given for the lower than expected value of ethylene loading at low liquid flowrates. The first is based on the observation that after the first day of operation, the solution showed visual darkening as associated with oxidation in section 5.5. Possibly some fraction of the active copper was depleted by this oxidation leading to a lower equilibrium value than measured with the autoclave experiments. If this were the case, the solution was stable enough such that additional time in the continuous absorption/regeneration process did not produce further loss of capacity. No autoclave equilibrium work was attempted to find the absorption behavior of a darkened oxidized solution. The second possible explanation for the low ethylene loading is that the dynamics of mass transfer and reaction were too slow to reach equilibrium in the contactor used. However, the kinetics of the ethylene complexation reaction were shown in section 7.3.2 to be

instantaneous, so it is not likely that a taller column or a packing with more active area would yield a higher concentration of ethylene in the liquid product at the pinch condition studied.

For these low liquid flowrate experiments, the regeneration temperature was set to 70ºC, and the absorber temperatures ranged from 20.8ºC and 21.6ºC. From examination of the values of the liquid feed mole fractions from Table 8-3, the higher regeneration temperatures for the lower flowrate experiments did not lead to consistently lower values of x_f. The liquid feed mole fraction from case 11 at 0.010 was just as high as the highest value when the regeneration flask was set to 60ºC. This result implied that the regeneration efficiency was not a strong function of the temperature of the regeneration flask.

In order to determine the maximum recovery of ethylene in the feed, the process was run with low gas rates and moderate liquid flow rates. From Table 8-3 gas flowrates of 0.95 SLPM and 1.63 SLPM were used in cases 10 and 14, respectively, with liquid flowrates of about 20 lb/hr each. The gas product mole fractions for each of these cases were 0.005 and 0.014 corresponding to ethylene recovery of 0.99 and 0.95. While these low gas flowrates enabled very high ethylene removal, the loading of the liquid product was relatively low at ethylene mole fractions of 0.011 for case 10 and 0.015 for case 14. These concentrations are less than half those achieved with moderate gas rates. To achieve high values of ethylene recovery with acceptable ethylene loadings, the absorption column would certainly require more height (i.e. equilibrium stages) with the current packing. The ethylene recovery for all of the experiments with the ethylene/nitrogen blend as a function of L/G ratio is shown in Figure 8-2.

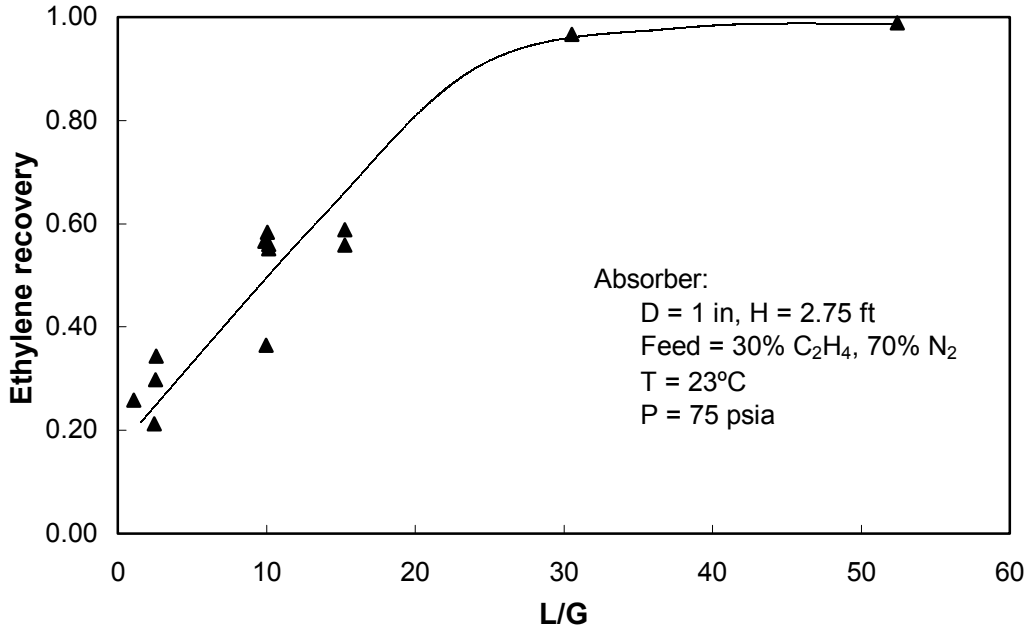

Figure 8-2. Ethylene recovery as a function of L/G

As the gas rates decreased and/or liquid rates increase, ethylene recovery increased linearly until reaching the asymptotic limit of 1.0. Separate experiments performed at the same L/G showed significant scatter such as at L/G = 10 and at L/G = 2.5. As discussed previously, this scatter is likely due to inefficient regeneration of the liquid causing the feed liquid to have a considerably amount of ethylene. Figure 8-3 shows the relationship between the mole fraction of ethylene in the feed liquid with ethylene recovery. A higher concentration of ethylene entering with the feed corresponds to a lower driving force, which yields a lower recovery of the feed gas. For the two values of L/G shown, the trend of ethylene recovery with x_f seems to be identical. Due to the influence of the regeneration efficiency on ethylene recovery, the nitrogen stripping gas rate was increased as discussed previously for the ethylene/ethane experiments.

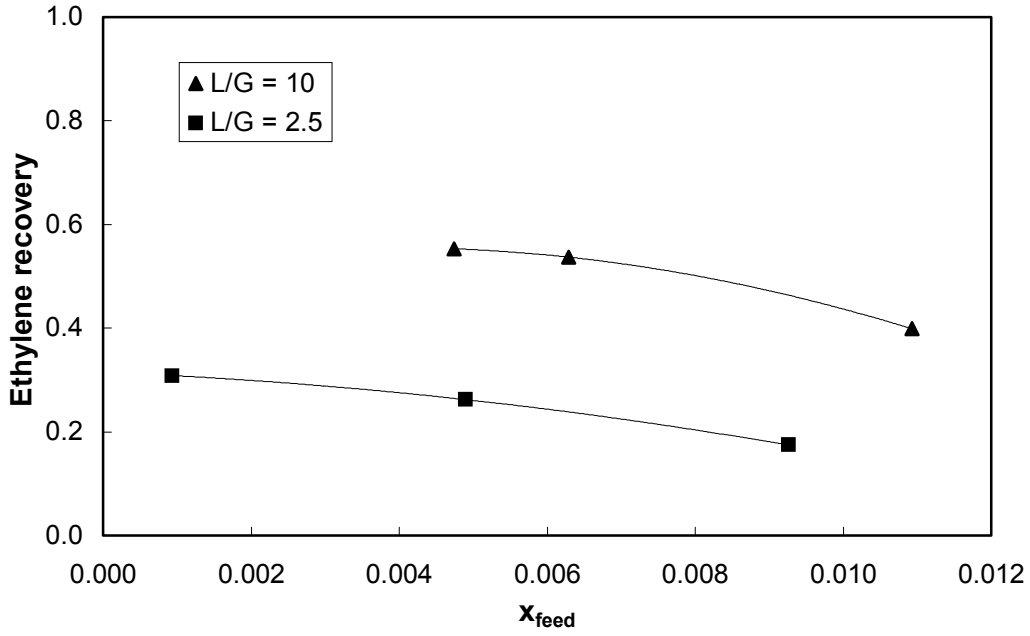

Figure 8-3. Ethylene recovery as a function of x_f

8.3 50% Ethylene / 50% Ethane

In order to investigate the loading and selectivity of an olefin/paraffin mixture in the absorption solution in the continuous process, experiments were performed with a 50% ethylene / 50% ethane gas blend. For this absorption process, both gases in the feed were soluble in the liquid, so there was no carrier gas. The liquid solution was still assumed to be nonvolatile, and the regeneration flask temperature was maintained at 60ºC for all experiments. Whereas a number of experiments were repeated with the ethylene/nitrogen blend to confirm the stability of the solution and the reliability of the experimental technique, only six experiments were conducted with the ethylene/ethane gas.

8.3.1 Stream compositions

The overall and ethylene component material balances given in equations (8-1) and (8-3) are still valid, but the ethane material balance must be included in order to solve for the stream flowrates.

$$V_f y_{f,2} - V_p y_{p,2} = L_p x_{p,2} - L_f x_{f,2} \tag{8-6}$$

where the *1* and *2* subscripts are used to denote the ethylene and ethane components, respectively. Like the ethylene/nitrogen experiments, analysis of gas and liquid samples gave values for y_p, x_p, and x_f for ethylene and ethane. Since the liquid was nonvolatile, an additional restraint exists that the gas product mole fractions must sum to unity.

$$y_{p,1} + y_{p,2} = 1 \tag{8-7}$$

For most samples, the sum of the quantitative results in equation (8-7) was between 0.9 and 1. As before, quantification was accomplished by using a filled vial from the feed gas cylinder. These results confirm the earlier suspicion that the syringe injection from the product gas was not completely efficient. Since equation (8-7) must be true, the observed concentrations were normalized such that the ratio of the gases in the quantitative calculation was the same.

$$y_{p,i} = \frac{y'_{p,i}}{\sum y'_{p,j}} \tag{8-8}$$

where the quantitative results are denoted by the prime symbol $'$. The analytical results from the gas product compositions calculated from equation (8-8) and the liquid mole fractions of both ethylene and ethane are given in Table 8-4. Cases 1 – 5 were run at absorber temperatures between 22ºC and 23ºC while case 6 was run at a higher temperature of 34ºC.

Table 8-4. Analytical results from ethylene/ethane experiments

Case	Gas Flow (SLPM)	Liquid Flow (lb/hr)	Vapor product		Liquid product		Liquid feed	
			$y_{p,1}$	$y_{p,2}$	$x_{p,1}$	$x_{p,2}$	$x_{f,1}$	$x_{f,2}$
1	3.37	14.9	0.37	0.63	0.030	0.0081	0.0026	0.00005
2	3.37	19.9	0.34	0.66	0.030	0.0082	0.0050	0.00011
3	4.95	20.2	0.40	0.60	0.028	0.0079	0.0041	0.00010
4	1.02	20.0	0.008	0.99	0.016	0.0108	0.0029	0.00021
5	1.58	19.9	0.03	0.97	0.019	0.0081	0.0039	0.00015
6	3.19	14.9	0.42	0.58	0.022	0.0069	0.0042	0.00012

The values for all cases except case 5 are averages of at least two replicate samples per result, but the analytical results in case 5 are from a single sample on each stream. The average RSD of the gas product results for both ethylene and ethane was less than 0.5%. Because both gases of the binary mixture could be detected by the GC, a great improvement in the accuracy of the gas sampling technique was observed over the ethylene/nitrogen case. The liquid product results showed an average RSD of 5%, and the liquid feed results showed an average RSD of 20%. The precision of HS-GC for the liquid analysis was comparable to that observed with the ethylene/nitrogen case. The mass balance for the ethylene/ethane experiments showed excellent convergence for nearly every case with a convergence of within 5% as calculated by equation (8-5) for both ethylene and ethane. Case 5 was the only experiment that failed to converge with an error of 0.44 moles of ethylene and 0.63 moles of ethane corresponding to a percentage of the average number of moles transferred of 24% and 117%.

From Table 8-4 the ethane concentration in the liquid product remained relatively constant for the ambient temperature cases 1 – 5. From section 6.3.3, the equilibrium behavior of ethane in a mixed gas followed Henry's law with a slope of 0.00254 mol·(L psia)$^{-1}$, so the equilibrium concentration of ethane at a partial pressure

of 37.5 psia is 0.095 mol/L corresponding to a mole fraction of 0.0083. The data in Table 8-4 agrees very well with this value, so the ethane most likely reached equilibrium in the absorber for all flow conditions studied. Figure 8-4 shows that the ethane mole fraction in the liquid product stream is relatively constant with the L/V_{feed} ratio. The ethylene concentration in the liquid product seemed generally to increase with gas flow rate, corresponding to lower values of L/V_{feed}. The ethylene concentration did not reach the equilibrium mole fraction predicted by the model of 0.054. From Figure 8-4 L/V_{feed} ratios from about 7 to 10 yield an ethylene mole fraction of 0.030, which was far below the equilibrium value. This loading was comparable to case 12 in the ethylene/nitrogen experiments that had a corresponding L/V_{feed} ratio of 7 with a mole fraction of 0.029 in the liquid product.

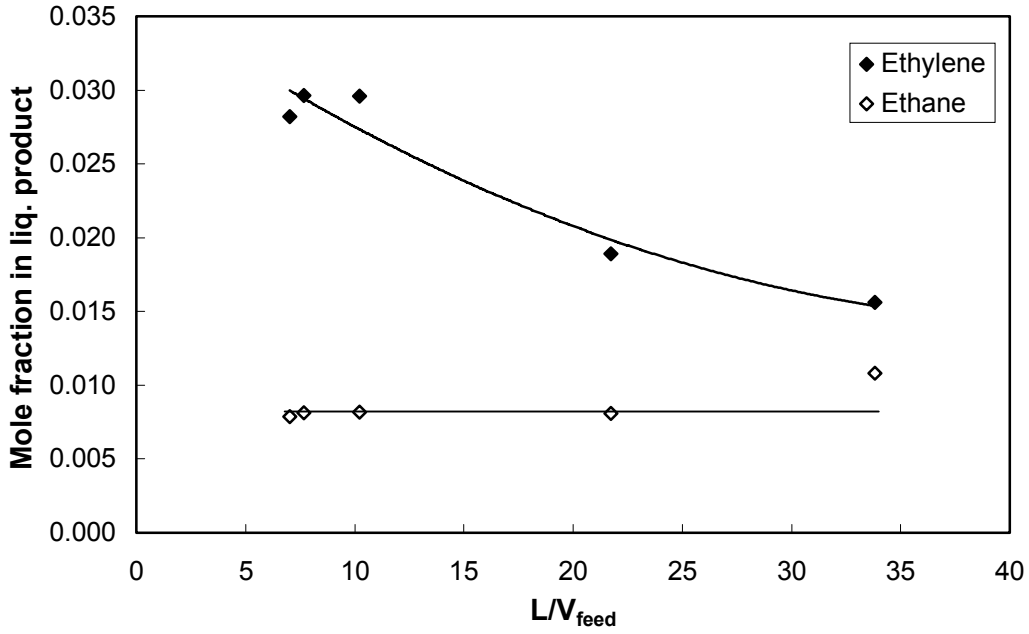

Figure 8-4. Mole fraction in liquid product as a function of L/V_{feed}

Compared to the ethylene/nitrogen experiments, the regeneration in the ethylene/ethane experiments from Table 8-4 was more effective at removing

ethylene. By maintaining the stripping gas flowrate near the flood point, the highest mole fraction ethylene in the liquid feed was 0.0050 for case 2, which was less than half the highest value in the ethylene/nitrogen of 0.0103 for case 11. Even though the regeneration efficiency for ethylene was higher than previous experiments, the degree of ethane stripping was much higher than ethylene. For each case, the mole fraction ethane in the liquid feed was less than 2% of its value in the liquid product while ethylene was only reduced 10% to 20% of its value in the liquid product. This difference is probably due to the inefficient usage of heat in the regeneration step. Since the heat was applied to the flask after the liquid passed through the regeneration column, the liquid at decomplexation temperature did not experience the mass transfer zone of the stripping column. Instead, the degree of regeneration observed was due to the reduced partial pressure from the lower total pressure of the regeneration side and the nitrogen stripping gas. The equilibrium for ethylene and ethane at ambient temperature in Figure 6-6 accurately shows that ethylene still has considerable capacity at reduced partial pressure compared to ethane.

8.3.2 Selectivity

The gas recovery calculated by equation (8-4) is shown in Figure 8-5 as a function of the ratio of solute-free liquid rate to total gas feed rate. The total gas feed rate was used because the feed did not contain a carrier gas. The limit of ethylene recovery is approached around a L/V_{feed} ratio of 20, which is similar to the ethylene/nitrogen experiments that show the same behavior around a L/G of 30 corresponding to a L/V_{feed} ratio of about 20. At higher L/V_{feed} ratios, the ethane recovery continues to improve, while nearly all of the ethylene is removed from the gas. The discrepancy in the ethane data for the point at a L/V_{feed} ratio of 22 corresponds to case 5 which showed the worst convergence of the material balance, so the accuracy of this point is doubted.

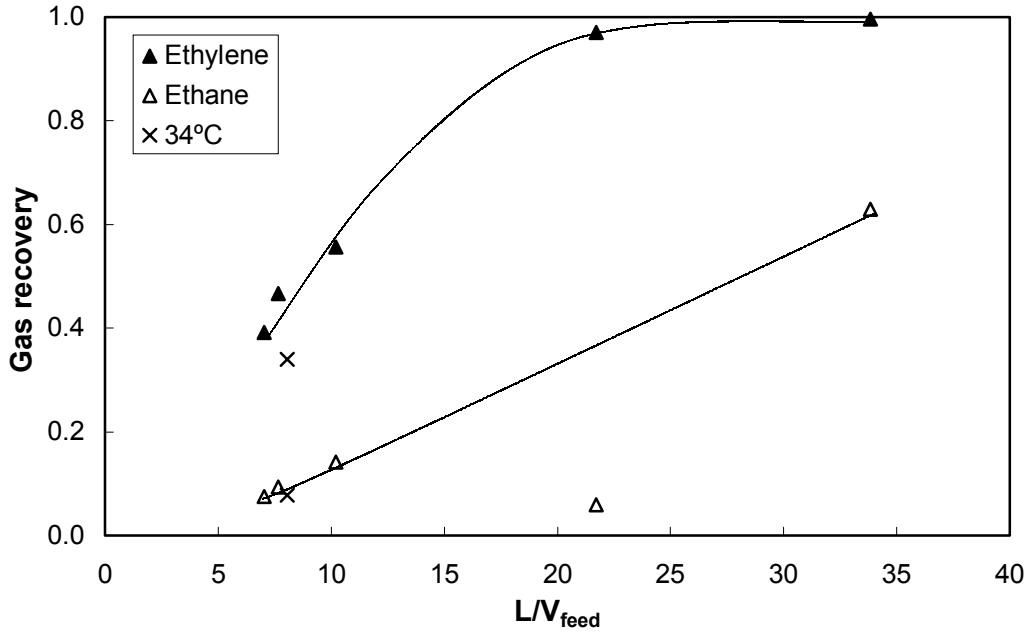

Figure 8-5. Gas recovery as a function of L/V_{feed}

Since the kinetics of the complexation reaction were thought to be instantaneous, the experiment at 34ºC was performed as a check. If a higher absorber temperature had significantly improved the ratio of ethylene recovery to ethane recovery of the process, then the reaction would be finite due to Arrhenius behavior of the rate coefficient. For an already instantaneous reaction, a higher temperature would not be expected to improve the absorption, but instead, the absorption would suffer due to a lower equilibrium constant. The experiment at 34ºC confirmed the instantaneous complexation reaction by showing a loss of recovery of ethylene compared to the ambient temperature cases. Since the ethylene recovery decreased at least as much as the ethane recovery, the selectivity towards ethylene was not improved as a result of the higher absorption temperature.

The observed selectivity of the absorption process at given liquid and gas flowrates can be defined as the ratio of ethylene to ethane in the product liquid.

$$Selectivity = \frac{x_{p,1}}{x_{p,2}} \tag{8-9}$$

A plot of the absorber selectivity as a function of gas recovery is given in Figure 8-6. The maximum selectivity was around 3.7 at low ethylene recoveries, which also correspond to low L/V_{feed} ratios. Since the selectivity based on physical solubility alone was 1.3 from section 6.3.6, some chemical effects were certainly present. However, the predicted equilibrium selectivity was around 7 for the partial pressures of gases studied. In order to achieve higher selectivities, a column with more packing height or more mass transfer area would have been required. At higher ethylene recoveries, the tradeoff between selectivity and recovery was evident as the selectivity decreased to the lowest value of about 1.4. Since this approaches the physical solubility value, this was likely near the minimum possible selectivity of the system. The selectivity for the 34ºC experiment was about 3.3.

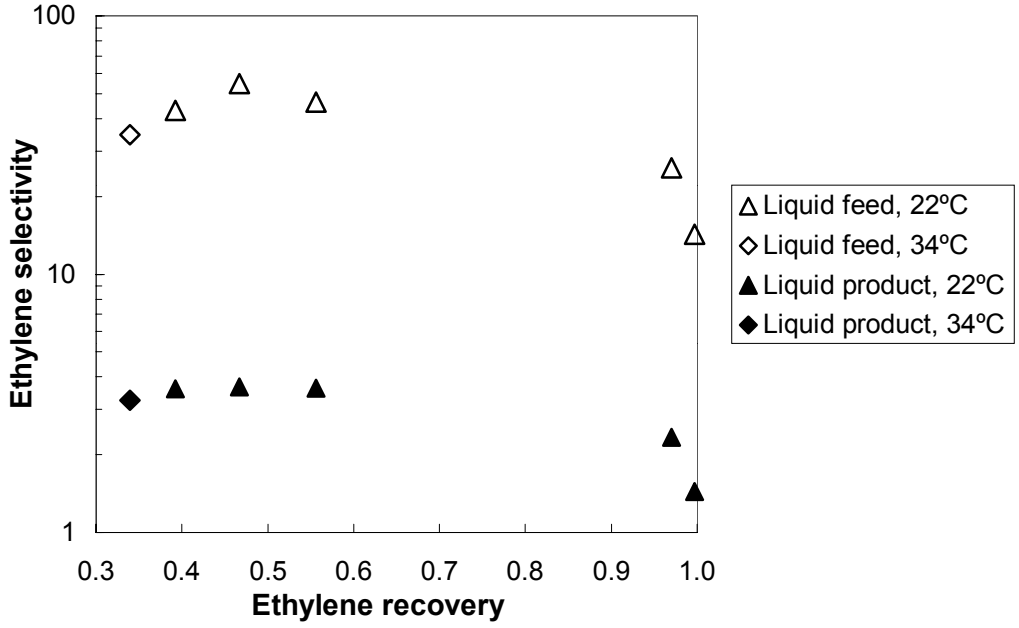

Figure 8-6. Ethylene selectivity versus recovery

By examining the liquid returning to the absorber, another feature of the regeneration process arises. If the selectivity is defined based on the feed stream instead of the product stream, much higher ethylene to ethane ratios are found.

$$Selectivity = \frac{x_{f,1}}{x_{f,2}} \tag{8-10}$$

Since the absorber feed stream is the effluent from the regeneration section, the selectivity based on the feed in equation (8-10) is actually a measure of the regeneration efficiency. According to Figure 8-6, the selectivity of the feed stream is over an order of magnitude higher than the product stream. From this information, a much more efficient process could be designed by recovering the purified ethylene product from a second regeneration unit with more severe desorption conditions. Since the regeneration efficiency of the current setup was not influenced by the flask temperature but instead was influenced by the stripping gas flowrate, the addition of heat in the regeneration column was poorly utilized. The second regeneration step should employ heat along with a high mass transfer coefficient in order to drive off the remaining complexed ethylene and take advantage of the higher ethylene to ethane selectivities at these conditions.

8.4 Conclusion

From the results of the ethylene/nitrogen experiments, the solution proved to be robust with time because no loss of capacity was observed in liquid product concentration over the five weeks that passed between the first and last experiments at similar flow conditions. The ethylene capacity of the solution seemed to remain stable despite repeated transfers of the liquid between the flow process and the glove box. The analysis of experimental samples from both gas blends produced an acceptable degree of error for most cases, but certain experiments encountered poor convergence of the material balance due to the lack of replicate samples or operating times that were less than the required times for steady-state. The maximum ethylene

loading of the copper solution was found to be significantly less than the equilibrium value, but the ethane absorption reached equilibrium for every case studied.

The process was capable of recovering high percentages of the ethylene in the feed gas, but high recovery was at the expense of lower selectivity because the ratio of ethylene to ethane exiting the absorber was less than expected. More packing height was expected to alleviate this shortcoming to some extent; however, it was thought that the liquid experienced a chemical change such that the absorption equilibrium capacity was decreased due to oxidation of some fraction of the active copper(I) sites. This change would have caused a lower ethylene capacity than expected from the autoclave experiments. In spite of the equilibrium limitations, the selectivity was nearly three times greater than that possible as a result of physical solubility alone. Overall, the continuous process proved that the absorption solution was capable of purifying an olefin-paraffin stream into an olefin-rich and a paraffin-rich stream without any noticeable loss of performance over about six weeks of operating time.

Chapter 9.
Discussion and Recommendations

9.1 Copper solution

Ethylene absorption solutions were prepared by using a combination of copper halide salt, aromatic nitrogen-containing ligand, and amide solvent. The preferred solution was determined to contain CuCl with aniline as ligand due to superior ethylene loading observed in CV and autoclave experiments. The most significant solution properties considered were copper molarity, volatility, viscosity, and stability. A high copper molarity was desirable because more copper in solution gives more sites for ethylene complexation. The solubility limit was reached for the benzylamine-CuBr-DMF and aniline-CuBr-DMF solutions before the desired copper molarity was obtained. The other solutions were not prepared beyond about 1.1 M copper due to the literature recommendation that the molarity for an organic copper solution should not exceed around 1 M [21]. This limit was given because even though a higher copper molarity yields a higher ethylene absorption capacity, a higher solution viscosity also results, which causes pumping difficulties and hinders mass transfer characteristics. The aniline-CuCl-NMP solution at about 1.1 M was found to have a viscosity about twice that for a copper-free aniline-NMP solution. Future work could include examining copper molarities up to the solubility limit and finding the viscosity behavior as a function of copper molarity. Since the kinetics of the absorption reaction have been shown to be instantaneous, the increased pumping costs and mass transfer resistance with a higher copper molarity solution may be unacceptable despite the benefit of increased ethylene capacity.

A comparison of the boiling point and vapor pressure of the solvents used revealed that NMP was considerably less volatile than DMF. The use of NMP would

result in much less solvent stripped into the gas phase in a vapor-liquid contacting device. Even though the volatility of the ligand was thought to be slightly less important than the volatility of the solvent due to the strong coordination with the copper(I) ions, aniline was an acceptable choice due to its high boiling point and low vapor pressure at absorption and desorption conditions. The stability of all copper solutions was poor when exposed to air showing mild to drastic color changes. The pyridine-CuCl-DMF solution was the most unacceptable because it solidified within a short period of time. The remaining solutions darkened considerably, but the exact oxidation mechanism and products were unknown. A more detailed study into the chemistry behind these changes could give valuable information into the reversibility of the oxidation process to recover the copper(I) state. A better understanding of solution degradation could also suggest potential additives as oxidation inhibitors.

9.2 Equilibrium and kinetics

The equilibrium and kinetics of ethylene absorption were investigated with the autoclave apparatus, and the data were found to show good agreement with a simple reaction model that was first-order in ethylene and copper. The equilibrium showed that most of the chemical complexation took place at ethylene partial pressures below about 50 psia. Beyond this point, the equilibrium curve showed the same slope as predicted by physical solubility alone. The capacity of the copper solution for chemical complexation was found to be significantly lower than the actual concentration of copper(I) ions able to form a 1:1 ethylene-copper complex. One possible reason for this discrepancy was that ligand substitution effects were neglected in the model. In order to include the ligand exchange reactions, knowledge of the free ligand concentration and/or the coordination number or distribution of coordination numbers of the copper complexes would be valuable information.

The selectivity of ethylene to ethane absorption was found to be greatest at lower pressures creating a tradeoff with capacity for the optimum absorption pressure.

Both high ethylene capacity and high ethylene to ethane selectivity are preferred, but these two effects act in opposite directions with ethylene pressure. The purity required for polymer-grade ethylene is not possible in a simple absorber/stripper process based on equilibrium selectivity alone even at sub-atmospheric operating pressures. Since the kinetic experiments found the absorption of ethylene to be instantaneous, the best operating pressure for an ethylene absorption design should be determined from selectivity rather than capacity. With an instantaneous reaction, a lower pressure could be used to achieve higher selectivity than possible from equilibrium alone. At atmospheric pressure, a contacting device with high mass transfer and short contact times could theoretically achieve a selectivity exceeding the mixed gas equilibrium selectivity value of 12.

The modeling of the reaction kinetics showed the instantaneous, reversible model to exhibit a good fit with the experimental data. The diffusivity ratio D_A/D_B was calculated as 5 from fitting the model to the data. Further work that would lend validity to this model would be to experimentally find the diffusivity of the ethylene-free copper(I) species in solution. One possible method that has been successful for the measurement of copper diffusivity is to use an open-ended capillary cell where a certain concentration of isotopic copper is allowed to diffuse into a bulk solution, and the contents of the capillary are analyzed after a fixed time [51]. With the calculated value of D_B, the instantaneous model could be employed much more confidently. In addition to gaining accuracy in the kinetic model at ambient temperature, additional equilibrium experiments at higher temperatures should be performed approaching regeneration conditions up to 80ºC. With this information, a much more efficient process for desorption of absorbed gases could be designed. Another recommendation for future work is to perform the autoclave equilibrium experiment on a sample of a mixed ethylene-ethane stream from an actual industrial process stream. Repeated experiments should confirm that the absorption solution is robust

enough to handle the impurities present before attempting implementation on a larger scale.

9.3 Flow process

The continuous absorption/regeneration process demonstrated the trends predicted by the equilibrium and kinetic models. In every experiment the ethane reached the predicted absorption equilibrium and showed nearly complete regeneration. The ethylene absorption fell short of the equilibrium value even in the low liquid rate experiments probably due to partial oxidation of the solution at the beginning of the flow experiments. In order to confirm this suspicion, autoclave equilibrium experiments should be performed with a visibly oxidized solution to determine the effects of oxidation on ethylene absorption capacity. The flow process could be improved by using additional packing height or packing with more active surface area to increase the number of equilibrium stages and achieve higher recovery at low L/V ratios.

Besides using more packing height, the process could be improved by revamping the regeneration section with a two-step design. By designing the process using pressure and temperature swings, it may be possible to purify the olefin with a two-step regeneration process. By first driving off the physically absorbed paraffin (with a substantial amount of olefin) with a reduced pressure column, the olefin-rich solution could be treated in a second desorption stage with high temperature to recover a high purity product. Recall that Keller et al. [61] suggested a similar process flow shown in Figure 2-9 with a vent column operated at a pressure slightly below the absorber pressure to remove physically absorbed components. In the revamped first regeneration step of this process, a column similar to the current design should suffice, but the use of nitrogen as a stripping gas should be avoided because dilution of the product gases is undesirable. Instead, a fraction of the purified ethylene product could be used if necessary, and the gas exiting the vent column

could be returned to the absorber to recover any stripped ethylene. The liquid exiting the vent column would then be stripped of physically absorbed gases, and it could be heated before entering the second column, which should have considerably more packing height than the current column. According to the results from regeneration of the solution in the autoclave experiments, low-pressure steam should provide a sufficient temperature driving force in the heat exchanger prior to the second column. With these improvements, the flow process would be significantly improved and ready for a test on a skid scale with an industrial mixed ethylene-ethane stream.

Appendix A.
Equipment & Setup

A.1 Pressure transducer check

In order to check the accuracy of the pressure transducer before the autoclave experiments were begun, the readouts from the transducer and the gauge were compared for autoclave pressures over a range from 50 psia to 300 psia. The gauge used was newly acquired from US Gauge, and it was checked against another trusted gauge before being secured to the autoclave. The gauge pressure and the transducer readout were converted to psia and plotted in Figure A-1. Since the transducer values deviated from the gauge values more at higher pressures, the transducer had an obvious slope error at 0.831. After repair by the manufacturer, the transducer agreed very well with the gauge showing a slope of 1.009. The intercept of this fit is simply a function of the zero point of the transducer and could easily be corrected by a fine adjustment screw. The gauge pressure was also recorded along with the transducer pressure for all autoclave experiments, and the linear fit was periodically checked to avoid any error across experiment sets due to instrument drift.

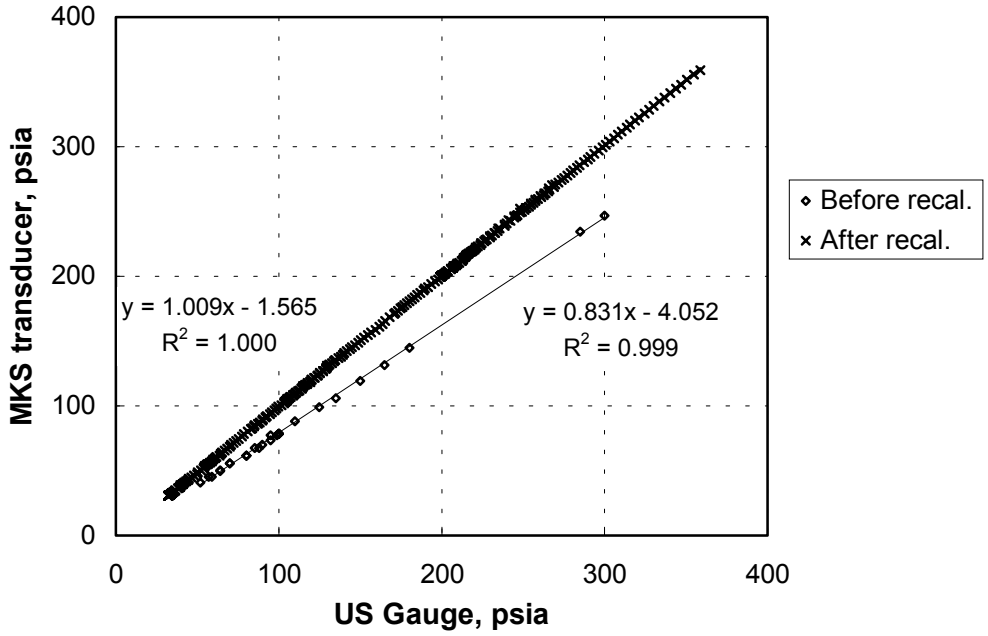

Figure A-1. Gauge and transducer pressure before and after recalibration

A.2 Sample calculation of moles ethylene absorbed

The procedure for calculating the moles of ethylene absorbed consists of iterating the mass balance in the gas phase with the gas law equations. From the autoclave condition before charging the absorption gas, the quantity of nitrogen in the gas phase $n_{nitrogen}$ was known as 1.14 mmol nitrogen for this sample calculation. The total moles of gas at any given time are given by

$$n_{\text{total}} = \frac{V_{\text{autoclave}}}{R}\left(\frac{P}{ZT}\right)_{\text{autoclave, time}} \qquad \text{(A-1)}$$

At 10 minutes into the sample experiment, the system pressure was 22.0 psia and the temperature was 23.0ºC (296.2K). The value of Z given by equation (3-8) is dependent on B from equation (3-9), which is a function of the unknown mole fraction of the gas. The value of the mole fraction of ethylene is guessed and used to

find the number of moles of ethylene in gas from equation (3-18). The material balance for the moles in the gas phase is the target cell that is iterated to zero as given by

$$\left(n_{\text{total}} - n_{\text{ethylene}} - n_{\text{nitrogen}}\right) * 10{,}000 \stackrel{?}{=} 0 \qquad \text{(A-2)}$$

where the 10,000 factor is included for improved convergence. In the data analysis, a goal seek macro was used to converge equation (A-2) for each data point, but a sample calculation is given in Table A-1 for the iterative results with an initial guess of 0.99 for the ethylene mole fraction. The convergence was improved from this case until the fourth step where the target value from equation (A-2) was nearly zero at an ethylene mole fraction of 0.957. With the ethylene mole fraction, the partial pressure of ethylene was calculated as 21.0 psia, and the number of moles of gas absorbed was found from equation (3-7) to be 50.0 mmol.

Table A-1. Iteration of an autoclave experiment at 10 minutes

Value	Iteration			
	1	2	3	4
$y_{ethylene}$ (guess)	0.99	0.95	0.96	0.957
B	-141.5	-133.7	-135.6	-135.0
Z	0.9913	0.9918	0.9917	0.9917
n_{total} (mmol)	25.81	25.80	25.80	25.80
$n_{ethylene}$ (mmol)	25.56	24.51	24.77	24.69
target cell	-8.529	1.790	-0.789	-0.015

A.3 Calibration of MKS gas flowmeter

The gas flowmeter used in the continuous absorption/regeneration experiments measured gas flow by thermal conductivity over a Wheatstone bridge circuit. Since different gases and gas blends have different thermal conductivity, the instrument needed to be calibrated for each gas used. The calibration experimental

setup shown in Figure A-2 consisted of a soap-bubble flowmeter to measure the flowrate of the gas. The same gas cylinders used in the continuous flow experiments were connected to the MKS flowmeter via a Nupro plug valve. A Whitey needle valve on the downstream side of the MKS flowmeter was used to adjust the flowrate to the desired value. The soap-bubble flowmeter had a 1 L capacity with markings at every 10 mL. The flowrate was measured by using a stopwatch to find the time for a bubble film to proceed over a given volume (e.g. from 0 to 1000 mL).

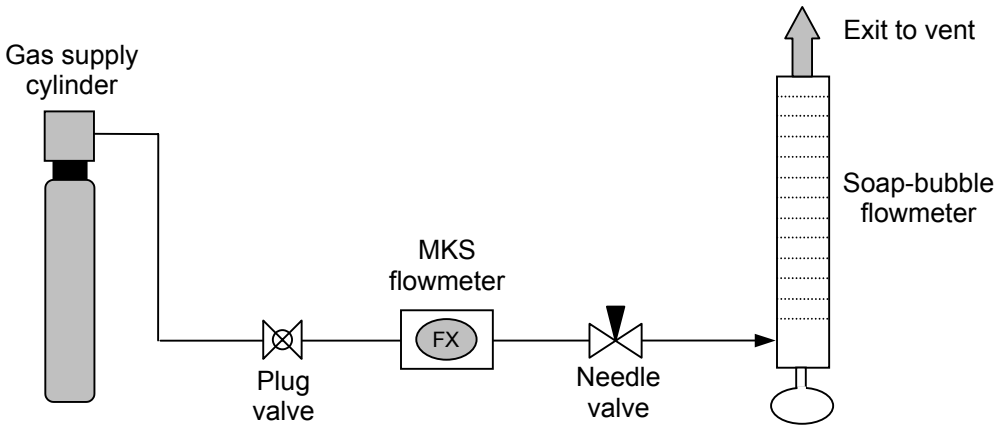

Figure A-2. MKS flowmeter calibration experimental setup

Results from the calibrations for nitrogen, 30% ethylene/70% nitrogen, and 50% ethylene/50% ethane are shown in Figure A-3, Figure A-4, and Figure A-5, respectively. In order to make sure that the MKS flowmeter did not have a predisposition for error with gas pressure, two different gas pressures were used for each calibration. The pressure setting of the cylinder regulator was found to have no effect on the flowrate for all of the gases. For the nitrogen calibration, the MKS readout was less than half of the actual flowrate with a ratio of 0.419 from the slope of the calibration. This result was surprising because the meter was supposedly calibrated for nitrogen flow; however, since the calibration was very linear with an R^2

value of 0.999 with no significant deviation up to about 6 SLPM on the soap-bubble meter, the MKS flowmeter was deemed reliable as long as the calibration factor was used.

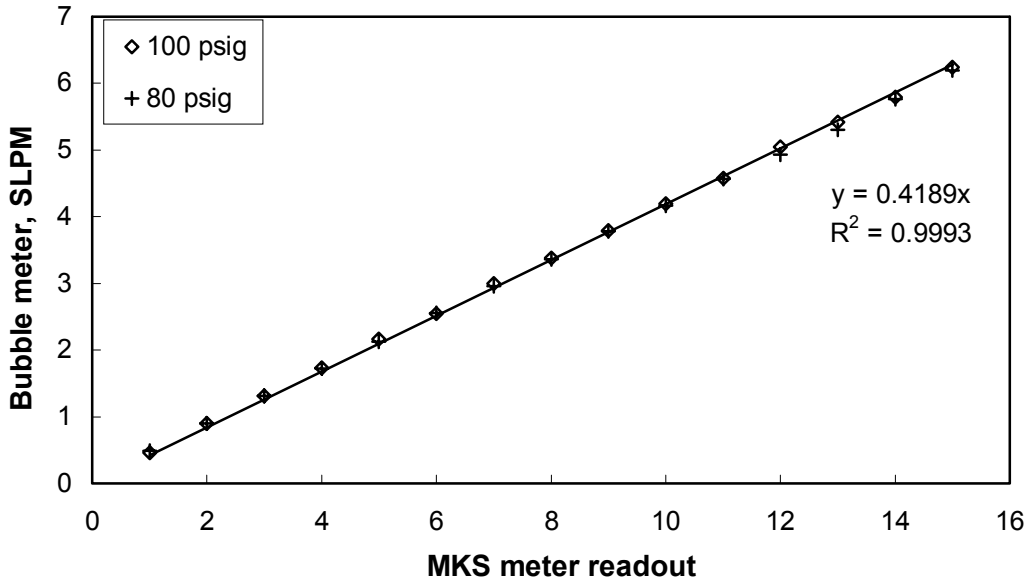

Figure A-3. Calibration curve for nitrogen

For the ethylene blends, the slopes of the calibration curves were lower than pure nitrogen at 0.323 for ethylene/nitrogen and 0.259 for ethylene/ethane. As with nitrogen, these curves were very linear with R^2 values over 0.999. The range of flowrates studied in the continuous process corresponded to corrected flowrates between 1 SLPM and 5 SLPM, which was well within the range of the calibrations.

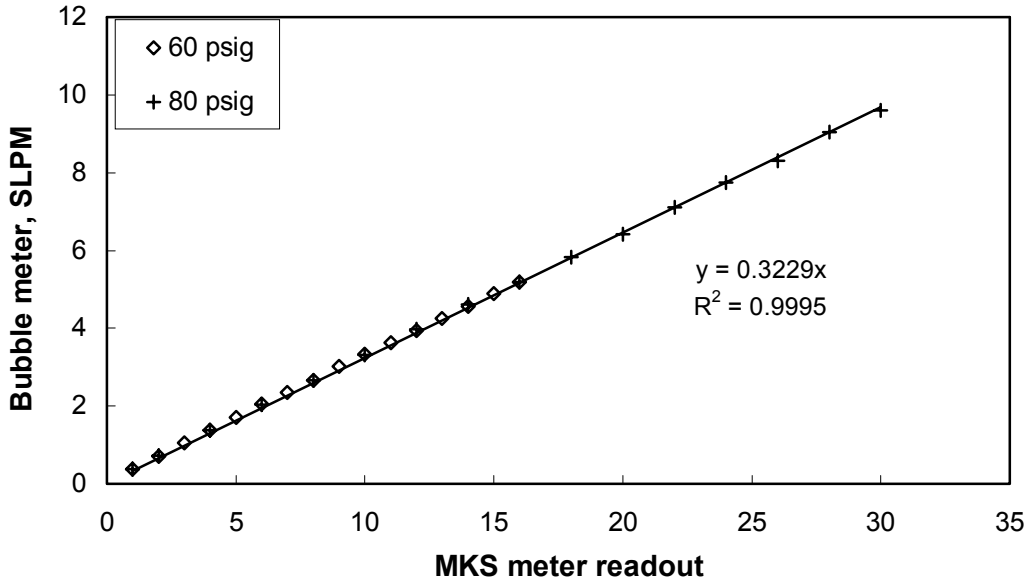

Figure A-4. Calibration curve for 30% ethylene/70% nitrogen

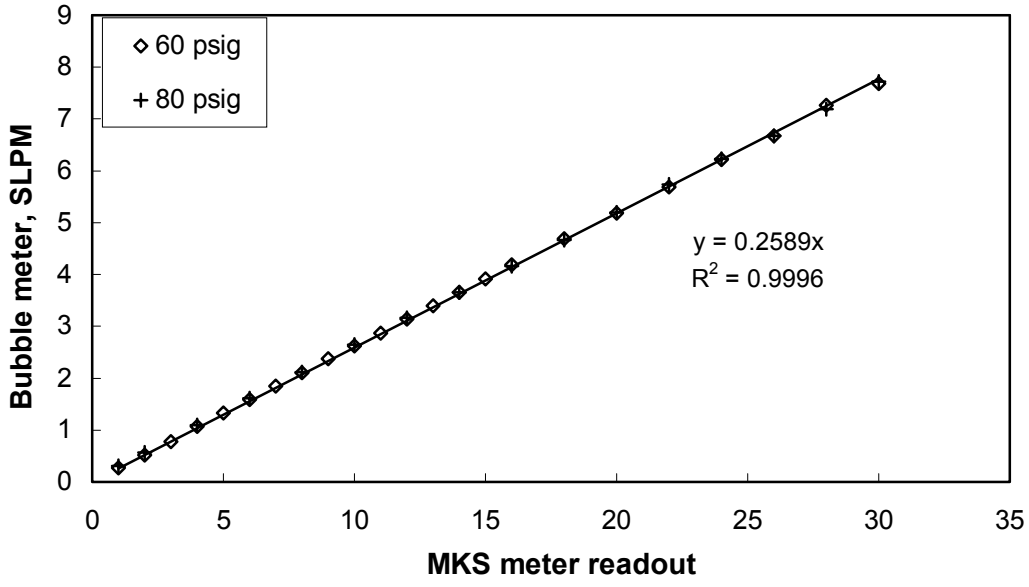

Figure A-5. Calibration curve for 50% ethylene/50% ethane

A.4 Design calculations for concentric tube heat exchanger

To cool the copper solution from the regeneration section, a concentric tube heat exchanger was designed to reduce the solution temperature from 60ºC to 30ºC. Since additional heat was expected to be lost from air cooling of the $^1/_4$" tubing between the heat exchanger and the absorption column entry, an outlet temperature of 30ºC from the exchanger was considered sufficient. The chilled water was available at a flowrate of about 1 GPM (0.06 kg/s) at about 7ºC. As shown in Table A-2, the properties of water were found at 7.5ºC, and the properties for aniline and NMP were found at the median temperature of about 45ºC. Since the specific heat and thermal conductivity of the copper solution were unknown, these properties were estimated from the average of a 1:1 mixture of aniline and NMP. The viscosity was found previously in section 5.3.

Table A-2. Properties used in heat transfer calculations (from [120])

	T_m ºC	c_p J/kg·K	μ cP	k W/m·K
Water	7.5	4198	1.42	0.582
Aniline	45	2312	2.1	0.171
NMP	45	1818	0.95	0.191
Solution	45	2065 [a]	4.0 [b]	0.181 [a]

[a] calculated from an 1:1 aniline-NMP mixture [b] from Figure 5-1

Since $^1/_4$" Swagelok tubing was used for the liquid stream throughout the continuous flow process, the hot solution was maintained as the fluid through the inside tube to prevent contamination from leaky fittings. The flowrate for design of the heat exchanger was 20 lb/hr (0.0025 kg/s), which was the most common liquid flowrate used in the experiments. The chilled water flowed through the annular region, which was constructed from $^1/_2$" Swagelok tubing. The exchanger and all chilled water tubing was wrapped with 1"-thick foam pipe insulation, so the heat loss

to the environment was minimized; therefore, the heat flux through the outer wall of the annulus was neglected. The heat transfer rate from the energy balance for the hot fluid is given by

$$q = \dot{m}_h \cdot c_{p,h}(T_{h,i} - T_{h,o}) = 0.0025\frac{kg}{s} \cdot 2065\frac{J}{kg \cdot K} \cdot (60 - 30)°C = 156.1W \quad \text{(A-3)}$$

Similarly, an energy balance on the cold fluid gives the water outlet temperature

$$T_{c,o} = \frac{q}{\dot{m}_c \cdot c_{p,c}} + T_{c,i} = \frac{156.1W}{0.06\,kg/s \cdot 4198\,J/kg \cdot K} + 7°C = 7.6°C \quad \text{(A-4)}$$

Since the water outlet temperature is very close to the inlet temperature, the inner tube can be assumed to have a constant surface temperature. The required heat exchanger length is related to the total rate of heat transfer by

$$q = U \cdot A \cdot \Delta T_{lm} \quad \text{(A-5)}$$

where U is the overall heat transfer coefficient, A is the area of heat transfer, and ΔT_{lm} is the log-mean temperature difference. These species are represented by the following equations

$$A = \pi \cdot D_i \cdot L \quad \text{(A-6)}$$

$$\Delta T_{lm} = \frac{(T_{h,i} - T_{c,o}) - (T_{h,o} - T_{c,i})}{\ln\left[(T_{h,i} - T_{c,o})/(T_{h,o} - T_{c,i})\right]} = \frac{(52.4 - 23)K}{\ln(52.4/23)} = 35.7K \quad \text{(A-7)}$$

$$U = \frac{1}{\frac{1}{h_i} + \frac{D_i \ln(D_o/D_i)}{2k_{st}} + \frac{D_i}{D_o h_o}} \quad \text{(A-8)}$$

where D_i is the inner diameter of the inside tube 0.0046 m, D_o is the outer diameter of the inside tube 0.0064 m, h_i and h_o are heat transfer coefficients of the tube and annulus regions, and k_{st} is the thermal conductivity of the steel tube 13.4 W/m·K. The Reynolds number for the water is given by

$$\text{Re} = \frac{4 \cdot \dot{m}_c}{\pi(D_{o,i} + D_o)\mu} = \frac{4 \cdot 0.06\,kg/s}{\pi \cdot 0.0173m \cdot 1.42 \cdot 10^{-3}\,Ns/m^2} = 3110 \quad \text{(A-9)}$$

where $D_{o,i}$ is the inner diameter of the outer tube 0.0109 m. Since $2300 < \mathrm{Re} < 10^4$, the water flow is in the transition region between laminar and turbulent. Incropera and DeWitt [53] suggest that the Gnielinski correlation is an appropriate correlation for the transition flow region to find the Nusselt number.

$$\mathrm{Nu} = \frac{(f/8)(\mathrm{Re}-1000)\mathrm{Pr}}{1+12.7(f/8)^{1/2}\left(\mathrm{Pr}^{2/3}-1\right)} = \frac{0.0053(2100)10.26}{1+12.7(0.0053)^{1/2}\left(10.26^{2/3}-1\right)} = 25.7 \qquad \text{(A-10)}$$

where f is the friction factor determined to be 0.042 from the Moody diagram [53] at a relative roughness of 0.0003 and a Reynolds number of 3110. The heat transfer coefficient of the annular region is calculated by

$$h_o = \frac{\mathrm{Nu}\cdot k_c}{D_{o,i}-D_o} = \frac{25.7\cdot 0.582 W/m\cdot K}{(0.0109-0.0064)m} = 3270\frac{W}{m^2\cdot K} \qquad \text{(A-11)}$$

where $D_{o,i} - D_o$ is the hydraulic diameter for the annulus.

For the hot liquid through the inner tube the Reynolds number is

$$\mathrm{Re} = \frac{4\cdot \dot{m}_h}{\pi\cdot D_i\cdot \mu} = \frac{4\cdot 0.0025\, kg/s}{\pi\cdot 0.0046m\cdot 4.0\cdot 10^{-3}\, Ns/m^2} = 175 \qquad \text{(A-12)}$$

Since $\mathrm{Re} < 2300$, the flow of the solution is laminar, and the Nusselt number for a constant surface temperature is 3.66 [53]. The heat transfer coefficient for the inner tube is given by

$$h_i = \frac{\mathrm{Nu}\cdot k_h}{D_i} = \frac{3.66\cdot 0.181 W/m\cdot K}{0.0046m} = 144\frac{W}{m^2\cdot K} \qquad \text{(A-13)}$$

The overall heat transfer coefficient from equation (A-8) can now be calculated as

$$U = \frac{1}{\frac{1}{144\frac{W}{m^2K}} + \frac{0.0046m\cdot \ln(0.0064/0.0046)}{2\cdot 13.4\frac{W}{m\cdot K}} + \frac{(0.0046/0.0064)}{3270\frac{W}{m^2K}}} = 139\frac{W}{m^2K} \qquad \text{(A-14)}$$

Rearranging equations (A-5) and (A-6) and solving for the required length gives

$$L = \frac{q}{\pi U D_i \Delta T_{lm}} = \frac{156.1W}{\pi \cdot 139 \frac{W}{m^2 K} \cdot 0.0046m \cdot 35.7K} = 1.6m = 5.2ft \qquad \text{(A-15)}$$

Following this result the heat exchanger was conservatively built with a length of 6 ft, and a Nupro needle valve was installed on the chilled water line to permit reduction of the water flowrate if the exchanger over-cooled the process liquid.

A.5 Data and results from equilibrium experiments

Table A-3 gives the results from equilibrium experiments of ethylene absorption with the aniline-CuCl-NMP solution.

Table A-3. Equilibrium values of ethylene absorption into aniline-CuCl-NMP

Date	Charge gas (P – pure, M – mixed)	Partial pressure, psia	Temperature, ºC	Gas absorption, mol/L
4/4/02	ethylene, P	117.3	25.9	0.791
4/8/02	ethylene, P	181.3	26.4	0.935
4/9/02	ethylene, P	148.0	25.8	0.886
4/11/02	ethylene, P	88.8	26.0	0.815
4/12/02	ethylene, P	61.2	26.1	0.705
4/15/02	ethylene, P	36.6	25.8	0.596
4/17/02	ethylene, P	15.9	25.9	0.463
4/18/02	ethylene, P	186.1	25.9	1.023
4/19/02	ethylene, P	152.3	25.6	0.967
2/6/03	ethylene, P	89.7	28.8	0.769
2/7/03	ethylene, P	77.6	28.7	0.736
2/27/03	ethylene, P	95.6	26.4	0.813
3/3/03	ethylene, P	97.8	25.3	0.841
3/3/03	ethylene, P	80.8	26.5	0.770
3/6/03	ethylene, P	97.6	25.3	0.871
3/20/03	ethylene, P	98.6	24.5	0.915

3/21/03	ethylene, P	73.4	23.9	0.815
3/24/03	ethylene, P	57.6	23.6	0.715
3/25/03	ethylene, P	36.7	23.7	0.618
3/26/03	ethylene, P	30.6	23.1	0.605
3/27/03	ethylene, P	25.5	24.0	0.561
3/28/03	ethylene, P	17.7	23.6	0.496
4/4/03	ethylene, P	14.8	23.4	0.458
9/9/03	ethylene, M	14.2	23.5	0.421
9/9/03	ethylene, M	21.7	25.0	0.521
9/9/03	ethylene, M	27.9	25.8	0.587
9/11/03	ethylene, M	3.2	23.5	0.178
9/11/03	ethylene, M	7.2	24.9	0.311
9/11/03	ethylene, M	10.9	25.6	0.390
9/11/03	ethylene, M	15.0	26.1	0.495
9/11/03	ethylene, M	25.2	26.6	0.558
9/18/03	ethylene, M	16.4	23.6	0.447
9/18/03	ethylene, M	27.2	25.2	0.609
9/22/03	ethylene, M	4.3	23.8	0.242
9/22/03	ethylene, M	9.3	24.7	0.409
9/22/03	ethylene, M	15.4	25.5	0.508
4/1/04	ethylene, P	8.3	27.6	0.250
4/14/04	ethylene, P	7.9	26.4	0.250

Table A-4 gives the results from equilibrium experiments of ethane absorption with the aniline-CuCl-NMP solution.

Table A-4. Equilibrium values of ethane absorption into aniline-CuCl-NMP

Date	Charge gas (P – pure, M – mixed)	Partial pressure, psia	Temperature, ºC	Gas absorption, mol/L
4/29/02	ethane, P	235.9	24.9	0.393

4/30/02	ethane, P	193.7	24.6	0.371
5/1/02	ethane, P	157.2	24.5	0.323
5/2/02	ethane, P	120.6	24.5	0.257
5/3/02	ethane, P	90.5	24.2	0.193
5/6/02	ethane, P	64.6	24.7	0.136
5/8/02	ethane, P	37.2	25.4	0.074
5/9/02	ethane, P	14.7	25.0	0.016
9/9/03	ethane, M	39.4	23.5	0.115
9/9/03	ethane, M	52.6	25.0	0.141
9/9/03	ethane, M	62.6	25.8	0.153
9/11/03	ethane, M	14.9	23.5	0.037
9/11/03	ethane, M	26.7	24.9	0.073
9/11/03	ethane, M	34.9	25.6	0.094
9/11/03	ethane, M	46.9	26.1	0.096
9/11/03	ethane, M	52.2	26.6	0.131
9/18/03	ethane, M	43.0	23.6	0.122
9/18/03	ethane, M	61.3	25.2	0.150
9/22/03	ethane, M	15.6	23.8	0.045
9/22/03	ethane, M	28.1	24.7	0.074
9/22/03	ethane, M	38.3	25.5	0.097
3/11/04	ethane, P	25.9	24.0	0.049
3/18/04	ethane, P	23.5	24.2	0.049
3/19/04	ethane, P	25.7	24.8	0.055
3/20/04	ethane, P	24.7	24.5	0.053
3/22/04	ethane, P	24.5	24.4	0.048
3/24/04	ethane, P	23.7	24.3	0.050
3/25/04	ethane, P	24.4	24.5	0.051
3/26/04	ethane, P	24.3	24.7	0.052
3/29/04	ethane, P	43.3	24.3	0.074

Table A-5 gives the results from equilibrium experiments of ethylene absorption with the aniline-NMP solution.

Table A-5. Equilibrium values of ethylene absorption into aniline-NMP

Date	Charge gas (P – pure, M – mixed)	Partial pressure, psia	Temperature, ºC	Gas absorption, mol/L
9/9/02	ethylene, P	160.1	24.6	0.542
9/10/02	ethylene, P	192.1	24.3	0.597
9/11/02	ethylene, P	151.0	24.1	0.481
9/12/02	ethylene, P	121.2	25.2	0.389
9/13/02	ethylene, P	80.0	24.9	0.265
9/16/02	ethylene, P	57.3	24.5	0.180
12/8/03	ethylene, P	43.3	23.4	0.151
12/8/03	ethylene, P	47.0	22.3	0.154
12/8/03	ethylene, P	44.2	23.3	0.148
12/8/03	ethylene, P	43.6	23.4	0.142
12/8/03	ethylene, P	40.5	23.3	0.132
12/16/03	ethylene, P	65.6	22.4	0.224
12/16/03	ethylene, P	120.0	23.5	0.400
12/16/03	ethylene, P	95.9	23.4	0.330
12/16/03	ethylene, P	20.8	23.1	0.065
12/16/03	ethylene, P	91.7	23.4	0.314
1/30/04	ethylene, P	22.4	24.9	0.069
2/2/04	ethylene, P	23.6	23.9	0.066
2/2/04	ethylene, P	22.3	24.8	0.058
2/3/04	ethylene, P	21.4	24.2	0.073
2/4/04	ethylene, P	22.6	24.2	0.078
2/5/04	ethylene, P	21.7	23.9	0.078
2/7/04	ethylene, P	24.0	24.0	0.083
2/9/04	ethylene, P	20.8	23.7	0.072
2/10/04	ethylene, P	38.3	24.9	0.137

2/11/04	ethylene, P	22.6	24.0	0.079
2/12/04	ethylene, P	38.7	24.4	0.138
2/13/04	ethylene, P	23.3	23.9	0.089
2/16/04	ethylene, P	38.6	25.1	0.137
2/17/04	ethylene, P	22.8	24.0	0.078
2/18/04	ethylene, P	23.2	23.5	0.080
2/20/04	ethylene, P	23.9	22.2	0.083
2/24/04	ethylene, P	39.1	23.6	0.141
2/25/04	ethylene, P	15.7	23.8	0.050

Table A-6 gives the results from equilibrium experiments of ethane absorption with the aniline-NMP solution.

Table A-6. Equilibrium values of ethane absorption into aniline-NMP

Date	Charge gas (P – pure, M – mixed)	Partial pressure, psia	Temperature, ºC	Gas absorption, mol/L
8/29/02	ethane, P	185.6	24.9	0.434
8/30/02	ethane, P	166.3	25.6	0.411
9/3/02	ethane, P	151.8	25.5	0.360
9/4/02	ethane, P	133.6	25.1	0.331
9/5/02	ethane, P	106.1	24.9	0.258
9/6/02	ethane, P	84.5	24.6	0.208
9/7/02	ethane, P	50.5	24.9	0.114
2/26/04	ethane, P	25.8	24.2	0.070
2/27/04	ethane, P	24.5	23.9	0.066
2/28/04	ethane, P	23.7	24.4	0.065
3/1/04	ethane, P	23.4	23.8	0.064
3/2/04	ethane, P	41.0	24.2	0.120
3/3/04	ethane, P	15.6	24.4	0.042

Table A-7 gives the results from equilibrium experiments of ethylene absorption with the CV comparison solutions.

Table A-7. Equilibrium values of ethylene absorption of CV solutions in DMF

Date	Solution composition	Partial pressure, psia	Temperature, ºC	Gas absorption, mol/L
9/30/03	Pyridine-CuCl	23.4	23.8	0.140
10/2/03	Pyridine-CuCl	19.1	23.7	0.122
10/2/03	Pyridine-CuCl	27.4	24.3	0.175
10/2/03	Pyridine-CuCl	40.2	25.5	0.260
10/2/03	Pyridine-CuCl	57.9	26.3	0.375
10/3/03	Pyridine-CuCl	12.1	23.6	0.077
10/3/03	Pyridine-CuCl	75.2	25.0	0.492
10/3/03	Pyridine-CuCl	121.6	25.7	0.794
10/3/03	Pyridine-CuCl	151.9	26.4	0.987
10/6/03	Pyridine-CuCl	90.7	23.9	0.577
10/6/03	Pyridine-CuCl	107.5	24.9	0.682
10/6/03	Pyridine-CuCl	142.8	26.0	0.901
10/6/03	Pyridine-CuCl	165.5	26.4	1.043
10/6/03	Pyridine-CuCl	185.2	27.1	1.167
10/7/03	Pyridine-CuCl	147.5	23.7	0.857
10/7/03	Pyridine-CuCl	223.2	25.7	1.318
10/7/03	Pyridine-CuCl	263.4	26.6	1.564
10/7/03	Pyridine-CuCl	292.5	22.7	1.843
10/7/03	Pyridine-CuCl	334.0	24.5	2.083
10/21/03	Pyridine-CuBr	24.9	22.7	0.118
10/21/03	Pyridine-CuBr	59.5	24.1	0.289
10/21/03	Pyridine-CuBr	91.3	24.2	0.449
10/21/03	Pyridine-CuBr	133.1	24.5	0.660
10/21/03	Pyridine-CuBr	168.7	25.0	0.844
10/22/03	Pyridine-CuBr	18.3	22.7	0.089

10/22/03	Pyridine-CuBr	52.9	23.1	0.265
10/22/03	Pyridine-CuBr	75.7	23.3	0.381
10/22/03	Pyridine-CuBr	143.3	23.9	0.725
10/22/03	Pyridine-CuBr	194.8	24.5	0.992
10/24/03	Aniline-CuCl	13.9	24.3	0.428
10/24/03	Aniline-CuCl	44.5	24.9	0.639
10/24/03	Aniline-CuCl	76.2	25.3	0.787
10/27/03	Aniline-CuCl	135.9	23.8	0.967
10/27/03	Aniline-CuCl	213.5	24.6	1.288
10/27/03	Aniline-CuCl	215.6	24.9	1.296
10/27/03	Aniline-CuCl	232.0	25.4	1.359
10/27/03	Aniline-CuCl	247.5	25.7	1.421
10/28/03	Aniline-CuCl	20.6	23.2	0.432
10/28/03	Aniline-CuCl	40.1	24.0	0.565
10/28/03	Aniline-CuCl	93.6	24.9	0.823
10/28/03	Aniline-CuCl	169.0	25.7	1.132
11/3/03	Aniline-CuBr	18.7	23.5	0.353
11/3/03	Aniline-CuBr	38.7	24.0	0.537
11/6/03	Aniline-CuBr	21.1	23.4	0.344
11/6/03	Aniline-CuBr	60.2	25.0	0.648
11/6/03	Aniline-CuBr	97.0	25.7	0.888
11/7/03	Aniline-CuBr	42.9	23.6	0.518
11/7/03	Aniline-CuBr	83.9	24.5	0.780
11/10/03	Aniline-CuBr	60.1	23.6	0.630
11/10/03	Aniline-CuBr	106.7	24.2	0.916
11/11/03	Aniline-CuBr	100.9	23.2	0.854
11/11/03	Aniline-CuBr	138.9	23.9	1.053
11/11/03	Aniline-CuBr	183.2	25.0	1.268
11/11/03	Aniline-CuBr	219.3	25.3	1.437
11/13/03	Benzylamine-CuBr	28.1	22.6	0.216
11/13/03	Benzylamine-CuBr	60.1	23.5	0.435

11/13/03	Benzylamine-CuBr	100.2	24.0	0.685
11/13/03	Benzylamine-CuBr	137.1	25.0	0.903
11/13/03	Benzylamine-CuBr	162.3	25.3	1.044
11/13/03	Benzylamine-CuBr	181.3	25.6	1.150
11/13/03	Benzylamine-CuBr	197.5	26.0	1.241
11/13/03	Benzylamine-CuBr	214.3	26.4	1.332
11/14/03	Benzylamine-CuBr	31.9	23.2	0.246
11/14/03	Benzylamine-CuBr	58.0	24.0	0.424
11/14/03	Benzylamine-CuBr	88.9	24.8	0.615
11/17/03	Benzylamine-CuBr	14.1	22.8	0.110
11/17/03	Benzylamine-CuBr	39.3	23.9	0.299
11/17/03	Benzylamine-CuBr	122.0	24.8	0.802
11/20/03	Benzylamine-CuCl	15.5	22.7	0.158
11/20/03	Benzylamine-CuCl	35.5	23.1	0.334
11/20/03	Benzylamine-CuCl	73.0	24.0	0.602
11/20/03	Benzylamine-CuCl	128.5	24.8	0.926
11/20/03	Benzylamine-CuCl	158.1	25.8	1.086
11/21/03	Benzylamine-CuCl	24.8	23.0	0.243
11/21/03	Benzylamine-CuCl	74.1	23.8	0.607
11/21/03	Benzylamine-CuCl	180.9	24.9	1.196
11/21/03	Benzylamine-CuCl	215.7	25.5	1.372
11/25/03	Benzylamine-CuCl	58.4	23.4	0.484
11/25/03	Benzylamine-CuCl	100.9	24.5	0.753
11/25/03	Benzylamine-CuCl	162.3	25.1	1.085

A.6 Data and results from kinetic experiments

Table A-8 gives the data and results from kinetic experiments of ethylene absorption with aniline-CuCl-NMP at 260 rpm. The liquid volume in the autoclave

was 97.3 cm^3 and the number of moles of ethylene charged from the gas bomb was 0.0327.

Table A-8. Kinetic data and results for ethylene absorption at 260 rpm

Elapsed time from stirrer start, min	Partial pressure, psia	Temperature, ºC	Absorption rate, mol/s
0.0	27.1	25.9	
0.5	26.5	25.7	2.03E-05
1.0	26.0	25.7	1.97E-05
1.5	25.6	25.5	1.91E-05
2.0	25.1	25.5	1.85E-05
2.5	24.6	25.5	1.79E-05
3.0	24.2	25.4	1.74E-05
3.5	23.7	25.4	1.68E-05
4.0	23.3	25.5	1.63E-05
4.5	23.0	25.4	1.58E-05
5.0	22.6	25.5	1.53E-05
5.5	22.2	25.5	1.48E-05
6.0	21.9	25.4	1.44E-05
6.5	21.5	25.3	1.39E-05
7.0	21.2	25.3	1.35E-05
7.5	20.8	25.5	1.31E-05
8.0	20.5	25.5	1.27E-05
8.5	20.2	25.4	1.23E-05
9.0	19.9	25.5	1.19E-05
9.5	19.7	25.5	1.15E-05
10.0	19.4	25.4	1.11E-05
10.5	19.1	25.5	1.08E-05
11.0	18.9	25.5	1.05E-05
11.5	18.6	25.4	1.01E-05
12.0	18.4	25.5	9.81E-06

12.5	18.2	25.6	9.51E-06
13.5	17.7	25.6	8.94E-06
14.5	17.3	25.8	8.40E-06
15.5	16.9	25.7	7.91E-06
16.5	16.5	25.7	7.45E-06
17.5	16.2	25.7	7.03E-06
18.5	15.8	25.7	6.64E-06
19.5	15.5	25.7	6.28E-06
20.5	15.2	25.8	5.95E-06
21.5	14.9	25.7	5.65E-06
22.5	14.6	25.8	5.37E-06
23.5	14.4	25.9	5.11E-06
24.5	14.1	25.9	4.88E-06
25.5	13.9	25.9	4.67E-06
26.5	13.7	26.0	4.47E-06
27.5	13.5	26.0	4.30E-06
28.5	13.2	26.2	4.13E-06
29.5	13.0	26.1	3.97E-06
30.5	12.8	26.2	3.83E-06
31.5	12.7	26.3	3.69E-06
32.5	12.5	26.3	3.56E-06
34.5	12.1	26.4	3.31E-06
36.5	11.9	26.5	3.06E-06
38.5	11.6	26.5	2.79E-06
40.5	11.4	26.6	2.49E-06
42.5	11.2	26.7	2.15E-06
44.5	10.9	26.7	1.74E-06
46.5	10.8	26.7	1.25E-06
48.5*	10.6	26.8	
55.5	9.8	27.2	
60.5	9.3	27.3	

65.5	8.6	27.3	
71.5	8.3	27.3	
74.5	8.3	27.7	
76.5	8.3	27.6	
* Stirrer increased to 600 rpm			

Table A-9 gives the data and results from kinetic experiments of ethylene absorption with aniline-CuCl-NMP at 300 rpm. The liquid volume in the autoclave was 97.3 cm^3 and the number of moles of ethylene charged from the gas bomb was 0.0325.

Table A-9. Kinetic data and results for ethylene absorption at 300 rpm

Elapsed time from stirrer start, min	Partial pressure, psia	Temperature, °C	Absorption rate, mol/s
0.0	27.0	24.4	
0.5	26.5	24.4	2.48E-05
1.0	25.8	24.4	2.41E-05
1.5	25.2	24.4	2.34E-05
2.0	24.7	24.4	2.27E-05
2.5	24.1	24.3	2.20E-05
3.0	23.6	24.2	2.13E-05
3.5	23.1	24.3	2.07E-05
4.0	22.6	24.3	2.00E-05
4.5	22.1	24.3	1.94E-05
5.0	21.6	24.3	1.88E-05
5.5	21.1	24.2	1.82E-05
6.0	20.7	24.2	1.77E-05
6.5	20.3	24.2	1.71E-05
7.0	19.9	24.2	1.65E-05
7.5	19.5	24.2	1.60E-05

8.0	19.1	24.2	1.55E-05
8.5	18.7	24.2	1.50E-05
9.0	18.4	24.1	1.45E-05
9.5	18.1	24.2	1.40E-05
10.0	17.7	24.3	1.36E-05
10.5	17.4	24.4	1.31E-05
11.0	17.1	24.4	1.27E-05
11.5	16.8	24.4	1.23E-05
12.0	16.5	24.4	1.18E-05
12.5	16.2	24.5	1.14E-05
13.0	16.0	24.4	1.11E-05
13.5	15.7	24.4	1.07E-05
14.0	15.4	24.4	1.03E-05
14.5	15.2	24.5	9.96E-06
15.0	15.0	24.5	9.62E-06
15.5	14.7	24.6	9.29E-06
16.0	14.5	24.5	8.97E-06
16.5	14.3	24.4	8.66E-06
17.0	14.1	24.4	8.36E-06
17.5	13.9	24.4	8.07E-06
18.0	13.7	24.5	7.79E-06
18.5	13.5	24.6	7.51E-06
19.0	13.3	24.7	7.25E-06
19.5	13.2	24.7	7.00E-06
20.0	13.0	24.8	6.76E-06
20.5	12.8	24.8	6.52E-06
21.5	12.5	24.9	6.08E-06
22.5	12.2	24.8	5.67E-06
23.5	12.0	24.9	5.29E-06
24.5	11.7	24.9	4.94E-06
25.5	11.5	24.9	4.61E-06

26.5	11.2	24.9	4.32E-06
27.5	11.0	25.0	4.04E-06
28.5	10.8	25.0	3.80E-06
29.5	10.7	25.0	3.57E-06
30.5	10.5	25.0	3.36E-06
31.5	10.3	25.0	3.17E-06
32.5	10.2	25.1	2.99E-06
33.5	10.0	25.0	2.83E-06
34.5	9.9	25.1	2.69E-06
35.5	9.8	25.2	2.55E-06
36.5	9.6	25.3	2.42E-06
38.5	9.4	25.3	2.20E-06
40.5	9.2	25.5	1.98E-06
42.5	9.1	25.5	1.78E-06
44.5	9.0	25.5	1.57E-06
46.5	8.8	25.6	1.33E-06
48.5	8.7	25.7	1.07E-06
50.5	8.6	25.7	7.54E-07
52.5	8.5	25.9	3.80E-07
54.5*	8.4	25.9	
59.5	8.2	26.2	
62.5	8.0	26.3	
65.5	7.9	26.2	
68.5	7.9	26.3	
70.5	7.9	26.4	

* Stirrer increased to 600 rpm

Bibliography

[1] Alter, E.; Bruns, L. Process for Separating Off Olefins from Gases Containing Olefins. US Pat. 4,328,382. Iss. 05/04/1982.

[2] Baker, B.B. The Effect of Metal Fluoroborates on the Absorption of Ethylene by Silver Ion. *Inorg. Chem.* 1964, 3, 200-202.

[3] Bjacek, P. Petrochemical Capacity Additions to Slow in 2002-12. *Oil & Gas Journal*. December 15, 2003, 50.

[4] Blytas, G.C. Separation of Unsaturates by Complexing with Nonaqueous Solutions of Cuprous Salts. *Separation and Purification Technology*. Li, N.N., Calo, J.M., Eds.; Marcel Dekker: New York, 1992; Chapter 2.

[5] Brady, R.; Flynn, B.R.; Geoffroy, G.L.; Gray, H.B.; Peone, Jr., J.; Vaska, L. Electronic Spectral Studies of Planar Rhodium(I) and Iridium(I) Complexes Containing π-Acceptor Ligands. *Inorg. Chem.* 1976, 15, 1485-1488.

[6] Branan, D.M.; Hoffman, N.W.; McElroy, E.A.; Miller, N.C.; Ramage, D.L.; Schott, A.F.; Young, S.H. Anion Affinity of Carbonylbis(triphenylphosphine) rhodium(I) in CH_2Cl_2: Fluoride vs. Its Halide Analogues. *Inorg. Chem.* 1987, 26, 2915-2917.

[7] Budzelaar, P.H.M.; Timmermans, P.J.J.A.; Mackor, A.; Baerends, E.J. Bonding in the ground state and excited states of copper-alkene complexes. *J. Organomet. Chem.* 1987, 331, 397-407.

[8] Burns, R.L. Investigation of Poly(pyrrolone-imide) Materials for the Olefin / Paraffin Separation. Ph.D. Dissertation. The University of Texas at Austin, 2002.

[9] Buxton, G.V.; Green, J.C.; Sellers, R.M. Oxidation of Copper(I)-Olefin Complexes in Aqueous Solution by Oxygen and Hydrogen Peroxide. *J. Chem. Soc. Dalt. Trans.* 1976, 2160-2165.

[10] Caulton, K.G.; Davies, G.; Holt, E.M. Synthesis, Molecular Structures, Properties and Reactions of Halo- and Carbonyl(amine)copper(I) Complexes. *Polyhedron*. 1990, 9, 2319-2351.

[11] Cen, P.L. Adsorption Uptake Curves of Ethylene on Cu(I)-NaY Zeolite. *AIChE J.* 1991, 36, 789-793.

[12] Chang, C.S.; Rochelle, G.T. Surface Renewal Theory for Simultaneous Mass Transfer and Equilibrium Chemical Reaction. Presented at AIChE 88th National Meeting, Philadelphia, June 8-12, 1980.

[13] Chatt, J.; Duncanson, L.A. Olefin Co-ordination Compounds. Part III. Infra-red Spectra and Structure: Attempted Preparation of Acetylene Complexes. *J. Chem. Soc.* 1953, 2939-2947.

[14] Chemical Prices. *Chemical Market Reporter*. May 17, 2004.

[15] Chen, K.H.; Iwamoto, R.T. Tetracoordination of Copper(I) by Monofunctional Amines. *Inorg. Chim. Acta*. 1971, 5, 97-102.

[16] Chen, J.P.; Yang, R.T. A Molecular Orbital Study of the Selective Adsorption of Simple Hydrocarbon Molecules on Ag^+- and Cu^+-Exchanged Resins and Cuprous Halides. *Langmuir*. 1995, 11, 3450-3456.

[17] Corradini, P.; Guerra, G.; Cavallo, L. Do New Century Catalysts Unravel the Mechanism of Stereocontrol of Old Ziegler-Natta Catalysts? *Acc. Chem. Res.* 2004, 37, 231-241.

[18] Cossee, P. Ziegler-Natta catalysis. I. Mechanism of polymerization of α-olefins with Ziegler-Natta catalysts. *J. Catal.* 1964, 3, 80-88.

[19] Crookes, J.V.; Woolf, A.A. Competitive Interactions in the Complexing of Ethylene with Silver(I) Salt Solutions. *J. Chem. Soc., Dalt. Trans.* 1973, 1241-1247.

[20] Cymbaluk, T.H.; Tabler, D.C.; Johnson, M.M.; Nowack, G.P. Method for Preparing Olefin Complexing Reagents and Use Thereof. US Pat. 5,191,153. Iss. 03/02/1993.

[21] Cymbaluk, T.H.; Nowack, G.P.; Johnson, M.M. Copper(I) Carboxylate-Containing Olefin Complexing Reagents. US Pat. 5,523,512. Iss. 06/04/1996.

[22] Da Silva, F.A.; Rodrigues, A.E. Propylene/Propane Separation by Vacuum Swing Adsorption Using 13X Zeolite. *AIChE Journal*. 2001, 47, 341-357.

[23] Danckwerts, P.V. *Gas-Liquid Reactions*. McGraw-Hill: New York, 1970.

[24] Dewar, J.S. A Review of the π-Complex Theory. *Bull. Soc. Chim. Fr.* 1951, 18, C71-C79.

[25] Dunlop, A.K.; Blytas, G.C.; Bell, E.R. Separation of Hydrocarbons by Cuprous Salts. US Pat. 3,401,112. Iss. 09/10/1968.

[26] Ebrahimi, S.; Kleerebezem, R.; Van Loosdrecht, M.C.M.; Heijnen, J.J. Kinetics of the Reactive Absorption of Hydrogen Sulfide into Aqueous Ferric Sulfate Solutions. *Chem. Eng. Sci.* 2003, 58, 417-427.

[27] Eldridge, R.B. Olefin/Paraffin Separation Technology: A Review. *Ind. Eng. Chem. Res.* 1993, 32, 2208-2212.

[28] Forster, D. Relative Stabilities of Some Halide Complexes of Rhodium and Iridium. *Inorg. Chem.* 1972, 11, 1686-1687.

[29] Gagne, R.R.; Spiro, C.L.; Smith, T.J.; Hamann, C.A; Thies, W.R.; Shiemke, A.K. The Synthesis, Redox Properties, and Ligand Binding of Heterobinuclear Transition-Metal Macrocyclic Ligand Complexes. Measurement of an Apparent Delocalization Energy in a Mixed-Valent $Cu^{I}Cu^{II}$ Complex. *J. Am. Chem. Soc.* 1981, 103, 4073-4081.

[30] Galus, Z. *Fundamentals of Electrochemical Analysis*. Marcinkiewicz, S., Trans.; Reynolds, G. F., Trans. Ed.; Halsted: New York, 1976.

[31] Geiger, D.; Ferraudi, G. Photochemistry of Cu-Olefin Complexes: a Flash Photochemical Investigation of the Reactivity of Cu(ethylene)$^{+}$ and Cu(*cis*,*cis*-1,5-cyclooctadiene)$_2^{+}$. *Inorg. Chim. Acta*. 1985, 101, 197-201.

[32] Geiger, W.E. Electrochemistry of Cycloaddition Products of Olefins with Nickel Dithiolenes: A Reinvestigation of the Reduction of the 1:1 Adduct between $Ni(S_2C_2(CF_3)_2)_2$ and Norbornadiene. *Inorg. Chem.* 2002, 41, 136-139.

[33] Gerhartz, W., Ed. Ethylene. *Ullman's Encyclopedia of Industrial Chemistry*. 5th edition. VCH Verlagsgesellschaft: Weinheim, 1987, Vol. A10, pp 45-93.

[34] Gilliland, E.R.; Seebold, J.E.; Fitzhugh, J.R.; Morgan, P.S. Reaction of Olefins with Solid Cuprous Halides. *J. Am. Chem. Soc.* 1939, 61, 1960-1962.

[35] Gil-Rubio, J.; Weberndorfer, B.; Werner, H. A series of new fluororhodium(I) complexes. *J. Chem. Soc., Dalt. Trans.* 1999, 1437-1444.

[36] Haase, D.J.; Walker, D.G. The COSORB Process. *Chem. Engr. Prog.* 1974, 70 (5), 74-77.

[37] Haase, D.J.; Walker, D.G.; Ostrowski, P.C. Use of Amine-Aluminum Chloride Adducts as Alkylation Inhibitors in a Ligand-Complexing Process. US Pat. 4,317,950. Iss. 03/02/1982.

[38] Haase, D.J. Process for Removal of Selected Component Gases from Multi-Component Gas Streams. US Pat. 5,382,417. Iss. 01/17/1995.

[39] Hartley, F.R. Thermodynamic Data for Olefin and Acetylene Complexes of Transition Metals. *Chem. Rev.* 1973, 73, 163-190.

[40] Herberhold, M. *Metal p-Complexes. Part II: Specific Aspects*. Elsevier: New York, 1974; Vol. II.

[41] Hikita, H.; Asai, S.; Ishikawa, H.; Saito, Y. Kinetics of Absorption of Chlorine in Aqueous Acidic Solutions of Ferrous Chloride. *Chem. Eng. Sci.* 1975, 30, 607-616.

[42] Hines, A.H.; Maddox, R.N. *Mass Transfer Fundamentals and Applications*. Prentice Hall: Upper Saddle River, N.J., 1985.

[43] Hirai, H.; Kurima, K.; Komiyama, M. Ethylene Absorption by Solutions of Copper(I) Chloride and Amines in Methanol. *Chem. Soc. Jap., Chem. Let*. 1986, 671-674.

[44] Hirai, H.; Kurima, K.; Komiyama, M. Selective Solid Ethylene Adsorbent Composed of Copper(I) Chloride and Polystyrene Resin Having Amino Groups. *Poly. Mat. Sci. Engr.* 1986, 55, 464-468.

[45] Ho, W.S.W.; Doyle, G.; Savage, D.W.; Pruett, R.L. Olefin Separations via Complexation with Cuprous Diketonate. *Ind. Eng. Chem. Res.* 1988, 27, 334-337.

[46] Horowitz, H.H.; Tyler, W.E.,III. Olefin Separation Process. US Pat. 3,809,729. Iss. 05/07/1974.

[47] Horsley, G.F. Process for separating and recovering olefines from gases containing the same. British Pat. 291,186. Iss. 05/31/1928.

[48] Huang, Y.Y. Ethylene Complexes in Copper(I) and Silver(I) Y Zeolites. *J. Catal.* 1980, 61, 461-476.

[49] Huang, H.Y.; Padin, J.; Yang, R.T. Anion and Cation Effects on Olefin Adsorption on Silver and Copper Halides: Ab Initio Effective Core Potential Study of π-Complexation. *J. Phys. Chem. B*. 1999, 103, 3206-3212.

[50] Huang, H.Y.; Padin, J.; Yang, R.T. Comparison of π-Complexations of Ethylene and Carbon Monoxide with Cu^+ and Ag^+. *Ing. Eng. Chem. Res.* 1999, 38, 2720-2725.

[51] Hughes, M.A.; Middlebrook, P.D.; Whewell, R.J. Aspects of the Diffusion of Copper in Solutions Encountered during Solvent Extraction with Hydroxyoximes. *J. Inorg. Nucl. Chem.* 1977, 39, 1679-1682.

[52] Humphrey, J.L.; Seibert, A.F.; Koort, R.A. Separation Technologies Advances and Priorities. U.S. Dept. of Energy Report 12920-1, 1991.

[53] Incropera, F.P.; DeWitt, D.P. *Fundamentals of Heat and Mass Transfer*. 4th edition. John Wiley & Sons: New York, 1996.

[54] Jacobson, R.R.; Tyeklar, Z.; Farooq, A.; Karlin, K.D.; Liu, S.; Zubieta, J. A Cu_2-O_2 Complex. Crystal Structure and Characterization of a Reversible Dioxygen Binding System. *J. Am. Chem. Soc.* 1988, 110, 3690-3692.

[55] Jamal, A.; Meisen, A. Kinetics of CO induced degradation of aqueous diethanolamine. *Chem. Eng. Sci.* 2001, 56, 6743-6760.

[56] Jayaraman, A.; Yang, R.T.; Munson, C.L.; Chinn, D. Deactivation of π-Complexation Adsorbents by Hydrogen and Rejuvenation by Oxidation. *Ind. Eng. Chem. Res.* 2001, 40, 4370-7376.

[57] Joshua, W.P.; Stanley, H.M. Separation and recovery of olefines from gases containing the same. US Pat. 2,005,500. Iss. 06/18/1935.

[58] Kamau, P.; Jordan, R.B. Formation Constants of Copper(I)-Olefin Complexes in Aqueous Solution. *Inorg. Chem.* 2002, 41, 884-891.

[59] Karlin, K.D.; Kaderli, S.; Zuberbuhler, A.D. Kinetics and Thermodynamics of Copper(I)/Dioxygen Interaction. *Acc. Chem. Res.* 1997, 30, 139-147.

[60] Kelber, J.A.; Harrah, L.A.; Jennison, D.R. Theoretical Studies of $(CuC_2H_4)^+$ and $(CuC_2H_4)^0$: Application of CuCl on Polystyrene. *J. Organmet. Chem.* 1980, 199, 281-291.

[61] Keller, G.E.; Marcinkowsky, A.E.; Verma, S.K.; Williamson, K.D. Olefin Recovery and Purification via Silver Complexation. *Separation and Purification Technology*. Li, N.N., Calo, J.M., Eds.; Marcel Dekker: New York, 1992; Chapter 3.

[62] Kim, C.J.; Palmer, A.M.; Milliman, G.E. Absorption of Carbon Monoxide into Aqueous Solutions of K_2CO_3, Methyldiethanolamine, and Diethylethanolamine. *Ind. Eng. Chem. Res.* 1988, 27, 324-328.

[63] Kim, Y.H.; Ryu, J.H.; Bae, J.Y.; Kang, Y.S.; Kim, H.S. Reactive polymer membranes containing cuprous complexes in olefin/paraffin separation. *Chem. Commun.* 2000, 195-196.

[64] Kitagawa, S.; Munakata, M. Binuclear Copper(I) Complexes Which Reversibly React with CO. 1. Di-μ-halogeno-bis(2,2'-bipyridine)dicopper(I) and Its Derivatives. *Inorg. Chem.* 1981, 20, 2261-2267.

[65] Kitagawa, S.; Munakata, M.; Higashie, A. Effect of Substituents on the Charge Transfer Band of Copper(I) Complexes with 4-Monosubstituted Pyridines. *Inorg. Chim. Acta*. 1982, 59, 219-223.

[66] Kolb, B.; Ettre, L.S. *Static Headspace-Gas Chromatography: Theory and Practice*. Wiley: New York, 1997.

[67] Komiyama, M. Selective Absorption of Ethylene by Methanol Solutions of Copper(I) Chloride-Ethylenediamine Complex. *Chem. Eng. Technol.* 1989, 12, 356-357.

[68] Laddha, S.S.; Diaz, J.M.; Danckwerts, P.V. The N_2O Analogy: the Solubilities of CO_2 and N_2O in Aqueous Solution of Organic Compounds. *Chem. Eng. Sci.* 1981, 36, 228-229.

[69] Lang, L, ed. *Absorption Spectra in the Ultraviolet and Visible Region*; Academic Press: New York, 1973, Vol. XVIII.

[70] Leet, W.A.; Kulprathipanja, S. Reactive Separation Processes. *Reactive Separation Process*. Kulprathipanja, S., Ed.; Taylor & Francis: New York, 2002; Chapter 1.

[71] Lewin, A.H.; Michl, R.J.; Ganis, P.; Lepore, U.; Avitabile, G. Copper(I) Complexes: Synthesis and Crystal Structure of Tetrapyridine Copper(I) Perchlorate $(C_5H_5N)_4CuClO_4$. *Chem. Commun.* 1971, 1400-1401.

[72] Lide, D.R., Ed. *CRC Handbook of Chemistry and Physics*; CRC Press: Boca Raton, 81st Edition, 2000.

[73] Lin, Y.S.; Ji, W.; Wang, Y.; Higgins, R.J. Cuprous-Chloride-Modified Nanoporous Alumina Membranes for Ethylene-Ethane Separation. *Ind. Eng. Chem. Res.* 1999, 38, 2292-2298.

[74] Long, R.B.; Longwell, J.P.; Caruso, F.A.; DeFeo, R.J. Separation and Recovery of Complexible Ligands by Liquid Exchange. US Pat. 3,592,865. Iss. 07/13/1971.

[75] Long, R.B. Separation of Unsaturates by Complexing with Solid Copper Salts. *Recent Developments in Separation Science*. Li, N.N., Ed.; CRC Press: Boca Raton, FL, 1972; Vol. 1, pp 35-57.

[76] Merchan, M.; Gonzalez-Luque, R.; Nebot-Gil, I.; Tomas, F. A Pseudopotential ab initio Molecular Orbital Study of the Copper(I)-Ethylene System. *Chem. Phys. Let.* 1984, 112, 412-416.

[77] Monk, P. *Fundamentals of Electro-Analytical Chemistry*. John Wiley & Sons: Chichester, 2001.

[78] Morisato, A.; He, Z.; Pinnau, I.; Merkel, T.C. Transport Properties of PA12-PTMO/$AgBF_4$ Solid Polymer Electrolyte Membranes for Olefin/Paraffin Separation. *Poly. Mat. Sci. Engr.* 2001, 85, 96-97.

[79] Munakata, M. Kitagawa, S. The Chemistry of Copper(I) Complexes in Solution. *Copper Coordination Chemistry: Biochemical and Inorganic Perspectives*. Karlin, K.D., Zubieta, J., Eds.; Adenine Press: New York, 1983; pp 473-495.

[80] Munakata, M.; Kitagawa, S.; Kosome, S.; Asahara, A. Studies of Copper(I) Olefin Complexes. Formation Constants of Copper Olefin Complexes with 2,2'-Bipyridine, 1,10-Phenanthroline, and Their Derivatives. *Inorg. Chem.* 1986, 25, 2622-2627.

[81] Nymeijer, K.; Visser, T.; Assen, R.; Wessling, M. Olefin-Selective Membranes in Gas-Liquid Membrane Contactors for Olefin/Paraffin Separation. *Ind. Eng. Chem. Res.* 2004, 43, 720-727.

[82] Onda, K.; Sada, E.; Kobayashi, T.; Fujine, M. Gas Absorption Accompanied by Complex Chemical Reactions – I. Reversible Chemical Reactions. *Chem. Eng. Sci.* 1970, 25, 753-760.

[83] Pavlov, S.J.; Stepanova, V.A.; Bogdanova, O.V.; et al. Separating Unequally Saturated Hydrocarbons with Monovalent Copper Salt Solutions in β-Methoxypropionitrile. US Pat. 4,141,925. Iss. 02/27/1979.

[84] Pearson, R.G. Hard and Soft Acids and Bases. *J. Am. Chem. Soc.* 1963, 85, 3533-3539.

[85] Petitjean, L.; Pattou, D.; Ruiz-Lopez, M.F. Theoretical Study of the Mechanisms of Ethylene Polymerization with Metallocene-Type Catalysts. *J. Phys. Chem. B*. 1999, 103, 27-35.

[86] Pino, P.; Moretti, G. The impact of the discovery of the polymerization of the α-olefins on the development of the stereospecific polymerization of vinyl monomers. *Polymer*. 1987, 28, 683-692.

[87] Quinn, H.W.; Glew, D.N. Coordination Compounds of Olefins with Solid Complex Silver Salts: I. Coordination Compounds with Anhydrous Silver Fluoborate. *Can. J. Chem.* 1962, 40, 1103-1112.

[88] Randles, J.E.B. The Equilibrium between Cuprous and Cupric Compounds in Presence of Metallic Copper. *J. Chem. Soc.* 1941, 802-811.

[89] Ray, G.C. Recovery of olefin hydrocarbons. US Pat. 2,589,960. Iss. 03/18/1952.

[90] Robey, R.F. Concentration of olefins. US Pat. 2,245,719. Iss. 06/17/1941.

[91] Safarik, D.J.; Eldridge, R.B. Olefin/Paraffin Separations by Reactive Absorption: A Review. *Ind. Eng. Chem. Res.* 1998, 37, 2571-2581.

[92] Sanyal, I.; Mahroof-Tahir, M.; Nasir, M.S.; Ghosh, P.; Cohen, B.I.; Gultneh, Y.; Cruse, R.W.; Farooq, A.; Karlin, K.D.; Liu, S.; Zubieta, J. Reactions of Dioxygen (O_2) with Mononuclear Copper(I) Complexes: Temperature-Dependent Formation of Peroxo- or Oxo- (and Dihydroxo-) Bridged Dicopper(II) Complexes. *Inorg. Chem.* 1992, 31, 4322-4332.

[93] Sedriks, W. Olefins Industry Outlook: Trends, Uncertainties, & Implications. Presented at Process Economics Program Conference, Redwood Shores, CA, 1998.

[94] Sharma, V.K.; Millero, F.J. Determining the Stability Constant of Copper(I) Halide Complexes from Kinetic Measurements. *Inorg. Chem.* 1988, 27, 3256-3259.

[95] Sherwood, T.K.; Pigford, R.L.; Wilke, C.R. *Mass Transfer*. McGraw-Hill: New York, 1975.

[96] Shrier, A.L.; Danckwerts, P.V. Carbon Dioxide Absorption into Amine-Promoted Potash Solutions. *Ind. Eng. Chem. Res. Fund.* 1969, 8, 415-423.

[97] Smith, J.M.; Van Ness, H.C.; Abbott, M.M. *Introduction to Chemical Engineering Thermodynamics*, 5th ed.; McGraw-Hill: New York, 1996.

[98] Stack, T.D.P. Complexity with simplicity: a steric continuum of chelating diamines with copper(I) and dioxygen. *J. Chem. Soc. Dalt. Trans.* 2003, 1881-1889.

[99] Su, C.; Kuraoka, K.; Yazawa, T. Increasing the stability of silver(I) ions in inorganic-organic hybrid membranes for C_2H_4/C_2H_6 separation by using weakly self-coordinating anions of the silver salts. *J. Mat. Sci. Let.* 2002, 21, 525-527.

[100] Suenaga, Y.; Wu, L.P.; Kuroda-sowa, T.; Munakata, M.; Maekawa, M. Structure and ^1H NMR study of copper(I) complex with ethylene and tetramethylethylenediamine. *Polyhedron*. 1997, 16, 67-70.

[101] Sundaram, K.M.; Shreehan, M.M.; Olszewski, E.F. Ethylene. *Kirk-Othmer Encyclopedia of Chemical Technology*. 4th edition. John Wiley & Sons, Inc.: New York, 1994, Vol. 9, pp 877-915.

[102] Sunderrajan, S.; Freeman, B.D.; Hall, C.K. Fourier Transform Infrared Spectroscopic Characterization of Olefin Complexation by Silver Salts in Solution. *Ind. Eng. Chem. Res.* 1999, 38, 4051-4059.

[103] Sunderrajan, S.; Freeman, B.D.; Hall, C.K.; Pinnau, I. Propane and propylene sorption in solid polymer electrolytes based on poly(ethylene oxide) and silver salts. *J. Membr. Sci.* 2001, 182, 1-12.

[104] Sungpet, A.; Way, J.D.; Thoen, P.M.; Dorgan, J.R. Reactive Polymer Membranes for Ethylene/Ethane Separation. *J. Membr. Sci.* 1997, 136, 111-120.

[105] Suzuki, T.; Noble, R.D.; Koval, C.A. Electrochemistry, Stability, and Alkene Complexation Chemistry of Copper(I) Triflate in Aqueous Solution. Potential for Use

in Electrochemically Modulated Complexation-Based Separation Processes. *Inorg. Chem.* 1997, 36, 136-140.

[106] Teramoto, M.; Matsuyama, H.; Yamashiro, T.; Katayama, Y. Separation of Ethylene from Ethane by Supported Liquid Membranes Containing Silver Nitrate as a Carrier. *J. Chem. Engr. Jpn.* 1986, 19, 419-424.

[107] Terry, P.A.; Noble, R.D.; Swanson, D.; Koval, C.A. Electrochemically Modulated Complexation Process for Ethylene/Ethane Separation. *AIChE J.* 1997, 43, 1709-1716.

[108] Thompson, J.S.; Harlow, R.L.; Whitney, J.F. Copper(I)-Olefin Complexes. Support for the Proposed Role of Copper in the Ethylene Effect in Plants. *J. Am. Chem. Soc.* 1983, 105, 3522-3527.

[109] Tsou, D.T.; Blachman, M.W.; Davis, J.C. Silver-Facilitated Olefin/Paraffin Separation in a Liquid Membrane Contactor System. *Ind. Eng. Chem. Res.* 1994, 33, 3209-3216.

[110] Tyeklar, Z.; Jacobson, R.R.; Wei, N.; Murthy, N.N.; Zubieta, J.; Karlin, K.D. Reversible Reaction of O_2 (and CO) with a Copper(I) Complex. X-ray Structures of Relevant Mononuclear Cu(I) Precursor Adducts and the *trans*-(μ-1,2-Peroxo)dicopper(II) Product. *J. Am. Chem. Soc*. 1993, 115, 2677-2689.

[111] Uebele, C.E.; Grasselli, R.K.; Nixon, W.C.,Jr. Olefin Recovery Process. US Pat. 3,514,488. Iss. 05/26/1970.

[112] Van Krevelen, D.W.; Hoftijzer, P.J. Kinetics of Gas-Liquid Reactions. I. General Theory. *Rec. Trav. Chim.* 1948, 67, 563-586.

[113] Vaska, L. Reversible Activation of Covalent Molecules by Transition Metal Complexes. The Role of the Covalent Molecule. *Acc. Chem. Res.* 1968, 1, 335-344.

[114] Versteeg, G.F.; Blauwhoff, P.M.M.; Van Swaaij, W.P.M. The effect of Diffusivity on Gas-Liquid Mass Transfer in Stirred Vessels. Experiments at Atmospheric and Elevated Pressures. *Chem. Eng. Sci.* 1987, 42, 1103-1119.

[115] Wang, B.; Eldridge, R.B.; Lagowski, J.J. Olefin/Paraffin Separation by Reactive Absorption: An investigation of the application of electrochemistry (CV) to estimate complexation constants of metal ions with ethylene. Unpublished work. 2000.

[116] Wang, K.; Stiefel, E.I. Toward Separation and Purification of Olefins Using Dithiolene Complexes: An Electrochemical Approach. *Science*. 2001, 291, 106-109.

[117] Watts, H.G. Process of recovering ethylene from gaseous olefine mixtures containing the same. US Pat. 1,977,659. Iss. 10/23/1934.

[118] Xu, S.; Wang, Y.; Otto, F.D.; Mather, A.E. Kinetics of the Reaction of Carbon Dioxide with 2-Amino-2-methyl-1-propanol Solutions. *Chem. Eng. Sci.* 1996, 51, 841-850.

[119] Yanagihara, N.; del Castillo S., E.; Ogura, T. Determination of copper(I)-ethylene complexes, $[Cu(C_2H_4)]^+$ and $[Cu(C_2H_4)_2]^+$, with aid of EDTA titration of copper(I) and copper(II) ions. *Transition Met. Chem.* 1987, 12, 12-14.

[120] Yaws, C.L., Ed. *Chemical Properties Handbook*; McGraw-Hill: New York, 1999.

[121] Yang, R.T.; Kikkinides, E.S. New Sorbents for Olefin/Paraffin Separations by Adsorption via π-Complexation. *AIChE J.* 1995, 41, 509-517.

[122] Zeigler, T.; Rauk, A. A Theoretical Study of the Ethylene-Metal Bond in Complexes between Cu^+, Ag^+, Au^+, Pt^0, or Pt^{2+} and Ethylene, Based on the Hartree-Fock-Slater Transition-State Method. *Inorg. Chem.* 1979, 18, 1558-1565.

Vita

Travis Allen Reine was born on May 19, 1979 in Baton Rouge, Louisiana as the only son of Wayne and Emilie Reine. Travis graduated from Parkview Baptist High School in Baton Rouge, Louisiana in May 1996. He attended Louisiana Tech University from 1996 – 2000, and he graduated with a Bachelor of Science degree in Chemical Engineering, summa cum laude, in May 2000. During the summer of 1999, he worked at Environmental Resource Management (ERM) Southwest in Metairie, Louisiana as an intern. In August 2000, Travis entered the graduate school at The University of Texas at Austin. During the summer of 2002, he worked for Shell Chemical Company as a graduate intern at their Westhollow research facility in Houston, Texas. He received a Master of Science degree in Chemical Engineering from The University of Texas at Austin in May 2004. Upon graduation with his PhD degree, he plans to begin work with ExxonMobil Chemical Company in Baton Rouge, Louisiana.

Permanent Address: 40104 Alise Ave.
Prairieville, LA 70769

This dissertation was typed by the author.